AE3200-DSE, Final Report

Distributed Electric Propulsion (DEP) for Regional Transport Aircraft: E-gle

D. van Aken	4383184	R.R. Feith	4218272
S. Berning	4370589	M.W. Goderie	4363337
S. Boddu	4381866	S. Manjunatharao	4356055
N.G. Borst	4370457	V.B. Verhoeven	4391594
K. Engelen	4364546	E. Woeldgen	4275306

Delft University of Technology

PREFACE

This report is the last of a series of several reports to be delivered for the course module AE3200, Design Synthesis Exercise, by group 1 in the third year of the BSc Aerospace Engineering programme at Delft University of Technology, The Netherlands. The report consists of a detailed trade-off process to determine the optimal design that satisfies all the requirements and constraints. The project aims to investigate the use of Distributed Electric Propulsion (DEP) for cleaner aviation. The group comprises of ten motivated students working together to come up with potential results for the tasks to be accomplished. The educational goal of this project is to familiarise students with a multitude of skills including design, communication, team management and sustainable development. This report is aimed at anyone wanting to research on the subject of Distributed Electric Propulsion. Finally, the group would like to express their gratitude to their principal tutor, Dr. Ir. A. Sahai, and their coaches, Dr. X. Zhao and Ir. V. Pallichadath, for their constant support and mentoring throughout the execution of this project.

Report by Group 1:

Daan van Aken	4383184
Sjoerd Berning	4370589
Sumalik Boddu	4381866
Nick G. Borst	4370457
Koen Engelen	4364546
Rick R. Feith	4218272
Michiel W. Goderie	4363337
Shamitha Manjunatharao	4356055
Vincent B. Verhoeven	4391594
Elisabeth Woeldgen	4275306

Delft, April 2017

Cover photo: *Catia Render group 1.* –

EXECUTIVE OVERVIEW

One of the most severe problems mankind is currently facing, is the change in climate due to the emission of a large quantity of greenhouse gasses. Whereas most transportation industries are experiencing a shift towards the use of cleaner, renewable energy, the aviation industry is still largely dependant on kerosene. Therefore, the following need is found: *"In order to meet the environmental goals of NASA N+3 and Flightpath 2050, there is a need to design aircraft that efficiently use alternate cleaner energy sources over conventional propulsion techniques."*

Recent studies suggest that the use of electric propulsion can lead to an increase in propulsive efficiency, while also providing benefits in term of flight performance. These designs make use of distributed electric propulsion (DEP), meaning that small propellers, used in order to provide extra lift during landing and take-off, are distributed along the wing, whereas the propulsive propellers are placed on the tips of the wing. The DEP propellers will be folded when they are not required in order to minimise drag, as can be seen in Figure 1. The benefits of this configuration can be mainly attributed to three factors. First of all, as the distributed electric propellers, or high-lift propellers, increase the dynamic pressure over the wing during landing and take-off, these phases are no longer critical for the design of the wing. This means that the wing can be sized for cruise, reducing the surface area and enabling the aircraft to fly at higher lift coefficients, which in turn decreases the total drag. Secondly, the wingtip propellers lead to a large decrease in induced drag, leading to less power required, improving the aircraft's flight performance. Finally, electric motors, used to convert the energy from the batteries, are up to three times as efficient compared to combustion engines, leading to a reduction in energy consumption. These benefits can lead to a hybrid, electric aircraft, fulfilling the needs previously described. Therefore, the purpose of this report is: *Design a regional passenger transport aircraft with a range of at least 500 Nautical Miles (NM), that makes use of Distributed Electric Propulsion technology to produce thrust and is operational in 2030; with a group of 10 students within a duration of 10 weeks.*

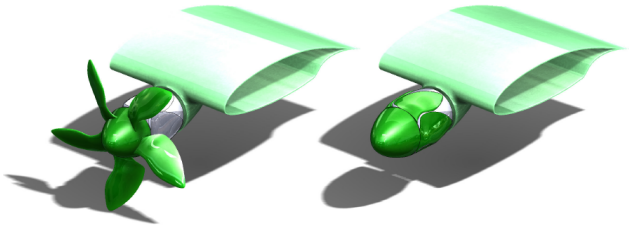

Figure 1: Five blade propeller design illustrating the blade folding mechanism [1]

First of all, a top-level concept design is performed, which is done by using design option trees. This method allows for all options for a certain design to be explored, while eliminating the unfeasible ones. An overview of all the design domains for which a design option tree is created is given in Table 1.

Table 1: Overview of the created design options trees

Design Options Trees	
Propulsion	Wing Configuration
Power Transfer	Fuselage Configuration
Power Generation	Empennage Configuration
Distributed Electric Propulsion	Landing Gear Configuration

From the initial design exploration, three subsystems stand out due to the large contribution to the final outcome and success of the design, namely the wing configuration, the power storage and the propulsion (including the distributed electric propulsion). Due to the limited time-frame of this project it is decided to first investigate these subsystems and compare the resulting design to current regional turboprops. During the midterm phase of the project, the goal is to find the most suitable concept for the need expressed above. In order to select the optimal choice within each subsystem several trade-offs are performed, which is done by first creating a trade-off strategy and selecting suitable trade-off criteria for each subsystem. Each criterion is then awarded a weight, after which each of the concepts is given scores, leading to a overview of which concepts best suits the design requirements.

During the trade-off of the power subsystem it is discovered that the current battery technology and battery forecast are not able to deliver enough battery specific energy per kg to reach a range of 500 NM. As can be observed from Figure 2 a lower battery specific energy results in a higher total mass and thus a value of 5 MJ/kg or 1400 W/kg of specific energy is necessary for batteries, in order to perform a fully electric flight whilst adhering to the weight budget. However, forecasts predict a value of 500 W/kg. For this reason, other options are investigated and extra research is done into the use of hydrogen or the use of hybrid propulsion, i.e. using a gas turbine in combination with batteries. Resulting from this, zinc-air and lithium-sulphur batteries are considered in the trade-off, as other batteries are either technologically immature or have a low specific energy. Furthermore, hydrogen storage both by compression tank and by cryo-compression tank are considered. The result from this trade-off can be seen in Figure 3. The zinc-air batteries are selected, as they have a high energy density and show beneficial properties overall.

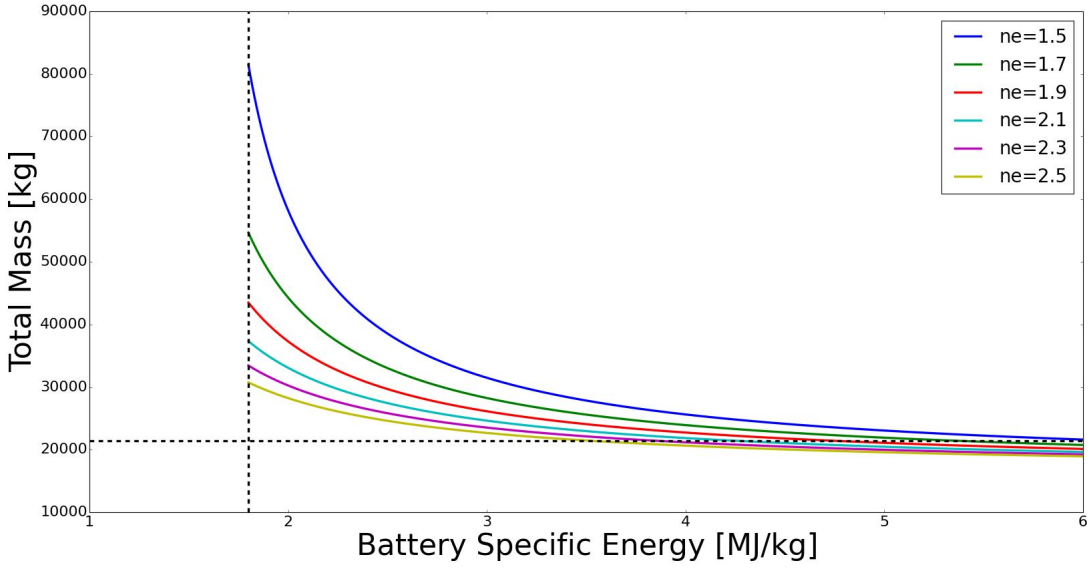

Figure 2: Maximum take-off weight as a function of battery specific energy for a fully electric flight, different lines representing different aircraft efficiencies. The vertical line represents the current battery specific energy

During the aerodynamic analysis, a high wing configuration is chosen, as this allows for a large clearance for the wingtip propellers. Moreover, a trade-off is made between a conventional wing, a canard wing and a box wing, as seen in Figure 3. It can be seen that for the wing configuration a conventional wing configuration was the ideal choice, since the canard and box wing option carry too much risk, are less stable and have a worse take-off and landing performance.

For the propulsion subsystem three trade-offs were performed that lead to the design choices of using propellers driven by conventional electric motors in combination with a hybrid turboprop, allowing for the use of multiple energy sources. This was mainly based on the fact that fans have a low efficiency, superconducting engines and turbo generates are too heavy and a turboprop is not compatible with DEP.

		Aerodynamics			Power				Propulsion						
		Wing Configuration			Power Storage				Propulsors		Electric Motors		Thrust Generation		
Criterion	Weight	Conventional	Canard Wing	Box Wing	Li-S Batteries	Zn-Air Batteries	Compression Tank	Cryo-Compression Tank	Propellers	Fans	Conventional	Superconducting	Turboprop	Turbo Generator	Hybrid Turboprop
Lift to Drag	4	4	5	5	-	-	-	-	-	-	-	-	-	-	-
Stability	3	5	2	3	-	-	-	-	-	-	-	-	-	-	-
Take-Off & Landing Performanc	3	5	3	4	-	-	-	-	-	-	-	-	-	-	-
Specific Energy	5	-	-	-	3	2	3	4	-	-	-	-	-	-	-
Energy Density	3	-	-	-	2	4	2	3	-	-	-	-	-	-	-
Degradation	3	-	-	-	2	3	3	3	-	-	-	-	-	-	-
Operating Cost	4	-	-	-	2	3	2	2	-	-	-	-	-	-	-
Safety	5|5|3	4	3	2	2	3	2	2	3	5	-	-	-	-	-
Technology Maturity	4|4|4	-	-	-	3	3	2	1	-	-	4	2	5	3	4
Power Density	5	-	-	-	-	-	-	-	-	-	4	5	-	-	-
Cost	2|3|2	-	-	-	-	-	-	-	4	2	3	2	5	3	4
Efficiency	5|5|3	-	-	-	-	-	-	-	5	1	3	5	5	4	4
Weight	3|4|5	-	-	-	-	-	-	-	3	2	4	1	4	1	3
Noise	4|2	-	-	-	-	-	-	-	3	5	3	4	-	-	-
DEP Compatibility	4	-	-	-	-	-	-	-	-	-	-	-	1	5	4
Emission	4	-	-	-	-	-	-	-	-	-	-	-	1	4	3
Total		66	50	51	57	70	56	60	63	52	82	76	73	76	79

Figure 3: Overview of the various trade-offs performed

Once the trade-off phase is completed, the selected concepts are designed and analysed in more detail. An overview of the most important design parameters can be seen in Table 3.

A parallel turbo-electric hybrid system is chosen because of the redundancy of the system and lower required power output from the gas turbine, which makes the design lighter and cheaper. An architecture of a parallel hybrid system is visualised in Figure 4. The configuration will have two hybrid turbo-electric propellers, which contain both one gas turbine, GE CT7 2A, and two electrical motors, Siemens SPD 60. Furthermore, there are twenty high-lift propellers distributed along the leading edge of the main wing, driven by an Emrax 268 electrical engine each. The thrust propellers have two blades, such that an optimal efficiency is reached. They use variable pitch propeller blades, in order to deliver constant power with respect to the velocity of the aircraft. The high-lift propellers have 8 propeller blades due to limited allowable propeller diameter. The energy for those engines comes partly from JET-A fuel and partly from Zn-Air batteries. The advantage of Zn-Air is the relatively high specific energy and energy density. Disadvantages are the charging time and life cycle of the battery. If demand rises and research is intensified these challenges can be mitigated. Battery swapping is preferred above battery charging, because charging takes more than 6 hours. Swapping reduces the turn around time making it possible to make more trips in comparison with Q300, which is cost efficient.

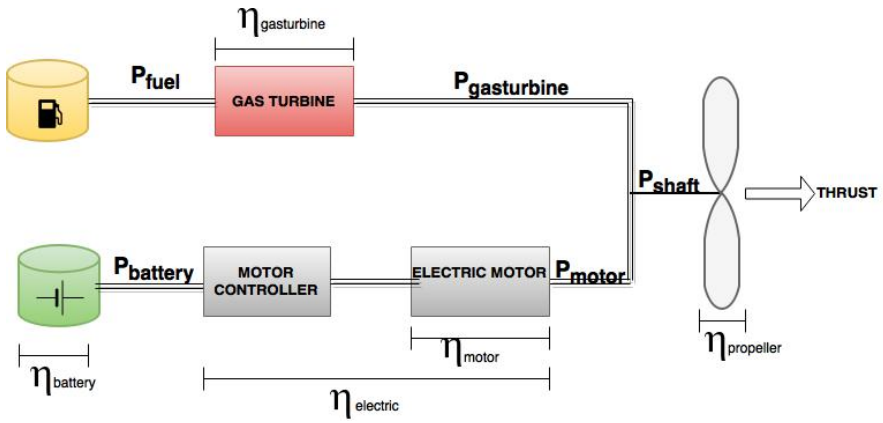

Figure 4: Architecture of a parallel turbo-electric configuration

It is found that the main drag reduction of the aircraft comes from the use of wingtip propellers and the smaller surface area, due to the fact that the wing can be sized for cruise conditions. The wingtip propellers reduce the induced drag by almost 35%, whereas the reduction in area of more than 30%, lowers the total drag by almost 30%. This reduction in drag leads to a improvement of the flight performance of the aircraft, as the power required reduces. The mass of the main wing is 2040 kg, which is slightly higher than the wing weight of similar aircraft. The fuselage mass is estimated to be 1528 kg, which is similar to reference values. Al-7050 and Al-2024 are the chosen materials for the wing structure. Al-7050 is chosen for its high strength, whereas Al-2024 for its favourable fatigue resistance.

The optimal cruising height for the E-gle is found to be 5000 m. This is because, for short distances, the benefit of lower drag at a high altitude does not outweigh the penalty of the extra energy and time needed to reach that altitude during the climb phase. This effect can already be observed at the maximum range design for (500 NM) and will thus be more profound at shorter range, which is what the aircraft will be most used at. Due to the aforementioned drag reduction, the E-gle is found to be much more fuel efficient than the Q300. For the same range of 500 NM the Q300 burned 1159 kg of fuel, whereas the E-gle only burns 320 kg of fuel. The battery mass for this mission is 5804 kg. Furthermore, an optimal efficiency is reached at a number of engines for which the cruise flight could be flown purely on electrical power. The design is highly sensitive to the specific energy of the battery. In Figure 5 can be seen how the specific energy influences the design. A battery specific energy lower than 400 Wh/kg will make the aircraft too heavy to meet the weight requirement of the E-gle.

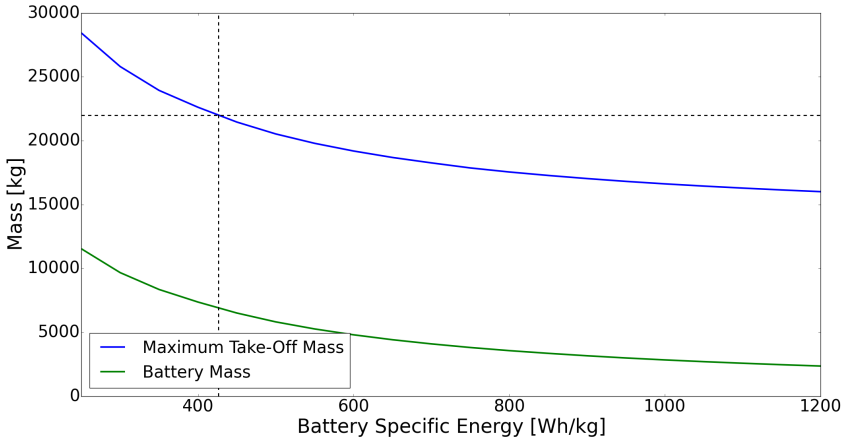

Figure 5: Maximum take-off mass and battery mass as a function of the battery specific energy

The noise does not meet the requirement stated in the project, but the noise level was 13.7 dB lower than the cumulative noise of the JAR-36 requirements and lower in all categories compared to the Bombardier Q300. The emission requirement is easily met with a total direct emission reduction of 72.4%, as can be seen in Table 2. If the emission of the production of the electrical energy is taken into account, the emission reduction reduces to 64.5%.

Table 2: Comparison of emissions between E-gle and Bombardier Q300

		E-gle [kg]	**Bombardier Q300 [kg]**
Fuel required over 500NM range		320	1159
Emissions	Emission index (EI) [g/kg]		
CO_2	3149	1007.68	3649.69
H_2O	1230	393.6	1425.57
SO_x	0.84	0.268	0.973
CO	4.875	1.56	5.65
NO_x	23.1077	7.394	26.781
HC	1.5637	0.500	1.812
Total emissions		**1411.002**	**5110.477**
Difference		**-72.39%**	

E-gle, being a new and innovative concept using futuristic technologies, is prone to quite a few risks. These risks must first be identified then, carefully assessed and analysed and finally, handled and mitigated to reduce their likelihood and consequence. One of the most important risks is a potentially low battery specific energy in the year 2025 as this will increase the weight quite drastically. Another important risk is power distribution and electric motor control failure. This increases the chance of fire during flight and a total failure of the system will make it very hard to land as the aircraft is dependent on the extra dynamic pressure on the wing created by the high-lift propellers. Finally, there is still an uncertainty in the required strength and stiffness of the wing, which can increase weight.

The market analysis states that busiest flight routes can be covered with a 500 NM range aircraft. According to the financial analysis the direct operating cost of the E-gle can be reduced with 32% compared to the Q300 making it financially more attractive than its competitors. However, the acquisition cost of the aircraft is 10% higher. This is mainly due to a major increase in the amount of electrical engines increasing the complexity of the system and thus increasing costs. An overview of the most important design parameters can be seen in Table 3.

Table 3: Aircraft Characteristics of the E-gle

Parameter	**Value**	**Unit**	**Parameter**	**Value**	**Unit**
Passengers	50	-	Aspect Ratio	15	-
Cruise Height	5000	m	DEP Engines	20 x 100	kW
Cruise Velocity	500	km/h	Electrical Engines	4 x 260	kW
Range	500	NM	Gas Turbine	2 x 1200	kW
MTOW	20446	kg	Take-Off Field Length	1090	m
OEW	8909	kg	Landing Field Length	1190	m
BW	5804	kg	Stall Velocity Sea Level	46.0	m/s
MFW	1288	kg	RD&T and Production Cost	16.1 million	USD
MPW	5000	kg	Direct Operating Costs	4.8 million	USD/year
Surface Area	39	m^2	Cumulative Certification Noise	86.1	dB
Wing Span	24.2	m	Direct Emission Reduction	72.4	%

Altogether, the E-gle, as shown in Figure 6, reduces emissions by having higher aerodynamic and propulsive efficiency, while reducing operating cost as well. In this way the E-gle contributes to a greener future in aviation in a financially attractive way.

Figure 6: Representation of the E-gle

List of Symbols

Roman Symbol	Description	Unit
a	Speed of sound	[m/s]
A	Area	[m^2]
	Aspect ratio	[-]
	Shear area	[m^2]
A_3	Area at parallel flow behind propeller	[m^2]
b	Wing span	[m]
B	Number of blades per propeller	[-]
b_{blown}	Blown span by DEP	[-]
c	Chord	[m]
$\bar{c}$	Average chord length	[m]
c_p	Power coefficient	[J/kgV^2]
C_{av}	Avionics cost	[USD]
C_D	Development support cost	[USD]
	Drag Coefficient	[-]
C_{D_0}	Zero-lift drag coefficient	[-]
C_{D_i}	Lift-induced drag Coefficient	[-]
C_{eng}	Engine production cost	[USD]
C_f	Skin friction coefficient	[-]
C_F	Flight test cost	[USD]
C_{int}	Interior cost	[USD]
C_l	Two-dimensional lift coefficient	[-]
C_L	Lift coefficient	[-]
$C_{L_{infty}}$	Lift coefficient free stream velocity	[-]
C_{L_α}	Lift slope	[rad^{-1}]
$C_{L_{\alpha_h}}$	Lift slope horizontal wing	[rad^{-1}]
$C_{L_{\alpha_{A-h}}}$	Lift slope main wing	[rad^{-1}]
C_M	Manufacturing material cost	[USD]
$C_{m_{ac}}$	Moment coefficient around ac	[-]
c_p	Specific fuel consumption	[kg/J]
$C_{P,B}$	Blade loading coefficient	[-]
cr	Climb rate	[m/s]
c_r	Root chord	[m]
C_{sp}	Spare parts cost	[USD]
c_t	Tip chord	[m]
D	Diameter	[m]
	Drag	[N]
D_i	Induced drag	[N]
e_0	Oswald efficiency	[-]
E	Energy	[Wh]
	Endurance	[s]
E_s	Specific energy	[Wh/kg]
f	Weight fraction	[-]
	Fuselage diameter	[m]
	Frequency	[s^{-1}]
F	Power factor	[-]
	Tip loss factor	[-]
	Force	[N]
f_{total}	Product of all fuel fractions	[-]
f_{max}	Frequency at which SPL is maximum	[s^{-1}]
FF	Form factor	[-]
g	Gravitational constant	[m/s^2]
H_E	Engine hours	[h]
H_{LG}	Landing gear height	[m]
H_M	Manufacturing hours	[h]
H_Q	Quality control hours	[h]
H_T	Tooling hours	[h]
H_{test}	Flyover height	[m]
h_{scr}	Screen height	[m]

Roman Symbol	Description	Unit
I	Area moment of inertia	[m^4]
	Sound intensity	[W/m^2]
i_p	Angle V_p with chord	[deg]
i_w	Wing incidence angle of attack	[deg]
J	Advance ratio	[-]
	Bessel function 1st order, 1st kind	[-]
k	Induced drag reduction factor	[-]
K_s	Torsional spring stiffness	[N/m]
$l_\parallel$	Eddy lengthscale	[m]
$l_\perp$	Eddy lengthscale	[m]
l_h	Arm length horizontal tail	[m]
L	Lift	[N]
L_{hub}	Length propeller hub	[m]
m	Harmonic	[-]
M	Mach number	[-]
	Moment	[Nm]
	Mass	[kg]
M_H	Helical blade tip mach number	[-]
M_t	Blade tip mach number	[-]
m	Aircraft mass	[kg]
n	Revolutions per second	[s^{-1}]
	Noy adjusted SPL	[dB]
N	Revolutions per minute	[min^{-1}]
	Number of wheels	[-]
ND	Noise factor for high lift devices	[-]
N_B	Number of blades	[-]
n_e	Integration benefit factor	[-]
n_{prop}	Number of propellers	[-]
N_{St}	Strouhal number	[-]
P	Power	[W]
	Static load	[N]
	Length potential core	[m]
	Pressure	[N/m^2]
P_a	Power available	[W]
P_{br}	Shaft power	[W]
P_D	Pitch distance	[m]
P_r	Power required	[W]
P_s	Power setting	[-]
p	Pressure	[Pa]
p_i	Points i-th criterion trade-off	[-]
q	Dynamic pressure	[N/m^2]
	Shear flow	[N/m]
	Source distribution	[m^7/s^3]
Q	Torque	[Nm]
	Interference factor	[-]
r	Distance from sound source	[m]
	Bladestation	[m]
r_e	Retarded radius	[m]
R	Range	[m]
R_e	Reynolds number	[-]
R_E	Wrap rate engineering	[USD/h]
R_M	Wrap rate manufacturing	[USD/h]
R_Q	Wrap rate quality control	[USD/h]
R_{ref}	Reference propeller radius	[m]
R_T	Wrap rate tooling	[USD/h]

Roman Symbol	Description	Unit
S	Surface area	[m^2]
S_e	Nozzle exit area	[m^2]
S_f	Flaps surface area	[m^2]
s_{land}	Runway length	[m]
S_{ref}	Reference area	[m^2]
s_{TO}	Take-off distance	[m]
S_{wet}	Wetted area	[m^2]
S_h	Horizontal surface area	[m^2]
St	Strouhal number jet	[-]
t	Thickness	[m]
T	Thrust	[N]
	Torque	[Nm]
T_c	Superconducting transition temperature	[K]
t	Thickness	[m]
t/c	Thickness over chord ratio	[-]
u	Upsweep angle	[rad]
U	Rotational velocity	[m/s]
U_C	Eddy convection velocity	[m/s]
V	Velocity	[m/s]
V_2	Take-off safety speed	[m/s]
V_3	Velocity at parallel flow behind propeller	[m/s]
V_A	Approach velocity	[m/s]
V_e	Exhaust velocity	[m/s]
V_h	Freemstream velocity horizontal tail	[m/s]
V_T	Touchdown velocity	[m/s]
V_{TO}	Take-off velocity	[m/s]
V_{ep}	Effective velocity behind propellers	[m/s]
V_p	Propeller slipstream velocity	[m/s]
V_{land}	Landing velocity	[m/s]
V_{LOF}	Velocity at lift-off	[m/s]
V_{req}	Required velocity	[m/s]
V_{scr}	Velocity at screen height	[m/s]
V_{stall}	Stall velocity	[m/s]
V_∞	Landing velocity	[m/s]
	Freestream velocity	[m/s]
ΔV	Induced velocity	[m/s]
W	Weight	[N]
	Width exhaust	[m]
W_b	Weight before cruise	[N]
W_e	Weight at end of cruise	[N]
w_i	Weight i-th criterion trade-off	[kg]
x/c	Maximum chamber location	[-]
x_{ac}	x-location of aerodynamic centre	[m]
y_1	Distance behind jet exhaust	[m]

Greek Symbol	Description	Unit
α	Angle of attack	[rad]
α_s	Stall angle of attack	[rad]
α_g	Geometric angle of attack	[rad]
β	Pitch angle	[rad]
	Prandtl-Gauert compressibility correction factor	[-]
δ	Turbulent boundary layer thickness	[m]
δ_f	Flap deflection angle	[rad]
η	Airfoil efficiency factor	[-]
η_c	Efficiency	[-]
η_p	Propeller efficiency	[-]
$\frac{d\epsilon}{d\alpha}$	Downwash	[-]
θ	Azimuth angle	[rad]
θ_e	Retarded radiation angle	[rad]
θ_p	Propeller folding angle	[rad]
λ	Taper ratio	[-]
Λ	Sweep angle	[deg]
μ	Dynamic viscosity	[Pa/s]
ρ	Air density	[kg/m^3]
ρ_0	Air density at sea level	[kg/m^3]
ρ_e	Nozzle exit density	[kg/m^3]
σ	Density ratio	[-]
	Normal stress	[N/m^2]
τ	Shear stress	[N/m^2]
τ_s	Turbulent eddy lifetime	[s]
ϕ	Vertical plane directional angle	[rad]
	Helix angle	[rad]
ψ_L	Noncompactness factor	[-]
ω	Density exponent	[-]
	Rotational speed	[rad/s]
$\tilde{\omega}$	Frequency adjusted for Re and V	[-]

Abbreviation	Description
AC	Alternating current
ACARS	Aircraft Communications Addressing and Reporting System
ADS-B	Automatic Dependent Surveillance-Broadcast
ALT	Alternator Master
BAT	Battery Master
BMS	Battery Management System
BSFC	Brake Specific Fuel Consumption
BW	Battery Weight
CAS	Calibrated Airspeed
CFD	Computational Fluid Dynamics
CFRP	Carbon Fibre Reinforced Polymers
CG	Centre of Gravity
DC	Direct Current
DDL	Design Development Logic
DOC	Direct Operational Cost
DEP	Distributed Electric Propulsion
DR	Driving Requirements
DSE	Design Synthesis Exercise
FBD	Functional Breakdown Diagram
FFD	Functional Flow Diagram
GDP	Gross Domestic Product
GPS	Global Positioning System
GPU	Ground Power Unit
GR	Gear Ratio
GSP	Gas Turbine Simulation Program
HLP	High-lift Propellers
HTS	High Temperature Superconductor
HW	Hardware
KR	Key Requirements
LCC	Life Cycle Cost
LP	Low Pressure
MAC	Mean Aerodynamic Chord
MTOM	Maximum Take-off Mass
MTOW	Maximum Take-off Weight
MFW	Maximum Fuel Weight
MPW	Maximum Payload Weight
OEM	Operational Empty Mass
OEW	Operational Empty Weight
OBS	Organisational Break-down Structure
PDS	Power Distribution System
PEM	Proton Exchange Membrane
PL	Payload
RAMS	Reliability, Availability, Maintainability and Safety
RC	Rate of Climb
RD	Research and Development
RDT	Requirements Discovery Tree
RPM	Revolutions per Minute
SHF	Single Super high Frequency
SOFC	Solid Oxide Fuel Cell
SOFC-GT	Solid Oxide Fuel Cell Gas Turbine
SPL	Sound Pressure Level
SW	Software
TAS	True Air Speed
TO	Take-off
TOP	Take-off Parameter
TPM	Technical Performance Management
TRL	Technology Readiness Level
TSFC	Thrust Specific Fuel Consumption
VHF	Very High Frequency
WBS	Work Breakdown Structure
WFD	Work Flow Diagram

CONTENTS

1

INTRODUCTION

Over the past century, the consumption of fossil fuels in means of transportation has increased exponentially. Although they have many benefits, these types of fuel lead to the emission of large quantities of greenhouse gasses, such as carbon dioxide and nitric oxides. This leads to changes to the climate such as elevated sea levels and increased sea and air temperatures, negatively impacting and possible threatening life on earth. It is therefore of paramount importance that use is made of cleaner, renewable energy sources such as solar or wind energy. Although other transportation industries such as the automotive and railway industry are shifting towards the use of renewable fuels, the aircraft industry still largely relies on kerosene. This leads to the following need present in the world of aviation: *In order to meet the environmental goals of NASA N+3 and Flightpath 2050, there is a need to design aircraft that efficiently use alternate cleaner energy sources over conventional propulsion techniques*.

Recent studies suggest that the use of electric propulsion can lead to an increase in propulsive efficiency, while also providing benefits in term of flight performance [1, 2]. These designs make use of distributed electric propulsion (DEP), which means that small propellers are distributed along the wing in order to provide extra lift during landing and take-off, with the propulsive propellers being placed on the tips of the wing. The benefits of this configuration can be mainly attributed to three factors. First of all, as the high lift propellers increase the dynamic pressure over the wing during landing and take-off, these phases are no longer critical to the design of the wing. This means that the wing can be sized for cruise, reducing the surface area and enabling the aircraft to fly at higher lift coefficients. Secondly, the wingtip propellers lead to a large decrease in induced drag, leading to less power required, improving the aircraft's flight performance. Finally, electric motors, used to convert the energy from the batteries, are up to three times as efficient compared to combustion engines which leads to a reduction in energy consumption. These benefits can lead to a hybrid or electric aircraft, fulfilling the needs previously described. Therefore, the purpose of this report is: *Design a regional passenger transport aircraft with a range of at least 500 Nautical Miles (NM), that makes use of Distributed Electric Propulsion technology to produce thrust and is operational in 2030; with a group of 10 students within a duration of 10 weeks*.

The report is structured such that it represents the functional flow of work throughout the different phases of the design of the aircraft, named the E-gle. First of all, a market analysis is performed in Chapter 2 in order to get an indication of what the main needs and competitors are for the E-gle. Next, in Chapter 3 the mission is analysed, leading to a set of requirements for different phases of the aircraft's use. Following from this, Chapter 4 describes the resource budget for the various subsystems as well as visualising how they interact. Next, analyses are performed for various subsystems of the aircraft, in order to optimise the design. These can be found in Chapter 5 through Chapter 10. Furthermore, it describes the operations, logistics, maintenance and production of the aircraft. Now that the design and all the aspects accompanying it are determined, a final design evaluation is performed in Chapter 13. This concerns aspect such as performing a sensitivity analysis, assessing the risks of the design, analysing its total cost, developing a sustainable development strategy and checking the RAMS (Reliability, Availability, Maintainability and Safety) characteristics. This chapter also includes the compliance matrix, giving an overview of which previously set requirements have been met and in which section a justification can be found. To conclude the report, Chapter 14 provides an overview of the further design and production phases and Chapter 15 gives a final overview of design.

2

Market Analysis

This chapter contains the market analysis. First, the aircraft market forecast is discussed, after which the market for the product being designed, the E-gle, is looked into. This study is based on the market predictions of three large aviation companies: Airbus [3] , Boeing [4] and Bombardier [5]. To begin with, the market demand for aircraft in general is explained in Section 2.1. Next, the important stakeholders that are involved in the mission are analysed in Section 2.2. Following, Section 2.3 presents the competition that currently exists and how its affects the market for E-gle. Finally, the position of the market is explained in Section 2.4. Details on cost analysis and return on investment can be found in Section 13.3.

2.1. Market Demand

The demand for aircraft is expanding at an alarming rate the last couple of decades. The number of passenger and cargo aircraft is increasing with a rate of 4.5% per year. This will lead to a total market in 2030 of around 31,000 aircraft and 37,700 aircraft in 2035. This growth is estimated by analysing the GDP of the largest countries (G7) and by taking into account age, tourism and urbanisation [3]. The increase in market will keep on growing for the next 30 years and beyond. The predicted number of aircraft by Boeing is presented in Figure 2.1.

Region	Asia	North America	Europe	Middle East	Latin America	C.I.S.	Africa	World
2015 Fleet								
Large Widebody	270	100	170	140	-	50	10	740
Medium Widebody	540	320	360	320	20	20	60	1,640
Small Widebody	860	750	440	250	140	140	80	2,660
Single Aisle	4,540	4,010	3,370	590	1,280	650	430	14,870
Regional Jets	140	1,730	270	70	110	170	110	2,600
Total	6,350	6,910	4,610	1,370	1,550	1,030	690	22,510
2035 Fleet								
Large Wide-body	70	60	100	320	-	50	-	700
Medium Wide-body	1,590	460	610	840	40	70	80	3,690
Small Wide-body	2,340	1,150	1,140	610	350	170	300	6,060
Single Aisle	12,560	6,630	5,920	1,660	3,110	1,380	1,020	32,280
Regional Jets	310	1,520	150	80	160	230	60	2,510
Total	16,970	9,820	7,920	3,510	3,660	1,900	1,460	45,240

Figure 2.1: Boeing Market Forecast [4]

The largest growth of the market is present in the Asia, the Middle East and South America. This has to do with their economy which is increasing rapidly, especially the middle-class. Some drops in aircraft market growth are present due to financial crises or wars, but after these crises the market stabilises. In 2009, there was a large decrease in GDP, as well as in the number of aircraft orders, due to the economic crisis. Afterwards, the orders went up again, due to the fact that air travel became more frequent and hence, had a large demand.

2.2. STAKEHOLDERS

The E-gle has a lot of different persons, groups and companies involved in its use and design. These are referred to as stakeholders, an overview of the main ones is presented in Figure 2.2. In the middle of the diagram the E-gle itself is located. Next to it, the other main groups of stakeholders are presented, which are split into separate stakeholders. These stakeholders should all be taken into account to acquire a strong market position and a good and safe aircraft.

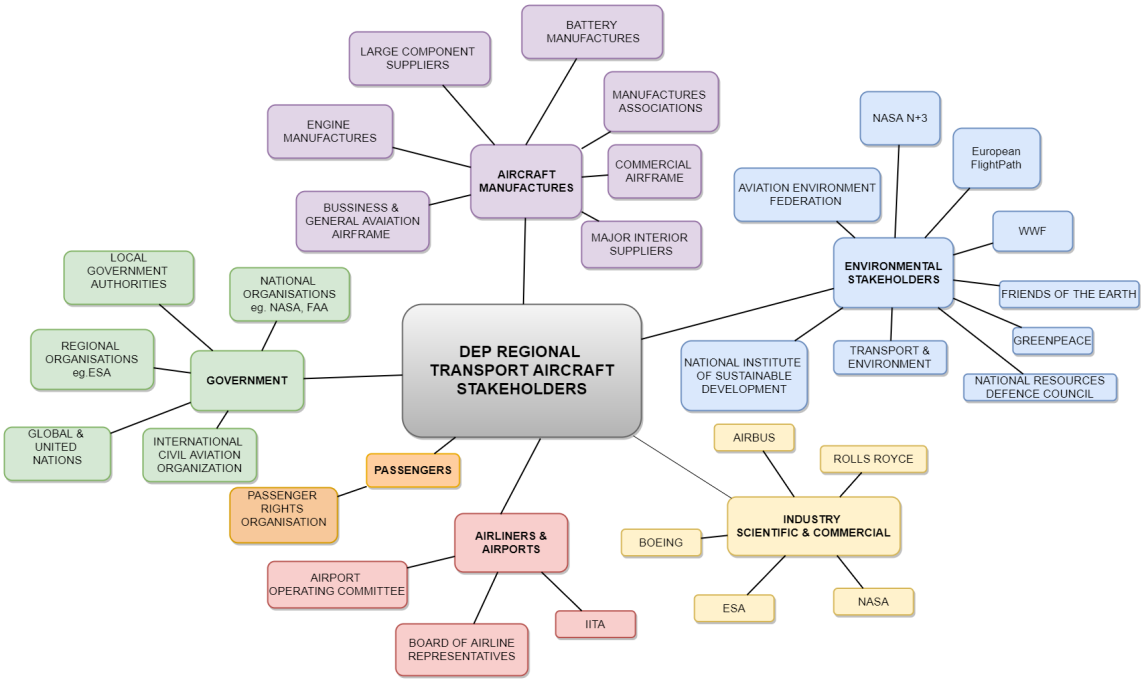

Figure 2.2: E-gle stakeholders

2.3. COMPETITION

For the E-gle to be successful, there is the need to replace the current turboprop Bombardier Q300 by 2030. This is a 50 passenger aircraft with a range of 924 NM.

From Table 2.1, it can be concluded that the acquisition cost of a similar aircraft should be around $17 million. If the aircraft is more expensive, it needs to be lower in fuel cost or maintenance cost than the other conventional aircraft to be a desirable option. For the E-gle, an acquisition cost of $18.7 million is expected, which is a 10% increase, with respect to the Q300. However, the direct operational costs of the E-gle are expected to be 26.2% lower than that of the Q300. This means that, despite the higher acquisition cost, the aircraft is still beneficial to operate for airlines. The reasoning behind the values for the acquisitions cost and the direct operational costs can be found in Section 13.3.

Table 2.1: Important parameters of comparable aircraft missions

Aircraft Model	No. of passengers	MTOW [kg]	Range [NM]	Max Cruise Speed [kts]	Acquisiton Cost [$ million]	Fuel Cost [¢ per seat per NM]
Bombardier Q300 [6]	50	19,505	924	285	17	10.84
Fokker 50 [7]	46	20,820	1110	286	17.5	15.95
Embraer ERJ 140 [8]	44	20,099	1250	-	17	14.83
ATR 42-500 [9]	48	18,600	716	300	12.1	25.94
Tupolev Tu-124 [10]	45	38,000	658	405	16	-

In terms of competition, several companies are working on electrical and DEP aircraft. For example Airbus, NASA, Uber, Siemens and Pipistrel. These companies should be checked on a regular basis to see how their market position is and on what topics they work. With these companies can also be cooperated to increase the quality of the product and prevent mistakes.

2.4. MARKET POSITION

To make an evaluation of the where the aircraft stand in the market, an estimation of the price, as from Section 13.3, is required. It is concluded that, in order keep the acquisition cost of a single aircraft sufficiently low, the number of aircraft produced needs to be at least 281. Moreover, the direct operational cost are discussed in Subsection 13.3.2. This will result in a market share of 10% of the total regional jets market of 2030-2035. The number of Q300 sold is 263 [11]. The required sold aircraft is therefore not an easy task to be done. This requires good advertisement to sell all the aircraft while still maintaining the cost requirements. However this aircraft will have a lower DOC as specified in Subsection 13.3.2. This will reduce the cost of the aircraft over its lifetime significantly.

The range of the E-gle is also specialised in the range of 500 NM, which makes it more efficient on these ranges. Besides, the busiest air routes are also in this range. Finally the turn around time decreases, due to the swapping battery mechanism.

It is important to note that E-gle is a unique aircraft in the market. This opens different markets and opportunities for investors. Governments and companies can greatly influence the success of the E-gle. Special regulations might be taken due to its low noise, described in Section 12.2. This opens new possibilities to fly for example in different time slots or at different airport locations. The operation cost of the E-gle might even be more interesting when oil prices increase significantly due to crises, oil shortage or global warming. To advertise this, a lot of lobbying should be done with different companies and investors. A strong business plan needs to be established to cover the cost of production and design. This plan needs to cover all the financial aspect of the aircraft production. An overview of a general business plan can be seen in Figure 2.3.

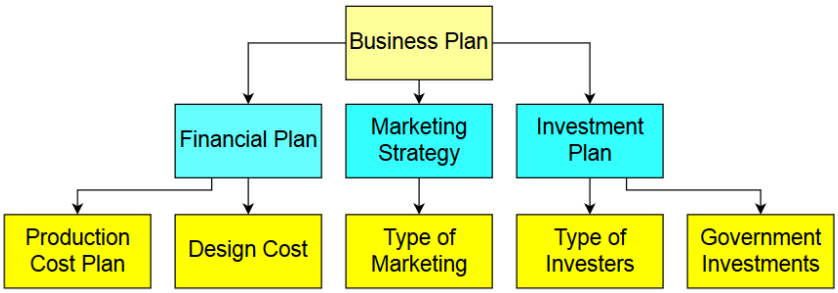

Figure 2.3: Overview of a business for the E-gle

3

Mission Analysis

In order to design an aircraft that best suits the requirements, constraints, needs and objectives; a mission analysis of E-gle's mission is performed. First, the mission profile of the aircraft is determined, based on the range requirements and regulations. Next, a functional analysis is performed by means of a functional flow diagram and a functional breakdown diagram, providing an overview of all different tasks the aircraft needs to perform. Based on this a set of requirements is set up and represented in the form of a requirement discovery tree.

3.1. Mission Profile

The mission profile gives an overview of the different phases the aircraft has to go through during a mission. Constructing the mission profile is the first step in determining the actions the aircraft needs to be able to perform. Figure 3.1 visualises this mission profile in which the different phases are indicated by a number. The mission can be split into two parts; the first part consists of phases 1 through 7, including 12 and makes up the normal flight procedure, the second part is the diversion flight procedure and consists of phases 8 through 11.

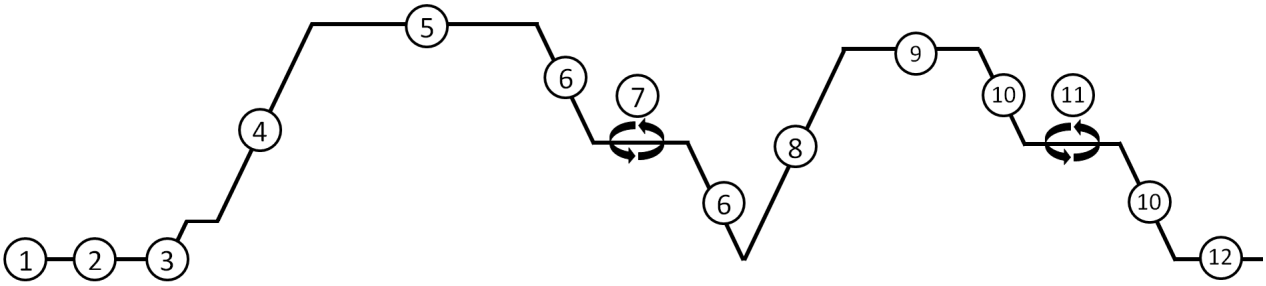

Figure 3.1: Mission profile diagram

The first phase of the normal flight procedure is starting up the engines (1). This phase is followed up by taxiing to the runway (2). After this the take-off phase (3) will be initiated. The next phase is the climbing phase (4) which is divided in 3 parts. First the aircraft climbs to an altitude of 1 km. At this altitude the aircraft will accelerate to a speed at which the rate of climb is maximum. Then the aircraft will continue its climb with a maximum rate of climb such that the cruise altitude will be reached in a minimum amount of time. During cruise flight (5) the aircraft will travel a large part of the total range of 500 NM. Naturally at the end of the cruise phase the aircraft will start descending (6). In the mission profile it is accounted for the possibility that the aircraft needs to wait before further descend. A loitering time of 5 min is an absolute minimum. In this design, a loitering time of 5% of the total mission time will be taken as a design value [12]. After loitering, the aircraft will descend and makes a landing attempt (7). The first phase of the diversion flight procedure is a new climb (8). Then the aircraft will travel to the nearest airport under cruise-like conditions (9). In the design of the aircraft a range of 100 NM has been chosen [12]. It should be noted that the flight range can be either increased, when nearby diversion options are available, or decreased if the diversion options are far away from the destination. Another option during this phase, is that the aircraft will loiter for 60 minutes [12]. After this phase the aircraft should still be able to loiter for 45 minutes above the alternative landing spot (11). Then the aircraft will initiate its second descend (10) and will attempt to land. In the last phase the aircraft will taxi and shut down its engines (12).

3.2. FUNCTIONAL ANALYSIS

In system engineering a functional analysis is done before the design is started, of which the results are presented in this section. First, the Functional Flow Diagram is shown and explained, after which the resulting Functional Breakdown is presented.

3.2.1. FUNCTIONAL FLOW DIAGRAM

To ensure all aspects of the process are thought of during the design phase, a Functional Flow Diagram (FFD) is created [13]. In a FFD all phases of the process of using the aircraft are shown in chronological order. Consecutive tasks are connected with arrows. In this project, some tasks have multiple predecessors with an AND function, meaning that both predecessors have to be completed before the next phase can begin. Some functions have a "GO/NO-GO" path depending on the outcome of the previous function. In the diagrams this is displayed with a "G" for functions that are completed successfully, "$\overline{G}$" shows the alternative path in case the task was unsuccessful. Alternative paths can also lead to different levels and are not always worked out at this stage. To ensure none of the phases are forgotten, an FFD consists of multiple levels. On level 1 the obvious phases (climb, cruise, etc) are mentioned. Next all phases are looked at in greater detail which results in a level 2 FFD for each phase. Following this, each sub-phase in level 2 is analysed again to create a level 3 FFD for each sub-phase. This process continues until all aspects and phases of the aircraft's lifetime have been analysed.

During the creation of the FFD's for this project, the same procedure is followed. However, since the allocated time for this project is limited, not all phases are worked out in great detail. The more general phases are kept at level 1, whereas phases that might differ from the traditional operational procedures are worked out to a second or third level.

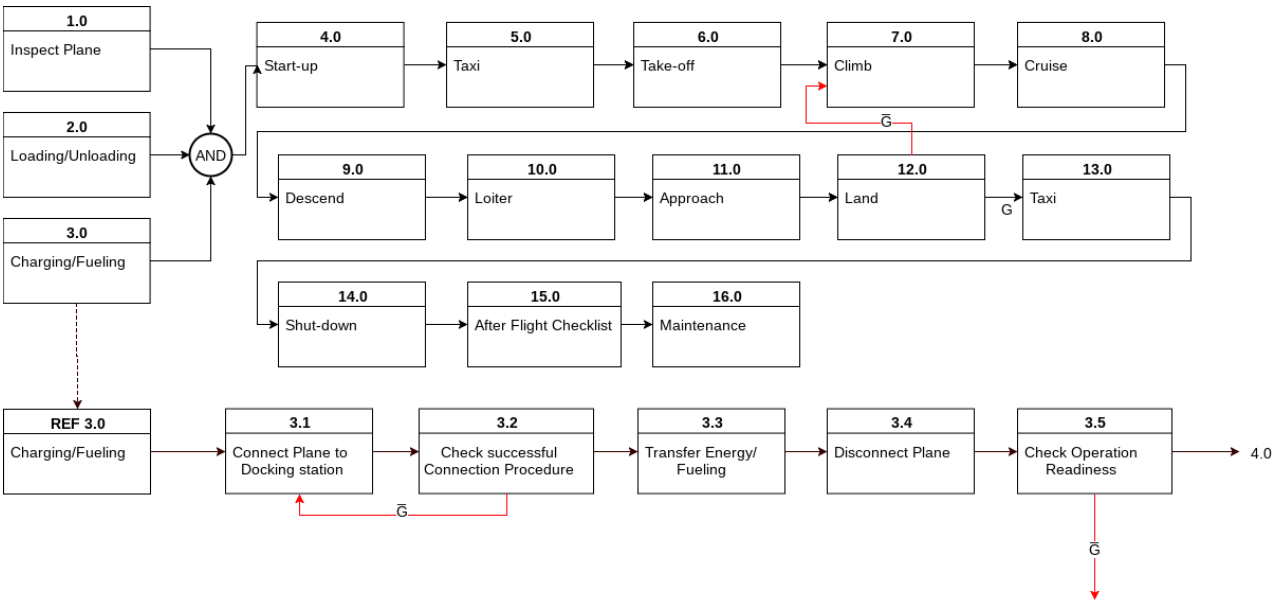

Figure 3.2: Level 1 Functional Flow Diagram of the operational cycle with Charging/Fueling phase explained up to level 2

In Figure 3.2 the FFD of the entire operational cycle is displayed at level 1 detail. Since "Charging/Fueling" is going to alter from traditional aircraft, this phase is worked out to level 2. Another phase that will be likely to change because the use of DEP is the take-off phase, therefore this phase is also worked out to level 2 with the critical sub-phases worked out to level 3. The results can be seen in Figure 3.3. Using DEP replaces complex conventional high lift devices which changes the take-off phase and procedures.

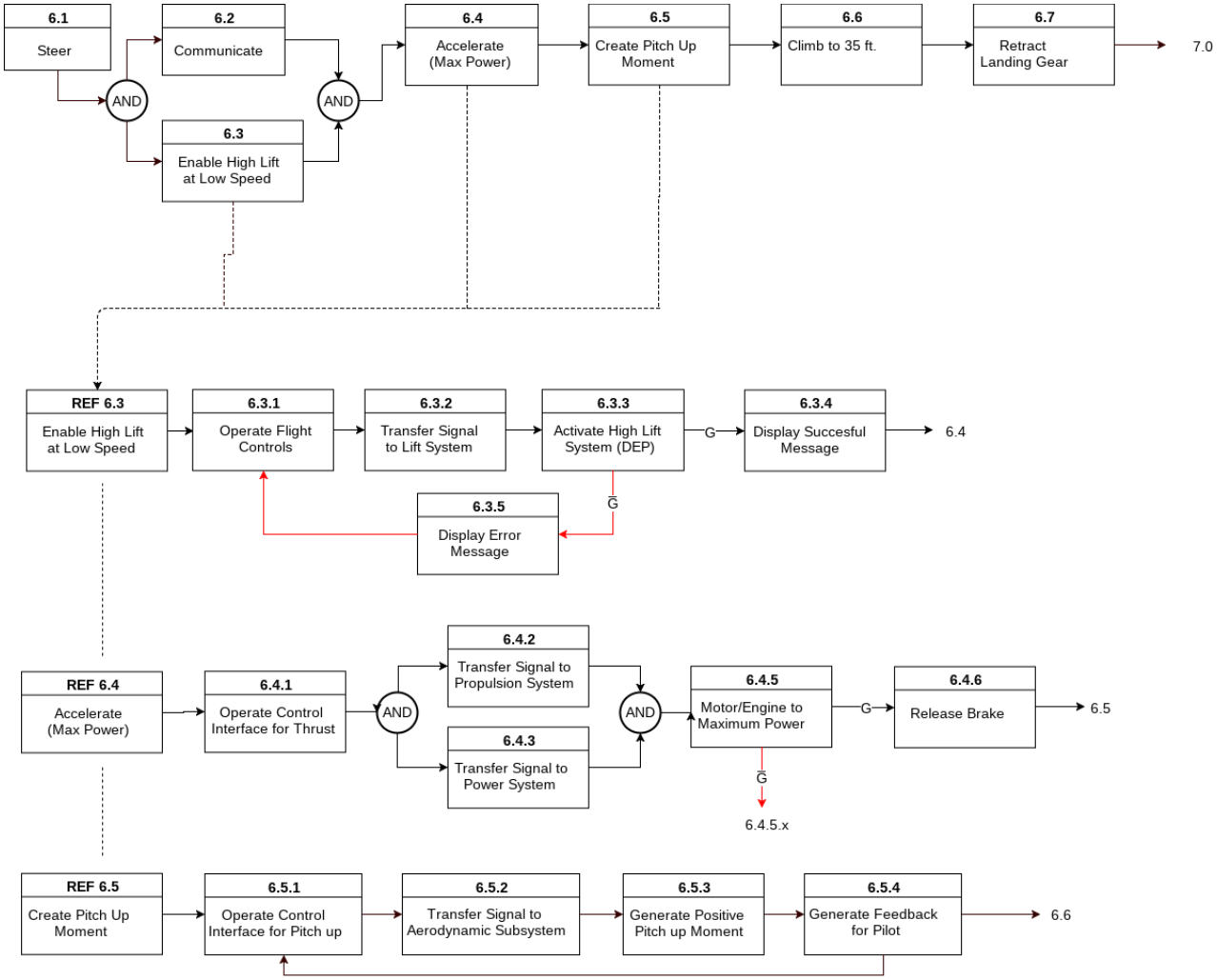

Figure 3.3: Functional Flow Diagram of the Take-off phase up to level 3

3.2.2. FUNCTIONAL BREAKDOWN

Before setting up all the requirements, a Functional Breakdown Diagram (FBD) is created in order to visualise the global functioning of the system. The FBD is an AND tree, which implies that all functions need to be achieved by the aircraft. Differing from the Functional Flow Diagram, the FBD shows all functions of the aircraft in a non-chronological order. This is done in order to group all functions in logical modules based on the type of function. Since this reduces the overall size of the diagram it is useful to get an overview of all the operations.

The Functional Breakdown Diagram of the entire aircraft is shown in Figure 3.4. This FBD is subdivided in three main categories: Perform Flight, Non-Flight and Passenger & Cargo Operations. The first category, Flight, consists of the functions the aircraft should be able to perform while flying. This includes all the phases from take-off to landing, taxiing is also included. Non-Flight operations are all operations that are required to keep the aircraft functional. This includes charging/fueling and maintenance. The last category includes all functions required for the payload.

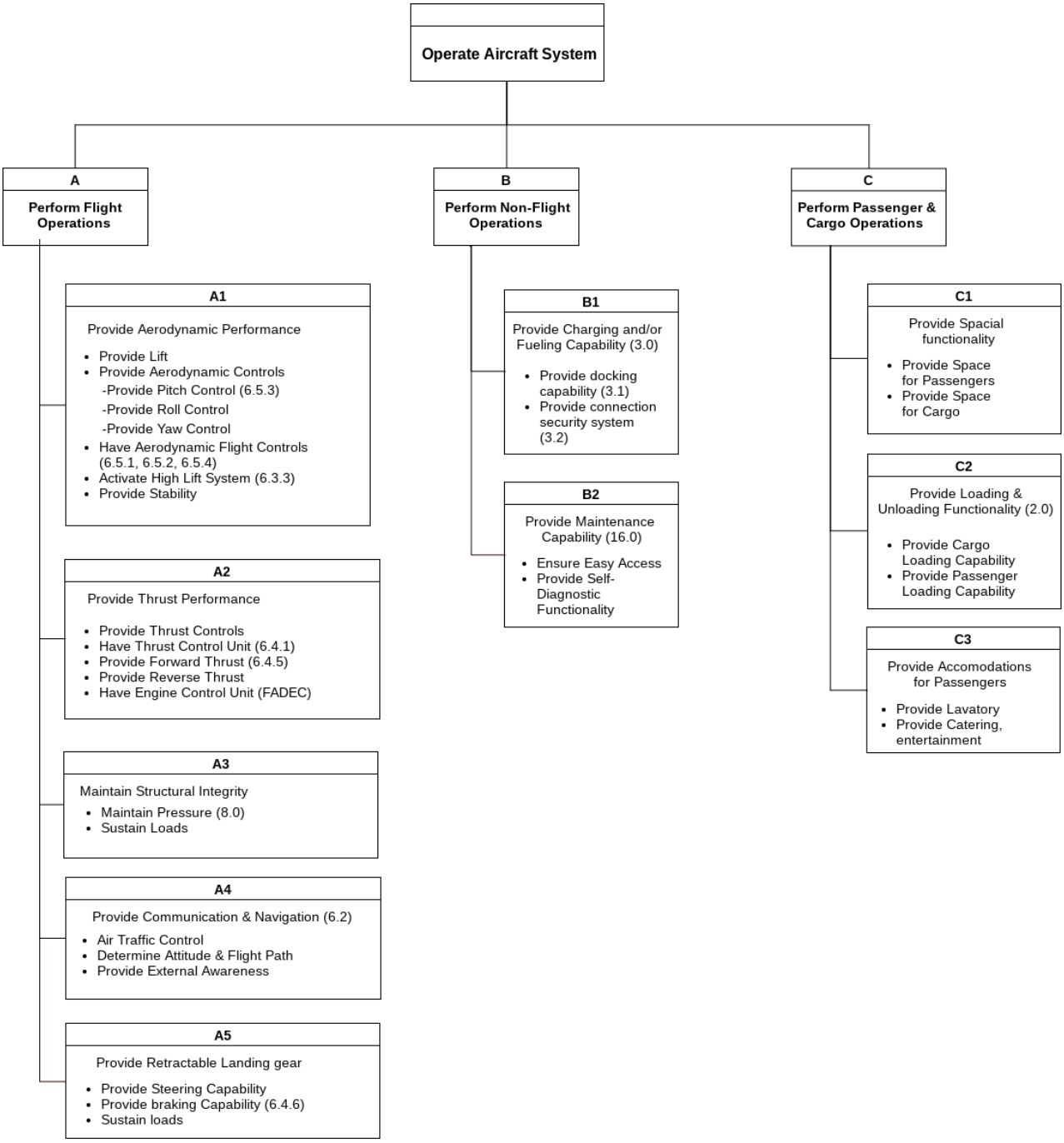

Figure 3.4: Functional Breakdown Diagram of the entire aircraft

3.3. REQUIREMENTS

In this section all the requirements that are also later expressed in the Requirements Discovery Tree (RDT) are listed in detail. The CS-25 requirements depend on the specific design decisions that are made, so no specific requirements from CS will be listed yet. First the constraints are listed in Subsection 3.3.1, after which the functional requirements are listed in Subsection 3.3.2. Moreover, key requirements and driver requirements are identified, key requirements are denoted by [KR] and driving requirements are denoted by [DR]. The requirements for the masses of various subsystems have been obtained from the mass budget estimation performed in Table 4.1

3.3.1. CONSTRAINTS

First, the constraints that the mission has to adhere to are looked at. These consist of cost, schedule and market.

Cost

CON-CST-01 [KR] The direct operating cost (DOC) shall be 25% lower than current regional aircraft.

CON-CST-02 [KR] The increase in purchase cost shall not be higher than 10% of the purchase cost of current regional aircraft.

Schedule

CON-SDL-01 The preliminary design shall be completed in ten weeks.

CON-SDL-02 The preliminary design shall be completed by ten designers.

Market

CON-MRK-01 [KR] The aircraft shall be market-ready by 2030.

3.3.2. TECHNICAL REQUIREMENTS

Next, all the technical requirements can be analysed. These are divided in Pre-Flight, In-Flight and subsystems.

Pre-Flight

Inspection

TEC-PRE-A01 Propellers shall be accessible for inspection.

Loading/Unloading

TEC-PRE-B01 The cargo holds shall be accessible via a cargo ramp.

TEC-PRE-B02 [KR] The aircraft shall have capacity for 50 passengers.

Charging/Fueling

TEC-PRE-C01 The aircraft shall be charged, from empty to full, within the turn around time of the Q300.

TEC-PRE-C02 The aircraft shall be fuelled, from empty to full as fast as the refuelling of the Q300.

TEC-PRE-C03 The charging and fuelling process shall pose no danger to anyone within or near the aircraft or charging equipment.

Maintenance

TEC-PST-B01 Routine maintenance items shall facilitate easy removal.

TEC-PST-B02 Hatches shall be placed in the wing and fuselage to allow for access and inspection.

Taxi

TEC-PRE-E01 The aircraft shall be sufficiently manoeuvrable to use general airport taxiways.

In-Flight

Take-off

TEC-INF-A01 [KR] The aircraft shall have a maximum take-off field length of 1200 m.

TEC-INF-A02 [DR] MTOW shall not exceed that of the Bombardier Q300 multiplied with a factor 1.1.

Climb

TEC-INF-B01 [DR] The aircraft shall have a climb rate as described in CS-25.119,121

Cruise

TEC-INF-C01 [KR] Range shall exceed 500 nautical miles with normal reserves.

TEC-INF-C02 [DR] Cruise speed shall be 500 km/h.

Landing

TEC-INF-D01 [KR] The aircraft shall have a maximum landing field length of 1100 m.

TEC-INF-D02 The landing gear shall be able to withstand a landing gear load of 2g.

Stability

TEC-INF-E01 [DR] The aircraft shall have stable eigenmodes.

TEC-INF-E02 The aircraft shall be stick-fixed stable.

TEC-INF-E03 The aircraft shall be stick-free stable.

Controllability

TEC-INF-E01 The aircraft shall have a turning performance as described in CS-25.

TEC-INF-E02 The aircraft shall be able to perform a cross wind landing procedure as described in CS-25.

TEC-INF-E03 The aircraft shall be able to have a take-off pitch rate as described in CS-25.

Subsystems

Power

TEC-SUB-A01 [DR] The design shall be made with a battery specific energy of 500 Wh/kg.

TEC-SUB-A02 The battery system shall have a casing that prevents fire from reaching other parts of the aircraft.

TEC-SUB-A03 [DR] The power subsystem shall stay within its mass budget of 6264 kg.

TEC-SUB-A04 Environmentally friendly disposal of the batteries shall be possible at end of life.

TEC-SUB-A05 The power subsystem shall be at least as safe as the power subsystem of Q300.

Structures

TEC-SUB-B01 [DR] No structure shall have plastic deformation below ultimate load.

TEC-SUB-B02 [DR] No (parts of a) structure shall fail below failure loads.

TEC-SUB-B03 Structures shall have sufficient stiffness to not limit operation of the aircraft due to operational forces.

TEC-SUB-B04 The structure shall be corrosion resistant.

TEC-SUB-B05 The structure shall be able to endure for 30 years.

TEC-SUB-B06 [DR] The structure shall stay within its mass budget of 4962 kg.

Propulsion

TEC-SUB-C01 [KR] DEP shall be used to provide thrust.

TEC-SUB-C02 [DR] The propulsion subsystem shall stay within its mass budget of 2196 kg.

TEC-SUB-C03 The propulsion subsystem shall adhere to CS-25E.

TEC-SUB-C04 [DR] The aircraft emissions shall be 50% lower compared to current conventional regional aircraft.

TEC-SUB-C05 [DR] The cumulative certification noise impact shall be 15 dB lower compared to current regional transport turboprop aircraft.

3.3.3. REQUIREMENT DISCOVERY TREE

All the requirements are structured in a Requirement Discovery Tree, as can be seen in Figure 3.5. In the requirement identifiers, the large boxes are indicated by a three letter code, the small boxes are indicated by a single letters and the individual requirements are indicated by numbers. The key requirements are indicated in bold and the driving requirements are underlined. The requirements are divided into technical requirements and constraints. The technical requirements can be further divided into pre-flight, in-flight and post-flight, which contain requirements for different subsystems. Requirements that have not been mentioned here are grouped in the remaining subsystems category.

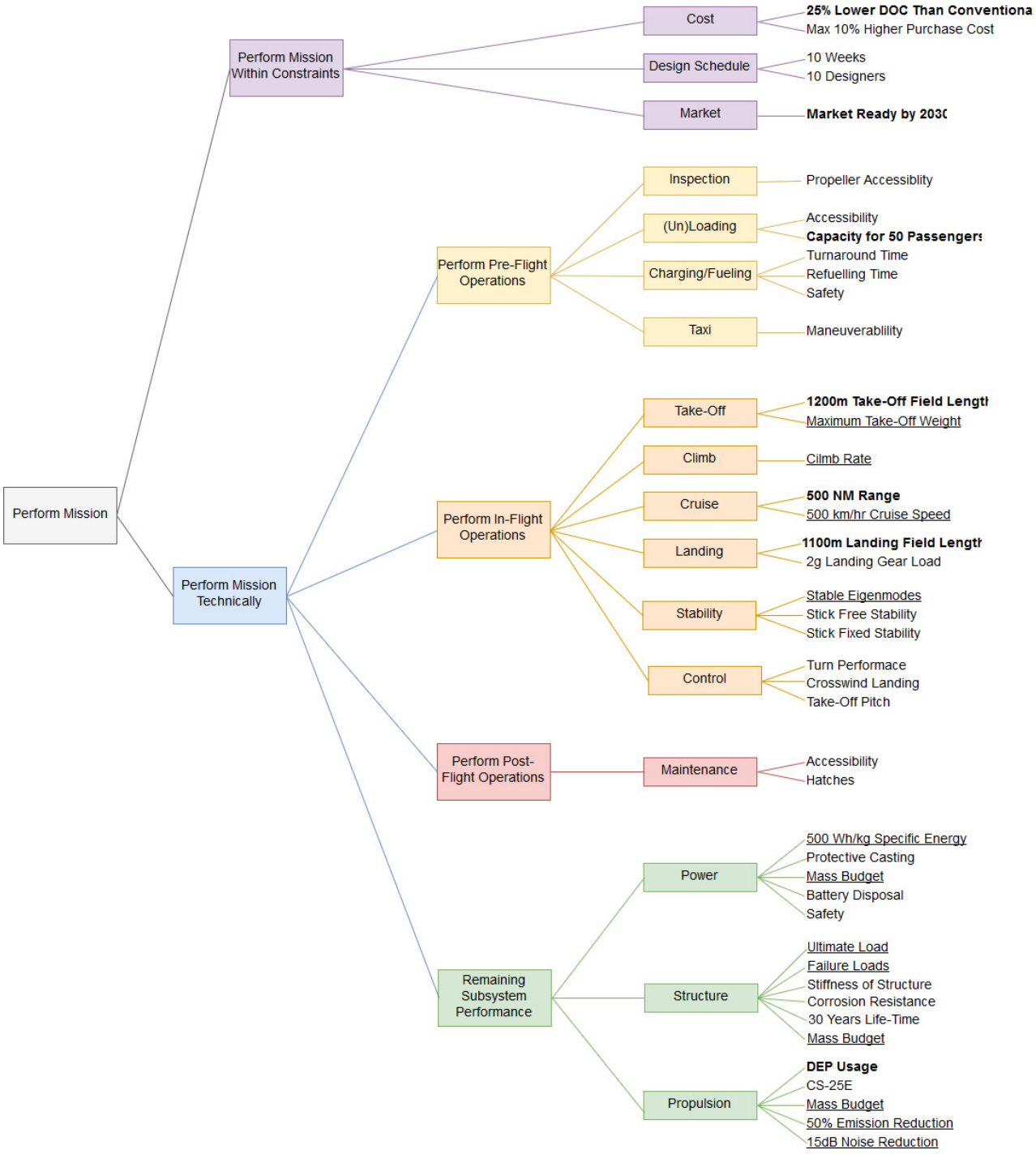

Figure 3.5: Requirement discovery tree

4

Subsystems Design

In this chapter, first an overview of the technical performance parameters is presented, including an indication of budget management, such as the mass budget. This is followed by various block diagrams (data handling diagram, hardware diagram, software diagram), giving an indication of how the various subsystems interact in terms of data and resources. Furthermore, a electric block diagram is presented, giving an indication of how the different parts of the electrical system are connected. Finally, a communication flow diagram is presented, to give an overview of the types of communication the aircraft will encounter during its lifetime and how it will handle them.

4.1. Technical Resource Budgets

Technical resource budgets are budgets that are set on the technical parameters of the design in order to ensure positive progress in the development of the project. Usually, the parameters considered here are the ones which have a large influence on the design and put limits to it. To ascertain whether the end product complies with the specified requirements, a tool named technical performance measurement (TPM) can be exploited. This method involves gathering information from statistical data of similar missions and then setting margins (or contingencies) to account for alterations in the design at later stages. Applying these contingencies at the initial stage of the design aids in achieving the specified performance at the time of product delivery. As the design matures, the contingency value tends to decrease and gradually reaches a null value. The following section first addresses the different parameters used through the design, after which the most important budgets determined at the beginning preliminary design are presented. Thereafter, the contingency throughout the different phases of the project are discussed. Finally, the budgets as they are right now are presented and an approach of how they will be managed in the future is discussed.

4.1.1. Technical Performance Parameters

There are some standard technical parameters that are considered when designing an aircraft. However, there are a couple of parameters specifically important for the design of the E-gle. First, the system efficiency is considered, which is defined as the energy effectively used during the flight compared to the energy stored on board for flight. This parameter gives an indication of the reduction in energy consumption due to integration benefits. Next, the internal spatial layout is taken into account, as the fuel tanks, landing gear, passengers, cargo and batteries all have to be fitted aboard the aircraft. The velocity increase needed from the DEP propellers during landing and take-off is also considered important for the design. As the aircraft uses new technologies, which might turn out to be expensive, the series production cost is also deemed important. Finally, the direct operating cost have to be monitored, as the aim is to decrease them compared to conventional regional turboprop. All the considered parameters can be seen below.

- Mass
- Power
- Range
- Computer capacity
- System efficiency
- Internal spatial layout
- Centre of gravity location
- Available engine power
- DEP velocity increase
- Series production cost
- Direct operating cost
- Production time
- Reliability
- Availability
- Maintainability

In addition to the above-mentioned technical parameters some other parameters are important to the design of the E-gle. Although these are not technical performance parameters, they are of importance and have to be monitored closely throughout the design. First of these is the specific energy of the batteries, as this has a significant impact on the design. Next is the aircraft's noise, as it is required to reduce this by 15 dB. Finally, the emissions are important, as it is required to reduce the overall emission of the aircraft by 50 percent.

For some of the aforementioned parameters, a budget can be made, in order to give an indication of which subsystem use what amount of a certain resource. Most importantly, this can be done for both the total mass of each of the aircraft's main components. First, an original mass budget constructed using a statistical method based on reference data [14], which was adapted to the expected changes due to the use of both DEP and new materials. This updated mass budget serves as the initial mass budget for the design of the E-gle and can be seen in Table 4.1. The mass budget aims for the design to be 18330 kg, being the requirement on the MTOW, including a 20% contingency.

Table 4.1: Initial mass budget of the E-gle

Component	**Mass** [kg]	**Updated Mass** [kg]	**Mass Change** [%]	**Component to Total Mass** [%]
Wing	2015	1510	-25	8.2
Tail	515	385	-25	2.1
Body	2000	1600	-20	8.7
Landing Gear	730	640	-12	3.5
Flight Controls	315	220	-30	1.2
Propulsion	1830	1830	0	10
Auxiliary Power	110	0	-100	0
Furnishing	1385	830	-40	4.5
Crew	280	280	0	1.5
Other Subsystems	1165	1165	0	6.4
Empty Mass	10345	8460	-18	46.1
Payload Mass	4650	4650	0	26.9
Energy Mass	3335	5220	57	28.5
Total Mass	18330	18330	0	100

4.1.2. CONTINGENCY MANAGEMENT

Aerospace designs tend to increase in mass during the design phase. Therefore, it is important to have a proper contingency management. Normally, the contingency decreases with design maturity. In Table 4.2 an overview is given of the contingencies for the technical performance parameters chosen in Subsection 4.1.1.

In the conceptual phase the contingencies of all the TPM are still rather high. This is because at this stage there is variety of concepts and the analysis on those concepts is not very extensive. In the preliminary phase only one concept is left on which a more detailed analysis can be done. This reduces the required contingency. During the next phase the concept will be worked out into detail. Therefore, again a lower contingency can be applied. In the production phase the finishing touch to the design will be done. The contingencies in this phase are very low. In operation the actual aircraft is developed and built. At that moment the contingency is equal to zero.

Table 4.2: Overview of the contingencies in percentage per technical performance parameter

Design maturity	Mass	Power	Range	Computer capacity	System efficiency	Internal spatial layout	Centre of gravity location	DEP Velocity Increase	Series production cost	Direct operating cost	Production time	Reliability	Availability	Maintainability
Conceptual	20	40	10	20	30	20	10	25	20	20	30	20	30	25
Preliminary	10	15	5	15	20	10	5	10	15	15	15	10	20	15
Detailed	5	5	2	10	10	5	3	5	10	10	5	5	10	10
Production	3	3	1	5	5	3	1	2	5	7	0	3	5	5
Operation	0	0	0	0	0	0	0	0	0	0	0	0	0	0

Note that the power contingency is in the beginning rather high, because there is a lot of uncertainty on the power that is consumed by the aircraft, as it is not known how much the electric engines will consume. However the contingency drops very fast in preliminary phase and on wards. The same applies for the DEP velocity increase. The contingency drops, because, via tests, the uncertainty of this parameter will go down. Furthermore, the system efficiency has a quite high contingency, because there is a lot of uncertainty in computing the efficiency of the total system. Especially in a hybrid electric aircraft, as there little known about the interaction of both power systems. Lastly the contingency increase from reliability to maintainability and availability. The reason for this is that maintainability is dependent on reliability and availability in its turn is dependent reliability.

4.1.3. ESTIMATED AND EVALUATED MASS BUDGETS

From performing a mass estimation for each of separate subsystems, as well as optimising for performance, the current mass budget of the aircraft can be drawn up, as seen in Table 4.3. It can be observed that the main increases in mass can be attributed to the wing and the horizontal and vertical stabilisers. The increase in wing mass can mainly be contributed to the presence of the wingtip propellers, causing additional stresses in the wings. However, the percentage the wing mass makes up of the total mass is similar to that of the original mass in Table 4.1. The tail mass increases as the initial estimate was made based on the use of light-weight composite materials, whereas the current weight estimation is based on statistical data, which does not take this into account.

Table 4.3: Current mass estimation compared to the initial mass budget

Component	Estimated Mass [kg]	Evaluated Mass [kg]	Mass Change [%]	Component to Total Mass [%]
Wing	1510	2045	35	10
Tail	385	537	39	2.6
Body	1600	1528	-4.5	7.8
Landing Gear	640	640	0	3.1
Flight Controls	220	220	0	1.1
Propulsion	1830	1563	-15	7.6
Auxiliary Power	0	0	0	0
Furnishing	830	830	0	4.1
Crew	280	280	0	1.4
Other Subsystems	1165	1165	0	5.7
Empty Mass	8460	8909	5.3	44
Payload Mass	4650	5000	7.5	25
Energy Mass	5220	6539	25	32
Total Mass	18330	20446	12	100

As all the above-mentioned masses are based on preliminary estimations, they have to be updates throughout the design. As the contingencies per subsystem decrease, the mass estimations per subsystem can be updated to a more accurate value. Once the mass budget has been updated, the design is iterated again, coming to a new energy mass and thus a new total mass. This approach is already applied throughout the current design phase, it is however important that this is still applied in future design. This will lead to an accurate mass budget up to the production phase, where masses can be accurately measured.

4.2. HARDWARE, SOFTWARE & DATA HANDLING DIAGRAM

The following section shows multiple diagrams concerning the flow of resources and information through the aircraft's subsystems as well as an indication of what actions the accompanying software should be able to perform. This is done by first making a data handling diagram followed by a hardware and a software diagram.

4.2.1. DATA HANDLING DIAGRAM

The data handling diagram can be seen in Figure 4.1. It indicates the flow of data through the main subsystems, as well as through the command and data handling centre. As most the aircraft systems are managed by software, it is of high importance that the command and data handling system is redundant. Therefore, a second set command and data handling system will installed on board. As this is only the very first stage of hardware design, no specific processors, encrypters, decrypters and data storage devices are selected. This is done in a later stage of the design when more is known about the software and hardware required for the operation of the aircraft. The energy needs of the on-board eletrical system of the aircraft are indicated in the diagram as 'On-Board System Needs'.

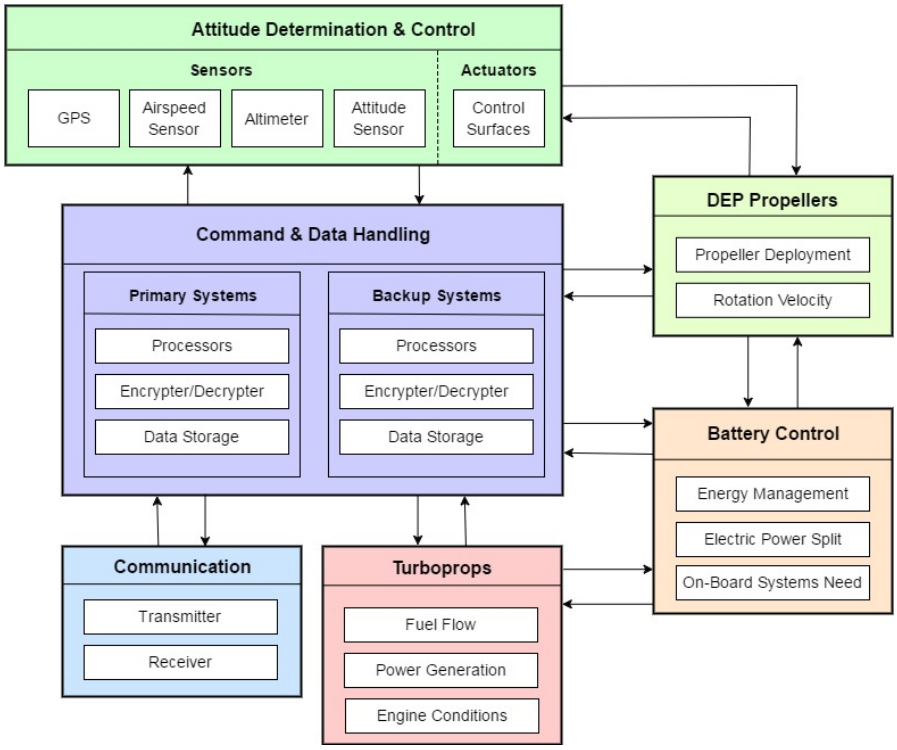

Figure 4.1: Data handling diagram of E-gle

4.2.2. HARDWARE DIAGRAM

The hardware block diagram, as shown in Figure 4.2 gives an illustration of the hardware components of the aircraft and how they are mutually interacted. The diagram is made to improve the understanding of the system. The hardware is divided in four components; propulsion, power, DEP and control. The diagram illustrates the features of each component and their mutual interaction.

From the cockpit, inputs are delivered to the propulsion, DEP and control system. These inputs have effect on the functioning of the aircraft and can be for instance certain values for the deflection of the control surface, for example when the pilot decides to descent and to make the aircraft ready for landing, he delivers inputs from the cockpit to the DEP component to unfold the high-lift propellers. In addition, he passes along an input to the control component to deploy the flaps and landing gear. The inputs delivered by the pilots go in parallel with data transferred from the cockpit to the power component. This data contains the information on how much energy has to be generated by either the batteries or the fuel to carry out the proceedings successfully.

An interesting feature of the propulsion component can be observed; additional mechanical power generated by the turboprop which is not immediately required by the wingtip propellers can be transferred to the batteries via the motor as electrical power as is discussed in Section 7.4.

4.2.3. SOFTWARE DIAGRAM

In order to make all the subsystems properly interact, as shown in the data handling and hardware diagrams, accompanying software has to be developed. As no software design has been performed, a top level software diagram is constructed, in order to generate an overview of which different types of software are required and what actions they should be able to perform. This software diagram can be seen in figure Figure 4.5. It gives an indication of how the specified software for different subsystems have to function, interact and what feedback they have to provide. Moreover, a data management block is including, allowing the data to be stored, accessed and checked for values about which the pilot need to be warned.

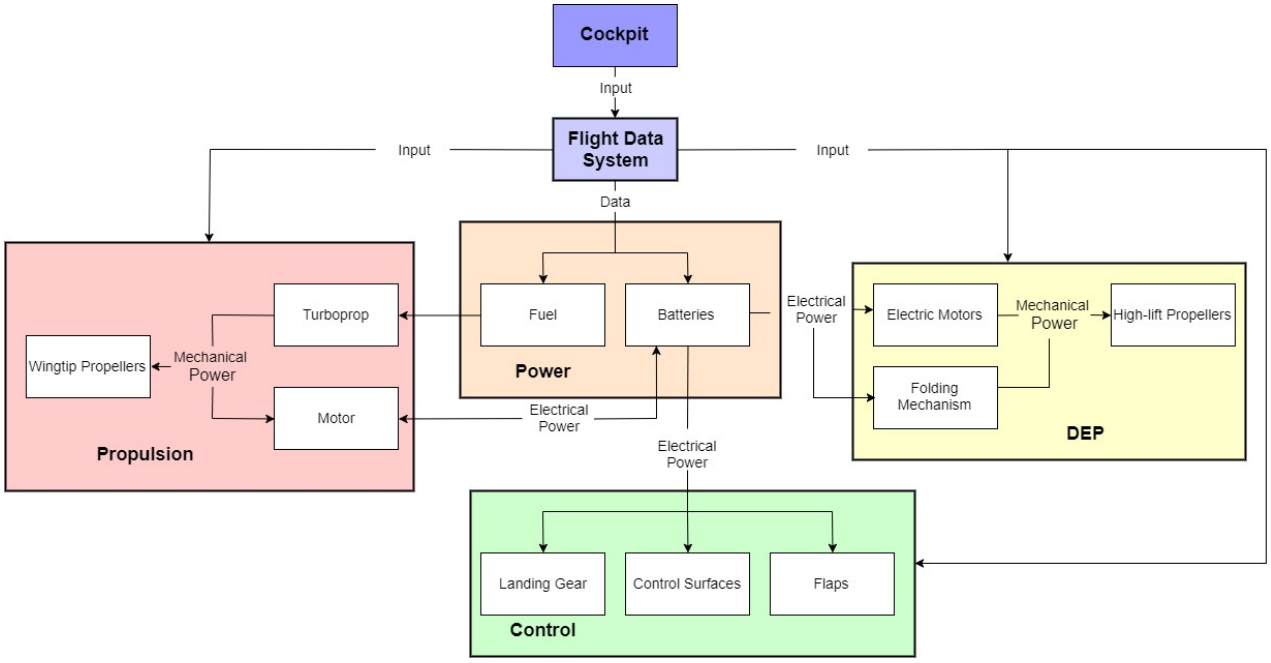

Figure 4.2: Hardware block diagram of E-gle

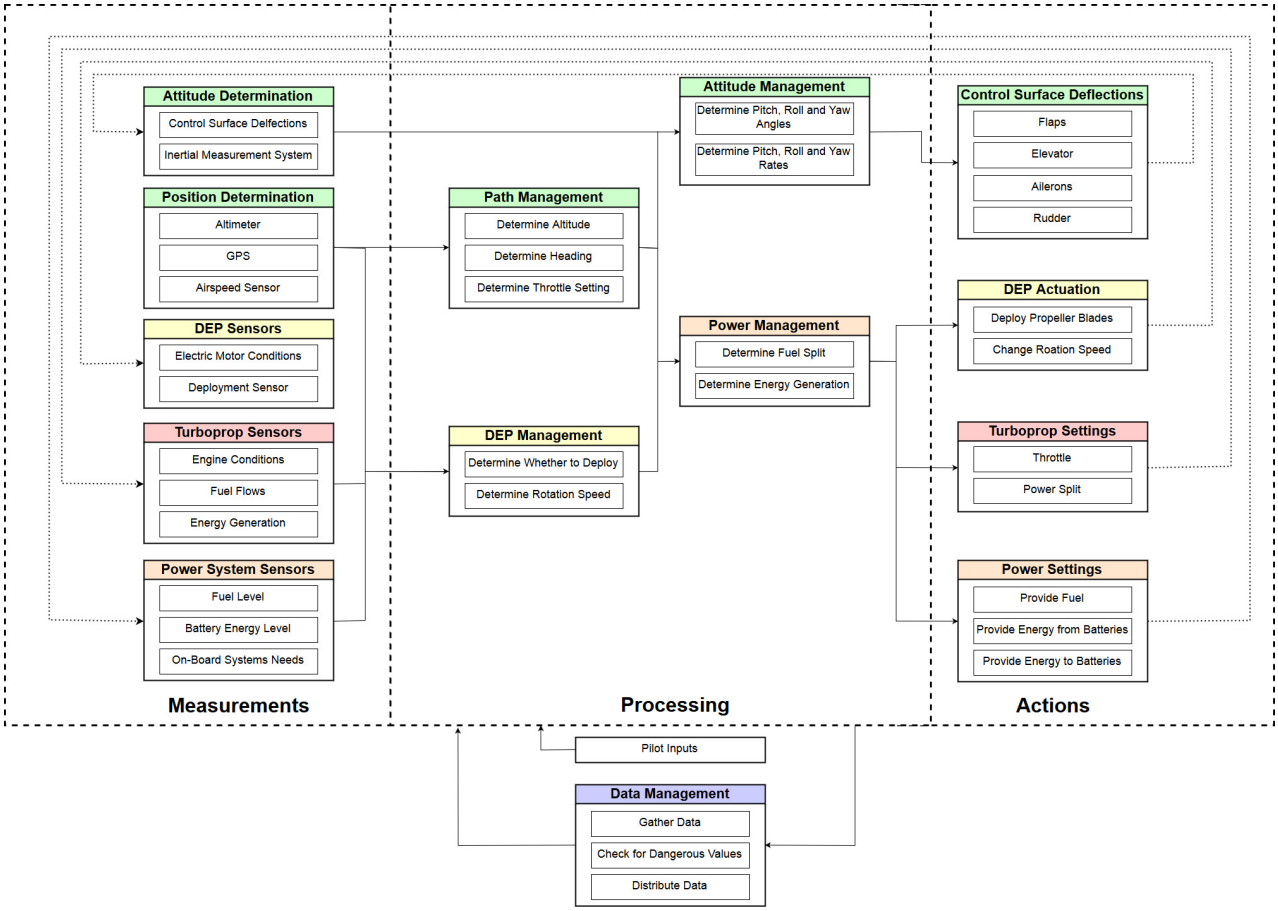

Figure 4.3: Software block diagram of E-gle

4.3. ELECTRICAL SYSTEM

The satisfactory performance of any modern aircraft depends to a very large degree on the continuing reliability of electrical systems. Being a electric hybrid aircraft, most of the flight equipment and system on E-gle are powered by the batteries. The turboprop engines provide power for the thrust propellers and excess power from here is used to recharge the batteries via the alternator.

The master switch consists of two separate switches, the battery master (BAT) and the alternator master (ALT). The battery master activates the battery contactor, which connects the battery to the aircraft's primary and avionics electrical busses. The alternator master activates the alternator by applying power to the alternator field circuit. These two switches provide electrical power to all the systems in the aircraft. Each device is attached to a bus bar through a circuit breaker.

The bus bar is made up of a thick copper strip connected to group of switches and circuit breakers with the same basic function. The avionic bus consists of the avionic equipment for control, monitoring, communication, navigation, weather, and anti-collision systems, all of which are located in the cockpit. Communications connect the flight deck to the ground and the flight deck to the passengers. Navigation systems help to determine the position and direction on and above the surface of Earth. These include a combination of satellite based and ground based systems.

The primary bus is connected to several major flight systems. The DEP system consists of the high lift propellers powered by one electric motor each. These motors are fed power from the battery. Further the motors are supported by motor controllers which are also run from the power from the battery. The parallel turbo-electric propulsion system consists of one turboprop parallel with two electric motors on either wing and the fuel feed system consists of pumps which require power. The batteries also supply power to the high lift and control surfaces. Further, interior lighting, air conditioning, toilets, kitchen and entertainment screens draw their power requirements from the primary power bus.

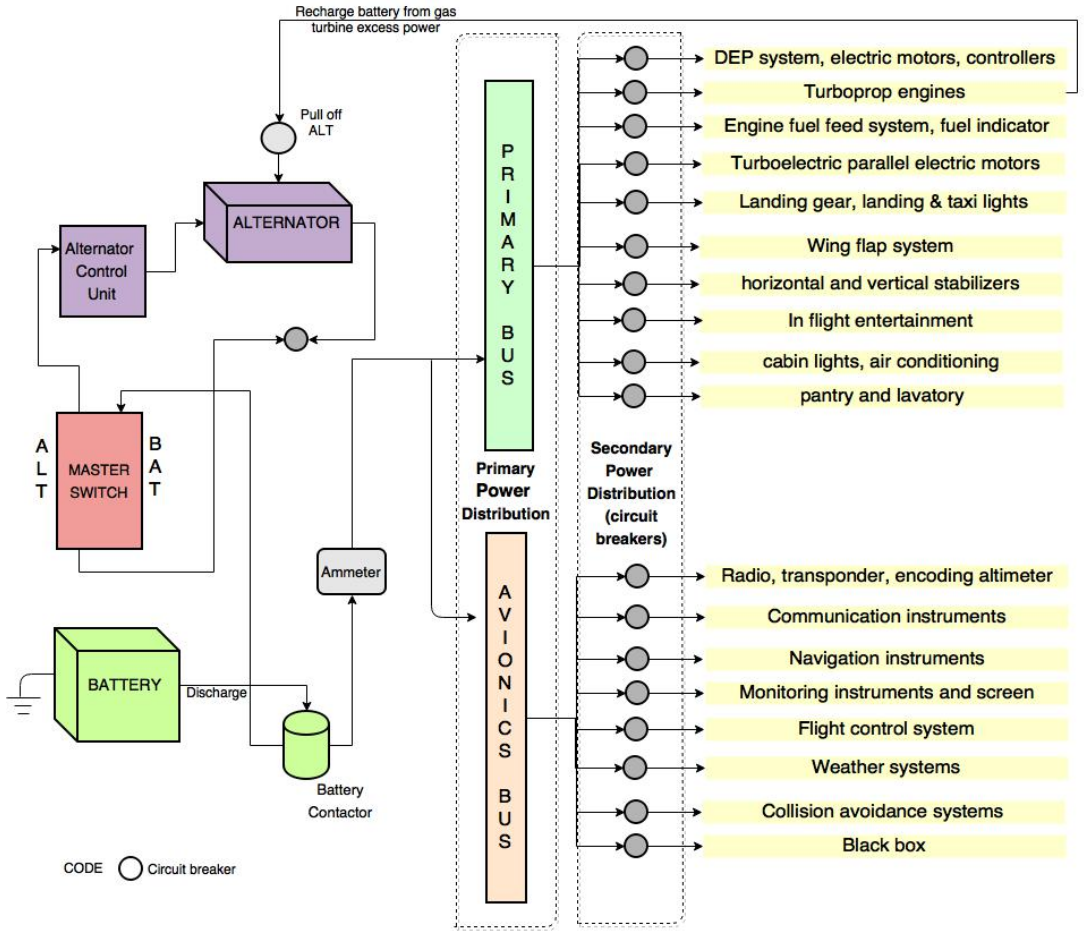

Figure 4.4: Electrical block diagram

4.4. COMMUNICATION FLOW DIAGRAM

Communication flow involves data transmission and reception between aircraft or between aircraft and ground. In order to ensure safe aircraft operations, it is highly essential to have a well devised communication system in the aircraft. The communication system on E-gle is shown in Figure 4.5 and the various components are discussed in detail below [15]. The radio communication ground segment consists of a Very High Frequency radio (VHF), VHF Omni-directional Range (VOR), Distance Measuring Equipment (DME), Airport Surveillance Radar (ASR), Instrument Landing System (ILS) and finally the Non-Directional Beacon (NDB).

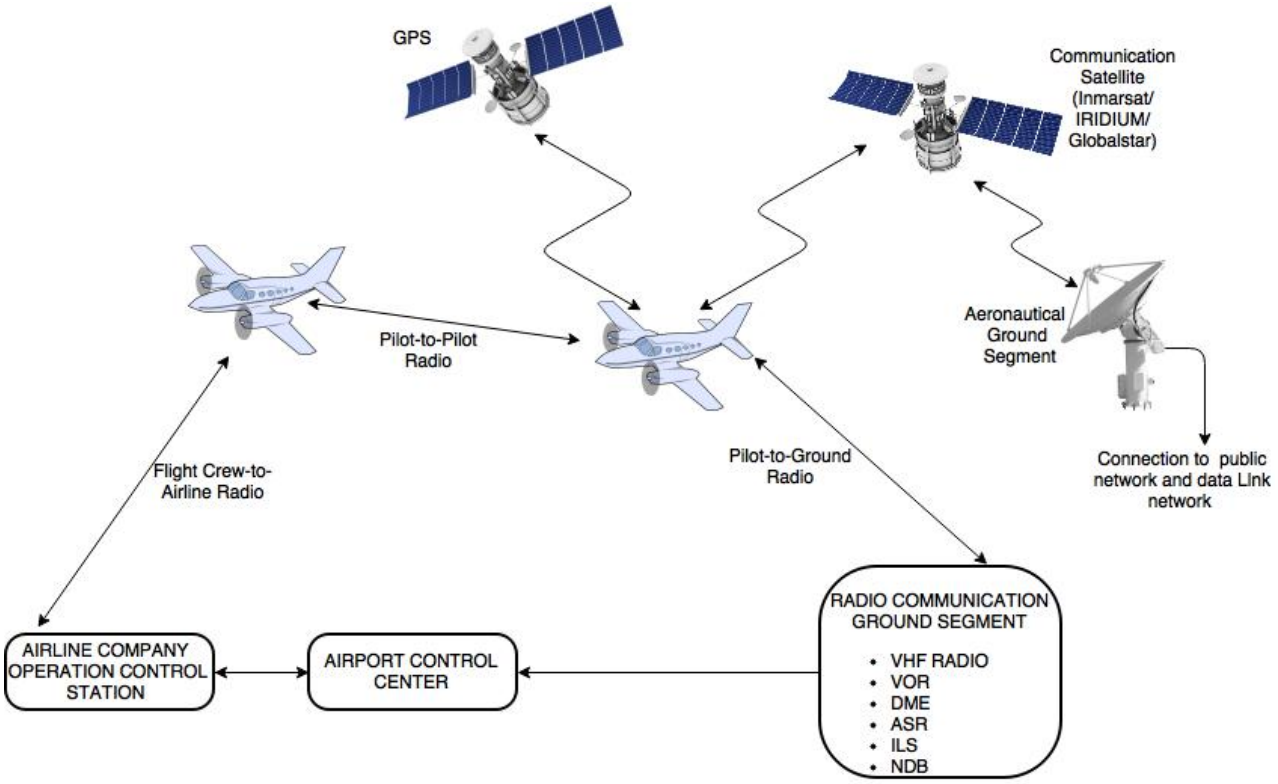

Figure 4.5: Aircraft external communication flow illustration

Human/ Voice Radio Communications

Radio communication is the backbone of air traffic control. The E-gle will be equipped with multiple radios to facilitate communication between pilot-to-ground, pilot-to-pilot and flight crew-to-airline; to enable efficient operations and control through dense air traffic regions. These radios are the communications medium for air traffic control, where pilots receive navigation guidance as verbal instructions from aircraft controllers. The flight crew-to-airline radio is meant to enable communication between the flight crew and the airline operations without disturbing the pilot. This way, they can communicate about the reservations, the airline schedule, etc. Lastly, communication between pilots during flight is also possible with this mean of communication. Those radio communications for civil aircraft use a range of very high frequency (VHF) between 108 and 137 MHz.

Transponders

Transponders are used for any machine-to-machine communication. Communication is done by producing a response when receiving a radio-frequency interrogation. They are used in addition of human/voice radio communication in order to reduce the workload of the pilots and the controllers, by reporting pressure altitude. The ones used in controlled air space used mode C or S transponders. The mode C transponders transmit pressure altitude information and the mode S transponders limit the radio-frequency interrogations and enables automatic collision avoidance. Transponders receive the interrogations on a single super high frequency (SHF) and transmit on another SHF.

GPS
Global Positioning System (GPS) is composed of three segments: user, space and control. The last two are owned by the United States, however Russia and China have their own GPS satellite constellations and Europe is developing theirs, called Galileo. The space segment is composed of several satellites transmitting to the control segment the position and time of the GPS by a single SHF signal. The control segment has for objective to keep the satellites in the right orbits and to maintain their health and status. Finally, the user segment, composed of the receiver equipment, calculates the exact location and time of the user using the transmitted information. This system is used by civilians from all around the world and military users from the United States and their allied. GPS transmission is done using two frequencies, L1 and L2, modulated to a nominal one.

ADS-B
The Automatic dependent surveillance-broadcast (ADS-B) system relies on two components: a GPS navigation source and a datalink, the ADS-B unit. This unit, usually a modified Mode S transponder, operates at 1090 or 978 MHz. The system transmits the position determined periodically by the GPS, together with the identification, altitude and velocity, to the air traffic control ground segment in order to track the aircraft. The position can also be transmitted to other aircraft, to warn the pilots about the position of the aircraft in the surroundings. The real-time position information provided by this system is more accurate than the information determined with current radar-based systems. This is the reason why more and more aircraft are equipped with this technology.

ACARS
The Aircraft Communications Addressing and Reporting System (ACARS) is a digital datalink system for transmission of short messages between aircraft and ground stations via airband radio or satellite. ACARS refers to the complete air and ground system, consisting of equipment on board, equipment on the ground, and a service provider.

5

AERODYNAMICS

In order to investigate the effect of the DEP concept, aerodynamic analyses are performed. First, the general planform of the aircraft is discussed in Section 5.1, such that the main parameters are known. Next, the aircraft will be optimised for cruise condition, leading to a wing design and its corresponding aerodynamic performance in Section 5.2. Consequently, the performance of the design is evaluated during both take-off and landing, investigating the effect of the high lift propellers in Section 5.3. Finally, the verification and validation procedures used are presented in Section 5.4.

5.1. WING PLANFORM

The wing planform is described in this section. This consist of several different main parameters. These parameters are explained in Subsection 5.1.1 to Subsection 5.1.6. Many parameters described in this chapter are unfortunately based on reference aircraft and assumptions from reports [16, 17]. Most of these parameters can be determined later during the design phase using wind-tunnel tests and computational fluid dynamics (CFD). These computations however exceed the time and the resources available and thus the parameters are analysed as thoroughly and detailed as possible for this stage. The wing surface used is determined in Subsection 5.2.2.

5.1.1. ASPECT RATIO

The aspect ratio of a wing is the span divided by the chord of the aircraft. This influences the lift curve and the drag created by the aircraft. The aspect ratio influences the C_L as can be in Figure 5.1.

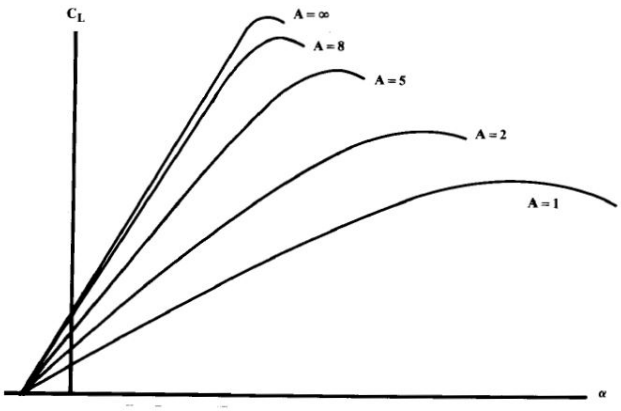

Figure 5.1: Effect of aspect ratio on lift [16]

The initial aspect ratio was estimated using a scaling factor acquired [1]. The aspect ratio of a comparable regional turboprop, the Bombardier Q300, was multiplied with this factor to achieve an aspect ratio of 19.02 [18]. The higher the aspect ratio, the better it is for the aerodynamics of the aircraft, because it reduces the induced drag, however in a structural sense this will be too heavy. An optimum had to be found between a high aspect ratio and acceptable structural weight. The final chosen value for aspect ratio is chosen to be 15, which is explained in more detail in Chapter 9.

5.1.2. SWEEP

Sweep is normally used to reduce the effects of trans- or supersonic velocities. The sweep can theoretically be placed directly on the mach cone, to prevent the supersonic effects, however this is not practical for high and low speed aircraft [16]. In addition to this, sweep also provides positive dihedral stability. Roughly 10 degrees of sweep provides 1 degree of dihedral effect. However with sweep the wing surface is required to be increased to provide the same lift. This requires an larger and therefore heavier wing.

For the E-gle a swept back wing is chosen to reduce the structural weight, instead of a forward swept wing, since outside of stall performance, aerodynamically there is no difference between a forward and aft swept wing. An oblique wing is not considered, since this reduces wave drag, which is not present in low speed flight. A variable-sweep wing is not applied, since low sweep is required and the mechanism to allow variable sweep increases the weight significantly [17].

The initial sweep of the aircraft is selected from historical data and depends on the maximum Mach number of the aircraft. The sweep what results form this data is a leading edge sweep of 4 degrees. This is a common value for regional aircraft with the cruise speed of the E-gle [16, 19].

5.1.3. TAPER

The taper ratio of the aircraft is primarily chosen to reduce the induced drag on the wing. The lowest induced drag is achieved with an elliptical lift distribution. A taper ratio of 0.5 for low sweep aircraft almost resembles the elliptical distribution with around one percent difference [16]. Also for wingtip propellers the use of a more elliptical planform is preferred as can be seen in Figure 5.2b, due to an increased reduction in induced drag. A higher or a lower aspect ratio results in a worse drag reduction. An elliptical or an optimal wing for tip drag is best suited. Therefore, for the E-gle a taper ratio of 0.5 is chosen as it suites the DEP and the relative low airspeed at which the E-gle flies and its low sweep. This is also in accordance with the Bombardier Q300, which has a taper of 0.5. The taper can be tuned later using software or wind tunnel tests, which is the way it is done in the aerospace industry.

5.1.4. SPAN AND CHORD

Span
The span of the aircraft is fixed with the surface and the aspect ratio of the wing. The total required span is calculated using Equation 5.1. This results in a span of 24.2 m, from the values given in Subsection 5.2.2 and Subsection 5.1.1.

$$b = \sqrt{A \cdot S} \tag{5.1}$$

In CS-25 [20] there is no requirement that limits the span of an aircraft, however a larger span does require larger storage, maintenance halls, etc. Which results in a higher operational cost.

Chord
The chord of the aircraft depends on aspect ratio, taper, span, leading edge sweep and quarter chord sweep. First the quarter chord sweep needs to be calculated with Equation 5.2, using the leading edge sweep. This formula is derived from geometrical relations from the wing. This formula establishes an approximate relation between the leading edge sweep and the quarter chord sweep. Next the root chord is estimated using Equation 5.3 [21]. This formula relates the root chord with other parameters.

$$\tan(\Lambda_{c/4}) = \tan(\Lambda_{LE}) - \frac{1-\lambda}{A \cdot (1+\lambda)} \tag{5.2}$$

$$c_r = \frac{2b[\tan(\Lambda_{LE}) - \tan(\Lambda_{c/4})]}{(1-\lambda)} \tag{5.3}$$

Finally the tip chord can be calculated in a straightforward manner by multiplying it with the taper ratio. This can be seen in Equation 5.4, the result of which is a root chord of 2.15 m and a tip chord of 1.08 m.

$$c_t = \lambda \cdot c_r \tag{5.4}$$

5.1.5. TWIST

The wing twist is used to prevent tip stall and optimise the lift for a certain lift coefficient. However, the twist only optimises one lift coefficient in particular. For the other phases the wing produces more drag. As an initial twist angle, a twist of 3 degrees is selected. To optimise this number in a later stage advanced software or wind tunnel test can be done to tweak this number.

5.1.6. DIHEDRAL

The dihedral generally influences the stability of the aircraft. As a first order estimate guidelines are used. A general aviation high wing aircraft generally has a dihedral of zero to two degrees [16]. As an initial value for the dihedral the value of the Q300 is chosen, which is equal to 2 degrees. This value can later be tuned using software during the detailed design phase and wind tunnel tests.

5.2. CRUISE OPTIMISATION

The benefits of using high-lift propellers result in the possibility to size the wings for optimal cruise flight. In this section, different parameters of the aircraft are determined which result in the lowest drag possible for this flight phase.

5.2.1. WINGTIP PROPELLERS

As was determined previously [18], it is beneficial in terms of the performance of the aircraft to place the thrust propellers on the tip of the main wing [1, 22]. The potential benefits and downsides of this placement are further explored in the following section. The main benefits of the wingtip mounted thrust propellers comes from the interaction between the propellers and the wingtip vortices. This is experienced in an increase in propulsive efficiency or a decrease in induced drag, depending on whether the propellers are positioned in front of the wing or behind the wing, respectively. As the propellers of the E-gle are fitted in front of the wing, a decrease in induced drag can be obtained. However, this requires the propeller to be counter-rotating with respect to the vortices, as the induced drag is increased otherwise [23]. This decrease in induced drag can also be seen as an increase in effective aspect ratio and depends on multiple variables. First, both a lower aspect ratio and a higher lift coefficient are beneficial in terms of drag reduction [24], as can be seen in Figure 5.2a. Moreover, the shape of the lift distribution has a larger impact on the effectiveness of the wingtip propellers, as can be seen in Figure 5.2b. Finally, the rotational speed of the propeller has an influence on the drag reduction, mainly requiring the windmilling speed to be reached [25].

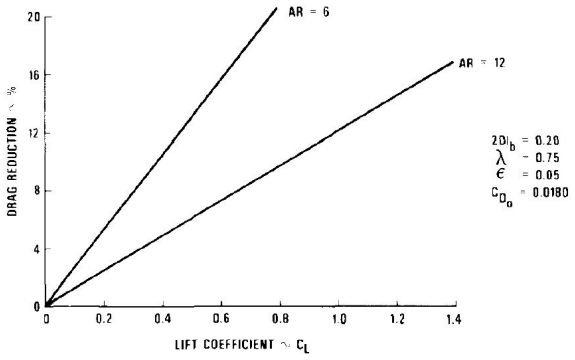

(a) Influence of aspect ratio and lift coefficient on drag reduction [23]

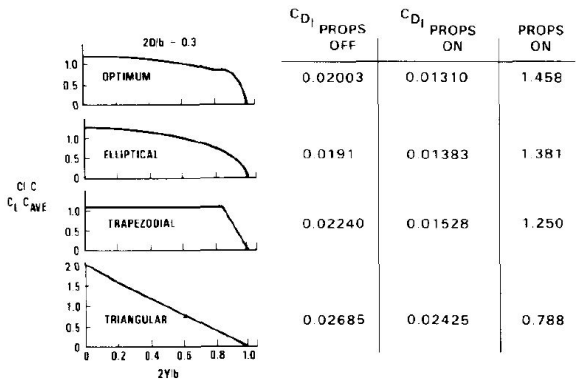

(b) Influence of lift distribution on induced drag [23]

Figure 5.2: Parameter influence on induced drag reduction

Although the influencing parameters are known, it is difficult to make an accurate prediction of the reduction in induced drag without using an extensive numerical model. However, an estimation can be made based on literature and other design studies. For a lower value of both the aspect ratio and the lift coefficient, research studies conclude that the reduction in induced drag ranges from 32 to 40 percent [23–25]. Moreover, a design study for a smaller aircraft using DEP has been performed, simulating the effects of wing tip propeller using CFD analyses, resulting in a induced drag reduction of 34 percent [26]. Therefore, reduction in induced drag for the E-gle is estimated to be around 35 percent.

Two of the major downsides of having the thrust propellers on the wing tips are the increased impact of flutter and the increased structural loading on the wings in non-flight situation. These effects will be discussed in Chapter 9 and will be considered during the further design, possible resulting in design alterations.

5.2.2. DRAG DETERMINATION

Since the sizing of the aircraft for cruise flight results in a reduction in required wing surface area, the drag will decrease accordingly. In this section, the benefits are analysed in further details and results are obtained regarding several aerodynamic characteristics.

During cruise, the aircraft has to generate just enough lift to compensate the weight acting downwards. Because the velocity is set at 500 km/h at an altitude of 5000 m (which will be determined in Chapter 10), an optimal combination between the lift coefficient and the surface area has to be found leading to the smallest drag. The lift coefficient's reduction will results in a diminishing lift-induced drag, however a smaller wing surface causes a reduction in overall drag.

The aerodynamic drag acting on the aircraft can be divided in two parts: the lift-induced drag and the zero-lift drag which is a combination of form, skin friction and interference drag. Combining both drag components results in Equation 5.5 for the total drag. Both drag coefficients will be discussed in more detail below.

$$D = D_i + D_0 = (C_{Di} + C_{D0}) \cdot \frac{1}{2}\rho V^2 \cdot S \tag{5.5}$$

Zero-lift Drag Coefficient

To determine the zero-lift drag coefficient (C_{D0}) the component buildup method [16] is used, which estimates the subsonic parasite drag of each component. The distinction is made between the main wing, fuselage, horizontal tail, vertical tail and nacelles. The nacelles contain the operating wingtip and folded high-lift propellers and engines. C_{D0} is determined with Equation 5.6.

$$C_{D0} = \frac{\Sigma\left(C_{f_c} FF_c Q_c S_{wet_c}\right)}{S_{ref}} + C_{D_{misc}} + C_{D_{L\&P}} \tag{5.6}$$

The drag is a summation of the attribution of each component indicated with subscript c. Due to the placement of the folded high-lift propellers in front of the wing, the flow is assumed to be turbulent. Hence, the skin friction coefficient (C_{f_c}) is determined with Equation 5.7, where the Reynolds number R for each component is obtained with Equation 5.8. The component Form Factor (FF) determines the pressure drag due to viscous separation and depends on the dimensions of each component. Equation 5.9 determines the Form Factor for the wings, Equation 5.10 for the fuselage and Equation 5.11 for the nacelles. The effect of interference on the component drag is estimated with the interference factor (Q) which results from the mutual interference between different components. The wetted area of each component is presented by S_{wet_c} and S_{ref} is the main wing reference area. The up sweep at the aft side of the fuselage causes extra drag and is responsible for the miscellaneous drag ($C_{D_{misc}}$). The drag due to up sweep can be determined with Equation 5.12 where u is the up sweep angle in radians and A_{max} the maximum cross-sectional area of the fuselage.

During take-off and landing, flaps and the landing gear are also taken into account by $C_{D_{misc}}$, which is discussed in more detail in Section 5.3. The last part of C_{D0} is the addition of leakage and protuberance ($C_{D_{L\&P}}$) which accounts for the momentum loss due to leakage and attributes like antennas, lights and manufacturing defects. The occurrence of leaking has to be limited, however the E-gle has to provide air for the batteries, causing drag. The increment in parasite drag due to leakage and protuberance is estimated to be 10 percent.

$$C_f = \frac{0.455}{(\log(R))^{2.58}(1 + 0.144M^2)^{0.65}} \tag{5.7}$$

$$R = \frac{\rho V l_c}{\mu} \tag{5.8}$$

$$FF = \left[1 + \frac{0.6}{(x/c)_m}\left(\frac{t}{c}\right) + 100\left(\frac{t}{c}\right)^4\right]\left[1.34M^{0.18}(\cos\Lambda_m)^{0.28}\right] \tag{5.9}$$

$$FF = 1 + \frac{60}{f^3} + \frac{f}{400} \tag{5.10}$$

$$FF = 1 + \left(\frac{0.35}{f}\right) \tag{5.11}$$

$$C_{D0_{up}} = \frac{3.83 u^{2.5} A_{max}}{S_{ref}} \tag{5.12}$$

The contribution of each component is shown in Figure 5.3, where it can be clearly seen that the main wing and fuselage are the main cause of drag.

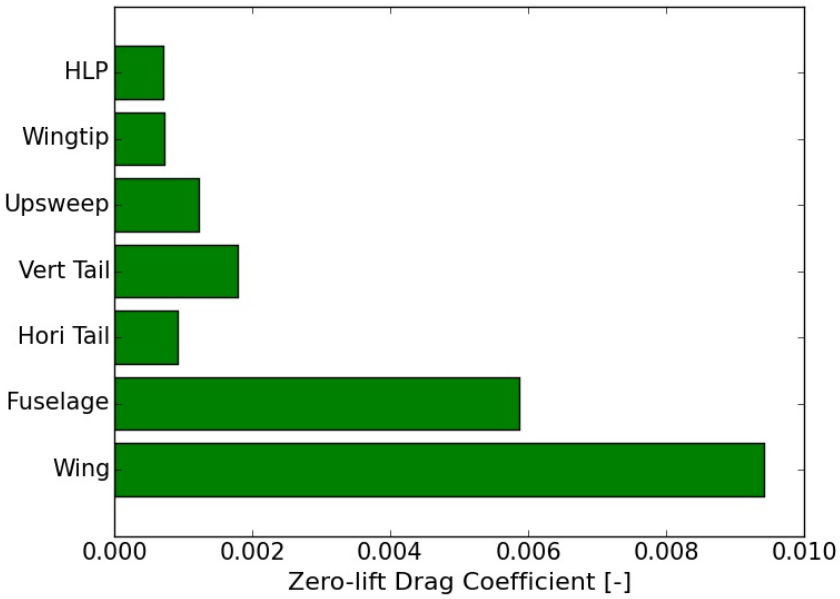

Figure 5.3: Component contribution to zero-lift drag coefficient during cruise

Lift-induced Drag Coefficient

As the parasite drag is independent of the lift generated, the lift-induced drag increases quadratically with increasing lift coefficient. Furthermore, the lift-induced drag coefficient C_{D_i} is dependent on the aspect ratio, the Oswald efficiency factor e_0 and the integration factor K due to the wingtip propellers and is presented by Equation 5.13.

$$C_{D_i} = K \cdot \frac{C_L^2}{\pi A e_0} \tag{5.13}$$

To minimise the lift-induced drag, the aspect ratio A has to be maximised. However, there are limits for the maximum value of A considering structures and weight. To account for a non-elliptical lift distribution and the occurrence of separation drag the Oswald efficiency factor has been introduced. It depends on basic geometrical aspects and is estimated with Equation 5.14 [27]. The value for K is analysed in Subsection 5.2.1 and accounts for the 35 percent decrease in lift-induced drag due to the wingtip propellers. The value of K is therefore 0.65.

$$e_0 = \frac{1}{1.08 + \frac{0.028(t/c)_{max}}{C_L^2} \pi A} \tag{5.14}$$

Both components of the drag have been analysed resulting in the knowledge how the drag behaves with different inputs. Correspondingly, the optimal values for surface area and lift coefficient can be determined leading to the lowest drag. The flow chart in Figure 5.4 presents the procedure applied.

The flowchart delivers the optimal geometrical values for the E-gle during cruise. These values are shown in Table 5.1 and compared to the Bombardier Q300. It is very clear that designing the E-gle for cruise results in a significant reduction in wing surface area leading to an overall smaller drag. To operate at this smaller wing surface, a higher cruise

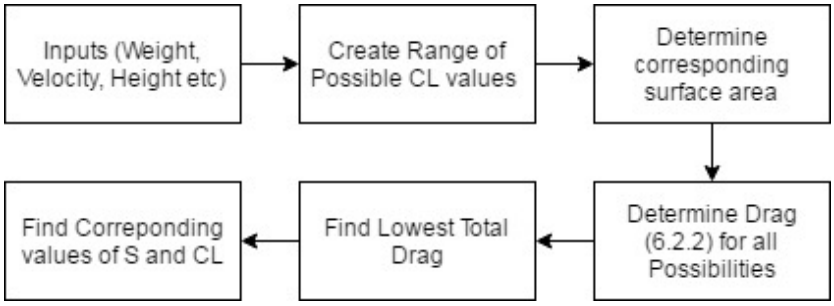

Figure 5.4: Flow Chart to determine optimal values during cruise

C_L is required. The zero-lift drag coefficient is smaller compared to the Bombardier mainly due to a smaller wing. The induced drag coefficient is larger with respect to the Bombardier despite the 35% reduction due to wingtip propellers. The higher cruise lift coefficient is responsible for the increase in the induced drag coefficient. Eventually, the total drag during cruise is much lower compared to the Bombardier which therefore results in a significant reduction in required energy.

Table 5.1: Cruise parameters E-gle

Concept	$C_D[-]$	C_{D_0} [-]	C_{D_i} [-]	C_L [-]	Drag [N]	L/D [-]	S [m^2]
E-gle	0.0332	0.0227	0.0105	0.75	9374	22.6	39.1
Q300	0.0348	0.025	0.0098	0.57	13895	16.8	56.2

From the values obtained using the flow chart, the drag polar is generated in Figure 5.5. To minimise the energy required during cruise, the most left point on the curve is chosen as the design point and is indicated with a red cross.

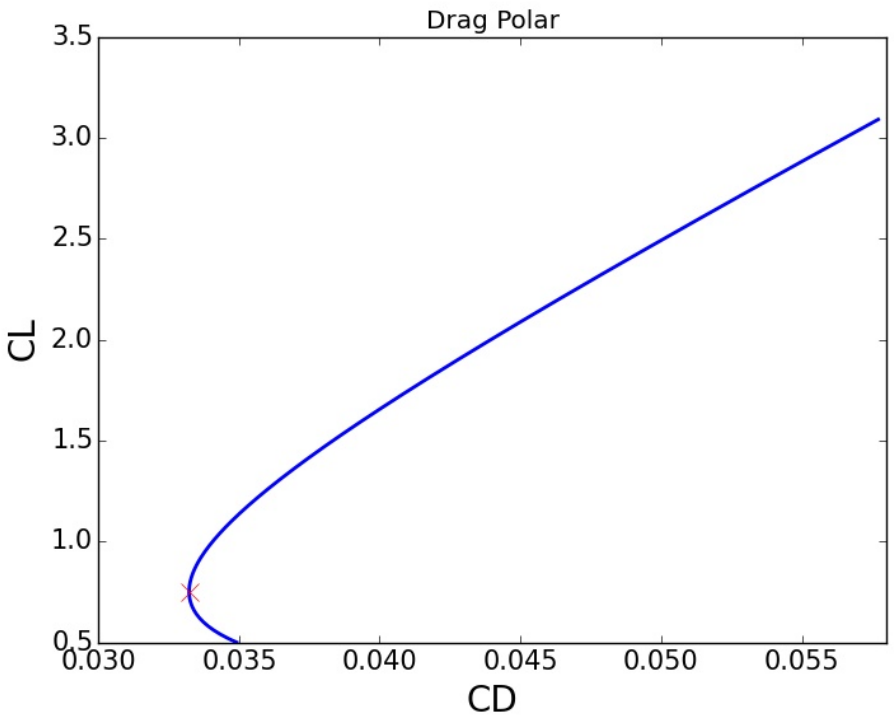

Figure 5.5: Drag polar for cruise conditions

5.2.3. CRUISE LIFT

The airfoil was already defined [18], but is made thicker to have a stronger wing to hold the wingtip propellers as will be explained in more detail in Chapter 9. The NACA4415 was chosen because reliable measurement data is available showing proper aerodynamic coefficient values [28]. To convert the two-dimensional C_l of the airfoil to the three-dimensional C_L of the wing, DATCOM is used [21]. Three main factors have influence on the slope of the lift curve: the aspect ratio A, compressibility effect M and sweep angle Λ. The slope for the three-dimensional wing can be calculated with Equation 5.15.

$$\frac{dC_L}{d\alpha} = C_{L_\alpha} = \frac{2\pi A}{2 + \sqrt{4 + \left(\frac{A\beta}{\eta}\right)^2 \left(1 + \frac{\tan^2 \Lambda_{0.5C}}{\beta^2}\right)}} \tag{5.15}$$

$$\beta = \sqrt{1 - M^2} \tag{5.16}$$

Here, β is the Prandtl-Gauert compressibility correction factor as expressed in Equation 5.16, η the airfoil efficiency factor and $\Lambda_{0.5C}$ is the sweep angle measured at half chord length. To determine the value of the lift coefficient at a certain angle of attack α, Equation 5.17 can be used. α_{0L} is the zero lift angle of attack and is a characteristic of the airfoil.

$$C_L = C_{L_\alpha} \alpha - C_{L_\alpha} \alpha_{0L} \tag{5.17}$$

This equation does not take into account stall. Therefore, for aircraft flying at a Mach number higher than 0.2 Equation 5.18 applies.

$$C_{Lmax} = \left[\frac{C_{Lmax}}{C_{l_{max}}}\right] C_{lmax} + \Delta C_{Lmax} \tag{5.18}$$

Values for $\left[\frac{C_{Lmax}}{C_{lmax}}\right]$ and ΔC_{Lmax} are obtained [16] and are a function of M, sweep and the leading edge sharpness parameter, which equals 3.12 for the NACA4415. $C_{l_{max}}$ is an airfoil characteristic, this has to be chosen carefully for the right Reynold's number. The corresponding stall angle α_s can be found with Equation 5.19. $\Delta\alpha_{C_{Lmax}}$ depends on M, sweep and the leading edge sharpness parameter [16].

$$\alpha_s = \frac{C_{Lmax}}{C_{L\alpha}} + \alpha_{0L} + \Delta\alpha_{C_{Lmax}} \tag{5.19}$$

Combining Equation 5.15 to 5.19, the three-dimensional lift gradient during cruise can be generated. This lift curve is presented in Figure 5.6 and is based on the lift gradient, zero-lift angle of attack, C_{Lmax} and the stall angle. The vertical dashed red line indicates the angle of attack required for the cruise lift coefficient calculated in Subsection 5.2.2.

During cruise it is convenient to know at what speed the aircraft will stall. Stall occurs when the aircraft cannot generate enough lift to keep itself on flight level. The C_{Lmax} during cruise is calculated with Equation 5.17 and visualised in Figure 5.6. Therefore, the stall speed (V_{stall}) during cruise flight is calculated with Equation 5.20.

$$V_{stall} = \sqrt{\frac{W_{cruise}}{C_{Lmax} \frac{1}{2} \rho S}} \tag{5.20}$$

The stall speed equals 105.1 m/s which is much smaller than the cruise speed. Therefore, varying the speed during cruise will not cause stall.

5.3. LANDING & TAKE-OFF PERFORMANCE

The main benefit of DEP lies in the fact that the main wing can be sized for cruise, whereas the propellers distributed along the leading edge can be used to enhance the take-off and landing performance. First, the effects of the flaps, that are used to generate both lift and drag during landing is explored. Next, the effect of the high-lift propellers on the landing and take-off performance is evaluated, after which the performance of the aircraft in terms of lift and drag is analysed.

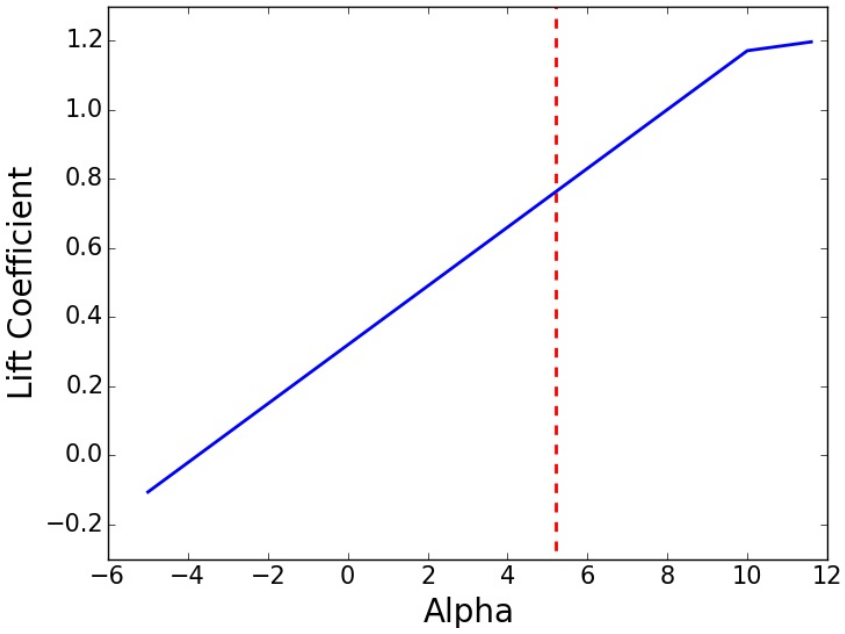

Figure 5.6: Lift gradient E-gle during cruise

5.3.1. FLAPS

The main wing's area is sized for the cruise phase to reduce the overall drag. To achieve successful landing and take-off, the high-lift propellers increase the dynamic pressure to compensate for the smaller wing area. The high-lift propellers are supported by flaps to lower the required propeller power resulting in less energy required to take-off and land.

The advantage of using flaps is the large increase of the lift coefficient. The benefits of this increase are the possibility to safely operate at very low speed in combination with the cruise sized wings. The disadvantages are the increase in weight due to the mechanical complexity and the additional drag. Operational high-lift propellers contribute significantly to the total thrust generated by the aircraft, with the result that the additional drag due to the flaps is of great importance during landing to be able to decelerate.

The simplest flap configuration is the split flap [17], making the increase in wing weight due to flaps minimal. Another advantage of the split flap is that it acts much like a spoiler at full deflection, resulting in the required drag during landing. The split flaps also deliver a reasonable amount of extra lift to support the high-lift propellers [28]. The maximum lift coefficient during take-off and landing increases due to split flaps from 1.512 to 2.43 with a flap deflection of 60 degrees.

The zero-lift drag increases considerably during take-off and landing due to the use of flaps. Equation 5.21 presents the zero-lift drag coefficient due to the deployment of split flaps [29], where the first part of the right-hand side represents the flap profile drag increment, the second part the induced drag increment due to flaps and the last part is responsible for the interference drag increment due to flaps.

$$C_{D0_{flaps}} = \Delta C_{D_{prof_{flap}}} + \Delta C_{D_{i_{flap}}} + \Delta C_{D_{int_{flap}}} \tag{5.21}$$

The contribution of the profile drag can be calculated with Equation 5.22. The factor 0.16 is the two-dimensional profile drag increment for split flaps [29] and depends on the thickness of the wing and the deflected angle.

$$\Delta C_{D_{prof_{flap}}} = 0.16 \cdot cos(\Lambda_{c/4}) \frac{S_f}{S} \tag{5.22}$$

The induced drag increment due to flaps can be estimated with Equation 5.23. Where the 0.08 is a empirical constant for the split flap depending on aspect ratio and the flap's span length. The last contribution to the flap's drag coefficient is the interference drag increment represented by Equation 5.24.

$$\Delta\Delta C_{D_{i_{flap}}} = 0.08^2 \cdot (\Delta C_{L_{flap}})^2 \cdot cos(\Lambda_{c/4}) \tag{5.23}$$

$$\Delta C_{D_{int_{flap}}} = -0.15 \cdot \Delta C_{D_{prof_{flap}}} \tag{5.24}$$

5.3.2. HIGH-LIFT PROPELLERS

The concept of high-lift propellers is based on the fact that the propellers increase the local dynamic pressure and increase the lift the main wing generates [1]. There are multiple studies available that provide a method capable of analysing the effects of high-lift propellers, which are used during the following analysis [30–33].

First of all, the two dimensional geometry of the wing and the propellers is considered. This geometry can be seen in Figure 5.7, where ϕ is the angle between the propeller blades and the freestream velocity. Furthermore, V_∞ is the freestream velocity and α_g is the angle with respect to the chord line. It can be observed that α_g is the geometric angle of attack of the airfoil, which in this case correspond to the maximum lift coefficient, as is used for landing and take-off, including flaps. Finally V_p is the slipstream velocity of the propeller and i_p is the angle it makes with the chord. This angle can be described as the inclination of the propeller with respect to the airfoil chord and has a major impact on the performance of the high-lift propellers.

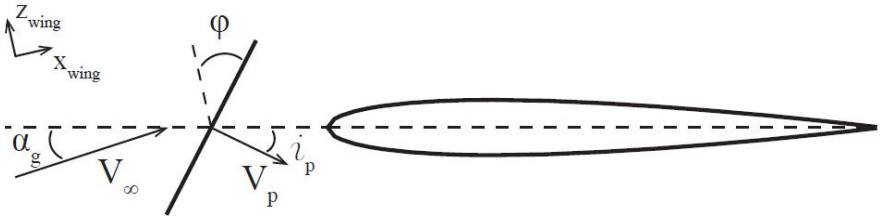

Figure 5.7: 2D geomerty of the high lift propellers [31]

For the use of the high-lift propellers it is most beneficial if the the freestream velocity is perpendicular to the propeller blade (or parallel to the propeller slipstream velocity) [34]. This means that the inclination angle is equal in magnitude and opposite in sign compared to the geometric angle of attack. Although this orientation is very beneficial in terms of landing and take-off performance, it provides a major downside. Larger nacelles are required, in order to incorporate the inclination angles. Combining this with the downward inclination of the nacelles during cruise, leads to a significant increase in drag of the nacelles during the other flight phases. It is concluded that the potential lift benefits from the high inclination angle are outweighed by the aforementioned increase in drag [30]. In order to minimise the drag during the other flight phases, but still gain some of the benefits from a negative inclination angle, the inclination angle is chosen equal to the geometric angle of attack during cruise. This results in an inclination of -6.4°. The slipstream from the propeller changes the effective angle of attack on the wing. This effective angle of attack behind the propeller α_{ep} is defined as the angle between the effective velocity behind the propeller V_{ep} and the chord line, as can be seen in Figure 5.8.

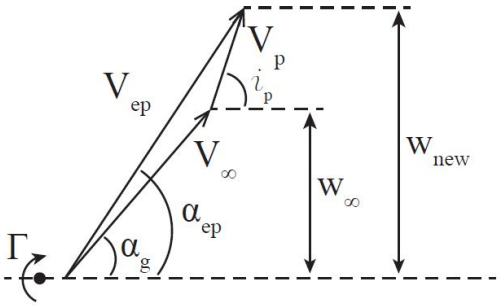

Figure 5.8: Vector diagram illustrating the effective angle of attack behind the propeller [31]

From this geometry, expressions for both of these quantities can be derived, as can be seen in Equation 5.25 and Equation 5.26.

$$V_{ep} = \sqrt{V_\infty^2 + V_p^2 + 2V_\infty V_p \cos(\alpha_g + i_p)} \tag{5.25}$$

$$\alpha_{ep} = \arctan\left(\frac{V_\infty \sin(\alpha_g) - V_p \sin(i_p)}{V_\infty \cos(\alpha_g) + V_p \cos(i_p)}\right) \tag{5.26}$$

Now that all the geometrical aspect are known, the slipstream velocity of the propeller can be estimated, which is of importance during the further design. An important parameter in these calculations is the percentage increase in lift compared to the total lift. Which can be calculated as in Equation 5.27 [31], where q_{eq} can be calculated using V_{ep} and the air density at sea level.

$$\frac{\Delta L'}{L'_\infty} = \frac{\Delta q}{q_\infty} = \frac{q_{ep}\left[\sin(\alpha_{ep})/\sin(\alpha_g)\right] - q_\infty}{q_\infty} \tag{5.27}$$

Next, a required value for the increase in lift is determined, already including the aforementioned flaps. This can be done by comparing the weight of the aircraft during either take-off or landing and comparing it to the lift generated at that instant, leading to Equation 5.28.

$$\frac{\Delta L'}{L'_\infty} = \frac{W - \frac{1}{2}\rho_0 C_{L_{max}} S V_\infty^2}{\frac{1}{2}\rho_0 C_{L_{max}} S V_\infty^2} \tag{5.28}$$

First Equation 5.25 and Equation 5.26 can be substituted in Equation 5.27, after which its right hand side can be set equal to the right hand side of Equation 5.28. This leaves an equation that can be solved numerically for the propeller slipstream velocity V_p.

The method described above is for a 2D wing, completely immersed in wide-slipstream flow, for which some correction have to made in order to apply to the real world case. First of all, for a wing with a constant twist angle, the extension made to three dimensions can be made using the percentage of the wing that is actually blown by the propellers, as in Equation 5.29 [31].

$$\frac{\Delta C_L}{C_{L_\infty}} = \left(\frac{\Delta L'}{L'_\infty}\right)\left(\frac{b_{blown}}{b}\right) \tag{5.29}$$

The effect of a finite slipstream height can be accounted for using the multiplicative factor β. This factor lies between zero and one and is to be multiplied with the propeller slipstream velocity in Equation 5.25 and Equation 5.26. It depends on the (average) slipstream height, how far the propeller is placed in front of the wing and the ratio between the slipstream speed far downstream and the freestream velocity [33]. An estimation of β can be made using overflow simulations for varying parameters, as seen in Figure 5.9.

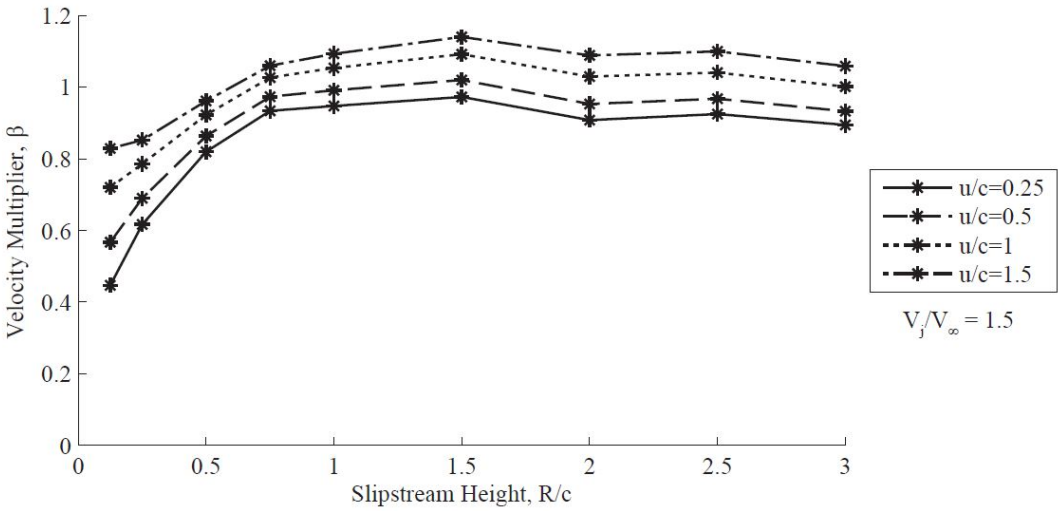

Figure 5.9: Beta as a function of the propeller dimensions [30]

By combining Equation 5.25 to 5.29 the required velocity increment by the high-lift propellers V_p can be calculated. This velocity increment is required to achieve a sufficient amount of dynamic pressure over the wing to be able to take-off and land. V_p during take-off is 27.27 m/s and during landing 20.52 m/s. The difference between the two flight phase values is due to the higher MTOW and lower velocity during take-off compared to landing.

5.3.3. DRAG EVALUATION

The drag has already been evaluated for the cruise phase in Subsection 5.2.2. During take-off and landing the drag coefficient will change due to the different conditions and the deployment of the landing gear and flaps. In this subsection differences with respect to cruise flight are analysed and the corresponding values for the drag are determined.

During take-off and landing, the velocity and the altitude is different compared to cruise. This has an effect on the Reynolds number, Mach number and the density. Changes in these parameters result in a different value for the zero-lift coefficient. The deployment of the flaps and the landing gear will also have an effect on C_{D0}. Due to the lower velocity, a higher lift coefficient is required to prevent the aircraft from descending too fast or even falling from the sky. The increase in lift coefficient has major influence on the lift-induced drag. The application of high-lift propellers influences the Oswald efficiency factor [30], increasing the lift-induced drag significantly. The velocity during take-off and landing is different, therefore the drag will be analysed for both situations. The use of high-lift propellers increases the dynamic pressure around the wing, resulting in an increased wing drag.

Landing

During the landing phase, the touch-down velocity is determined in Section 10.4 and equals 48.6 m/s. This is dependent on how much drag and reverse thrust can be produced during the landing phase. The critical weight during landing is obtained when landing happens immediately after take-off. The critical weight during landing is shown in Equation 5.30. The change in velocity results in a lower Mach and Reynolds number, increasing the skin friction coefficient in Equation 5.7. On the other hand, a lower Mach number decreases the form factor of the wings in Equation 5.9. The increase in density due to the fact that take-off and landing occur at sea level results in an increase in the Reynolds number. The dynamic viscosity μ increases with lowering the altitude meaning a decrease in the Reynolds number.

$$W_{land} = 0.98 \cdot \text{MTOW} \tag{5.30}$$

Due to the transitions mentioned above, the zero-lift drag coefficient will likely increase. This increase will be supported by the deployment of the flaps and landing gear. The influence of the flaps on the drag has already been evaluated in Subsection 5.3.1. The landing gear drag can be best estimated by comparing to test data for similar landing gear arrangements. A streamlined wheel and tire are chosen resulting in $\frac{0.18}{S_{ref}}$. Also the strut is streamlined and results in $\frac{0.05}{S_{ref}}$. 20 percent is added to the total value of the landing gear drag to account for mutual interference between the components. In Figure 5.10 the contribution of the flaps and landing gear are visualised compared to the other components. It is more than clear from this figure that mainly the flaps add a large contribution to the overall drag during landing and take-off.

$$C_{D_{lg}} = 1.2 \cdot \frac{0.18 + 0.05}{S_{ref}} \tag{5.31}$$

To generate the required amount of lift, the E-gle flies at maximum angle of attack and the flaps are deployed to increase the lift coefficient. The lift-induced drag will therefore increase significantly. Next to that, the high-lift propellers have a negative influence on the Oswald efficiency factor because the high-lift propellers create very jagged lift distributions. Simulations were performed to estimate Oswald efficiency factor with blowing propellers [30]. Based on these observations, Equation 5.32 is obtained to calculate e_0 when the high-lift propellers are active.

$$e_0 = \frac{(V_a - (V_a)_{max})^2}{(V_a)^2_{max}} (e_{max} - e_{min}) \tag{5.32}$$

Where $(V_a)_{max}$ is set at 29.2 m/s, e_{max} = 0.8 and e_{min} = 0.43. V_a is the average axial velocity from the high-lift propellers downstream. After the aircraft has performed the touchdown, additional speed brakes on the wing are deployed and generate a D/q value of 1.6 times the speed brakes' frontal area. These devices are used to have the aircraft slow down properly to meet the landing distance requirement as will be discussed in Chapter 10 in more detail. The speed brakes are located on 60 percent of the span and the height is 20 cm. The additional drag delivered by the speed brakes (D_s) is shown in Table 5.2.

Take-off

The take-off speed differs from the landing speed. The take-off speed depends on how much thrust the aircraft can generate during this phase to accelerate. From Section 10.4 the take-off velocity is equal to 46.0 m/s. The weight during take-off is set to be equal to the maximum take-off weight, resulting in Equation 5.33.

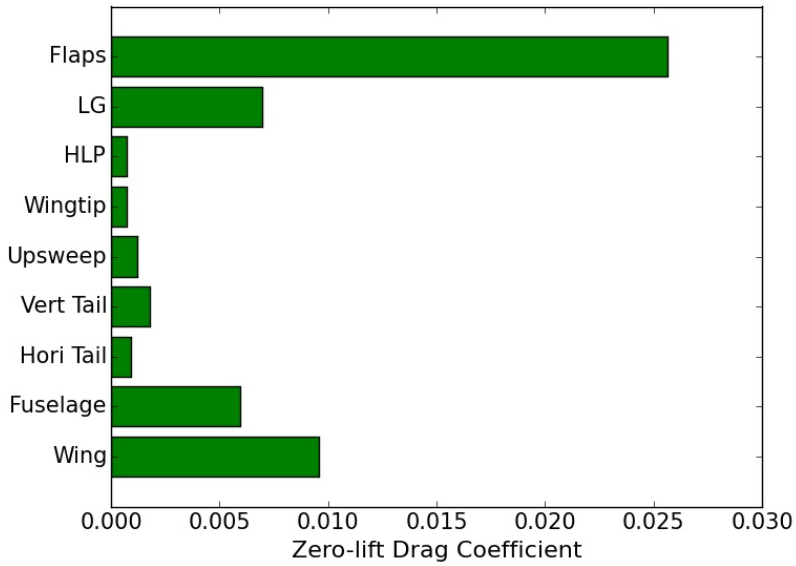

Figure 5.10: Component contribution to zero-lift drag coefficient during landing

$$W_{TO} = \text{MTOW} \tag{5.33}$$

During take-off, the landing gear and flaps are also deployed. Therefore in the landing phase Equation 5.21 and 5.31 apply. The total drag during take-off will be slightly different in comparison to landing due to the different velocity. The high-lift propellers increase the dynamic pressure of the wing and therefore also the drag. The dynamic pressure around the wing results in more overall wing drag. This can be visualised with Equation 5.34.

$$D_{wing} + D_{induced} = (C_{D_0} + C_{D_I}) \cdot \frac{1}{2}\rho(V + \Delta V)^2 \cdot S \tag{5.34}$$

During take-off and landing, the induced drag is extraordinary large due to the high lift coefficient due to flaps, the much lower Oswald efficiency factor and higher dynamic pressure due to the high-lift propellers. Everything discussed in this chapter so far combined, results in the drag characteristics during take-off and landing. They are presented in Table 5.2.

Table 5.2: Drag characteristics during take-off and landing

Phase	Drag [N]	$D_0[N]$	$D_i[N]$	$D_s[N]$	$\Delta V[m/s]$	$e_0[-]$
Take-off	21184	6975	14209	-	27.27	0.43
Landing	33176	7785	11795	13595	20.52	0.46

5.3.4. LIFT EVALUATION

To obtain the lift characteristics during take-off and landing, the same procedure is applied as in Subsection 5.2.3. The characteristics are determined without the use of the high-lift propellers to gain knowledge about stall and maximum lift coefficient. When these parameters are known, the additional contribution of the high-lift propellers can be obtained as is described in Subsection 5.3.2. During take-off and landing, the same flap settings are used to generate the maximum amount of lift. The only parameter that differs between take-off and landing is the velocity. The speed during take-off is slightly lower compared to landing. This results in a small variation in Mach number, influencing both η as β in Equation 5.15. However, this leads to a very small and negligible difference in the lift gradient. Therefore the lift during take-off and landing will not be treated separately.

The lift during take-off and landing is generated as in Subsection 5.2.3 using Equation 5.15 to 5.19. The values of β, η, C_{L_α}, α_{0L}, $\Delta C_{L_{max}}$ and $\Delta_{\alpha_{C_{Lmax}}}$ change due to the different conditions compared to cruise [16]. From that, the lift curve during take-off and landing is presented in Figure 5.11. The maximum lift coefficient is 2.43 and can be achieved by deploying flaps and flying at the highest angle of attack just before stall.

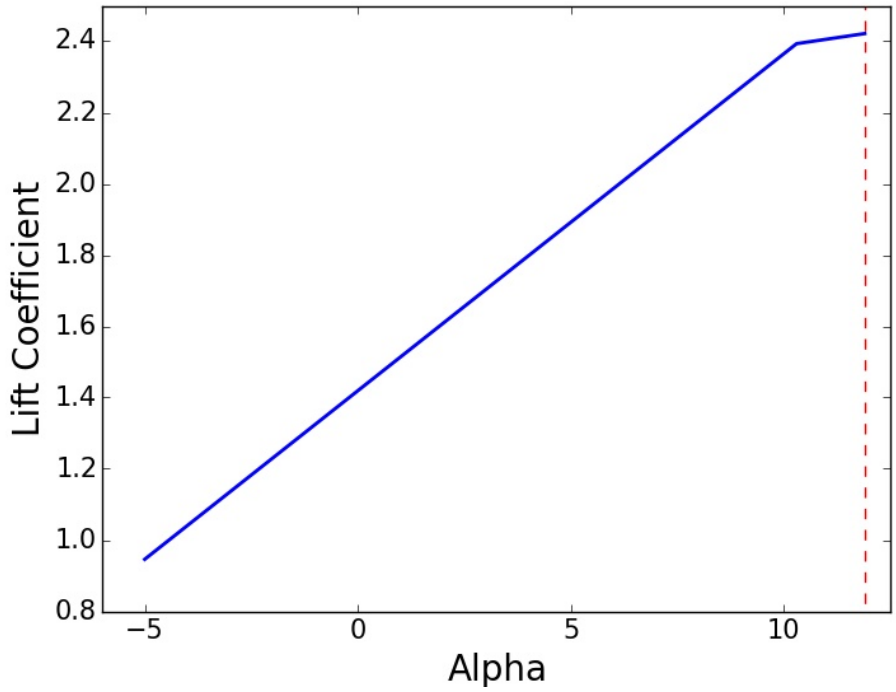

Figure 5.11: Lift gradient E-gle during take-off and landing

During take-off and landing, the occurrence of stall has to be avoided. The stall speed without the use of high-lift propellers is generated to get an idea how high the velocity has to be to take-off and land without the benefits of distributed electric propulsion. The critical mission phase is take-off because the related weight is higher. The stall speed during take-off is therefore presented by Equation 5.35.

$$V_{stall} = \sqrt{\frac{\text{MTOW}}{C_{Lmax}\frac{1}{2}\rho S}} \tag{5.35}$$

The stall speed equals 58.7 m/s, which is much higher than the take-off or landing speed. Therefore the high-lift propellers have to compensate for the low velocity and small wing surface area.

5.4. VERIFICATION & VALIDATION

In this chapter several calculations are performed regarding drag, lift and high-lift propeller performance. To ensure these calculations are correct and applicable to the E-gle, verification and validation are performed. First verification will be done by code verification and calculation verification. Secondly, the aerodynamics calculations are validated to proof that it usable to solve real world problems.

5.4.1. VERIFICATION

To simulate the aerodynamic behaviour of the E-gle during the flight, calculations are done which need to be verified. Verification of the aerodynamics can be done in two steps; code verification and calculation verification. Valid verification provides evidence that the calculations are done correctly.

Code Verification
To check the correctness of several parts of the program independently, a unit test is performed. A valid and successful unit test proves that the code is useful for different inputs. For all codes (cruise, take-off and landing) all units are tested by changing the input values and observing if the output values change as expected, both the deviation as the relation (linear, quadratic, etc) are inspected. The codes perform as expected. An example of the zero-lift drag coefficient's unit test is presented in Table 5.3.

Table 5.3: Unit test for zero-lift drag during cruise

Increased Parameter	Expected Effect	Actual Effect
Altitude	Decrease	Decrease
Velocity	Increase	Increase
Sweep	Decrease	Decrease
Wetted Area	Increase	Increase
Thickness Airfoil	Increase	Increase
Diameter Fuselage	Increase	Increase
Main Wing Surface	Decrease	Decrease
Upsweep Angle	Increase	Increase

It might not be obvious that an increase in wing surface results in a lower zero-lift drag coefficient, however, Equation 5.6 verifies the observation that the zero-lift drag coefficient decreases with increasing surface area due to the fact that the contribution of each component is divided by the reference surface area. Therefore, the result is a lower zero-lift drag coefficient when the surface area increases. The unit test as presented above is also performed for other parts of the code.

Calculation Verification
After code verification has been performed, no program errors remain. However, to be certain that the programs are correct, calculation verification has to be done. During this procedure the problem is solved with very simplistic input values, making it possible to do it by hand as well. These outputs are compared and if they show the same result the code is verified. Calculation verification is done for the aerodynamics program and no errors were found.

5.4.2. VALIDATION

During validation, computational predictions are compared to experimental outcomes and the possible deviations are explained. In this chapter no large models are present but mainly calculations for drag and lift during all flight phases. These calculations are done with the help of literature [16, 21, 30, 35]. It is assumed that these literature sources are reliable. Therefore, no validation will be performed on these studies.

It can however not be assumed that the outcomes of these calculations agree exactly with experimental data. For the computation of the drag and lift, some of the values are obtained through reference data. These data give a very good approximation of certain values for the E-gle, however it will not predict the values exactly. Next to that, assumptions are made in the literature to simplify the calculations in this stage of the design. This results in a small error for the values of the E-gle compared to the final real word data. The sensitivity analysis in Section 13.1 gives an extensive insight in consequences of certain deviations in the design. Eventually, proper testing have to be performed in later design phases to eliminate these small errors.

6

Stability and Control

An important feature of the design of the E-gle is its stability and controllability, both in cruise and during landing and take-off. First of all, the horizontal stabiliser is sized and the wing is placed, to ensure longitudinal stability. Additionally, the vertical stabiliser is sized, taking engine failure into account. Next, the control surfaces (ailerons, elevator and rudder) are sized for the appropriate critical conditions. Finally, both the static and dynamic stability are analysed, making use of the DATCOM method. A general idea of the aircraft lay-out can be seen in Appendix A.

6.1. Horizontal Stabilser Sizing

In this section the stabilser is sized by determining first the most forward and aft c.g. of the aircraft by means of a loading diagram for three different wing positions. Next the stability and controllability line are plotted. Afterwards the final location of the wing and the area of the horizontal stabiliser are determined. Finally the different planform parameters are determined and analysed.

6.1.1. Longitudinal Stability Determination

To ensure static longitudinal stability the tail needs to be sized and the location of the wing needs to be determined, which is done with a loading diagram and scissor plot [36]. First, the c.g. is needed of the OEW to plot the loading diagram. It is important to note that in the current design stage, the fuselage dimensions of the Q300 are used. From this, the centre of gravity of the fuselage can be found and is estimated to be located at 39 percent of the fuselage length from the nose of the aircraft [17]. After this the wing weight from Section 9.2 together with the engine weights is assessed for three different locations being at 30, 40 and 50 percent from the nose. Next, for these different wing locations the total loading plots are created using a Python program after which the location of baggage, seats, fuel and batteries are selected or taken from the Q300. For the mass, baggage is estimated to be 20 kg per person. The passengers including hand luggage are estimated to be around 80 kg [18]. The battery mass and the fuel mass is calculated in Chapter 10. Components are loaded from front to back or from the back to front. Both cases are shown in Figure 6.1. On the x-axis the centre of gravity is shown divided by the MAC and on the y-axis the total weight of the aircraft is shown. The aircraft is loaded in the following order: cargo (baggage), window passengers, aisle passengers, batteries and fuel. The most aft and the most forward c.g. are calculated for the different wing placements and shown in Table 6.1. These values are later used to optimise the horizontal stabiliser size and the main wing position.

Table 6.1: Overview of centre of gravity possition for different wing positions

Wing position [% of L_f]	**Front most c.g.** [X_{cg}/MAC]	**Aft most c.g.** [X_{cg}/MAC]
30	1.529	0.885
40	0.304	-0.19145
50	-0.91938	-1.2768

Next, the stability and controllability of the aircraft are ensured. First the stability line needs to be determined. The formula used to determine the lateral stability is shown in Equation 6.1. The centre of gravity is the same as for the loading diagrams. $C_{L\alpha_h}$ and $C_{L\alpha_{A-h}}$ are calculated with the DATCOM formulae [35] and the selected main wing airfoil. The down wash $d\epsilon/d\alpha$ is estimated for a high wing to be 0.1. The mean aerodynamic chord and the surface of the wing were already determined in Chapter 5. The velocity relation between the horizontal stabiliser and the main wing V_h/V for a high wing is equal to one, due to the fact that the tail is not directly in the wake of the wing. Lastly a margin is added of 5 percent of the MAC to ensure stability.

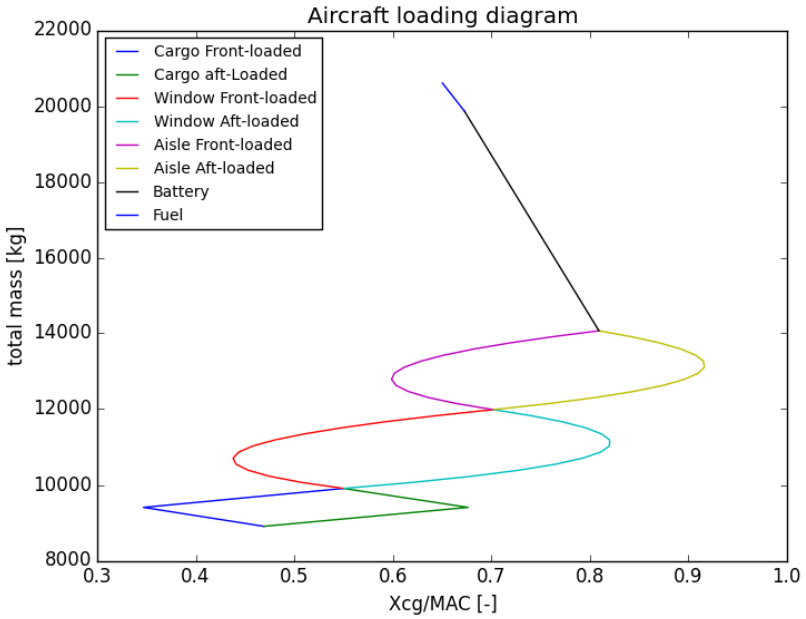

Figure 6.1: Loading diagram for a wing location of 35 percent.

For controllability a different line is plotted, whose formula is shown in Equation 6.2. The moment around the aerodynamic centre ($C_{m_{ac}}$) is a property of the airfoil and different parameters [36]. The lift coefficient of the horizontal tail is estimated using statistical data of fixed tail aircraft. Finally, the two lines can be plotted using a python program. On the x-axis the longitudional position of the centre of gravity divided by the MAC is plotted and on the y-axis the ratio of wing surface area over horizontal stabiliser area is plotted, which is shown in Figure 6.2a. The section above the stability and controllability line is considered stable and controllable. Next the data from Table 6.1 is plotted and visualised in Figure 6.2b. These graphs now can be fitted to achieve an optimal minimum horizontal stabiliser size and wing position. The optimum wing position is where the stability limit crosses the maximum c.g. and where the controllability limit crosses the minimum c.g. This is located at 0.11 Sh/S and a wing leading edge position of 35% of the fuselage length from the nose of the aircraft. The combination of the plots can be seen in Figure 6.3. The minimum and maximum c.g. location graph is shifted down by 0.27 to fit the other graph.

$$\bar{x}_{cg} = \bar{x}_{ac} + \frac{C_{L\alpha_h}}{C_{L\alpha_{A-h}}}\left(1 - \frac{d\epsilon}{d\alpha}\right)\frac{S_h l_h}{S\bar{c}}\left(\frac{V_h}{V}\right)^2 - 0.05 \tag{6.1}$$

$$\bar{x}_{cg} = \bar{x}_{ac} - \frac{C_{m_{ac}}}{C_{L_{A-h}}} + \frac{C_{L_h}}{C_{L_{A-h}}}\frac{S_h l_h}{S\bar{c}}\left(\frac{V_h}{V}\right)^2 \tag{6.2}$$

6.1.2. HORIZONTAL STABILISER PLANFORM

The planform of the horizontal stabiliser is determined in this section. First the airfoil needs to be selected for the horizontal stabiliser. The horizontal stabiliser may not stall before the wing stalls, therefore, a relatively thick airfoil needs to be selected. Also a symmetrical airfoil is preferred, since due to fuel consumption, the c.g. can shift and positive lift is required. For the E-gle this is not very critical, as a low amount of fuel is loaded, but for safety it is still applied. The selected airfoil for the horizontal stabilser is NACA 0012, due to the late stalling behaviour [28, 37].

The wing itself is selected to be a fixed tail, since a high manoeuvrability is not required and this would result into an increase in the weight of the aircraft. Also for a high wing configuration a fixed tail is commonly used. The aspect ratio of the horizontal stabiliser is normally chosen to be two thirds of the aspect ratio of the main wing. However this is structurally not feasible due to the rudder deflection which induces high bending moment on the tail, combined with an elliptical lift distribution not being required for a tail. Thus the final value for the tail aspect ratio is selected to be 6, which is on the high side for tail aspect ratios.

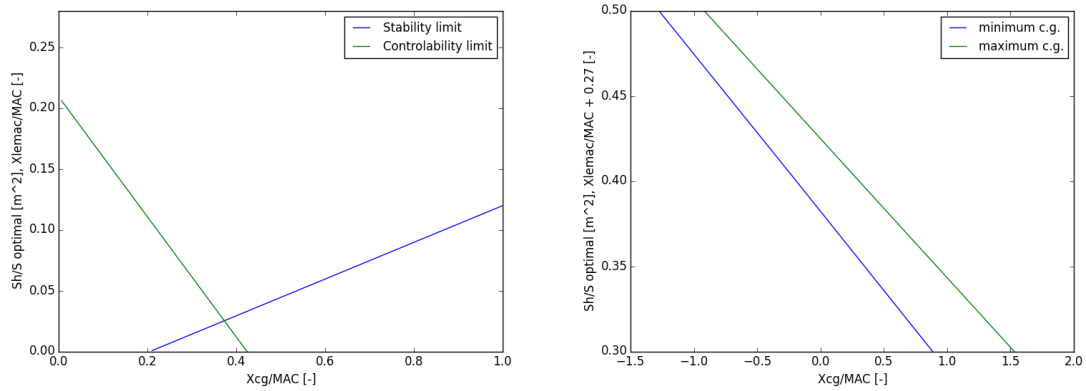

(a) Longitudinal stability and controllability of the aircraft (b) Minimum and maximum centre of gravity locations.

Figure 6.2: Longitudinal stability plots

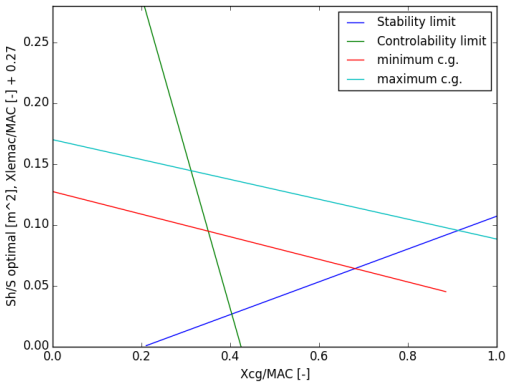

Figure 6.3: Centre of gravity location and stability and controllability combination

The taper ratio of the horizontal stabiliser for low sweep aircraft is normally between 0.7 and 1. For the initial selection a taper ratio is 0.7 selected to maintain structural strength. This number can be tweaked in the final design after more extensive wind tunnel tests. The leading edge sweep of the horizontal stabiliser is selected to be the same as for the main wing, which can also be changed after other components have been designed in more detail or if it increases stability during tests [37]. The dihedral of the tail is not easy to analyse at this stage of design and thus as a first estimate the dihedral is taken to be the same as the main wing, which is 2 degrees.

The location of the horizontal stabiliser depends on the length of the arm, the wing incidence angle and the wing stall angle. For this the horizontal vertical position should be between 2.5 and 4 m height. The formula used for this is depicted in Equation 6.3 and Equation 6.4 [37]. The vertical location of the horizontal wing is placed at the end of the vertical tail and is located at a height of 2.9 m.

$$h_t = l \cdot \tan(\alpha_s - i_w + 3) \tag{6.3}$$

$$h_t = l \cdot \tan(\alpha_s - i_w - 3) \tag{6.4}$$

6.2. VERTICAL STABILISER SIZING

In the following section, the vertical stabiliser is sized. First, the area is determined by analysing the case of engine failure for different flight conditions. Next, the planform is determined using statistical data.

6.2.1. VERTICAL STABILISER AREA

As the engines of the E-gle are located on the wingtips, the case of an engine failure is critical for the sizing of the area of the vertical stabiliser. It has to be able to counteract the moment induced by an engine failure, using a slight angle of attack on the vertical stabiliser and using the rudder. This is done by first selecting an initial area from reference aircraft, which is analysed for different engine failure cases. From statistics, it can be found that the vertical tail volume coefficient for regional turboprop aircraft is 0.8. An estimate of the area can be made by combining this with the previously determined surface area of the main wing, mean chord and the tail arm, which was chosen to be similar to that of the Q300. This results in a preliminary area for the vertical stabiliser of 8.4 m^2. Next, it is checked whether this area is able to withstand an engine failure scenario in take-off, cruise and landing. For this analysis, it is assumed NACA0012 is used as the airfoil for the vertical stabiliser, as explained in Subsection 6.2.2.

Take-Off & Climb
Whenever one of the engines fails during the climb take-off or climb, the flight is aborted as soon as possible. However, regulation require that the aircraft is able to maintain a certain climb angle. As the engines are sized for this condition, this requirement is met. However, the moment this asymmetric thrust induces has to be counteracted. This can be done by deploying the high-lift propellers, as they provide a significant amount of thrust, reducing the moment in two ways. First, the propellers on the side opposite to the working engine directly counteract the moment. The propellers on the side of the working engine allowing to be set to a lower setting, this also reduces the moment as the high-lift propellers have a shorter moment-arm than the main engine. This would require an angle of attack of approximately 3° for the vertical tail, without using the rudder. Using rudder, this lift coefficient can easily be obtained, therefore the vertical stabiliser is sufficiently large for an engine failure in cruise.

Cruise
During cruise, the high-lift propellers can not be used, meaning that the remaining engine has to provide the thrust equal to the drag in cruise. The moment generated from this can then be calculated. This leads to a required vertical fin lift coefficient of 0.53, which requires an angle of attack of around 5° (without rudder). Using rudder, this lift coefficient can easily be obtained, therefore the vertical stabiliser is sufficiently large for an engine failure in cruise.

Descent & Landing
During the approach and landing, the thrust required to be provided by the engines is relatively low, as the aircraft needs to reduce it speed. This means that when one of the engines fails, the high-lift propellers can be switched on, as they also provide a significant amount of thrust. This does, however, mean that the aircraft will have to fly at lower altitude and airspeed, as the high-lift propellers are more efficient in those ranges. As the main engines are not required to produce thrust in this case, no asymmetrical thrust case is present. This implies that a cross-wind landing with one engine inoperative is easier to do compared to a regular aircraft, as the rudder is not used for the asymmetrical thrust and can be fully used to counteract the crosswind. In case additional thrust is required on top of that of the high-lift propellers, the remaining engine can be used, while counteracting the moment it creates with the rudder.

6.2.2. VERTICAL STABILISER PLANFORM

The planform of the vertical stabiliser is determined using statistical data and design methodologies from mulitple aircraft design books [16, 17, 37, 38]. The planform is sized in term of airfoil, sweep, taper and aspect ratio, from which span and chord can be determined.

Airfoil
In order to ensure a symmetrical aircraft about the x-z plane, it is required to have a symmetrical airfoil on the vertical stabiliser. Moreover, the airfoil of the vertical fin is usually thinner than of the wing, in order to prevent compressibility effects. However, the airfoil can not be too thin, as t has to support the horizontal tail. For these reasons, a NACA0012 airfoil is selected.

Sweep
Implementing a sweep angle on the vertical stabiliser increasing the moment arms of the forces acting on both stabiliser, requiring a smaller area. However, it does negatively affect the directional stability of the aircraft, as the mass moment of inertia is increased. Compromising between the two and using reference data, a sweep angle of 35° is selected [37].

Taper
The implementation of taper on the vertical stabiliser allows for the use of sweep and increases directional control and stability of the aircraft, on the other hand, it increases complexity and weight. Reference data indicates a taper between 0.6 and 1 is common for T-tail aircraft [16], leading to a selected taper of 0.7, similar to that of the Q300.

Aspect Ratio
The main advantage of selecting a high aspect ratio for the vertical stabiliser is to increase the aerodynamic efficiency. The major downside is the increased bending moment at the root, and the increased effect of both fatigue and flutter. Reference data indicate the aspect ratio to be between 0.7 and 1.2 for T-tail aircraft [16]. Taking all this into consideration and comparing with references aircraft, gives an aspect ratio for the vertical stabiliser of 1.

Span and Chord
From the aforementioned parameters of the vertical stabiliser, both the span, tip chord, root chord and average chord can be determined from geometry to be 2.9 m, 2.36 m, 3.37 m and 2.9 m, respectively.

Overview
Now that the area and the planform of both the horizontal and vertical stabiliser are determined, the weight can be determined using Equation 6.5 and Equation 6.6 [16]. An overview of the planform parameters of both the horizontal and vertical stabiliser can be seen in Table 6.2.

$$W_h = 0.016(N_z \cdot MTOW)^{0.414} q^{0.168} S_h^{0.896} \left(\frac{100\,t/c}{\cos(\Lambda)}\right)^{-0.12} \left(\frac{A}{\cos^2(\Lambda_h)}\right)^{0.043} \lambda_h^{-0.02} \tag{6.5}$$

$$W_v = 0.073\left(1 + 0.2\frac{H_t}{H_v}\right)(N_z \cdot MTOW)^{0.376} q^{0.122} S_v^{0.873} \left(\frac{100\,t/c}{\cos(\Lambda_v)}\right)^{-0.49} \left(\frac{A}{\cos^2(\Lambda_v)}\right)^{0.357} \lambda_v^{0.039} \tag{6.6}$$

Table 6.2: Overview of horizontal and vertical stabiliser planform parameters

Planform Parameter	Unit	Horizontal Stabiliser	Vertical Stabiliser
Airfoil	-	NACA0012	NACA0012
Area	m^2	4.29	8.4
Aspect Ratio	-	6	1
Taper Ratio	-	0.7	0.7
Sweep	deg	4	35
Span	m^2	5.08	2.9
Average Chord	m	0.846	2.9
Weight	N	1118	4155

6.3. CONTROL SURFACE SIZING

It is of high importance that the aircraft is controllable in all necessary flight conditions, for which the control surface has to be sized accordingly. The following section focuses on the sizing of the ailerons, elevator and rudder, for their respective critical control conditions.

6.3.1. AILERON SIZING

The ailerons are located at the trailing edge of each main wing and used to control the roll motion. The roll motion is a movement around the aircraft's longitudinal axis which often results in a change in flight path. The ailerons are located on the outer portion of the wing to generate a more effective roll moment. The effectiveness is dependent on how good the operating aileron is at generating a desired rolling moment. The produced rolling moment is a function of aileron deflection, size and location compared to fuselage centre line. Since the effect of the control surfaces is lowest at lower velocity, the ailerons will be designed for the take-off phase. The E-gle is a class II aircraft and the critical take-off phase results in a required bank angle of 30 degrees in 1.8 seconds [37]. Because it is not desired to over design the ailerons due to cost and complexity, the time to achieve the bank angle has to be just below 1.8 seconds.

When the aileron has maximum deflection, the aircraft rolling moment (L_A) is given by Equation 6.7. C_{rl} is the aircraft rolling moment coefficient when the aileron has maximum deflection and can be obtained by Equation 6.8. The maximum deflection of the aileron is δ_A and $C_{l_{\delta A}}$ is the aileron rolling moment coefficient derivative calculated with Equation 6.9.

$$L_A = \frac{1}{2}\rho V_{TO}^2 \cdot SC_{rl}b \tag{6.7}$$

$$C_{rl} = C_{l_{\delta A}}\delta_A \tag{6.8}$$

$$C_{l_{\delta A}} = \frac{2C_{L_{\alpha_w}}\tau C_r}{Sb}\left[\frac{y^2}{2} + \frac{2}{3}\left(\frac{\lambda - 1}{b}\right)y^3\right]_{y_i}^{y_o} \tag{6.9}$$

The outer (y_o) and inner span (y_i) location of the aileron determine the location on the main wing's span. $C_{L_{\alpha_w}}$ is the lift slope of the main wing and τ is the aileron effective parameter depending on the aileron-to-wing chord ratio. The aircraft rolling moment is used to generate the steady-state roll rate (P_{ss}) in Equation 6.10.

$$P_{ss} = \sqrt{\frac{2 \cdot L_A}{\rho(S_w + S_h + S_{vt})C_{D_R} \cdot y_D^3}} \tag{6.10}$$

The wing horizontal/tail vertical tail rolling drag coefficient (C_{D_R}) is chosen from reference data [37]. The parameter y_D is defined as the distance between the rolling drag center and the aircraft's center of gravity. The bank angle (Φ_1) when the aircraft reaches the steady-state roll rate is defined by Equation 6.11. The mass moment of Inertia around the roll axis is defined by Equation 6.12 [16]. The non dimensional radii of gyration ($\vec{R}$) is based on reference aircraft [16].

$$\Phi_1 = \frac{I_{xx}}{\rho y_D^3(S_w + S_h + S_{vt})C_{D_R}} \ln\left(P_{ss}^2\right) \tag{6.11}$$

$$I_{xx} = \frac{b^2 W \vec{R}_x^2}{4g} \tag{6.12}$$

$$\dot{P} = \frac{P_{ss}^2}{2\Phi_1} \tag{6.13}$$

$$t_2 = \sqrt{\frac{2\Phi_{des}}{\dot{P}}} \tag{6.14}$$

The aileron rolling moment produces an aircraft rate of roll rate ($\dot{P}$) which is valid until the steady-state roll rate is reached. The aircraft rate of roll rate is given by Equation 6.13 and determines the rolling speed. The time needed to reach the required bank angle of 30 degrees can be found with Equation 6.14. Now it can be checked if the size of the aileron is sufficient to meet the requirements. The aileron geometry is given in Table 6.3.

Table 6.3: Aileron characteristics

Parameter	Unit	Value
δ_a	deg	30
b_a	m	4.598
y_o	m	11.86
y_i	m	7.26
c_a	m	0.488
S_a	m^2	4.49
t_2	sec	1.79

6.3.2. ELEVATOR SIZING

The elevators are used to pitch the aircraft up and down and have to designed such that they can pitch the aircraft up enough during take-off and trim the aircraft during flight. This method is combined with statistical data to size the elevators [37]. Firstly, from statistics it can be determined that the maximum negative and positive elevator deflections are -30° and 20°, respectively. Moreover, the elevator span to tail span ratio ranges from 0.8 to 1. Since the tail is relatively small, a value of 1 is selected, to provide sufficient elevator area.

The pitching moment that has to be applied to the aircraft in order to take off is likely to be the most limiting case for the elevator. The average angular pitch acceleration for large transport aircraft is around $5°/s^2$. In order to make an estimation for the required elevator parameters, all the moments acting on the aircraft during take-off need to be determined, as seen from the position of the main landing gear. These moments consist of the weight, the lift, the drag, the aerodynamic moment, the thrust, the ground friction, the moment due to the acceleration and moment due to the rotation. This can be done by calculating the forces and acceleration they are due to, which can be combined with the aircraft dimensions. From this, the required lift from the horizontal tail is found using Equation 6.15, where I_{yy} is determined using Equation 6.16 and R_y is estimated to be 0.34 for a regional turboprop [16].

$$L_h = \frac{M_L + M_D + M_T + M_W + M_{ac} + M_a - I_{yy}\ddot{\theta}}{x_{ac_h} - x_{lg}} \quad (6.15)$$

$$I_{yy} = \frac{2 l_f W R_y^2}{4g} \quad (6.16)$$

Next, the angle of attack effectiveness of the elevator (τ_e) can be determined using Equation 6.17. Here, the elevator deflection is assumed to be the maximum negative value of -30 °. The angle of attack of the horizontal tail is calculated using an estimation for the downwash, based on the planform parameters.

$$C_{Lh} = C_{L_{\alpha_h}} (\alpha_h + \tau_e \delta_e) \quad (6.17)$$

Once the angle of attack effectiveness of the elevator is determined, the required chord of the elevator, compared to that of the horizontal tail can be obtained from Figure 6.4. From this, it can be concluded that the chord of the elevator is half of that of the horizontal tail, which is around the highest it can get. This was expected, as the horizontal tail has a small surface area and the engine provide a pitch down moment, due to the high wing configuration.

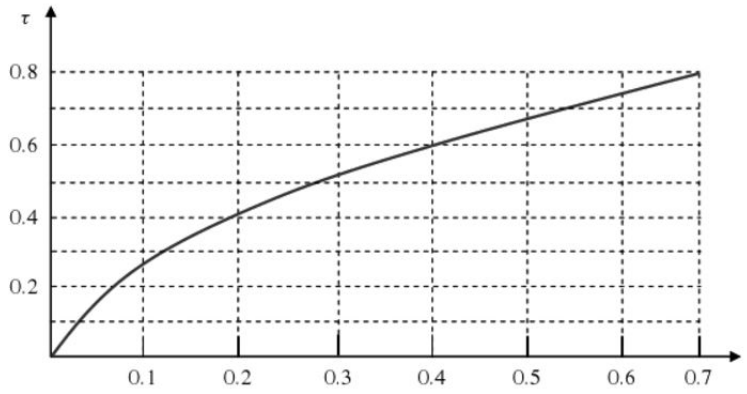

Figure 6.4: Angle of attack effectiveness as a function of elevator chord to tail chord ratio

Now that the elevator is sized for take-off, it has to checked whether this is sufficient for trimming the aircraft in flight. This is done by plotting the elevator deflection curve, indicating the required elevator deflection for a certain airspeed. The elevator deflection can be calculated using Equation 6.18, in which the parameters can be estimated using Equation 6.18 through Equation 6.21.

$$\delta_e = \frac{\left(\frac{Tz_T}{\bar{q}S\bar{c}} + C_{m_0}\right) C_{L_\alpha} + (C_L - C_{L_0}) C_{m_\alpha}}{C_L C_{m_{\delta_e}} - C_{m_\alpha} C_{L_{\delta e}}} \quad (6.18)$$

$$C_{m_\alpha} = C_{L_{\alpha_w}} (x_{ac} - x_{cg}) - C_{L_{\alpha_h}} \frac{S_h l_h}{S\bar{c}} \left(1 - \frac{d\epsilon}{d\alpha}\right) \quad (6.19)$$

$$C_{m_{\delta_e}} = -C_{L_h} V_h \tau_e \frac{b_e}{b_h} \quad (6.20)$$

$$C_{L_{\delta_e}} = C_{L_h} \tau_e \frac{b_e}{b_h} \frac{S_h}{S} \quad (6.21)$$

The elevator deflection curves for both take-off and cruise condition can be seen in Figure 6.5. Note that the most front and most aft centre of gravity position during flight are very similar, as only a small amount of fuel is consumed.

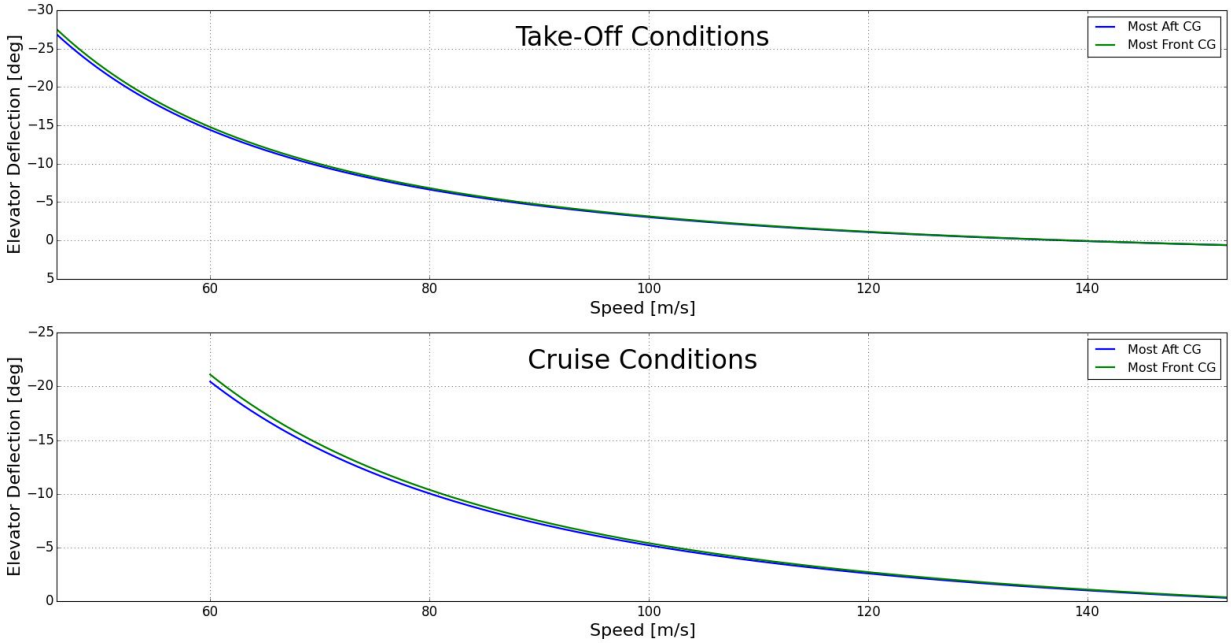

Figure 6.5: Elevator deflection as a function of airspeed for different centre of gravity positions and flight conditions

Form these graphs, it can be observed that the required elevator deflections for both the front and aft centre of gravity positions do not exceeded the aforementioned maximum deflections. It can therefore be concluded that the elevator is adequately sized. Moreover, it can be observed that the required elevator deflection becomes less negative when the airspeed increases. This implies that the derivative $d\delta_e/dV$ is positive, from which it can be concluded that the aircraft is statically stable.

6.3.3. RUDDER SIZING

Normally the aircraft's rudder is sized to prevent one engine failure and crosswind landing and take-off. Because the vertical tail has already been designed to keep the aircraft operative during one engine failure, the rudder will not be designed for it either. Therefore, the rudder is only designed to counteract crosswind.

To cope with crosswind, the rudder has to be able to keep the aircraft in a straight line over the runway during take-off and landing. The maximum cross-wind (V_W) considered is 30 knots (15.4 m/s). First, the corresponding sideslip angle (β) and total airspeed (V_T) can be calculated from geometry. The total airspeed is the vector sum of the cross-wind with the velocity of the aircraft. As critical speed $0.8V_{TO}$ is considered because also before the aircraft has taken off a straight line over the runway has to be fulfilled. Next, the aircraft side area (S_S) and its centre with respect to the centre of gravity (d_c) can be determined from aircraft geometry. Finally, a preliminary estimation of several stability derivatives has to be made, using Equation 6.22 to Equation 6.25 [37]. From reference data it is determined that the rudder span to vertical tail span ratio (b_R/b_V) is around 0.7, the vertical tail efficiency (η_V) is 0.97 and the angle of attack effectiveness of the rudder (τ_r) is 0.52, as obtained from the rudder chord to vertical chord ratio. The initial rudder chord is chosen from reference aircraft, however, it is changed when the rudder does not perform satisfactory in one of the critical cases. The maximum rudder deflection is set to be 30 degrees.

$$C_{n_\beta} = 0.8 C_{L_{\alpha_V}} \left(1 - \frac{d\sigma}{d\beta}\right) \eta_V V_V \tag{6.22}$$

$$C_{y_\beta} = -1.2 C_{L_{\alpha_V}} \left(1 - \frac{d\sigma}{d\beta}\right) \eta_V \frac{S_V}{S} \tag{6.23}$$

$$C_{n_{\delta_r}} = C_{L_{\alpha_V}} \eta_V \tau_R V_V \frac{S_V}{S} \tag{6.24}$$

$$C_{y_{\delta_r}} = C_{L_{\alpha_V}} \eta_V \tau_R \frac{b_R}{b_V} \frac{S_V}{S} \tag{6.25}$$

Next, Equation 6.26 and Equation 6.27 can be set up, which are dependent on both the rudder deflection (δ_r) and the crab angle (σ), which can be solved simultaneously in order to obtain the required rudder deflection [37].

$$\frac{1}{2}\rho b S V_T^2 \left(C_{n_o} + C_{n_\beta}(\beta - \sigma) + C_{n_{\delta r}}\delta_r\right) + \frac{1}{2}\rho C_{D_y} S_S V_W^2 d_c \cos(\sigma) = 0 \tag{6.26}$$

$$\frac{1}{2}\rho C_{D_y} S_S V_W^2 - \frac{1}{2}\rho S V_T^2 \left(C_{y_o} + C_{y_\beta}(\beta - \sigma) + C_{y_{\delta_r}}\delta_r\right) = 0 \tag{6.27}$$

From these equations a rudder deflection of 7.8 degrees follows. This means that the current design of the rudder is able to withstand cross-wind during take-off and landing.

6.4. DYNAMIC STABILITY ANALYSIS

In order to analyse the dynamic stability behaviour of the aircraft, the stability derivatives are determined using the DATCOM method. Using this, the longitudinal and lateral dynamic behaviour of the aircraft can be determined.

6.4.1. STABILITY DERIVATIVES

The dynamic stability is analysed using the DATCOM method [35, 39]. This method requires the weight of the aircraft, the planform of the aircraft and the main parameters concerning the control surfaces. These values can be obtained from the design of the multiple subsystems and from the CATIA drawings. Moreover, the flight conditions during each of the separate flight phases is required, as can be obtained from the performace analysis. A general overview of the planform used during the DATCOM anaylsis can be seen in Figure 6.6.

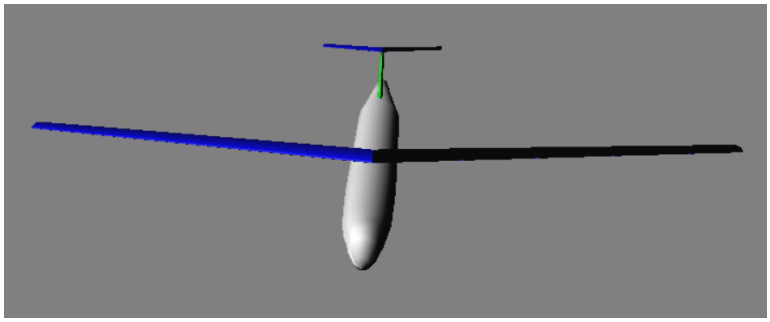

Figure 6.6: Overview of the input surface in DATCOM

From all the aforementioned data, a large quantity of the stability derivatives of the aircraft can be determined, as can be seen in Table 6.4. It is important to note that the values can diverge from the actual ones, they do, however, give an indication whether the aircraft is stable or not.

Table 6.4: DATCOM dynamic stability derivatives

C_{m_α} = 0.5524	C_{y_β} = -0.595	C_{l_β} = 0.0112	C_{n_β} = -0.2449
$C_{m_{\dot{\alpha}}}$ = -3.934	C_{y_p} = -0.0569	C_{l_p} = -0.688	C_{n_p} = -0.0872
C_{m_q} = -2.731	C_{y_r} = -	C_{l_r} = 0.0406	C_{n_r} = -0.0082
$C_{m_{\delta_e}}$ = -0.00694	$C_{y_{\delta a}}$ = -	$C_{l_{\delta_a}}$ = -0.2614	$C_{n_{\delta_a}}$ = 0
	$C_{y_{\delta_r}}$ = -	$C_{l_{\delta_r}}$ = -	$C_{n_{\delta_r}}$ = -0.001047

An important remark on Table 6.4, is that C_{n_β} is often not calculated correctly by DATCOM. Comparisons have shown deviations between DATCOM estimations and real world values. For example, the C-172 is calculated to have a negative C_{n_β}, whereas in reality this value is found to be positive [40]. This might be, because DATCOM can not handle high wings for this specific value. Therefore, the value of C_{n_β} is calculated using the formula presented in Equation 6.22.

6.4.2. LONGITUDINAL STABILITY

Once the aerodynamic derivatives are known using the procedure explained in Subsection 6.4.1, the stability of the design can be investigated. If, after a small deviation from the equilibrium due to a disturbance, the system returns to its original condition the design is considered stable. If the system deviates even more from its equilibrium state it is said to be unstable. When nothing happens after a deviation from the equilibrium state, the system is neutrally stable. In order to analyse the eigenmodes of the aircraft, the non-dimensionalised masses and inertias are needed, as can be calculated using Equation 6.28 through Equation 6.33.

$$\mu_c = \frac{m}{\rho S \bar{c}} \tag{6.28}$$

$$\mu_b = \frac{m}{\rho S b} \tag{6.29}$$

$$K_X^2 = \frac{I_{xx}}{mb^2} \tag{6.30}$$

$$K_Y^2 = \frac{I_{yy}}{m\bar{c}^2} \tag{6.31}$$

$$K_Z^2 = \frac{I_{zz}}{mb^2} \tag{6.32}$$

$$K_{XZ} = \frac{J_{xz}}{mb^2} \tag{6.33}$$

The homogeneous form of the equations of motion for a disturbed symmetric aircraft [41] are presented in matrix form in Equation 6.34.

$$\begin{bmatrix} C_{X_u} - 2\mu_c D_C & C_{X_\alpha} & C_{Z_0} & 0 \\ C_{Z_u} & C_{Z_\alpha} + (C_{Z_{\dot{\alpha}}} - 2\mu_c) D_c & -C_{X_0} & C_{Z_q} + 2\mu_c \\ 0 & 0 & -D_c & 1 \\ C_{m_u} & C_{m_\alpha} + C_{m_{\dot{\alpha}}} D_c & 0 & C_{m_q} - 2\mu_c K_Y^2 Dc \end{bmatrix} \begin{bmatrix} \hat{u} \\ \alpha \\ \theta \\ \frac{q\bar{c}}{V} \end{bmatrix} = \underline{0} \tag{6.34}$$

These equations are used to determine the longitudinal stability of the E-gle. Because DATCOM does not deliver derivatives in X and Z direction and only a preliminary estimation of the stability of the aircraft is required, the equations are going to be simplified for each eigenmotion [41]. Two different oscillations will be discussed; the short period and the phugoid motion. The phugoid motion is a relatively slow and lightly damped oscillation. The short period motion has a shorter period and is highly damped compared to the phugoid.

Short Period Motion

To determine the short period's stability, Equation 6.34 will be simplified. The first approximation made is that the airspeed remains constant during the motion, this eliminates the first column. This implies that also the forces in X-direction become zero meaning the first row disappears. Secondly, it is assumed that the initial steady flight condition is level, resulting in the negation of the third column. The third and last assumption made is that during the short period motion, the trajectory of the E-gle is a straight line. As a result the second row can be omitted. Equation 6.35 shows the results of these simplifications.

$$\left(C_{m_\alpha} + C_{m_{\dot{\alpha}}} D_c + C_{m_q} D_c - 2\mu_c K_Y^2 D_c^2\right)\theta = 0 \tag{6.35}$$

From this the characteristic equation can be derived to find the eigenvalues of the short period motion. The design is stable in this specific motion if the real parts of the complex eigenvalues and all real eigenvalues are negative. This would result in the disturbed motion to converge back to the original conditions. The characteristic equation is shown in Equation 6.36. From this equation the eigenvalues are obtained and presented in Table 6.5. Because the eigenvalues are complex and contain a negative real part, the short period motion is said to be stable.

$$\left(-2\mu_c K^2\right)\lambda_c^2 + (C_{m_{\dot{\alpha}}} + C_{m_q})\lambda_c + C_{m_\alpha} = 0 \tag{6.36}$$

Phugoid Motion
The phugoid will follow the same procedure as the short period motion by simplifying Equation 6.34. The first assumption made is that the angle of attack remains constant during the whole motion resulting in the omission of the second column. secondly, the pitch rate is said to be constant during the motion resulting in neglecting the fourth row. Next, it is assumed that C_m and C_{X_0} are zero. The last simplification is the negation of C_{Z_q} because it is much smaller than $2\mu_c$. These approaches result in Equation 6.37.

$$\begin{bmatrix} C_{X_u} - 2\mu_c D_C & C_{Z_0} & 0 \\ C_{Z_u} & 0 & 2\mu_c \\ 0 & -D_c & 1 \end{bmatrix} \begin{bmatrix} \hat{u} \\ \theta \\ \frac{q\bar{c}}{V} \end{bmatrix} = \underline{0} \tag{6.37}$$

From this matrix the quadratic characteristic equation is derived to obtain the eigenvalues of the phugoid motion. This characteristic equation is shown in Equation 6.38 and the corresponding eigenvalues are presented in Table 6.5. These eigenvalues are determined by applying the following approximations in Equation 6.39 to Equation 6.41 [41]. Because the eigenvalues are complex and contain negative real parts, the phugoid motion is stable.

$$\left(-4\mu_c^2\right)\lambda_c^2 + \left(2\mu_c C_{X_u}\right)\lambda_c - C_{Z_u}C_{Z_0} = 0 \tag{6.38}$$

$$C_{X_u} = -2C_D \tag{6.39}$$

$$C_{Z_0} = -C_L \tag{6.40}$$

$$C_{Z_u} = -2C_L \tag{6.41}$$

6.4.3. LATERAL STABILITY

Next, the lateral stability of the aircraft can be determined, using the stability derivatives calculated previously. The asymmetric equations of motions of the aircraft can be seen in homogeneous form in Equation 6.42.

$$\begin{bmatrix} C_{Y_\beta} + (C_{Y_{\dot{\beta}}} - 2\mu_b)D_b & C_L & C_{Y_p} & C_{Y_r} - 4\mu_b \\ 0 & -0.5D_b & 1 & 0 \\ C_{l_\beta} & 0 & C_{l_p} - 4\mu_b K_X^2 D_b & C_{l_r} + 4\mu_b K_{XZ} D_b \\ C_{n_\beta} + C_{n_{\dot{\beta}}} D_b & 0 & C_{n_p} + 4\mu_b K_{XZ} D_b & C_{n_r} - 4\mu_b K_Z^2 D_b \end{bmatrix} \begin{bmatrix} \beta \\ \varphi \\ \frac{pb}{2V} \\ \frac{rb}{2V} \end{bmatrix} = \underline{0} \tag{6.42}$$

These equations of motion are used to determine the dynamic behaviour of three eigenmotions of the aircraft, namely the Dutch roll, the aperiodic roll and the spiral motion.

Dutch Roll Motion
The first asymmetrical eigenmotion is the Dutch roll. In order to obtain its eigenvalues, the assumption is made that no rolling motion occurs during this eigenmode. This implies that both the second and third equations can be omitted, as well as the second and third column. Furthermore, the assumption is made that all the second order derivatives (with respect to the time derivative of β) are equal to zero, leaving the equations of motion in the form of Equation 6.43.

$$\begin{bmatrix} C_{Y_\beta} - 2\mu_b D_b & -4\mu_b \\ C_{n_\beta} & C_{n_r} - 4\mu_b K_Z^2 D_b \end{bmatrix} \begin{bmatrix} \beta \\ \frac{rb}{2V} \end{bmatrix} = \underline{0} \tag{6.43}$$

The eigenvalues of this matrix equation can be found by solving Equation 6.44.

$$\left(8\mu_b K_Z^2\right)\lambda_b^2 - \left(2\mu_b\left(C_{n_r} + 2K_Z^2 C_{Y_\beta}\right)\right)\lambda_b + 4\mu_b C_{n_\beta} + C_{Y_\beta} C_{n_r} = 0 \tag{6.44}$$

The eigenvalues resulting from this can be seen in Table 6.5. It can be observed that the Dutch roll is a periodic eigenmotion, as the eigenvalues contain an imaginary part. Moreover, the Dutch roll can be assumed to be stable, as the real part of the eigenvalues is negative.

Aperiodic Roll Motion
The second asymmetrical eigenmotion is the aperiodic roll and is characterised by the motion after an input of the ailerons. The ailerons cause a rolling moment, resulting in a higher lift on the wing the aircraft is rolling to. This causes a rolling moment opposite to the already occurring moment. In other words, the initial rolling moment is damped out.

Because the aperiodic roll is a very fast motion, there will be no time for yaw or sideslip effects to appear. Therefore, and r equal zero. Due to the very fast motion, the equations for the yawing moment and lateral forces (rows 1 and 4) can be omitted. This results in Equation 6.45. From this equation the eigenvalue can be determined with Equation 6.46.

$$(C_{l_p} - 4\mu_b K_X^2 D_b)\frac{pb}{2V} = 0 \tag{6.45}$$

$$\lambda_b = \frac{C_{l_p}}{4\mu_b K_X^2} \tag{6.46}$$

The value for C_{l_p} was determined by DATCOM in Subsection 6.4.1 and is given in Table 6.4. The motion of the aperiodic roll is shown in Table 6.5 and the eigenvalue only consists of a real negative part. This means no oscillation occurs but only a converging damping motion.

Spiral Motion
The third and last asymmetrical eigenmotion is the spiral motion. As this motion is very slow, linear and angular acceleration can be neglected, only leaving the time derivative accompanied to the kinematic equation. Furthermore, the derivatives of C_Y with respect to the roll rate and the yaw rate can be omitted, this results in the system of equations as can be seen in Equation 6.47.

$$\begin{bmatrix} C_{Y_\beta} & C_L & 0 & -4\mu_b \\ 0 & -0.5D_b & 1 & 0 \\ C_{l_\beta} & 0 & C_{l_p} & C_{l_r} \\ C_{n_\beta} & 0 & C_{n_p} & C_{n_r} \end{bmatrix} \begin{bmatrix} \beta \\ \varphi \\ \frac{pb}{2V} \\ \frac{rb}{2V} \end{bmatrix} = \underline{0} \tag{6.47}$$

As there is only one time derivative in the system of equations, the eigenvalue can be determined easily using Equation 6.48.

$$\lambda_b = \frac{2C_L\left(C_{l_\beta}C_{n_r} - C_{n_\beta}C_{l_r}\right)}{C_{l_p}\left(C_{Y_\beta}C_{n_r} + 4\mu_b C_{n_\beta}\right) - C_{n_p}\left(C_{Y_\beta}C_{l_r} + 4\mu_b C_{l_\beta}\right)} \tag{6.48}$$

As can be seen in Table 6.5, the eigenvalue has a very small positive value. This mean that the aircraft has an unstable spiral motion. However, as previously mentioned, the spiral motion is a very slowly progressing motion. This means that the pilot has a long time to correct for the aircraft entering a spiral, and thus it does not pose a threat to the aircraft safety. In fact, an unstable spiral is not uncommon for aircraft, however, it is important that the pilots are aware that the aircraft has this property.

Overview
In Table 6.5, an overview of all the parameters of the various eigenmotions can be seen. As discussed in the preceding paragraphs, all modes except the spiral motion are stable. Moreover, the table shows the period, natural frequency, damping coefficient and time to halve the amplitude for each of the eigenmotions. As expected, the short period has a high natural frequency and a short half-time, whereas the phugoid has a low frequency and a large half-time.

6.5. VERIFICATION & VALIDATION

For the stability and control of the E-gle, verification and validation is performed to check if the codes are correct and if the designs meet their specifications and requirements. First verification will be done for the horizontal and vertical stabiliser, followed by the control surfaces, finishing with the dynamic stability. Finally, validation will be discussed for all of these fields.

Table 6.5: Overview of the eigenvalues of the various eigenmodes

Eigenmode	Eigenvalue [-]	Period [s]	Half-Time [s]	Natural Frequency [rad/s]	Damping [-]
Short Period	$-0.00181 \pm 0.0252\,j$	2.90	4.45	2.17	0.07
Phugoid	$-3.77 \cdot 10^{-5} \pm 0.00120\,j$	60.8	214	0.103	0.03
Dutch Roll	$-0.00228 \pm 0.0784\,j$	14.0	53.0	0.45	0.029
Aperiodic Roll	-0.484	-	0.25	2.78	0.70
Spiral	$9.81 \cdot 10^{-3}$	-	-	0.0056	-0.031

6.5.1. VERIFICATION

In Section 6.1 the size of the horizontal stabiliser is determined by producing a loading diagram and a scissor plot. Numerical examples are available for these diagrams and plots [36]. Values of these examples are implemented in the produced codes and exactly the same results come out as in the examples. Because the results from the code for the loading diagram and the scissor plot correspond exactly to the example's outcomes, the codes are verified.

The control surfaces are designed in Section 6.3 and checked if they meet certain requirements. These designs rely on methods presented in literature [37]. Numerical examples are presented in this study which are used to verify the calculations for the control surfaces. Using the same inputs in the codes as in the examples of the literature results in exactly the same outputs. To conclude, the calculations for the control surfaces are verified.

In order to verify the stability derivatives calculated using the DATCOM method, some of the derivatives can be calculated by hand. This can be done using Equation 6.22 to Equation 6.25 and Equation 6.49 to Equation 6.51.

$$C_{m_\alpha} = C_{N_\alpha} \frac{x_{cg} - x_{ac}}{\bar{c}} - C_{N_{\alpha_h}} \left(1 - \frac{d\epsilon}{d\alpha}\right) \left(\frac{Vh}{V}\right)^2 \frac{S_h l_h}{S\bar{c}} \tag{6.49}$$

$$C_{m_q} = -1.1 C_{N_{\alpha_h}} \left(\frac{V_h}{V}\right)^2 \frac{S_h^2 l_h}{S\bar{c}^2} \tag{6.50}$$

$$C_{m_{\dot{\alpha}}} = -C_{N_{\alpha_h}} \left(\frac{V_h}{V}\right)^2 \frac{d\epsilon}{d\alpha} \frac{S_h l_h^2}{S\bar{c}^2} \tag{6.51}$$

Most of the stability derivatives calculated by hand have the same sign and order of magnitude as the ones obtained from DATCOM. This is considered to be sufficient to regard the method as verified, as stability derivatives are difficult to accurately predict without using wind tunnel test or CFD methods. The only stability derivative showing significant deviation is C_{n_β}. As discussed in Subsection 6.4.1, this is a recurring problem of the DATCOM method, resulting in the use of the analytically obtained value for this stability derivative.

6.5.2. VALIDATION

The calculations performed to obtain values for the stabilisers and control surfaces are presented by literature [36, 37]. These literature sources are assumed to be reliable, therefore no validation will be performed regarding these sources. However, it has to be taken into account that these methods are partially based on reference aircraft data, meaning the outcome of the calculations will not perfectly match the final real world performance. Therefore, proper testing is required before the aircraft is taken into use.

In order to validate the DATCOM method, a comparison between the determined values and real world values is made [40]. It can be seen that almost all the determined stability derivatives have the same sign and order of magnitude as the real world values. Moreover, the values obtained for the analysis of the E-gle and other aircraft were analysed. This leads to the conclusion that both the DATCOM method and the numerical model of the E-gle modelled into it are validated.

7

PROPULSION

In this chapter, the propulsion system of the E-gle is discussed. Firstly, the system description is given in Section 7.1. Section 7.2 presents the analysis of the propellers. Then in Section 7.3, the performance of a component of the chosen concept, the gas turbines, is discussed. Furthermore, in Section 7.4, selection of electric motors is performed. Finally, the complete propulsion architecture is illustrated in Section 7.6.

7.1. PROPULSION SYSTEM DESCRIPTION

The propulsion system of the E-gle consists of two parts. A parallel turbo-electric hybrid system consisting of turboprop engine and electric motors to generate thrust by powering the two thrust propellers placed at the wing tips and a DEP high-lift propeller system, wherein the DEP propellers are driven by electric motors. These systems are discussed in Subsection 7.1.1 and Subsection 7.1.2.

7.1.1. TURBO-ELECTRIC HYBRID SYSTEM

In the parallel hybrid propulsion system, the electric motor works in conjunction with the gas turbine, that is both the mechanical power output and the electrical power output are connected in parallel to drive the thrust propeller. The electric motor is mounted to the existing propeller shaft and may either add power to the propeller shaft from the battery, or charge the battery by acting as a generator and capturing power from the turbine. Figure 7.1 shows a diagram of a parallel hybrid system. One important advantage of this system is that since the electric motor is added to the propulsion system, less power output is required from the turboprop engine and thus the engine can be lighter and cheaper with a lower power output yielding lower specific fuel consumption. Another advantage is that it benefits from redundancy because of the two separate power trains [42, 43].

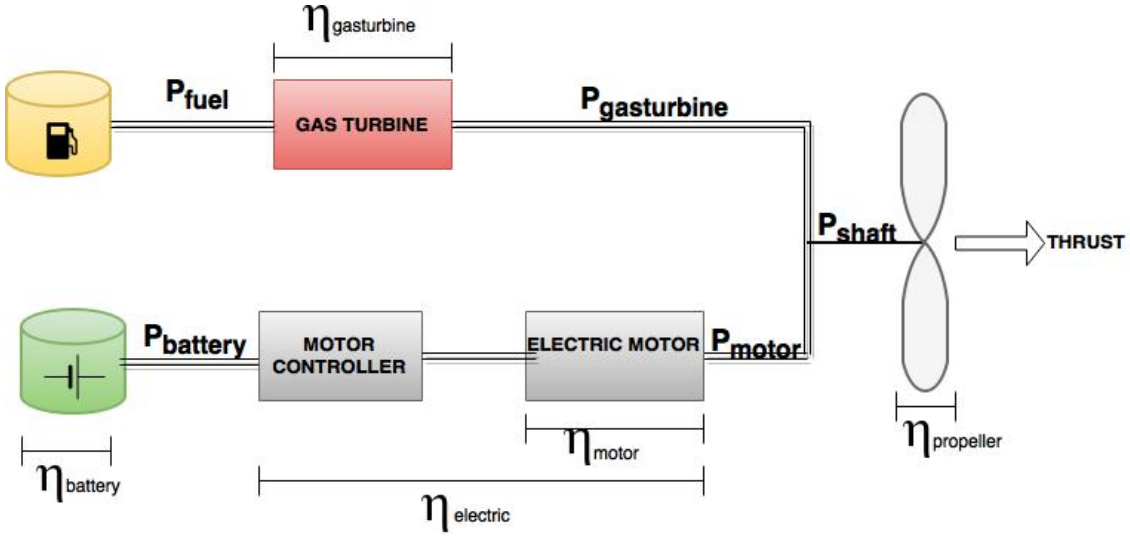

Figure 7.1: Concept 3 architecture; parallel turbo-electric configuration

This configuration despite of the many advantages, is accompanied by a small drawback of increased complexity of mechanical coupling because power has to be regulated and blended from the two power sources. This problem is solved by adding a clutch to the parallel system between the electric motor and the gas turbine. This makes it possible to have either electric motor only mode, gas turbine only mode or a combination of both. A combination of both turbine and motors working is used in the more power intensive phases of the flight such as during takeoff. During cruise, since the power required for thrust generation is much lower it sufficient to keep either one of the power trains operating while the other one can stay off or in flight idle condition in case of the gas turbine. The flight idle condition is when the gas turbine is set on lowest allowable power setting.

During the electric motor only mode, the system runs completely on battery power, during which the clutch will disengage the turbine from the propeller shaft. Another option is for the turbine to spin with the propeller while the electric motor is disconnected from the shaft, this way of operating adds parasitic frictional drag to the propulsion system and hurts efficiency and hence is not preferred.

A second option is to use the system as a power assist hybrid wherein the propulsion system is always powered by the turbine, with the electric motor only providing a boost in power during certain phases of flight. In all of the modes, the motor can be used to provide power during certain phase of the flight, and then be used as a generator in another phase of the flight to recharge the batteries. During the mission profile optimisation of the E-gle discussed in Chapter 10, it is seen that it is most efficient to have the cruise phase assisted by battery power while the gas turbine remains in flight idle. Design of the gas turbine and electric motors for the parallel hybrid system are further discussed in Section 7.3 and Section 7.4. Detailed analysis of the turboprop engine propellers is performed in Subsection 7.2.1.

7.1.2. DEP HIGH-LIFT PROPELLER SYSTEM

Although the primary function of propellers is typically to generate thrust, the E-gle equipped with distributed electric propulsion will also utilise propellers whose main purpose will be to function as high-lift devices. These "high-lift propellers" distributed over the wing's leading edge, act as a form of high lift device by increasing the dynamic pressure over the sections of the wing in the propeller's slipstream, thus increasing the total lift produced [33]. Similar to conventional high lift devices, these propellers are only operated at low speeds such as take-off and during high speed flight (cruise), they are folded and stowed against the nacelles to reduce drag. Using high-lift propellers will result in relatively small wings that will require blowing from propellers to meet the low-speed performance requirements. These propellers are driven by electric motors which are powered by batteries. A detailed analysis of the high lift propellers is carried out in Subsection 7.2.2 to determine their power, torque and sizing requirements. Based on the power requirements, the electric motor sizing is performed in Subsection 7.4.4. An illustration of the high lift propeller system is shown in Figure 7.2.

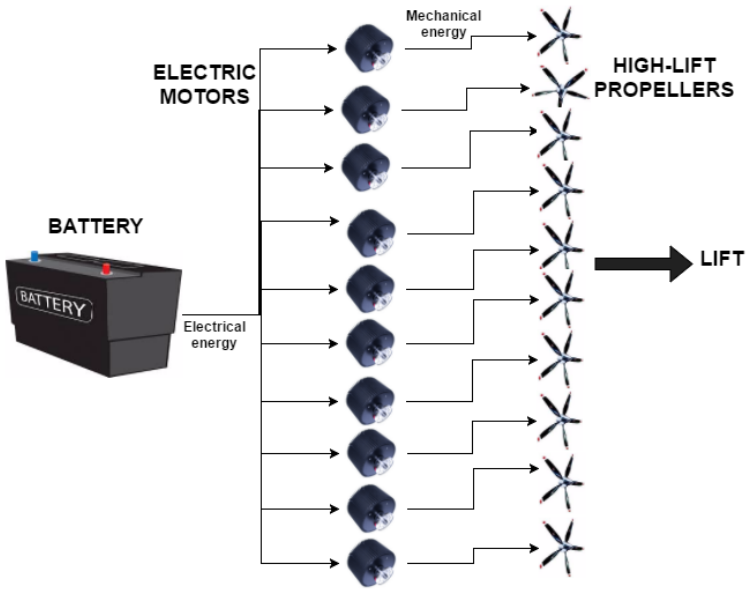

Figure 7.2: DEP high lift propeller system powered by electric motors

7.2. PROPELLERS

In this section the propeller performance will be determined for the thrust propellers in Subsection 7.2.1 and for the high lift propellers in Subsection 7.2.2. After that the way the propeller geometry is determined for both propellers is shown in Subsection 7.2.3 and the folding mechanism for the high lift propellers is considered in Subsection 7.2.4. Next a weight determination is performed in Subsection 7.2.5, finally the results are presented in Subsection 7.2.7.

7.2.1. THRUST PROPELLER PERFORMANCE

The thrust propeller is a variable pitch, constant speed propeller designed to be optimal at high velocities. First the equation that is used to determine the thrust is looked at, from which its required values can be gathered and then determined. Throughout this subsection, the book *General Aviation Aircraft Design: Applied Methods and Procedures* by S. Gudmunddsson is used [44].

The thrust is determined with a third degree polynomial, where its coefficients A through D are determined with Equation 7.2, where the subscript c denotes the cruise condition, $static$ denotes stand-still and max the maximum velocity. From this it follows that the thrust at a velocity of zero, maximum and cruise has to be determined along with the required shaft power P and the propeller efficiency at cruise η_{p_c}.

$$T(V) = A \cdot V^3 + B \cdot V^2 + C \cdot V + D \tag{7.1}$$

$$\begin{bmatrix} 0 & 0 & 0 & 1 \\ V_c^3 & V_c^2 & V_c & 1 \\ 3V_c^2 & 2V_c & 1 & 0 \\ V_{max}^3 & V_{max}^2 & V_{max} & 1 \end{bmatrix} \begin{bmatrix} A \\ B \\ C \\ D \end{bmatrix} = \begin{bmatrix} T_{static} \\ T_c \\ \frac{-\eta_{p_c} \cdot P}{V_c^2} \\ T_{max} \end{bmatrix} \tag{7.2}$$

First the propeller efficiency is determined at V_c and V_{max}. The efficiency at V_{max} is necessary in order to determine the required shaft power, which is done by using a propeller efficiency map, suitable for the turboprops of a regional aircraft. This plot requires both the advance ratio and the power coefficient, thus these have to be determined next by using equations Equation 7.3 and Equation 7.4, in which D is the propeller diameter.

$$J = \frac{60 \cdot V}{RPM \cdot D} \tag{7.3}$$

$$C_P = \frac{P}{\rho \left(\frac{RPM}{60}\right)^3 D^5} \tag{7.4}$$

The propeller diameter D is calculated via Equation 7.5, where the aim is to have a tip speed of 0.8 times the speed of sound a in order to have the highest tip speed without producing shock waves, sized for cruise velocity and altitude.

$$D = \frac{60 \cdot \sqrt{V_{tip}^2 - V_c^2}}{RPM \cdot \pi} = \frac{60 \cdot \sqrt{(0.8a)^2 - V_c^2}}{RPM \cdot \pi} \tag{7.5}$$

This diameter can be reduced to meet the maximum allowable value with equation Equation 7.6, where a diameter with a certain amount of blades is equivalent to a smaller diameter with a higher number of blades [44]. The number of blades is indicated with N_B, n is the rotations per second, k is a constant and is equal to 0.75. As a first estimate the chord is assumed independent of diameter to considerably simplify calculations, so the ratio of the propeller surface areas $\frac{S_{old}}{S_{new}}$ is changed to $\frac{D_{old}}{D_{new}}$. This is not entirely accurate, but necessary to progress. A detailed chord calculation method is presented in Subsection 7.2.3.

$$V^2 \cdot D_{new} + (\pi n k)^2 D_{new}^3 = \left(V^2 \cdot D_{old} + (\pi n k)^2 D_{old}^3\right) \left(\frac{N_{B_{old}}}{N_{B_{new}}}\right) \left(\frac{S_{old}}{S_{new}}\right) \tag{7.6}$$

This maximum allowable value is determined by a regulatory minimum required ground clearance, with a roll angle of 5° and a further clearance of 18 cm as can be seen in Figure 7.3, in which an aircraft with a low wing configuration is shown [20, 45].

The final parameter that needs to be determined is the power P, necessary to calculate its coefficient C_P. To assess the maximum required power, first the maximum thrust needs to be known, which is taken to be equal to the drag at maximum velocity divided by the number of engines which makes it 7957.2 N. By using this thrust value the required power P can be calculated with Equation 7.7 and was found to be 1686.7 kW.

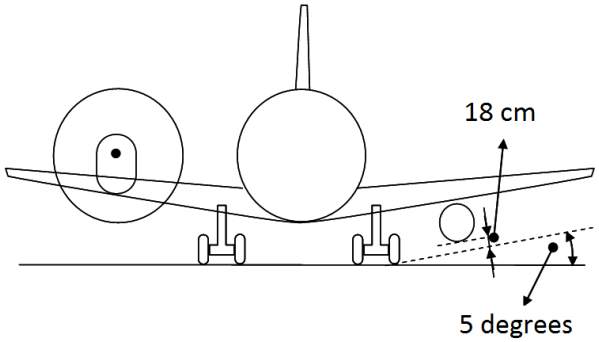

Figure 7.3: Required propeller ground clearance [45]

This calculation requires the propeller efficiency at maximum velocity, so care must be taken to ensure that via trial and error the value used here is identical to the value found at the end of the analysis. Since the required torque Q also needs to be met by the engine it also needs to be calculated, which is done with Equation 7.8 and was found to be 15339.4 Nm.

$$P_{TP} = \frac{T_{max} \cdot V_{max}}{\eta_{p_{max}}} \tag{7.7}$$

$$Q_{TP} = \frac{30 \cdot P_{TP}}{\pi \cdot RPM} \tag{7.8}$$

To size the propeller, the RPM of the engine is tweaked until the efficiency at cruise and maximum speed are at the most optimal. The resulting RPM was found to be 1050, which resulted in an optimal diameter of 3.92 m. The efficiency map with the results is shown in Figure 7.4, where an efficiency for V_{cruise} of 0.875 and for V_{max} of 0.86.

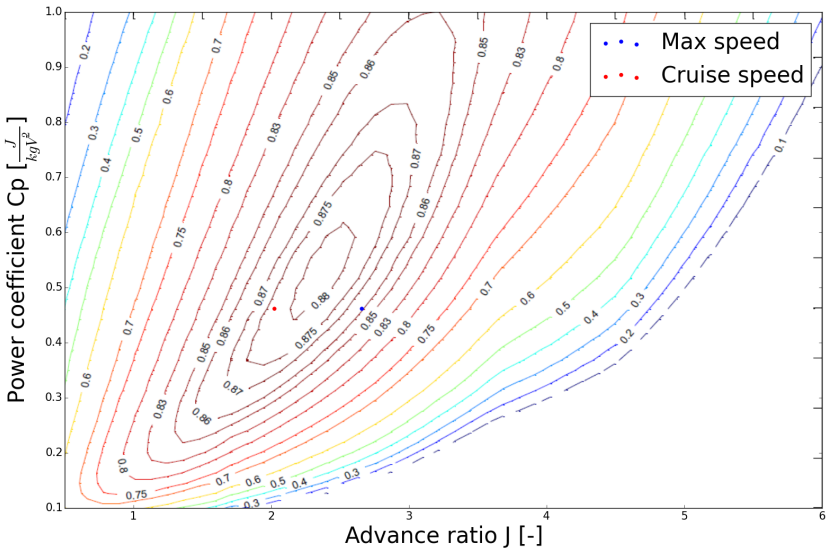

Figure 7.4: Propeller efficiency map

With a known required power, both the thrust at stand-still and cruise velocity can be calculated with the equation Equation 7.9 and Equation 7.10 respectively, where A_{prop} is the circular area described by the propeller and $A_{spinner}$ is the frontal area of the spinner, which will be determined in Subsection 7.2.3.

$$T_{static} = 0.85 \cdot P^{2/3} \cdot \sqrt[3]{2\rho A_{prop}} \cdot \left(1 - \frac{A_{spinner}}{A_{prop}}\right) \quad (7.9)$$

$$T_{cruise} = \frac{P_{TP} \cdot \eta_{p_{cruise}}}{V_{cruise}} \quad (7.10)$$

Finally Equation 7.2 can be filled in and $T(V)$ is known. Since the power is constant, the efficiency as a function of velocity can be calculated using Equation 7.11. Both the propeller efficiency and thrust functions are presented in Figure 7.5.

$$\eta_{p_{TP}}(V) = \frac{T(V) \cdot V}{P} = \frac{A \cdot V^4 + B \cdot V^3 + C \cdot V^2 + D \cdot V}{P_{TP}} \quad (7.11)$$

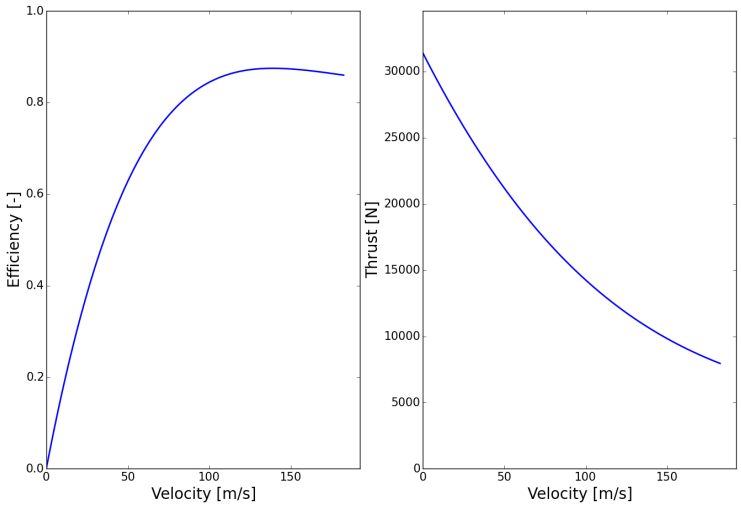

Figure 7.5: Propeller efficiency and thrust of the thrust propeller

7.2.2. HIGH LIFT PROPELLER PERFORMANCE

The high lift (DEP) propellers are considerably smaller than the thrust propellers, as they are intended to accelerate the air over the airfoil and not to generate thrust. They are fixed pitch, constant speed propellers to reduce the weight and cost and increase reliability and maintainability. Again the book *General Aviation Aircraft Design: Applied Methods and Procedures* by S. Gudmunddsson is used [44]. Similarly to the thrust propellers, the thrust equation is looked at first after which its requirements are calculated.

$$T(V) = \left(\frac{T_{static} - 2T_{max}}{V_{max}^2}\right) V^2 + \left(\frac{3T_{max} - 2T_{static}}{V_{max}}\right) V + T_{static} \quad (7.12)$$

The thrust equation seen above requires the static thrust, thrust at maximum velocity for which the DEP propellers are used and the maximum velocity itself for which the DEP propellers are used. The maximum velocity was taken to be 80 m/s, for performance reasons.

First the power is determined by sizing the propellers such that the difference between the regulatory stall speed and the stall speed of the wing is met, which is called the required velocity V_{req}. This is done by first calculating the thrust that this speed difference generates with equation Equation 7.13, followed by an iterative procedure until the power and efficiency have converged, by using equations Equation 7.16 and Equation 7.17. In these equations the third subscript denotes the situation where the flow behind the propeller has become parallel again. Care must be taken to ensure that P_{DEP} does not exceed the maximum engine power of 100 kW and as such a diameter of 0.58 m was taken. With 20 propellers, the resulting spacing was found to be 0.27 m.

$$T = \rho \cdot A_3 \cdot V_3(V_3 + V) \quad (7.13)$$

$$A_3 = \frac{A_{prop} \cdot V_{req}}{V_3} \tag{7.14}$$

$$V_3 = 2V_{req} - V \tag{7.15}$$

$$P_{DEP} = \frac{T \cdot V}{\eta_p} \tag{7.16}$$

$$\eta_p = \frac{2}{1 + \sqrt{\frac{2T}{A_{prop} \cdot V^2 \cdot \rho} + 1}} \tag{7.17}$$

With a small diameter comes a high RPM to reach a tip speed of 0.8 times the speed of sound and as such an RPM of 9,669.0 was found. Since the electric motor is limited to a maximum RPM of 4500, a gear ratio of 2.15 must be used. With this gear ratio GR, the torque that the engine must be able to deliver can be determined via Equation 7.18. A value of 43.54 Nm was found, which is well within the capabilities of the motor.

$$Q_{DEP_{motor}} = \frac{30 \cdot P_{DEP}}{\pi \cdot RPM \cdot GR} \tag{7.18}$$

The static thrust can be calculated using Equation 7.9, for which the power required by the DEP propellers P_{DEP} is used, along with the propeller and spinner areas. How the spinner area was determined will be shown in Subsection 7.2.3. Now that T_{static} and P_{DEP} have been found, the thrust at maximum velocity for the DEP propellers can be calculated as well by a similar iterative procedure, where now the power is given and the thrust and efficiency are iterated through with Equation 7.16 and Equation 7.17 until convergence has been found. Now that $T(V)$ is known, efficiency as a function of velocity can be easily determined as well with Equation 7.19. The thrust and efficiency equations are presented visually in Figure 7.6, along with the induced velocity.

$$\eta_{p_{DEP}} = \frac{T(V) \cdot V}{P_{DEP}} = \frac{\left(\frac{T_{static} - 2T_{max}}{V_{max}^2}\right) V^3 + \left(\frac{3T_{max} - 2T_{static}}{V_{max}}\right) V^2 + T_{static} V}{P_{DEP}} \tag{7.19}$$

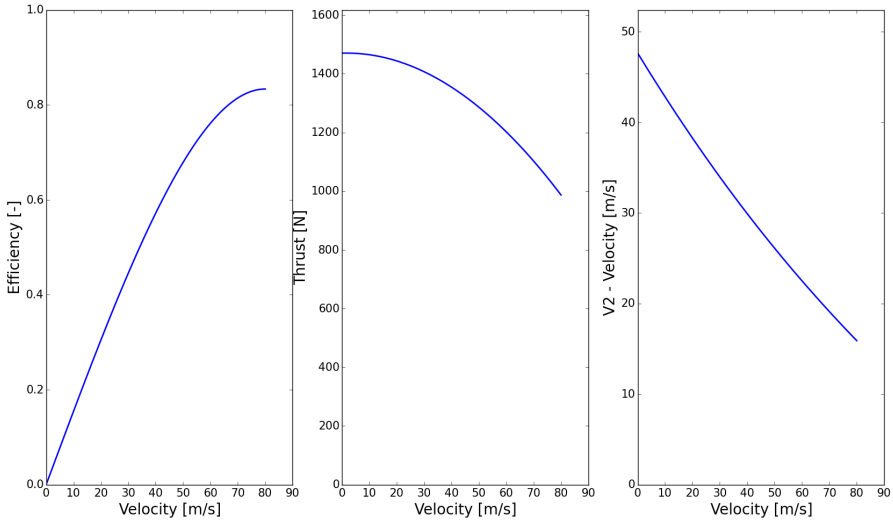

Figure 7.6: Propeller efficiency, thrust and induced velocity of the high lift propeller

7.2.3. PROPELLER GEOMETRY

In this section the propeller geometry is determined. First the equations to calculate the propeller angles are shown, after which the chord calculation is presented followed with an airfoil selection for both the thrust and the high lift propellers. The propeller pitch P_D, pitch angle β, helix angle ϕ and the propeller angle of attack α_p are calculated using equations Equation 7.20, Equation 7.21, Equation 7.22 and Equation 7.23 respectively.

The reference bladestation R_{ref} is used which is at 0.75 of the radius [44]. The angle of attack at their respective design conditions is 6.3° for the high lift propeller and 4.64° for the thrust propeller. How these values change with velocity for the thrust propeller is shown in Figure 7.7 and for the high lift propeller in Figure 7.8.

$$P_D \approx 643.6 \frac{V}{RPM} \frac{1}{\eta_p} \tag{7.20}$$

$$\beta = \tan^{-1}\left(\frac{P_D}{2\pi R_{ref}}\right) \tag{7.21}$$

$$\phi = \tan^{-1}\left(\frac{\pi \cdot R_{ref} \cdot RPM}{30 \cdot V}\right) \tag{7.22}$$

$$\alpha_p = \beta - \phi \tag{7.23}$$

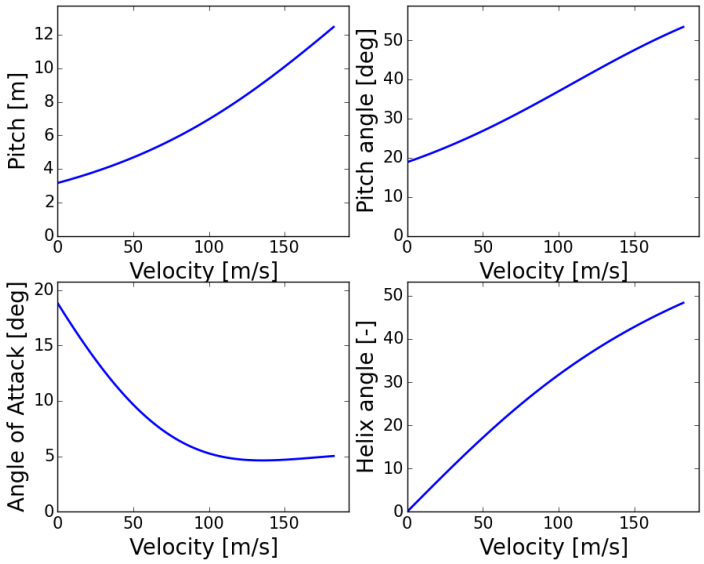

Figure 7.7: Pitch and propeller angles of the thrust propeller

By using the angles of attack for the design condition of the thrust and high lift propellers, the most optimal airfoil can be selected. For the thrust propellers this was the E853, with its optimum C_l/C_d value at around 4° and for the high lift propellers the E1200 was selected since it has a wider high C_l/C_d range, ranging from roughly 5° to 10°, which is more suitable for a fixed pitch propeller [46].

The chord distribution $c(r)$ can be calculated using equations Equation 7.24, where r is the bladestation which runs from the hub radius to the radius R, α_i is the induced angle of attack which was taken to be three degrees [44], N_B is the number of blades and $C_{l_{prop}}$ is the lift coefficient of the propeller [47]. The tip loss factor $F(r)$ can be calculated using Equation 7.25 and the angle of attack α_∞ can be calculated using Equation 7.26, where ω is the rotational speed of the propeller. The chord distribution of the high lift propeller can be seen in Figure 7.9 where one should note that the hub radius of 20 cm obstructs the propeller beyond that point.

$$c(r) = F(r)\frac{\pi}{2}\alpha_i(r)\frac{16r}{N_B \cdot C_{l_{prop}}}[\sin(\alpha_\infty(r)) + \alpha_i(r) \cdot \cos(\alpha_\infty(r))] \tag{7.24}$$

$$F(r) = \frac{2}{\pi}\cos^{-1}\left(e^{\frac{-N_B(1-r/R)}{2sin(\phi_{tip})}}\right) \tag{7.25}$$

$$\alpha_\infty(r) = \tan^{-1}\left(\frac{V}{\omega \cdot r}\right) \tag{7.26}$$

$$\phi_{tip} = \tan^{-1}\left(\frac{J}{\pi}\left[1+\frac{w_0}{4}\right]\right) \tag{7.27}$$

$$w_0(r) = \frac{2r\cdot\omega}{\cos(\alpha_\infty)\cdot[\cos(\alpha_\infty)-\alpha_i\cdot\sin(\alpha_\infty)]} \tag{7.28}$$

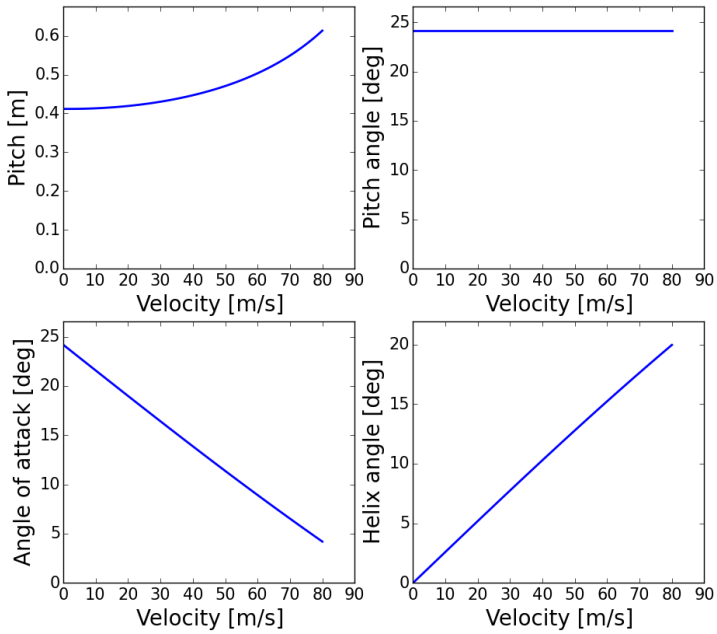

Figure 7.8: Pitch and propeller angles of the high lift propeller

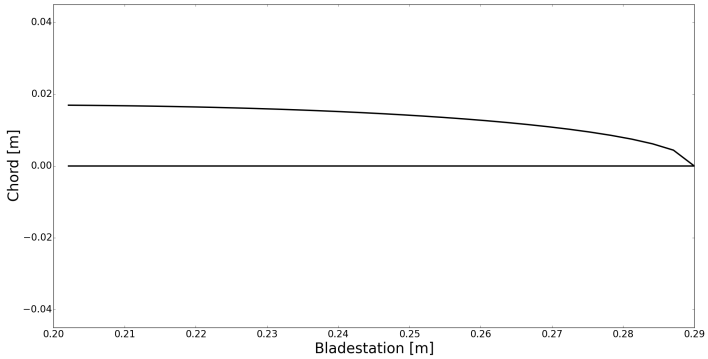

Figure 7.9: Chord distribution of the high lift propeller

7.2.4. HIGH LIFT PROPELLER FOLDING MECHANISM

The high lift propellers must be foldable to ensure lower drag when they are not operated. For the propeller folding mechanism there are two main options, powered or not powered. A powered folding mechanism uses the power from the propeller shaft or other motors, whilst a non-powered mechanism uses the centrifugal force of the shaft to open the blades and the aerodynamic forces to close them when they are not being used. The non-powered mechanism can therefore be a lot simpler and thus has lower cost, better maintainability and lower weight, which is why it is selected as the folding mechanism.

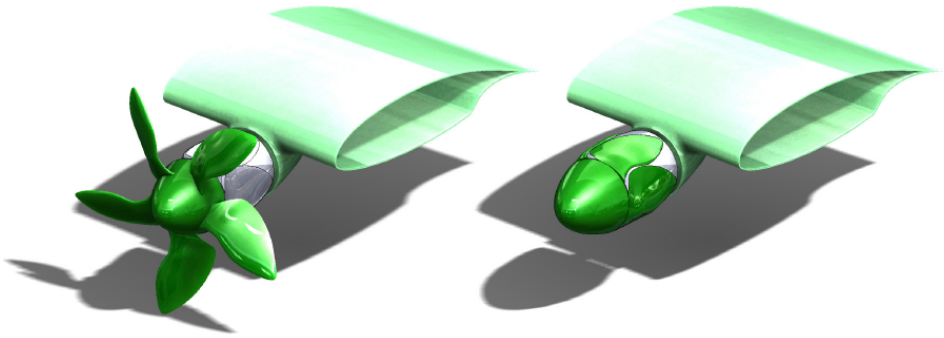

Figure 7.10: Five blade propeller design illustrating the blade folding mechanism [1]

To ensure that the propeller unfolds a spring can be used and to ensure that they do not vibrate in the wind an electronic magnet is applied on the propeller tip surface and the part of the nacelle that touches upon closing. To size the closing spring, the free body diagram was composed in Figure 7.11 after which by using moment equilibrium as seen in Equation 7.29 can be established, where F_D, F_G and F_C are the forces due to drag, gravity and the centrifugal rotation respectively. With this equation, the maximum required torsion stiffness K_S can be calculated using Equation 7.30. The forces are assumed to act in the middle of the blade.

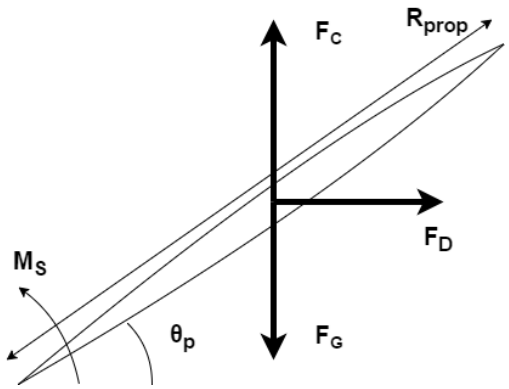

Figure 7.11: Schematic free body diagram of the folding propeller

$$M_S = K_S \cdot \theta_p > \frac{R}{2}\left[F_D \cdot \sin(\theta_p) + (F_G - F_C) \cdot \cos(\theta_p)\right] \tag{7.29}$$

$$K_{S_{max}} = \left(\frac{\frac{R}{2}\left[F_D \cdot \sin(\theta_p) + (F_G - F_C) \cdot \cos(\theta_p)\right]}{\theta_p}\right)_{max} \tag{7.30}$$

7.2.5. WEIGHT DETERMINATION

The propeller system weight consists of the propeller blades, the propeller hub, spinner and governor if applicable. Due to their large size and weight, carbon fibre was selected as the material choice for the thrust propellers. Since the weight of the high lift propellers is limited and in order to reduce production and maintenance cost, aluminium was selected instead.

The weight of the propeller blades can be determined by dividing the propeller into slices along the length of the blade from hub to tip, calculating the cross-sectional area A_{CS} for each chunk and then multiplying it with the length of the slice $r_{i+1} - r_i$ and the density of the material ρ_m.

$$M_B = \rho_m \cdot N_B \sum_{i=0}^{n} A_{CS_i} \cdot (r_{i+1} - r_i) \tag{7.31}$$

To calculate the weight of the propeller hub, its radius and length must be known. The radius of the thrust propeller hub was taken to be 30 cm and for the high lift propeller hub 20 cm, to fit the electric motors and nacelle behind it. The length L_{hub} is taken to be equal to the maximum chord of the propeller to ensure sufficient spacing. The weight of the hub can now be calculated with Equation 7.32.

$$M_{hub} = \frac{\pi}{2}\rho_m \cdot L_{hub} \cdot \left(R^2_{spinner} - R^2_{shaft}\right) \tag{7.32}$$

The spinner has the same radius R_{sp} as the hub to ensure smooth aerodynamic flow and is the shape of half an ellipsoid whose major axis is twice the hub radius. A thickness t_{skin} of 1 cm is chosen for the thrust propeller and high lift propellers to ensure sufficient impact stiffness.

$$M_{spinner} \approx 2\pi\rho_m \cdot t_{skin} \cdot \left(\frac{(2R_{sp}\cdot R_{sp})^{1.6} + (R_{sp}\cdot R_{sp})^{1.6} + (2R_{sp}\cdot R_{sp})^{1.6}}{3}\right)^{1/1.6} \approx 3.414\pi\rho_m \cdot t_{skin} \cdot R^2_{sp} \tag{7.33}$$

Finally the governor weight has to be determined. Since the high lift propellers are fixed pitch, only the thrust propellers will have them. The governor weight of a reference propeller was used, with a diameter of six metres and a power rating of two thousand horsepower, which was found to be 1.3 kg [48]. With all these components the total weight of the thrust propeller was found to be 32.0 kg and for the high lift propeller 1.85 kg.

7.2.6. PROPELLER VERIFICATION AND VALIDATION

To determine whether the propeller results are accurate, verification and validation must be performed. During programming each section of code has been independently verified to determine whether the results make sense and some functions have been verified using available data [44]. In order to present a more concise verification procedure, in this section only the verification of the most important and complicated part is presented, namely the thrust equations Equation 7.1 and Equation 7.12. The other data follows from these equations in a fairly straightforward manner.

In order to verify the thrust propeller the calculated T_{cruise} and thrust polynomial constants are compared with the data from the book *General Aviation Aircraft Design: Applied Methods and Procedures* by S. Gudmunddsson [44]. The input data are the following: a power of 65 HP, T_{static} of 546 lbf, T_{max} of 195 lbf, a V_{cruise} and V_{max} of 65 and 75 kts respectively and an efficiency at cruise of 0.75. The errors are very small, likely due to small rounding errors that are a result of using Imperial units.

Table 7.1: Comparison between the verification and calculated data for the thrust propeller

	T_cruise [lbf]	**A [-]**	**B [-]**	**C [-]**	**D [-]**
Calculated	244.4	-0.00105	0.150	-9.969	546.0
Book	244.0	-0.00101	0.145	-9.806	546.0
Error [%]	0.16	4.0	3.4	1.7	0.0

To verify the high lift propellers, the thrust and efficiency values that are calculated are compared with the book similarly to the thrust propellers. The verification data is presented in Figure 7.12, whilst the results are compared in Table 7.2. The overestimation of the efficiency and thrust is almost certainly due to lack of data on the spinner area. As such, it was assumed zero which would benefit the efficiency and thrust generated. Due to this and inaccuracies in reading the data, errors are expected. Due to the results being expected, the high lift propeller is taken to be verified.

Table 7.2: Comparison between the verification and calculated data for the high lift propellers

Velocity [kts]	**Efficiency (Calc.)** [-]	**Efficiency (Book)** [-]	**Error** [-]	**Thrust (Calc.)** [lbf]	**Thrust (Book)** [lbf]	**Error** [-]
V = 0 kts	0.0	0.0	0.0	1387.9	1300.0	6.8
V = 40 kts	0.445	0.43	3.5	1123.5	1050.0	7.0
V = 80 kts	0.711	0.69	3.0	897.5	850.0	5.6
V = 160 kts	0.888	0.85	4.5	560.3	550.0	1.9

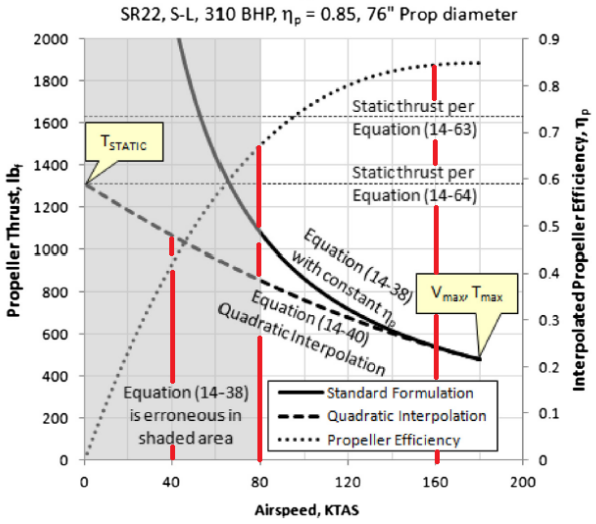

Figure 7.12: Verification data

7.2.7. PROPELLER RESULTS

The over-all results for the high lift and thrust propellers are presented below in Table 7.3

Table 7.3: Results for the high lift and thrust propeller

Parameter	Symbol	High lift propeller	Thrust propeller	Unit
Design conditions				
Design velocity	V_{des}	80.0	138.9	m/s
Maximum velocity	V_{max}	80.0	182.3	m/s
Required velocity	V_{req}	73.3	-	m/s
Design altitude	H_{des}	0.0	5,000.0	m
Performance				
Maximum power	P_{max}	94.74	1686.7	kW
Maximum torque	T_{max}	93.56	15,339.4	Nm
Static thrust	T_{static}	1470.2	31,430.7	N
Thrust at V_{max}	T_{max}	986.9	7,957.2	N
Thrust at V_{des}	T_{des}	986.9	10,626.0	N
Efficiency at V_{max}	$\eta_{p_{max}}$	0.833	0.86	-
Efficiency at V_{des}	$\eta_{p_{cr}}$	0.833	0.875	-
Geometry				
Diameter	D	0.58	3.92	m
Mean aerodynamic chord	MAC	0.013	0.243	m
Number of blades	N_B	8.0	2.0	-
Airfoil	-	E1200	E853	-
Pitch at V_des	P_D	0.61	9.33	m
Pitch angle at V_{des}	β	24.17	45.3	deg
Helix angle at V_{des}	ϕ	20.0	40.7	deg
Angle of attack at V_{des}	α_p	4.20	4.64	deg
Mass				
Mass blades	M_B	0.036	29.92	kg
Mass hub	M_{hub}	1.68	0.74	kg
Mass spinner	$M_{spinner}$	0.13	0.077	kg
Mass governor	$M_{governor}$	-	1.3	kg
Total mass	M_{prop}	1.85	32.03	kg

7.3. GAS TURBINE

The E-gle is equipped with two turboprop engines to provide the required thrust during flight. Being a parallel turbo electric hybrid propulsion system, these gas turbine engines operate in parallel with two electric motors on either wing to power the thrust propellers. The selection of suitable turboprop engines depends upon the power requirement, weight, cost and fuel efficiency. Several commercially available engines from manufacturers such as Pratt and Whitney, Rolls Royce and General Electric were examined based on this criteria.

Engines from General Electric belonging to the CT7 family were found to be most attractive due to their rugged, fuel efficient and exceptional performance accompanied with a low weight. The CT7 engine design has proven itself in harsh environments and has achieved over 37 million engine cycles. The turboprop variants of the CT7 engine family use the same core as the turboshaft engines, with a propeller gearbox fitted forward of the core. The chosen engine model GE CT7-2A is shown in Figure 7.13. The engine model is a front drive, turboshaft featuring a single-spool gas generator section consisting of a five-stage axial, single-stage centrifugal flow compressor, a through flow annular combustion chamber, a two-stage axial flow gas generator turbine, and a free or independent two-stage axial flow power turbine. The power turbine shaft is co-axial and extends to the front end of the engine onto which the propeller gearbox is integrated. A representation of the engine fitted with the gear box is shown in Figure 7.14.

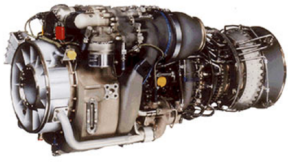

Figure 7.13: GE CT7-2A engine

Figure 7.14: Turboprop variant of the engine integrated with propeller gearbox

The physical and power specifications of the engine are shown in Table 7.4.

Table 7.4: CT7 2A Engine specifications

Physical Specifications	**Value**	**Unit**
Compressor stages	6	-
Overall length	119.4	cm
Overall width	66	cm
Overall height	63.5	cm
Dry weight	194.6	kg
Power Specifications		
Max. continuous power	1189	kW
Takeoff power	1212	kW
Output rpm	21000	rpm

7.3.1. GAS TURBINE SIMULATION PROGRAM ANALYSIS

In order to observe the efficiency of the turboprop engines throughout the flight, a detailed engine analysis is performed using the Gas turbine simulation program (GSP). GSP is a generic modelling tool developed by NLR, capable of modelling virtually any gas turbine engine configuration. GSP is primarily based on 0D-modelling (zero-D) of the thermodynamic cycle of the gas turbine. This implies that the flow properties are averaged over the flow cross section areas at the interface surfaces of the component models (inlet and the exit).

Table 7.5: Brake specific fuel consumption at various flight phases

Phase	Brake Specific Fuel Consumption[kg/ kW.h]
Taxing	0.287
Climb	0.272
Cruise	0.361
Descent1	0.719
Loiter	0.407
Descent2	0.830
Landing	0.874

Besides being a performance prediction tool, GSP is especially suitable for parameter sensitivity analysis such as: ambient (flight) condition effects analysis, installation (losses) effects analysis, analysis of effects of certain engine malfunctioning (including control system malfunctioning) and component deterioration effects analysis. Input for the analysis is based on the model configuration (e.g. fuel flow can be specified to calculate the generated power, or when the fuel flow is set as a state variable the power can be specified to calculate the corresponding fuel flow). By running the simulation, output data set in the component property window is displayed in a table, which can be visualized by a build-in graph tool. Data available includes the gas conditions (temperatures, pressures, mass flows, areas, speeds, etc) and the gas composition (gas species are available since GSP uses a full thermo-chemical gas properties model).

The chosen engine as modelled in GSP is shown in Figure 7.15. The model parameters are set according to the engine specifications and determined properties of the thrust propellers. The model is composed of one propeller, one inlet, one compressor, one combustion chamber, two turbines and one exhaust.

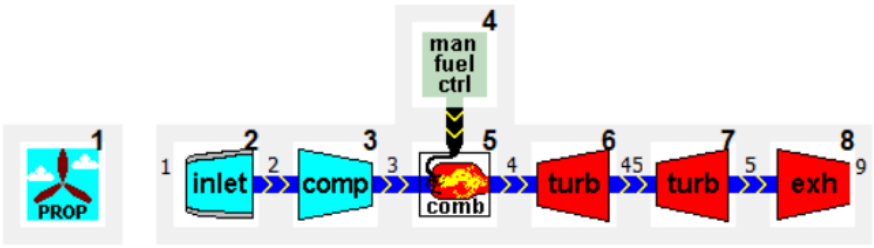

Figure 7.15: Turboprop engine model in GSP

It is possible to analyse the engine efficiency based on several parameters such as fuel consumption, brake specific and thrust specific fuel consumption. Fuel consumption is the amount of fuel burnt per unit time during the flight. Brake specific fuel consumption (BSFC) is a measure of the fuel efficiency of internal combustion engines with a shaft output. It is the rate of fuel consumption divided by the power produced. It may also be thought of as power-specific fuel consumption, for this reason. Thrust specific fuel consumption (TSFC) is used to describe the fuel efficiency of an engine design with respect to thrust output. TSFC may also be thought of as fuel consumption per unit of thrust. TSFC if particularly useful for turbojet and turbofan efficiency analysis, while for a turboprop, it makes sense to analyse BSFC since the direct output from the engine itself is the shaft power, which in turn powers the propellers, thereby producing thrust.

The model is simulated at various flight phases including taxi, take-off, climb, cruise, descent, loiter and landing. The power requirements for each phase is as determined in performance analysis in Chapter 10. The cruise altitude is at 5000 m. The resulting variation of brake specific fuel consumption over the course of the flight with shaft power is shown in Table 7.5 and Figure 7.16. It is visible from the graph the SFC increases when the engine delivers lower shaft powers. Hence it is possible to conclude that the turboprop efficiency is only good at high power.

Figure 7.17 displays the variation of SFC with flight altitude. The particular shape of the plot arises due to the various flight phases. Following the line starting from the bottom left is the take-off (1) and the climb till 5000 m altitude. Next, the SFC during cruise phase is represented by the first edge (2), which is then followed by the descent (3) till 1000 m.

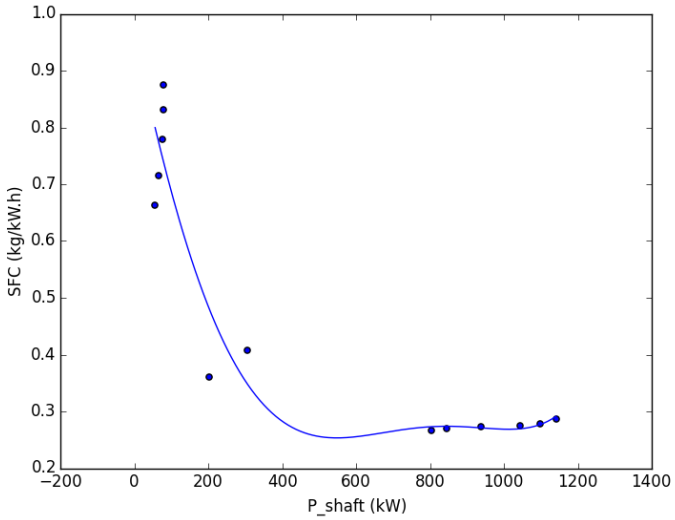

Figure 7.16: Engine shaft power vs. specific fuel consumption (SFC)

There is then the deviation which represents the loiter phase (4), followed by the second descent (5) and then landing (6).

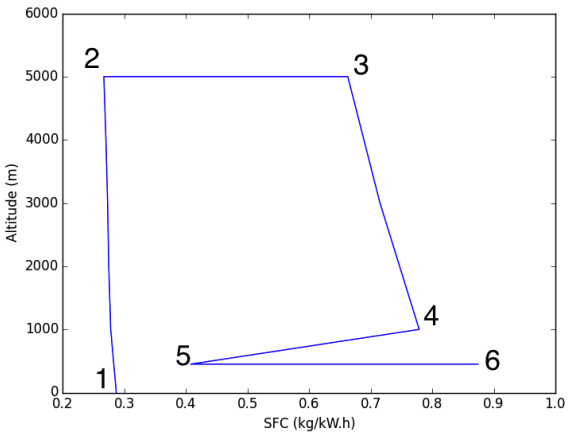

Figure 7.17: Engine specific fuel consumption (SFC) vs. altitude

GSP Validation
In order to validate the derived results for the chosen engine model, it is compared to a similar commercially available turboprop engine from Pratt & Whitney PW127. The PW127 is not modelled in GSP but rather its values for SFC and shaft power have been collected from the company data sheets. With these numbers, a plot of SFC against shaft power is made as shown in Figure 7.18. It can be observed that both the engines exhibit a comparable behaviour of the specific fuel consumption with changing shaft power. Furthermore, the SFC values for both engines are in the near range of each other. Hence the GSP model for the GE CT7-2A engine is considered to be validated.

7.4. ELECTRIC MOTORS

Electric motors (EM) are used to convert electrical energy into mechanical energy. They have a very broad variety of applications, explaining the numerous types of electric motors. They can be classified in different ways, based on their power source, their commutation, application, etc. This section presents the different categories of electric motors, a more advanced motor technologies will be discussed: permanent magnet (PM) motors.

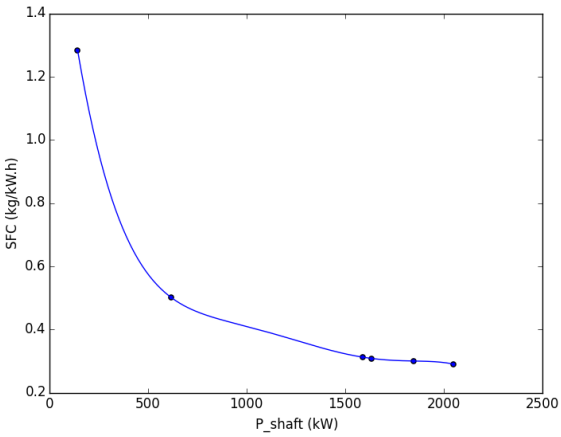

Figure 7.18: Engine specific fuel consumption (SFC) vs. shaft power for Pratt & Whitney Canada PW127 turboprop

Table 7.6: Pratt & Whitney PW127 Engine properties

Phase	Shaft Power kW	Brake Specific Fuel Consumption [kg/ kW.h]
Nominal idle (7%)	143	1.282
Approach (30%)	615	0.502
Max cruise (78%)	1590	0.312
Max climb (80%)	1635	0.308
Max contin. (90%)	1846	0.300
Take-off (100%)	2050	0.290

7.4.1. EVOLUTION AND CATEGORISATION OF ELECTRIC MOTORS

The first electric motor was created by Moritz Jacobi [1] in 1834. It was a single-phase alternating current (AC) induction motor. With the development of batteries, scientists' focus moved to direct current (DC) motors, powered by batteries. Quickly, interest about AC motors came back, and the three-phase AC induction motor was invented. Today, electric motors have not reached their full potential, and progress is being made every day to achieve greater energy efficiency. Any kind of electric motor is based on the principle of the interaction of magnetic field with current. The main two components are the stator and the rotor[2]. The first one is stationary and is composed of layers of steel lamination. Its core is hollowed, with a slot for conductive material such as wound or insulated copper wires. This slot is called a magnetic pole when the windings are energised with current. The second component, the rotor, rotates inside or outside the stator's core, delivering mechanical power by turning the shaft. It is composed of conductors, interacting with the magnetic field of the stator. The two components are separated by an air gap. It is desired to have a small air gap in order to limit the magnetising current needed. However, a minimum distance is required to avoid mechanical losses and noise problems. Although there are similarities between the different types of motors, the components and properties can differ with their working principles.

7.4.2. DC AND AC MOTORS

It can be seen from figure Figure 7.19 that the first two categories under EM are determined by the type of power source. The motor can be powered by alternating current (AC) sources such as power grid or generator and by direct current (DC) sources such as batteries. This breakdown structure presents one way of categorising the electric motors. However, other methods can be used, leading to other types of trees.

Direct Current Motors

[1] https://www.eti.kit.edu/english/1376.php[Online; accessed 15 June 2017]
[2] http://www.electrical-knowhow.com/2012/05/electrical-motors-basic-components.html[Online; accessed 8 June 2017]
[1] http://www.mogi.bme.hu/TAMOP/digitalis_szervo_hajtasok_angol/ch07.html[Online; accessed 14 June 2017]

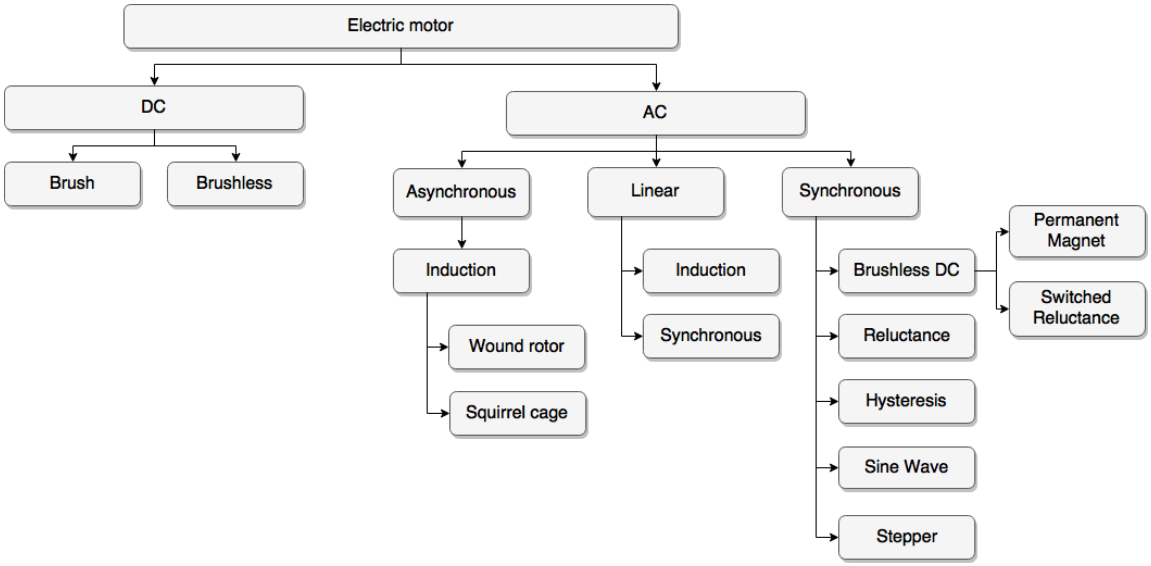

Figure 7.19: Categorisation of electric motors [1]

In a brushed DC motor, the stator is located on the outside and is usually composed of permanent magnets. The spinning armature, also called rotor, is located inside the stator. It is composed of electromagnets, creating a magnetic field when electricity is run through it.

There exists three ways to generate DC current. The first one is with the chemical reaction inside the battery. The second is to use a rectifier, converting AC to DC, and the last one is to use an AC generator with a commutator, producing DC. Direct Current supplies a constant voltage or current, and the current is flowing in only one direction. [2]

DC motors can be categorised into brush and brushless motors. A brushed motor has an electromagnet with two poles, composed of a rotating set of wound wire coils, also know as the armature or rotor. The direction of the current is reversed twice every cycle by the commutator. In this category, the commutator is a mechanical rotary switch. Because the current is reversed, the poles of the electromagnet interact with the poles of the permanent magnets located on the outside. With this polarity switch, the motor keeps on turning in the right direction.

A brushless motor is composed of three phases of driving coils in the inside, activated one after the other by an electronic commutator, and based on position sensors. These coils interact with the rotating permanent magnets located on the outside. The absence of brushes has several advantages such as low maintenance, low noise, high efficiency, reduced size, but is also more expensive to build and more complex to control.

Alternating Current Motors

An AC current is generated with an alternator, a particular type of generator. In an alternating current circuit, the current changes direction periodically. Therefore, the voltage reverses periodically as well. AC motors can be divided in two main categories: Synchronous and asynchronous motors. The difference between asynchronous (induction) and synchronous is the type of transfer of the rotor field excitation. This criteria refers to the ratio of the rotation speed of the energised field in the stator coils to the rotation speed of the rotor with its permanent magnets.

A single phase AC induction motor is based on the principle of electromagnetic induction to produce a motor torque. The two main components are the stator and the rotor. The stator is composed of laminated steel plates insulated from each other by a varnish or by oxidation. The lamination of these steel plates reduce losses. Windings are composed of several coils and their amount determines the number of phases of the motor. The usual types are the single phase and three phase AC motor. The rotor is composed of plates insulated from each other, placed in the shape of a cylinder.

A three-phase AC induction motor is based on the same principle, with the difference of having three coils placed in circle around the rotor. Each one is electrically powered by one of the three phase of alternating current. Providing the current to each coil sequentially, a rotating electrical field is generated. A 3 phase AC motor can also be used as an alternator. Induction motors always run at a speed that is lower than the synchronous speed.

[2] https://learn.sparkfun.com/tutorials/alternating-current-ac-vs-direct-current-dc[Online; accessed 8 June 2017]

The name of synchronous motors comes from the fact that the rotor is synchronous with the rotating magnetic field in the stator. The stator is similar to an induction motor and the rotor to a DC motor. The difference with induction motors is the origin of the flux in the air gap. In asynchronous motors, it is caused by magnets or field coil current from an external DC source, providing energy to a winding. In synchronous motors, the flux is generated by a component of the stator current. A synchronous motor is generally more efficient than an induction motor. This is the reason why synchronous AC electric motors were chosen in the design. To power the DEP propellers as well as acting in parallel with a gas turbine for the hybrid system for thrust propellers. Within the category of synchronous motors, another level can be added. Brushless DC, reluctance, hysteresis, sine wave and stepper motors. A particular look at brushless DC is taken: it is composed of the armature windings on the rotor and an AC generator with the field windings on the stator. There are also solid-state rectifier elements on the rotor shaft, their role being to rectify the output of the generator without brushes. Solid-state power electronic technology improves quickly. Most of the synchronous motors that are available on today's market are brushless because they need less maintenance.

An electric motor can have an axial [1]or radial flux. In an axial flux motor, the flux moves along the shaft. In a radial flux motor, the flux runs from the shaft towards the outside, all around the shaft, in the radial direction. An axial flux electric motor has a smaller ratio of axial length to diameter, explaining their other names pancake and flat motor. They can produce a high torque due to the low losses. Both types are used in motorsport but the axial flux motors are more common and are more efficient. They drive the shaft directly or with a small speed reduction.

7.4.3. PERMANENT-MAGNET MOTORS

The global market of permanent-magnet (PM) motor keeps on increasing, supported by the development of electric cars and the use of renewable sources of energy . They are more efficient than AC induction motors, are less expensive and require little maintenance due to their electronic control. Therefore, this motor was selected for the propulsion of this project. The permanent magnets, ferromagnetic materials which have strong magnetic properties, are integrated into the laminations of the rotor or fixed on the outer surface of the rotor. They create their magnetic field, which then interacts with the magnetic field in the stator to generate torque. The phase of the stator windings is electronically commutated, based on the feedback of the rotor's position. Several options for the electronic communication are feasible for this type of motor: using rotary encoder, sensors or even sensorless configurations. Using three position sensors called Hall-effect sensors inserted into the stator is very common to determine the rotor position.

With the electronic commutation, carbon brushes are not required anymore, justifying the increase in efficiency, reliability and longevity than standard brushed DC motors, operating on a similar principle. This similarity explains why permanent magnet motors are also called BLDC motors. The increase in performance can also be explained by the reduction in field excitation, explaining the lower energy consumption. PM motors are used with controls integrated or paired with a drive. Therefore, they perform well on applications with varied loads. They have the advantage of having a constant efficiency over a range of speeds.

The type of magnet used in PM motors is typically derived from rare-earth metals. China is the leading manufacturer of these rare-earth metals, providing over 90% of the entire market. Unlike specified in the name, rare-earth metals can be profusely found in China, but are very difficult to mine and to convert into components for the PM motors. Due to their high performance and other advantages, PM motors are known worldwide. Because environmental, geopolitical or other factor can have an enormous impact on the Chinese supply and its cost, many research groups are currently working on alternatives such as nanocomposite permanent magnets or ferrite magnets, abundant in nature.

7.4.4. DEP MOTORS

The electric motors for the DEP were selected based on the power required for the propellers, being 94.74 kW. The parameters of the motors presented in Table 7.7 were analysed to select the motor that fits the best the need of this design. It can be seen that the model 268 of the brand Emrax has a corresponding maximum continuous power, 100 kW, for only 20.3 kg. The power density is 4 kW/kg.

Studies estimate this value to double by 2025 [49]. Therefore, for the same amount of power and assuming that the density of all the components of the motor stay constant, the volume of the electric motor can be assumed to be half of the current volume.

[1] http://www.infolytica.com/en/applications/ex0072/ [Online; accessed 16 June 2017]

The motors for DEP will be placed behind the spinner, having a small diameter would allow the nacelle to be thinner. A new volume is calculated using the same width and reducing the diameter. Based on these assumptions and estimations, the motor has a width of 10.5 cm and a new diameter of 19.0 cm. The mass is also reduced by a factor of 2.

The maximum battery voltage is usually determined by technical rules and certifications. However, any certification exist for all electric or hybrid-electric regional transport aircraft of more than 19 passengers. Power loss by heat is related to the current squared. Keeping the current as low as possible is necessary to reduce the losses. The power is calculated by multiplying the current with the voltage. For a certain power, low current is therefore synonym of high voltage. High voltage increases complexity and cost of the electric motors.

Since the Emrax 268 is already designed for a maximum battery voltage of 700 V, this voltage is selected as voltage for the rest of the system. The voltage of most of the electric cars is around 300 and 400 V. But there exist other electric vehicles running on 700 V. The main reason to limit the voltage is safety. There is no maximum voltage that a human can withstand since it varies with many parameters. However, carrying a battery pack of 700 V would be more frightening than a battery of 9 V since any mishandling will electrocute the person.

A maximum voltage of 700 was selected for this design, assuming that progress will be made in the safety of a battery pack, especially for swapping them after every flight.

Table 7.7: Comparison between electric motors

Electric Motor	Mass[kg]	Max. continuous power[kW]	Power density [kW/kg]	Diameter[mm]
Joby JM1	2.75	13.2	4.8	154
Emrax 188	7	30	4.285	77
Emrax 208	9.4	40	4.255	208
Emrax 228	12.3	55	4.471	228
Emrax 268	20.3	100	4.926	268
Emrax 348	40	150	3.75	348
Siemens SP260D	50	260	5.2	418

7.4.5. PARALLEL HYBRID MOTORS

The parallel hybrid motors are placed on the same drive shaft connecting the gas turbine to the propeller[1]. These operate in parallel to produce the required mechanical energy to drive the thrust propellers and hence to propel the aircraft. When choosing these motors the various factors of importance include, maximum continuous power, power density, weight, technology maturity, efficiency and cost. The power requirements for the motors are determined in the mission profile optimisation in Chapter 10 and is found to be around 1.1 MW, i.e 0.55 MW from each parallel hybrid motors. With today's motor technology, even the strongest conventional motor built for electric vehicles, has a maximum power capacity of 260 KW. This motor is the SPD60 developed by the company Siemens. The characteristics of this motor are presented in Table 7.8. Since having one motor does not meet the power requirements, it is chosen to have 2 of these motors placed in parallel on either side of the wing in the parallel truboelectric configuration.

Table 7.8: Siemens SPD60 motor characteristics

Property	Value	Unit
Power continuous	260	kW
Maximum torque	2500	rpm
Efficiency at 260kW	95	%
Weight	50	kg
Power density	5.2	kW/kg
Diameter	418	mm
Length	300	mm

[1] https://sites.erau.edu/dbae/wp-content/uploads/sites/14/2014/12/hybrid_turboprop_video.gif[Online; accessed 14 June 2017]

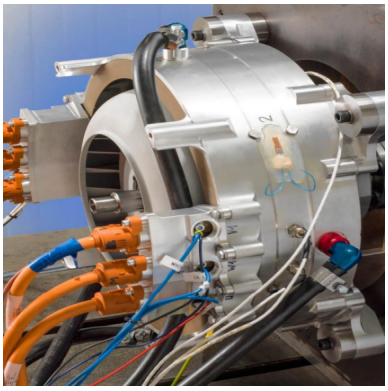

Figure 7.20: Siemens motor

7.5. COMPONENTS LINKED TO THE ELECTRIC MOTOR

Motor controller
An electric motor cannot run in a controlled way without a motor controller. It is the brain of the system, it controls the rate of energy that is being transferred between the battery and the motor. The batteries supply DC power and the motor controller converts it into three phase voltages, separated by 120°. Each of them control a different group of windinds in the stator, which are also placed with 120°between them. The permanent magnets in the rotor create a magnetic field with fixed poles, which will try to align its field with the rotating magnetic field of the stator. This will introduce a torque, spinning the electric motor in the same direction than the magnetic field of the stator. This rotational speed is the same as the one of the stator rotating magnetic field in steady state. This speed depends on the frequency of the three phase voltage. In a word, the motor controller controls the voltage and current supplied to the electric motor, controlling the speed and the torque.

Cooling
Any electrical system carrying current generates heat. It is necessary to control this heat in order to keep a good efficiency of the components. Discarding cryocooling or any other particular type of cooling, the available options for this application are liquid-cooled, air-cooled or combined-cooled. Air-cooled requires that an airflow passes along the system. If this can be easily satisfied, this system is a good, reliable and cheap method. However, it has several downsides and obstruction of the inlet is one of them. Liquid-cooling has advantages as well. A liquid-cooled motor for example can produce much higher continuous power and is an internal circuit. However, it adds complexity, weight and increases the overall cost. The motor controller that are compatible with the requirements of the overall propulsion architecture are liquid cooled. Therefore, having already the cooling pipes, pumps, etc, liquid-cooling is also selected for the electric motors.

Other components
Other components need to be considered in the propulsion system in order to increase the accuracy of estimation of the cost, volume and weight. Among others, the shaft, sensors, bearing, phase connectors and bracket can be mentioned. More details about these components can be found in the datasheet of the electric motor.

7.6. PROPULSION ARCHITECTURE

Layout of the complete propulsion system in E-gle is illustrated in Figure 7.21. Sizing of battery and fuel tanks is further described in Chapter 8.

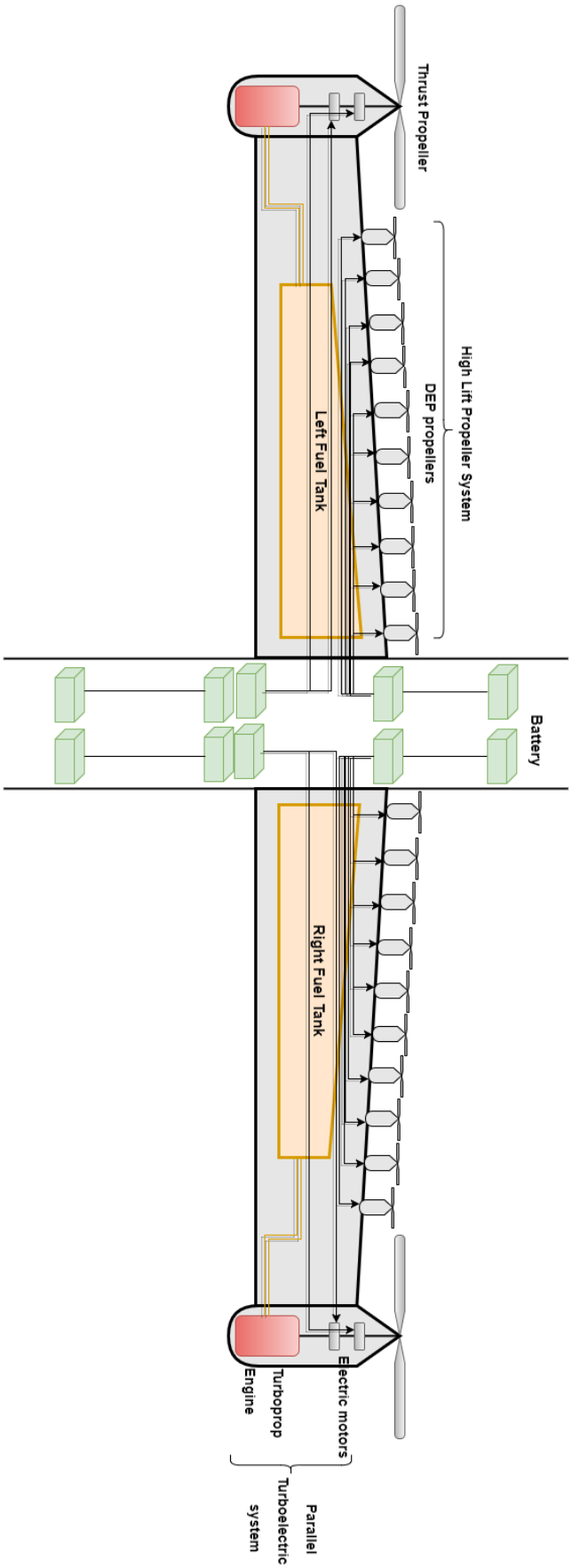

Figure 7.21: E-gle propulsion system architecture

8

POWER

In this chapter, the power subsystem is discussed. Since the E-gle is designed as a turbo-electric hybrid configuration, the power sources consist of batteries and fuel. The turboprop engines drive on the fuel, while the motors are driven by electrical energy from the batteries. The battery selection and design is described in Section 8.1. In Section 8.2 details of the fuel type and storage are given. Following is the power transmission via cables in Section 8.3.

8.1. BATTERY SELECTION & DESIGN

Most electric vehicles today use lithium-ion batteries, which have dominated the rechargeable battery market since their advent in the late 1990s. However, there are several disadvantages of these batteries namely: low specific energy, high cost, safety risks and limited supply of lithium and cobalt. These factors have led to intense research into alternative rechargeable battery technologies. Metal- air batteries are a great alternative as they display considerably high energy densities. This is due to the fact that oxygen is used as a reactant at the positive electrode and is stored outside of the battery until it is discharged.

Amongst all metal–air systems, zinc–air (Zn-air) batteries are the most practically viable choice. They possess several desirable features such as a high theoretical energy density, low cost, great safety, and environmental friendliness [50]. The theoretical energy density of zinc–air is 1086 Wh/kg, about 5 times higher than that of lithium-ion and its operational cost is estimated to be less than 90 USD/kWh, only a small fraction of that lithium-ion. Due to these attractive advantages, it is decided to use Zn-air batteries as the power source on E-gle. Zn-air batteries use oxygen from ambient atmosphere to produce electrochemical energy. They are typically composed of four main components: an air electrode comprising a catalyst-painted gas diffusion layer (GDL), an alkaline electrolyte, a separator, and a zinc electrode.

8.1.1. CHARGING & DISCHARGING MECHANISM

Discharge Mechanism
During discharge, the zinc–air battery functions as a power generator through the electrochemical coupling of the zinc metal to the air electrode in the presence of an alkaline electrolyte with an inexhaustible cathode reactant (oxygen) from the atmosphere. The reactions at both the electrodes are spontaneous thermodynamically and produce a theoretical voltage of 1.66 V.

The air electrode reaction:

$$O_2 + 2H_2O + 4\bar{e} \Leftrightarrow 4OH^-, E = 0.40V \tag{8.1}$$

The zinc electrode reaction

$$Zn + 2OH^- \Leftrightarrow ZnO + H_2O + 2\bar{e}, E = -1.26V \tag{8.2}$$

The overall reaction:

$$2Zn + O_2 \Leftrightarrow 2ZnO, E = 1.66V \tag{8.3}$$

Mechanical Recharging
Rechargeable Zn-air batteries for electric vehicles have been heavily investigated since 1975. Mechanically rechargeable and electrically rechargeable forms of the battery exist. In mechanically recharging zinc-air batteries, the battery is charged by removing spent zinc and re-supplying fresh zinc anode. These batteries are therefore designed with a means to remove and replace the discharged anodes or discharge products. The discharged anode or discharge products can be recharged or reclaimed external to the cell. This avoids the need for a bi-functional air cathode and the shape change problems resulting from the charge/discharge cycling of an in situ zinc electrode. This concept is however not widely adopted due to their short activated life, poor intermittent operation and high costs of setting up a network of zinc recharging and supplying stations. Hence the alternative electric recharging is a more attractive option for this design [50, 51].

Electrical Recharging
Electrically rechargeable zinc-air batteries use a bi-functional oxygen electrode so that both the charge process and the discharge process take place within the battery structure. The basic reactions of an electrically rechargeable zinc-air cell using a bi-functional oxygen electrode are shown in Figure 8.1. Advances in electrically rechargeable zinc-air cells are concentrated on developments in the bi-functional air electrodes and zinc electrodes.

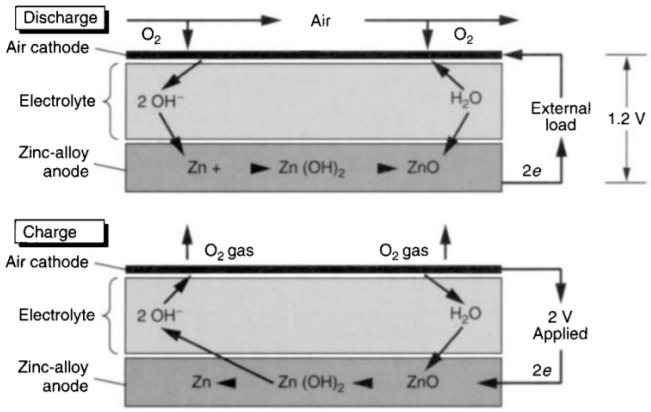

Figure 8.1: Basic operation of electrically rechargeable Zn-air cell [52].

A successful zinc electrode should have a high proportion of utilisable active material, be capable of high-efficiency recharging while being able to sustain its capacity over long period of time and over several hundred charge and recharge cycles. However, there are existing phenomena which try to limit the performance of the zinc electrodes, namely dendrite growth, shape change, passivisation and internal resistance, and hydrogen evolution.

To cope with these problems, a magnitude of strategies have been investigated. Solutions include using high surface area (3D) electrode structures, polymeric binders, carbon based electrode additives, heavy metal electrode additives, electrolyte additive and electrode coatings [50].

8.1.2. BATTERY CONFIGURATION

The type of Zn-air batteries to be used on E-gle use a planar bipolar configuration. This is a multi-cell configuration wherein several Zn-air cells can be stacked in series to raise the battery voltage the required level [52]. In the bipolar arrangement, each zinc electrode is paired with a single air electrode on only one side. Further, a series connection is made between the air and zinc electrode of the neighbouring cell via an electrically conductive bipolar plate, embedded with air channels. Contrarily, in a monoplanar arrangement, the zinc electrode is packed between two externally connected air electrodes and this unit is propagated over multiple cells.

Using a bipolar arrangement over a monoplanar set up has several advantages such as more efficient packaging of cells due to the absence of external wiring and an even distribution of current across the electrodes. As a result, bipolar configuration is preferred. Even so, care has to be taken to ensure that the air electrode is electrically conductive across its entire cross section and that a required pressure is maintained continuously to enable sufficient interfacial interaction between the electrodes and bipolar plates. Figure 8.2 depicts the difference between the two battery configurations[50].

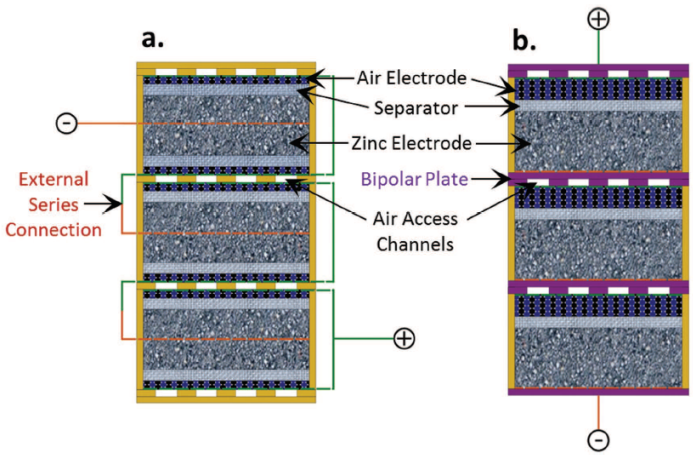

Figure 8.2: Multi-cell zinc–air battery configuration with: a) monopolar arrangement, and b) bipolar arrangement. Air access channels are depicted as going into the page [52].

The negative electrode consists of zinc particles in a paste form and the bi-functional air electrode consists of a membrane of carbon and plastic with appropriate catalysts. The electrolyte is potassium hydroxide with gelling agents and fibrous absorbing materials. A typical cell is rated at 100 Ah with an average operating voltage of 1.2 V. Specific energies up to 180 Wh/kg at the 5 to 10 h discharge rates and a battery life of about 1500 h have been achieved in today's technology. Technical limitations are limited power density and short charge-discharge cycles. However, taking into account large amount of technological research and improvements in battery technology, the makers of E-gle are confident that these minor issues will be overcome by 2025 and that the charge-discharge will reach 1000-1500 cycles [52], [50]. Table 8.1 provides the characteristics of the battery .

Table 8.1: Typical characteristics of electrically rechargeable Zn-air battery

Physical characteristics	**Value**	**Unit**
Cell size	33 x 35 x 0.75	cm^3
Cell weight	1.0	kg
Cell voltage		
Open-circuit	1.5	V
Average	1.2	V
High load	1.0	V
Charging	1.9	V
Energy density		
Current technology	180	Wh/kg
Predicted for 2025	470	Wh/kg
Temperature		
Operating	5 - 35	°C
Storage	-20 - 55	°C
Relative humidity		
Operating	20 - 80	%
Storage	5 - 95	%

It is highly essential that both charge rate and overcharging must be controlled. Overcharging will result in the generation of hydrogen at the negative electrode which will damage the cell and shorten life due to the corrosion of the air cathode. Furthermore, a critical factor in the design of the cell and battery is the means of controlling the flow of air into and out of the cell, which must be matched to the needs of the application. Excessive amounts of air could result in drying out the cell; too little air (oxygen-starved) will result in a drop-off of performance. The stoichiometric quantity of air required is 18.1 cm^3/min/A of continuous current. An air manager is used to control the flow of air by opening air access to the cathode during discharge and sealing the battery from the air when it is not in use to minimise self-discharge. A fan, powered by the battery, also is used to assist the airflow. It is highly essential that the air must be managed to remove carbon dioxide, and to provide humidity and thermal management.

The charging and discharging efficiency of a battery is largely dependent on its architecture. The electrical resistance of the battery is dependent on the number of cells connected in series or in parallel since the battery cells have a certain internal resistance. The battery weight and energy density density are independent of the bus voltage irrespective of the number of cells connected in series or parallel. If large currents are required then it is more efficient for the battery to have cells placed in parallel so that the voltage and the equivalent resistance is low. On the other hand, if current is not a leading parameter in the design of the battery then the voltage should be increased by placing the cells in series such that the losses can be decreased thereby increasing the battery efficiency [53].

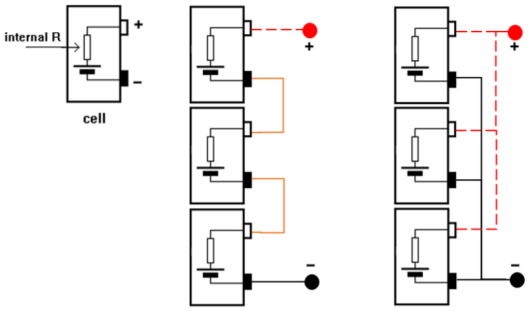

Figure 8.3: From left to right: single battery cell, 3 cells connected in series and 3 cells connected in parallel architecture [53].

Requirements for batteries in terms of power and voltage have been determined in Subsection 10.4.2 and Section 7.4. Based on these values and the typical characteristics of electrically rechargeable Zn-air batteries, it is possible to design for the number of cells required. Each cell is capable of delivering a voltage of 1.2 V. Arranging 584 cells in series results in the required voltage of 700 V. This results in a battery block as depicted in Figure 8.4. To provide the required power, a total 5804 kg of battery cells are required. This is achieved by placing 10 such battery blocks in a parallel configuration across the aircraft. These battery blocks are placed at different locations across the fuselage length. Locations where the battery blocks are placed are shown in Figure 7.21.

Table 8.2: Battery requirements

Property	Value	Unit
Battery energy	2727.88	MW
Energy density (estimated 2025)	470	Wh/kg
Battery mass	5804	kg
Voltage required	700	V
No. of cells required	5804	cells
No. of battery blocks	10	Blocks

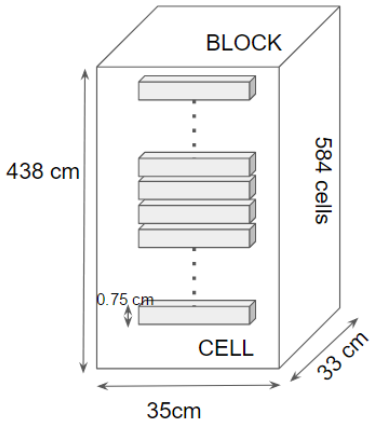

Figure 8.4: Single battery block consisting of 584 cells in series in a bipolar configuration capable of producing 700 V.

8.2. FUEL & STORAGE

E-gle uses Jet fuel A-1 for its fuel. The properties of this fuel are shown in Table 8.3. A total of 735 kg of fuel including the reserve is required per flight. Calculations for the fuel required is performed in Subsection 10.4.2.

Table 8.3: Jet fuel A-1 properties

Property	Value	Unit
Density	0.804	kg/l
Specific energy	42.80	MJ/kg
Energy density	34.7	MJ/l
Auto ignition temperature	210	°C
Flash point	38	°C
Freezing point	-47	°C

The fuel is stored in the wings wherein part of the structure of the wing is sealed with a fuel resistant two-part sealant to form a fuel tank. The sealed skin and structural members provide the highest volume of space available with the lowest weight. This type of tank is called an integral fuel tank since it forms a tank as a unit within the airframe structure. For fuel management purposes, the wing is sealed into separate tanks and includes a surge tank or an overflow tank, which is normally empty but sealed to hold fuel when needed. The engine fuel feed mechanism is a simplified system that combines gravity feed with an electric fuel pump as illustrated in Figure 8.5. Directly downstream of the selector valves are the fuel strainers and then an electric fuel pump for each engine. This pump draws fuel from the selected tank and sends it under pressure to the inlet side of the fuel injection metering unit. The metering unit for each engine provides the proper flow of fuel to the distribution manifold which feeds the injection nozzle of the engines. During manoeuvres, the long horizontal nature of an integral wing tank requires baffling to keep the fuel from sloshing. The wing ribs and box beam structural members serve as baffles. Further, baffle check valves are added specifically for this purpose. These valves allow fuel to move to the low, inboard sections of the tank but prevent it from moving outboard. They ensure that the fuel boost pumps located in the bottom of the tanks at the lowest points above the pumps always have fuel to pump regardless of aircraft attitude. Further, the integral fuel tanks have access panels or tank plates on the bottom surface of the wing for inspection and repairs of the tanks and other fuel system components. These aluminium panels are each sealed into place with an O-ring and an aluminium gasket for electrostatic bonding. An outer clamp ring is tightened to the inner panel with screws.

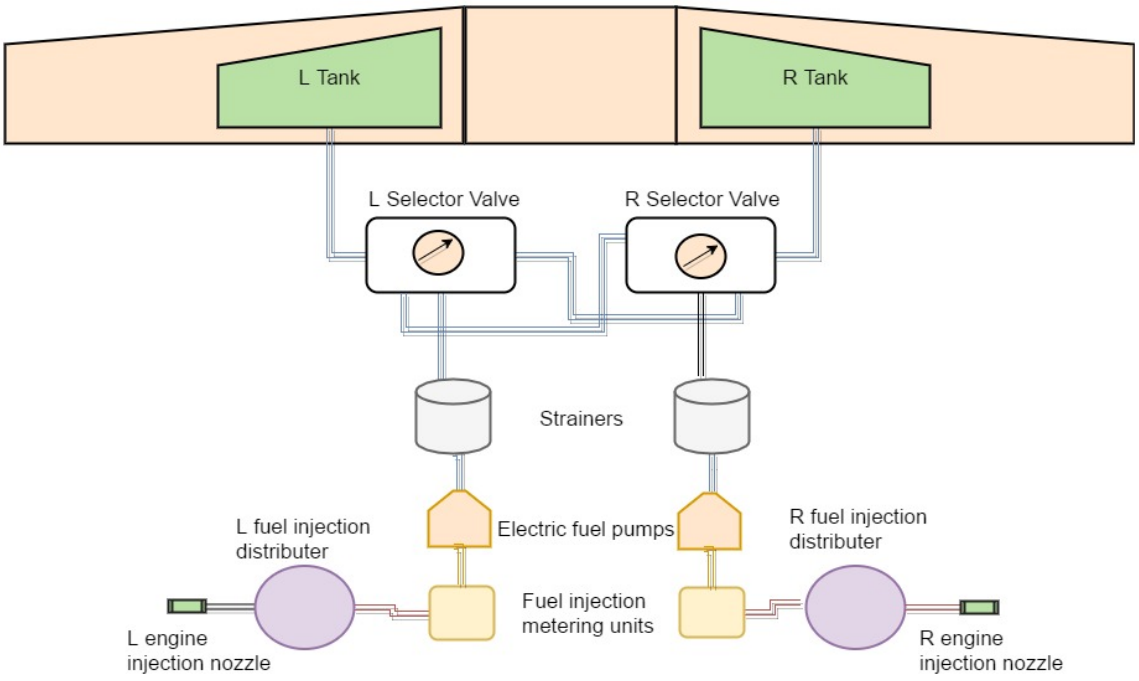

Figure 8.5: Fuel tanks and engine fuel feed system representation.

8.3. ELECTRICAL WIRING & POWER TRANSMISSION

Electrical wiring in E-gle consists of several different types of wires as discussed below:

- Airframe wires & cables for the flight deck, passenger area, wings and surface that control everything from fasten seat belt signs to complex fly-by-wire sub-systems.
- Power transmission cables for all power generation networks, that carry electrical energy for all major systems. These cables, called power feeders, are used to power motors and equipment, drawing energy from batteries.
- Fire-zone and high temperature area cables are used in hot areas, engines and the nacelle environment that carry signals and transmit energy. These wires are flame retardant and fire resistant.
- Coaxial cables used in radio/radar/anti-collision systems for communications and navigation.
- Data-bus, quad ethernet and optical fiber used for transferring signals and power to instrumentation and avionics, for communications and for multimedia and in-flight entertainment systems.
- Customised cables for specific applications that are used in cockpit, crew and passenger areas to meet special needs throughout the aircraft.

Wires for power transmission are very crucial for this mission and hence are discussed in detail. The power from the batteries needs to be transferred to the electric motors and to the other devices in the airframe. Further the batteries need to be recharged from the gas turbines. The transfer of energy is facilitated by means of cables with solid conductor. The cable consists of several layers as depicted in Figure 8.6. The conducting element is the conductor which transfers electricity from one location to another. It is necessary for the conductor to have the lowest weight with the lowest possible electrical losses. This element is surrounded by a non-conducting material called the shield, which is then surrounded by the insulator. The function of the shield and insulator is to isolate the conductor from other conducting materials in order to prevent short-circuiting.

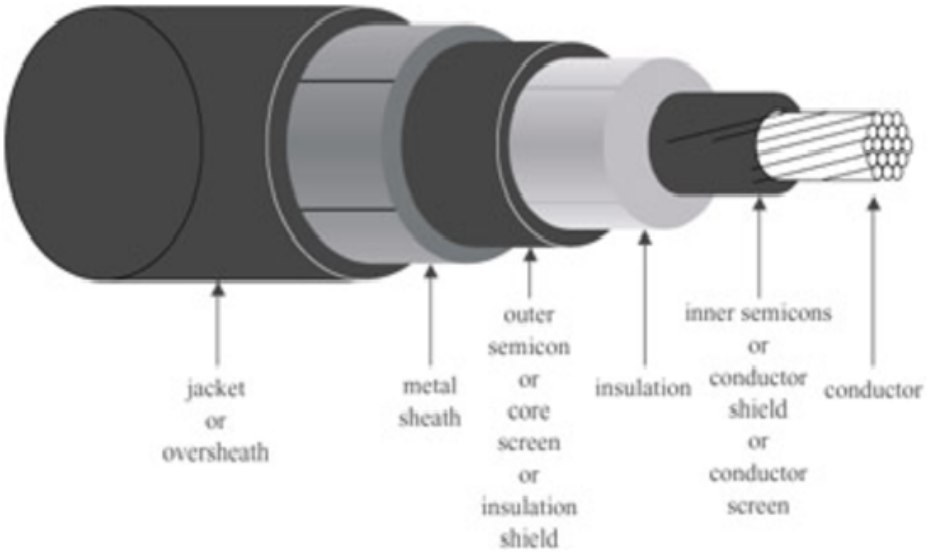

Figure 8.6: Transmission cable layout [53]

9

STRUCTURES & MATERIALS

Besides ensuring the aircraft is aerodynamically efficient, it is also necessary to evaluate if it is capable of handling the loads acting on it that are encountered during the different phases of the mission. To that end, a detailed structural analysis is performed in this chapter. The different loads that the structure has to cope with are identified in Section 9.2. Once all the forces and moments are known, it is possible to evaluate the corresponding stresses which is done in Section 9.3. Since the E-gle has a reasonably high aspect ratio, the wing structure is susceptible to flutter; this is analysed in Section 9.4.

9.1. FLIGHT ENVELOPE

In order to determine the loads acting on the aircraft the flight envelope has to be created. This envelope assesses all the load factors for every flight speed. The overall result can be seen in Figure 9.1. Here two envelopes are presented. The one starting at a value of zero is the manoeuvring load diagram, while the other starting at a value of one is the gust load diagram. The vertical dotted lines from left to right represent the stall speed, stall speed under peak manoeuvre load and cruise speed respectively. The highest equivalent airspeed that is reached represents the dive speed and is 31.25% higher than the cruise speed.

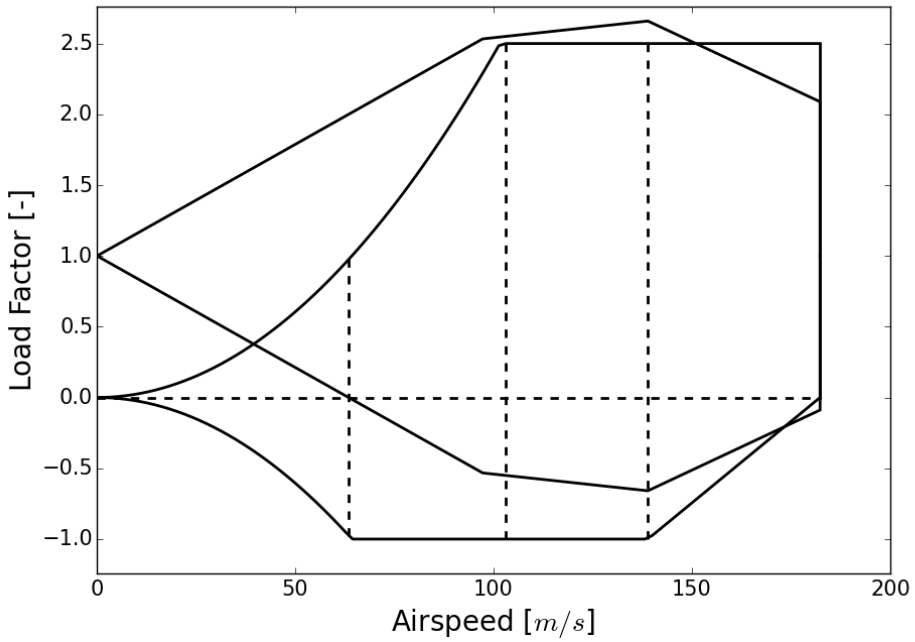

Figure 9.1: Flight envelope of the E-gle

9.2. LOADING

In order to ensure that the wing structure is designed properly, it is required to determine all the loads acting on the wing which are assessed in this section. For preliminary analysis, the lift distribution is assumed to be elliptical. To obtain the distribution of the weight over the wing, it is necessary to come up with an estimate for the dry wing weight. The wing structures can be broadly divided into primary and secondary structures. The components in each category can be viewed in Figure 9.2.

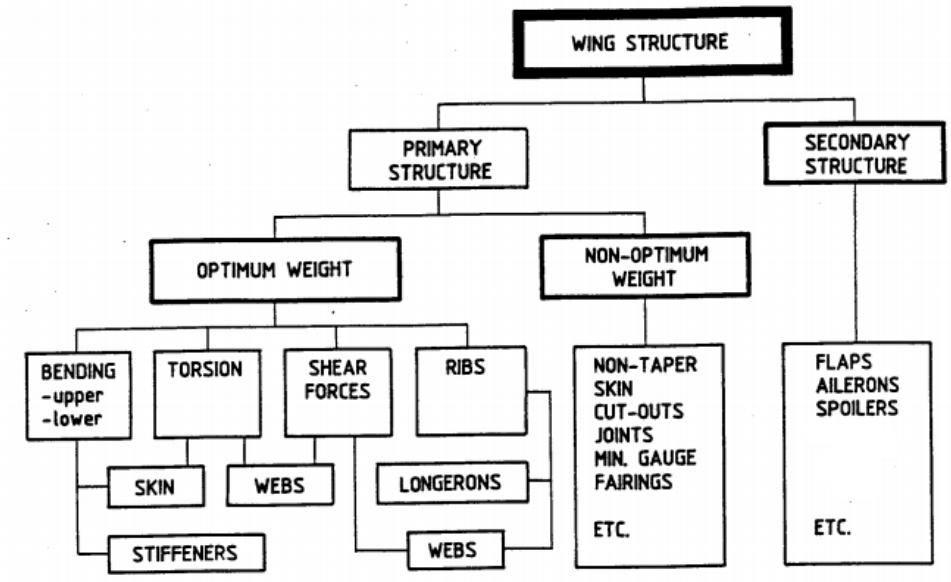

Figure 9.2: Subdivision of wing structure and weight contributions

According to Figure 9.2, the total wing weight can be formulated by Equation 9.1.

$$W_{\text{WING}} = W_{\text{PRIM}} + W_{\text{SEC}} \tag{9.1}$$

The primary weight of the wing is determined by considering the material between and including the front, rear spars and other attachments that are present. It also includes the centre section and contains three parts, as described by Equation 9.2.

$$W_{\text{PRIM}} = W_{\text{BASIC}} + \sum \Delta W_{\text{NO}} + \Delta W_{\text{ST}} \tag{9.2}$$

Here, W_{BASIC} is the minimum weight of the primary structure required to resist bending and shear loads, W_{NO} is the non-optimum weight that takes into account the penalties for joints, cutouts, mounts, and torsional loads and W_{ST} is the weight penalty to allow for stiffness requirements. The weight of the secondary structure includes the weight of flaps and ailerons. The type of flap being used for E-gle is a split flap which is already included the planform, so its weight does not need to be taken into account again. Hence, the secondary structure comprises of only the aileron weight, as can be seen in Equation 9.3.

$$W_{\text{SEC}} = W_{\text{a}} = 125\left[1 + 0.5\left(\frac{W_{to}}{10^6}\right)^{\frac{1}{4}}\right] S_{\text{a}} \tag{9.3}$$

Accordingly, the total wing weight can be calculated. This resulted in 2044.72 kg. This accounts for 10% of the aircraft total weight. A detailed wing weight estimation of E-gle is elaborated below. The method used for this computation is taken from the book *Development and Application of a Comprehensive, Design-sensitive Weight Prediction Method for Wing Structures of Transport Category Aircraft* by E. Torenbeek [54]. The reader is also referred to this book for the nomenclature of the symbols used in the equations of this section. The input values for this computation are obtained from different subsystems of the aircraft, see Table 9.1.

Table 9.1: Input parameters

Parameter	Symbol	Value	Unit
Design Weights			
Maximum Take-Off Weight	MTOW	200578.30	N
Maximum Landing Weight	MLW	196566.73	N
Maximum Zero Fuel Weight	MZFW	187943.02	N
Geometry			
Reference Area	S	39.07	m^2
Span	b	24.2	m
Mid-chord sweep angle	$\Lambda_{1/2}$	3	deg
Leading edge sweep angle	Λ_{LE}	4	deg
Root chord	c_r	1.5	m
Tip chord	c_t	0.5	m
Aspect ratio	A	15	-
Taper ratio	λ	0.33	-
Centre section span	b_{cs}	2.69	m
Thickness/chord ratio - root	t/c	0.15	-
Thickness/chord ratio - 40% span	t/c_{40}	0.15	-
Thickness at root	t_r	0.225	m
Taper ratio of wing tank	$\bar{\lambda}$	0.433	-
Design Conditions			
Design cruise speed	V_C	139	m/s
Design dive speed	V_D	182.43	m/s

First, the cantilever ratio is obtained from Equation 9.4 and Equation 9.5. Its lateral position can then be calculated by using Equation 9.6

$$b_{struct} = \frac{A \cdot S}{\cos(\Lambda_{1/2})} \tag{9.4}$$

$$R_c = \frac{b_{struct} - b_{cs}}{2 \cdot t_{cs}} \cdot \left(\frac{2}{3} + \frac{1}{3} \frac{t/c}{t/c_{40}} \right) \tag{9.5}$$

$$x_{cp} = \frac{2}{3\pi} + \frac{1+2\lambda}{6(1+\lambda)} \tag{9.6}$$

The mass parameter is computed according to Equation 9.7. This parameter is evaluated for the gust load and hence, the maximum zero fuel weight is used whilst the gust factor is calculated using Equation 9.8.

$$\mu = \frac{2 \cdot (MZFW/S)}{\rho g c C_{L_\alpha}} \tag{9.7}$$

$$K_g = \frac{0.88\mu}{5.3 + \mu} \tag{9.8}$$

To determine the critical root bending moment during manoeuvres the coordinate of the fuel must be known. Assuming that the tanks outboard of the fuselage contain fuel, Equation 9.9 yields the following.

$$\frac{\bar{y}}{b_F/2} = \frac{1 + 2\bar{\lambda} + 3\bar{\lambda}^2}{4(1 + \bar{\lambda} + \bar{\lambda}^2)} \tag{9.9}$$

Assuming the fuel tank span is 85% of the entire wing span, the coordinate of the fuel tank with respect to centre pressure is established with Equation 9.10.

$$\frac{x_F}{x_{cp}} = \frac{\frac{\bar{y}}{b_{F/2}} b_{F/2}}{x_{cp}(1 - \frac{b_{cs}}{b})} \tag{9.10}$$

The root bending moment for the manoeuvre load factor $n = 3.75$ is obtained from Equation 9.11.

$$M_{br} = 0.25 \cdot b_{struct} \cdot n_{ult} \cdot x_{cp} \cdot MTOW \cdot \left(1 - \frac{x_F}{x_{cp}}\left(1 - \frac{MZFW}{MTOW}\right)\right) \tag{9.11}$$

The root bending moment for the gust load factor $n = 2.5$ is obtained from Equation 9.12.

$$M_{br_{gust}} = 0.375 \cdot b_{struct} \cdot x_{cp} \cdot (MZFW + 0.5 \cdot k_g \cdot 1.225 \cdot 15.25 \cdot S \cdot CL_\alpha \cdot U_{de}) \tag{9.12}$$

The basic wing weight representing the bending and shear material and additionally, the rib weight for resistance against buckling, is given by Equation 9.13.

$$W_{BASIC} = \frac{1}{3} \cdot \frac{\rho g}{\bar{\sigma_r}} \cdot r \cdot n_{ult} \cdot MTOW \cdot b_{struct} \cdot x_{cp} \cdot \left(\frac{1.08}{\eta_t} \cdot R_c + 1.5 \cdot \frac{\bar{\sigma_r}}{\bar{\tau}}\right) + k_r \cdot \rho \cdot g \cdot S \cdot \left(t_{ref} + \frac{t_r + t_t}{2}\right) \tag{9.13}$$

To evaluate the non-optimum weight due to the engine mountings on the wing, Equation 9.14 can be used.

$$\Delta W_{NO} = 0.025 \cdot (1 + 0.2 \cdot N_{e,dep}) \cdot W_{p,dep} + 0.025 \cdot (1 + 0.2 \cdot N_{e,tp}) \cdot W_{p,tp} \tag{9.14}$$

Finally, by using Equation 9.15, the weight penalty for stiffness requirements can be estimated.

$$W_{ST} = 0.05 \cdot q_d \cdot 10^{-6} \cdot \frac{(b \cdot \cos \Lambda_{LE})^3 \cdot (1 - \sin \Lambda_{0.5})}{(t/c)^2 \cdot (1 - M_d \cdot \cos^2 \Lambda_{0.5})} \tag{9.15}$$

Now that all the contributions to the primary and secondary wing weight are know, it is possible to obtain the total wing weight. Besides the weight of the wing itself, the DEP and cruise propeller engines also introduce forces. The weights of these engine groups act as point loads on the wing. In case a propeller is spinning it also produces a certain thrust and torque. The lift distribution is assumed to be elliptical and is obtained by multiplying the ultimate load factor obtained from Section 9.1 by 1.5 times the maximum take-off weight. The drag distribution is obtained by multiplying the lift to drag ratio with the lift distribution. An illustration of the forces and moments on the wing can be visualised from Figure 9.3a. The main aspects that are visible in this image are the lift distribution and the tip propellers. The line pointing downwards is the weight of the fuselage group. The weight and drag of the wing are relatively small compared to the lift and the fuselage weight respectively. This is due to the fact that the wing weight is only 10% compared to the take-off weight and the lift to drag ratio is high.

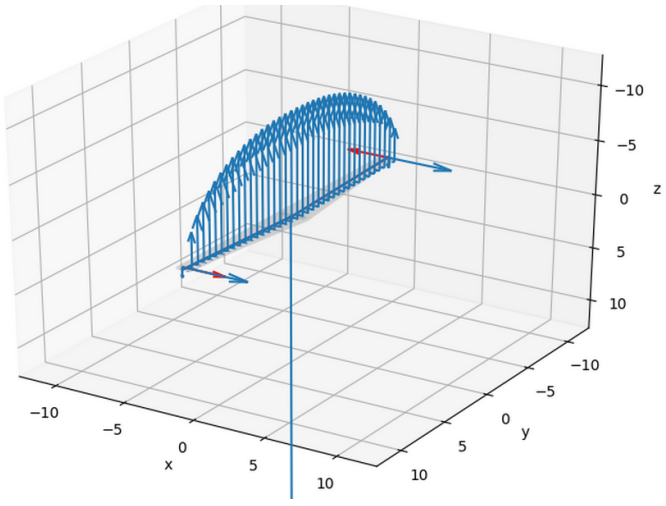

(a) Loading over the spanwise location of the wing. Blue and red vectors indicate forces and moments respectively

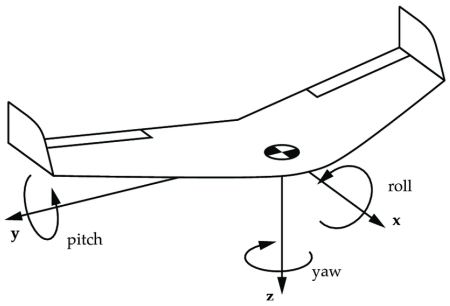

(b) Reference frame for an aircraft[1]

Figure 9.3: Loading over the wing and reference frame

Now that the loading on the wing is formulated, it is possible to evaluate the internal forces and moments in the structure for stress analysis. These internal loads differ during different mission phases, as can be seen from the plots in Figure 9.4. Here F_x, F_y and F_z are the forces in x, y and z respectively. The same holds for the moments M_x, M_y and M_z.

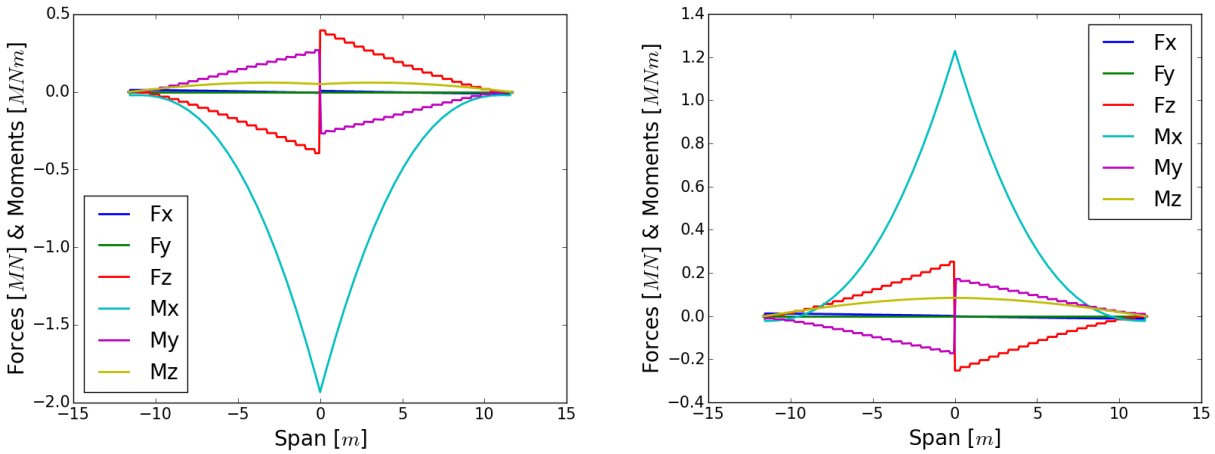

(a) Loading diagram for the pull-up manoeuvre

(b) Loading diagram for the dive manoeuvre

Figure 9.4: Internal loading diagrams for different mission phases

9.3. STRESSES

After the internal forces and moments are determined, the stresses can be determined based on the geometry of the wing. In order to assess the stresses in the structure, some assumptions need to be made. For simplicity, a basic wing box model is used with a symmetrical rectangular cross section, as can be seen in Figure 9.5. This results in a reduced moment of inertia as the height of the airfoil shape is neglected. Due to the fact that the wing box is symmetrical the shear centre coincides with the axes of symmetry. The wing box goes from 15% of the chord length to 70% of the chord length. The outer parts of the airfoil are used for equipment such as the DEP wiring system, an anti-icing system in the leading edge and a flap mechanism in the trailing edge, while the inside of the wing box is used in order to store fuel.

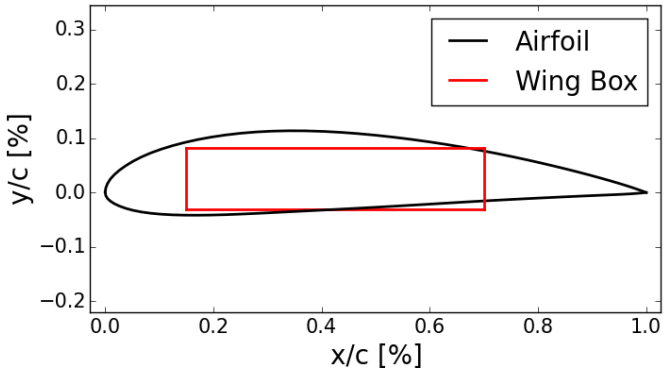

Figure 9.5: wing box cross section

For a given spanwise location it is assumed that the wing box has a constant thickness. This applies to both the leading edge and trailing edge spar and for the bottom and top plate. Furthermore, the assumptions are made that the stiffeners are assumed to be booms and the stresses are distributed equally throughout the skin thickness. Most importantly, the structure is assumed to be rigid. No second order effects due to the deflection are considered.

[1] https://www.researchgate.net/figure/40754972_fig2_Figure-32-Coordinate-system-of-the-body-attached-reference-frame-The-common-names-for [Online; accessed 26 June 2017]

The cross section is analysed at several locations on the wing including all the lift propeller locations. At these locations the total stress is determined by using the von Mises yield criterion. The von Mises criterion requires the normal and shear stresses acting on the structure in order to determine the total stress. These are discussed in Subsection 9.3.1 and Subsection 9.3.2 respectively [55].

9.3.1. NORMAL STRESSES

The stresses normal to the cross section are caused by three factors; two bending moments acting on the plane of the cross section and a force acting perpendicular to the cross section. The stresses caused by the force and bending moments can be calculated using Equation 9.16. Here the two fractions on the left represent the contribution due to the bending moments and the fraction on the right represents the contribution due to the axial force. Where I_x, I_z and I_{xz} are the moment of inertias for the given geometry, x and z are the distances with respect to the centroid and A is the cross sectional area of the wing box. Since the assumption was made that the wing box is symmetrical, I_{xz} becomes zero. Therefore the equation can be simplified resulting in Equation 9.17.

$$\sigma_y = -\frac{M_x I_z + M_z I_{xz}}{I_z I_x - I_{xz}^2} z + \frac{M_z I_x + M_x I_{xz}}{I_z I_x - I_{xz}^2} x + \frac{F_y}{A} \tag{9.16}$$

$$\sigma_y = -\frac{M_x}{I_x} z + \frac{M_z}{I_x} x + \frac{F_y}{A} \tag{9.17}$$

9.3.2. SHEAR STRESSES

In order to find the von Mises stress, the shear stress needs to be computed. The shear stresses are influenced by two shear forces and a torque. The contribution due to the torque is calculated by Equation 9.18. In this equation T represents the torque, which is equal to M_y from Section 9.2. Furthermore, t and A_E represent the skin thickness and the area enclosed by the wing box respectively.

$$\tau_T = \frac{T}{2tA_E} \tag{9.18}$$

The contribution due to the shear forces on the shear flow is calculated with Equation 9.19. Where the moment of inertias are denoted by I, t_s is the skin thickness and x and z are the distances from the centroid. In the summation the area of the booms are multiplied with either the offset of the boom to the centroid on the x axis or the y axis. Since the wing box was assumed to be symmetrical this equation can be simplified to Equation 9.20. The integral has to be evaluated over the entire circumference of the wing box. In order to save some time with the calculations this evaluation for the shear flow due to the shear force F_z is initiated in the middle of the bottom skin. Since the wing box was symmetrical, the shear center must also lie on the axis of symmetry. This implies that the bottom skin will have zero shearflow at the intersection with the symmetrical axis. For the shear force F_x this is done with the leading edge spar.

$$q = -\frac{F_z I_x - F_x I_{xz}}{I_z I_x - I_{xz}^2} \left(\int_0^s t_s z ds + \sum_{i:s_i \leq s} z_i A_i \right) - \frac{F_x I_z - F_z I_{xz}}{I_x I_z - I_{xz}^2} \left(\int_0^s t_s x ds + \sum_{i:s_i \leq s} x_i A_i \right) \tag{9.19}$$

$$q = -\frac{F_z}{I_z} \left(\int_0^s t_s z ds + \sum_{i:s_i \leq s} z_i A_i \right) - \frac{F_x}{I_x} \left(\int_0^s t_s x ds + \sum_{i:s_i \leq s} x_i A_i \right) \tag{9.20}$$

The shear stresses and shear flows are related by Equation 9.21, where t is the skin thickness. The total shear stress is computed by adding the contributions due to the forces τ_F and the contribution due to the torque τ_T.

$$\tau_F = \frac{q}{t} \tag{9.21}$$

9.4. FLUTTER

In addition to the stress constraint, the flutter of the wing must also be looked into. There are two main system parameters that have an effect on the flutter, the aspect ratio and number of high lift propellers. Alteration of these factors vastly affect the distribution of aerodynamic loading and structural stiffness. To determine how much extra weight the flutter institutes in the structure, an analysis performed by Gerogia Institute of Technology is used [56]. From reference, it can be noted that the increase in weight is about 6%. Hence, the total wing weight including flutter is 2167.39 kg.

9.5. MATERIAL SELECTION

To determine if the stresses in the wing structure exceed the maximum allowed stress, a material should be chosen. A large variety of materials can be used to build a wing structure. In order to select a material, an overview of suitable materials should be given. These materials include alloys from metals such as aluminium, steel and titanium. However, newer materials combinations such as composites might also be feasible. A selection can be made based on the properties of the materials.

While titanium alloys have high specific yield stresses and have a high corrosion resistance, they are almost ten times more expensive compared to aluminium alloys in order to support the same load. These titanium alloys are sometimes used in order to attach the engine to the wing. Furthermore these alloys are also used for military purposes as costs are not the primary driver for military aircraft.

Even though steel is cheap compared to aluminium, due to its high strength and high weight, the structures are generally thinner compared to aluminium. This makes the structure less resistant to compression and bending. Therefore, the eventual weight of the structure will have to increase in order to sustain the compression and bending loads [57].

For the E-gle's wing structure the alloys aluminium 7050 and 2024 are used. The aluminium 7050 alloy is commonly used in aerospace industries in order to make aircraft structures. Furthermore, it is known for its high yield strength compared to other aluminium alloys and has more resistance to corrosion compared to aluminium 2024, which is also often used in aircraft structures. The advantage of aluminium 2024 is that it has better fatigue properties. For this reason the E-gle's wing structure will consist out of both aluminium 7050 and 2024.

9.6. RESULTS

After all stresses are determined and the materials are chosen the von Mises stress can be compared with the yield stress of the selected materials. If the von Mises stress exceeds the yield stress the wing structure will fail at that point. This means that the structure needs to be reinforced at that location. Iterating this process until the entire structure sustains all the loads makes sure that the wing box is strong enough. This results in an initial weight. However, this method does not take into account buckling and therefore is increased by a structural reinforcement weight using methods from Torenbeek as explained in Section 9.2.

Both the weights of stress analysis and Torenbeek are compared and increased with a flutter increment of 6% as was obtained in Section 9.4. Both methods have disadvantages. The stress analysis has an empirical estimation for the buckling weight, while the method from Torenbeek doesn't include the engine placement. Since both methods neglect different aspects of the wing, the highest value of both values is used. This resulted in an overall wing mass of $2045kg$.

9.7. LANDING GEAR

The landing gear is one of the most critical components in an aircraft and its failure can be catastrophic. Thus, it is very important to carefully decide on its location. The main landing gear is positioned relatively to the wing, typically at 45-50% MAC, to guarantee ease of rotation during take-off. This corresponds to a typical location of 10-15% MAC behind the aft c.g. limit, which also prevents the aircraft from tipping over. In Chapter 6 a scissor plot has been generated that yields the most forward and most aft c.g. limits of the aircraft. The most aft c.g. is located at -8% MAC and hence, taking an average of 12.5%, the landing gear must be positioned at 4.5%. This is located 9.04 metres aft of the nose of the aircraft.

The landing gear consists of a single nose landing gear and two rear landing gears. The nose landing gear has two wheels and the rear landing gears have four wheels each. The load on each wheel can be calculated by using Equation 9.22 and Equation 9.23, for the number of main and nose wheels N [58].

$$P_{mw} = 0.92 \cdot W_{TO} / N_{mw} \tag{9.22}$$

$$P_{nw} = 0.08 \cdot W_{T0} / N_{nw} \tag{9.23}$$

With the static loads and by using the tire pressure of 80 psi of the Fokker F-27 [58], the tyre dimensions can be determined to be $32x11.4$ cm for the ones on the nose landing gear and $61x19.6$ cm for the rear landing gear [17]. For the rear landing gear an overall landing gear height of 1 m is used in order to achieve tip back angle of 13.3° [59]. Using empirical data, the total landing gear mass was determined to be 640 kg.

10

PERFORMANCE

In this chapter, the performance of the aircraft is discussed. First, the general approach used is addressed in Section 10.1. Following this a model for a reference aircraft, the Bombardier Q300, is given in Section 10.2 and a model for the hybrid electric aircraft, the E-gle, is given in Section 10.4. Section 10.5 presents the results of the model and Section 10.6 deals with the performance of E-gle with the chosen parameters.

10.1. OPTIMISATION APPROACH

To analyse and optimise the performance of E-gle for its mission a Python program is created. It uses the outputs from all subsystems to determine the most suitable mission profile and calculates the amount of fuel and batteries needed to perform the mission.

Since hybrid aircraft is a new concept that has not been developed previously, no statistical data could be found. Normally, the fuel weight needed for a certain flight mission is estimated using a weight fractions method. This method is based upon a decrease of weight by fuel burn. The flight mission is separated in different flight phases. Then the weight fraction of the several phases are gathered from statistical data except for the cruise and loiter phases. For these phases, the Breguet range equation is used. However, this method is not applicable for a hybrid electric aircraft. This is because there is no statistical data for regional hybrid electric aircraft. But more importantly, the weight of the aircraft will not vary if only electric energy is used. Therefore, a new approach to the problem needs to be taken.

The new method focuses on the power that is needed to perform the mission profile. Power is a much more universal way to approach the problem as both the electrical energy as well as the chemical energy of the fuel will be converted into mechanical energy in the shaft of the propeller. By using the specific fuel consumption (SFC) of the engines, the amount of fuel burned can be found. The total amount of electricity used can be found by determining the efficiency of the electrical system. Furthermore, the power generated by electrical engines and the power generated from the gas turbine can be set individually during each phase. By multiplying the power with time, the energy of all the phases can be obtained. A total efficiency for the aircraft can also be determined. The results can be used to analyse the power setting of each power source during each phase and an optimal power split (division of power between fuel and batteries) can be found. From the above data, the required energy from each source can be found and the battery and fuel mass can be estimated.

A model for both the Q300 and the E-gle was created with this new method. The power required for these models is estimated using the equations from *Introduction to Aerospace, Ruijgrok* and *Flight mechanics* [60–62]. After verifying and validating the models, they can be used to optimise the flight profile and calculate the required fuel and battery mass. The following sections elaborate in detail on the making of the models.

10.2. BASELINE MODEL: BOMBARDIER Q300

The reference aircraft that was chosen for this study is the Q300. The Q300 is a regional turboprop that can carry 50 passengers. In contrast to its predecessors this aircraft was not optimised for STOL (Short Take-Off and Landing), but rather for cruise performance and operational costs as airliners were more interested in these aspects. As the E-gle is also being optimised for cruise and low operational costs and also has to carry 50 passengers, the Q300 was found to be a suitable reference aircraft. The flight profile of the Q300 is closely related to the mission profile of the E-gle described in Section 3.1. The cruise height, cruise velocity and block range can be found in Table 10.1 along with other important aircraft characteristics that are used throughout this report.

Table 10.1: Q300 Characteristics

Parameter	Value	Unit	Parameter	Value	Unit
Passengers	50	-	Cruise Velocity	532	km/h
Range	924	NM	Cruise Altitude	7000	m
MTOW	19505	kg	Surface Area	56.2	m^2
OEW	11793	kg	Aspect Ratio	13.35	-
MFW	2528	kg	Engine	P&WC PW123s	-
MPW	6,124	kg	Number of Engines	2	-

10.2.1. ENGINE WARM-UP AND TAXI

During the first two phases of the flight the engines are started and used for taxiing to the take-off runway. Since the aircraft moves at low speed, the engines will operate close to idle setting. These phases use fuel and battery power but do not add to the distance flown. This is modelled by simply calculating the fuel burn using a fuel fraction of 0.999 [42], the battery power needed is calculated and multiplied by the total time to find the battery energy used during these phases.

10.2.2. TAKE-OFF

In the model for the take-off it was assumed that the engines are set to full throttle and thus have maximum power for take-off. Of course it is also possible to take-off at lower power setting in order to increase engine life, but that is not included in this model.[1] What still needs to be known is how long the aircraft needs to complete the take-off. In order to compute that, the take-off phases is split into a ground phase and an airborne phase. During the ground phase the aircraft accelerates to lift-off velocity. During this procedure the aircraft experiences two types of drag: friction drag from the ground and aerodynamic drag, which are estimated using Equation 10.1. In Equation 10.1 a $\mu_{friction}$ of 0.02 was used [61]. Note that the ground drag decreases with increasing velocity, while the aerodynamic drag increases. The thrust is estimated in Chapter 7. The equation can be used to compute the acceleration of the aircraft by dividing the net thrust, which is the total thrust minus drag, by the mass. The time can then be calculated using standard kinematic equations.

$$\frac{W}{g}\frac{dV}{dt} = T - C_{D_g}\frac{1}{2}\rho V^2 S - \mu_{friction}(W - C_{L_{TO}}\frac{1}{2}\rho V^2 S) \tag{10.1}$$

The airborne phase of the take off endures till the aircraft reaches a screen height of 15.2 m[61]. This phase was approximated using the method described in Subsection 10.2.3. As a check the total take-off distance is computed using simple kinematic equation. If the requirement is not met, the engine power will be increased.

10.2.3. CLIMB

There are multiple climb profiles to climb to cruise height according to [63]. In this model, a simplified climb profile was taken. It consists of the following 3 phases:

- Climb at V_2 with constant CAS to a height of 450 m.
- Accelerate to optimum climb velocity.
- Climb at optimum climb velocity with constant CAS to cruise height.

First and Second Climb
During the first part of the climb the aircraft will fly at the same CAS as the CAS at the end of the take-off phase. It climbs to an altitude at which the aircraft can accelerate to a more optimal velocity to climb. The differences between the two climbs is only the velocity they start with. During the whole climb the engines are assumed to work at full power in order to achieve the maximum rate of climb. In order to calculate how long the aircraft needs to generate maximum power, it is important to know the rate of climb, RC. The rate of climb can be used to compute the time over which the power is needed. If power and time are known, the total energy needed can be computed by battery mass estimations. The RC is determined by Equation 10.2 [62].

[1] https://www.skybrary.aero/index.php/Reduced_Thrust_Takeoff.[Online; accessed 19 June 2017]

$$RC = \frac{P_a - P_r}{W} - \frac{V}{g}\frac{dV}{dt} \tag{10.2}$$

The power available, P_a, changes with altitude. This is due to lower air densities at high altitudes. Lower density also implies a lower mass flow resulting in less power available. The temperature of the air will also be lower at higher altitudes, allowing more heat to be added to air. But this effect does not out weigh the effect of lower air density. Equation 10.3 is used to compute the power available at different air densities[60].

$$\frac{P_a}{P_{a,0}} = \left(\frac{\rho}{\rho_0}\right)^{0.75} \tag{10.3}$$

Furthermore, the power required, P_r, is essentially the drag of the aircraft times the true airspeed it flies at. The drag coefficient was computed by Equation 10.5. From this the drag was calculated by Equation 10.6. For the induced drag the lift coefficient was simply calculated using Equation 10.4.

$$L = \frac{1}{2} C_L \rho V^2 S \tag{10.4}$$

$$C_D = C_{D_0} + \frac{C_L^2}{\pi A e} \tag{10.5}$$

$$D_{aero} = \frac{1}{2} C_D \rho V^2 S \tag{10.6}$$

During the climb, the aircraft flies at constant CAS. This does not mean that the aircraft flies at a constant true airspeed. This change in true airspeed, $\frac{dV}{dt}$, is caused due to a change in air density. As can be seen in Equation 10.7 the true airspeed will increase with a decrease in density and thus will increase during the climb.

$$CAS = TAS\sqrt{\frac{\rho}{\rho_o}} \tag{10.7}$$

The optimal velocity to climb occurs at maximum excess power [62]. As the power available is constant over velocity, the optimal velocity occurs at minimum power required. For this flight condition the $\frac{C_L^3}{C_d^2}$ should be maximised[62], which will happen at the lift coefficient found in Equation 10.8. The corresponding velocity of this lift coefficient can be easily found using Equation 10.4. Knowing the acceleration, begin and end velocity, the time period can be computed using standard kinematics

$$C_L = \sqrt{3 C_{D_0} \pi A e} \tag{10.8}$$

Acceleration

During the second phase the aircraft will accelerate to an optimal velocity for the climb to cruise altitude. It is assumed that the aircraft will remain at the same altitude during the acceleration and that all the excess power i.e., power available minus power required, is used to accelerate the aircraft. This acceleration can then be determined by Equation 10.9.

$$\frac{dV}{dt} = \frac{P_a - P_r}{VW} \tag{10.9}$$

10.2.4. CRUISE

After the climb the aircraft will accelerate to cruise velocity. During cruise it is assumed that the lift is equal to the weight and the drag equal to the thrust. Therefore the power the engines will provide is equal to the power required. The C_L at which the aircraft is flying, is computed via Equation 10.4. This C_L will be used to calculate the drag with Equation 10.5 and Equation 10.6. As the weight decreases during the cruise, the C_L can decrease as well resulting in less drag and therefore, the power required will go down. Normally aircraft performs step climbs. As the weight decreases the aircraft is able to fly higher resulting in a lower density and also less drag. However, this effect is not implemented in the program.

10.2.5. DESCENT

The descent is split up into two phases. In the first phase, the aircraft will descent from cruise height to loiter height. After loitering, the second descent will be initiated where the aircraft will descend from loiter height to landing height. The first phase will start with the deceleration to a velocity the aircraft can glide as far as possible. Deceleration is acheived by returning the power setting to flight idle, which is 4% of maximum power [64]. The optimal velocity is reached when $\frac{C_L}{C_D}$ is maximised. The corresponding lift coefficient can be calculated using Equation 10.10 [62].

$$C_L = \sqrt{C_{D_0} \pi A e} \tag{10.10}$$

During descent, it is assumed that the engines are running on flight idle in order to minimise fuel consumption. The aircraft will maintain this velocity by having a fixed glide angle that ensures the component of the weight in longitudinal axis will compensate the drag. After the loiter phase, the second descent will take place. As the height difference of this descent is much lower that the first climb, the aircraft will not be accelerated to optimal glide range velocity. The aircraft will descend further at loiter velocity. The rate of descent is then computed by Equation 10.2 with a power available equal to the flight idle setting.

10.2.6. LOITER

After the first descent it is possible that the aircraft has to loiter for a certain period. In the model, a loiter time of 10 minutes was chosen. The velocity at which the aircraft can fly at maximal endurance occurs at minimum power required. The optimal lift coefficient for this condition can be found using equation Equation 10.8 [62]. The aircraft first needs to decelerate to a velocity at which the aircraft has this optimal lift coefficient, then it will loiter. Similar to the cruise phase, it is assumed that thrust equals the drag. The drag can be calculated using Equation 10.5 and Equation 10.6 as the lift coefficient is known. The power required was found by multiplying the drag with the velocity and this power will be equal to the power delivered by the engines.

10.2.7. LANDING

During landing the aircraft is assumed to fly at flight idle. The landing consists of a airborne phase and ground run. The airborne phase starts at screen height. The calculation is similar to the descent phase and will be done till a height of zero meters is reached. At this moment, the ground run starts. Equation 10.1 is used to compute the deceleration. It is assumed that thrust is zero and that the friction coefficient, or in this case the brake coefficient, is equal to 90% of the maximum brake coefficient of 0.8 [61]. Furthermore, there is a sudden true velocity decrease for the wing at touch down as the high lift propellers will be switched-off and will not provide an increase in dynamic pressure anymore. Therefore, brakes can be used more efficiently.

10.2.8. FUEL BURN

The fuel that is used by the gas turbine can be calculated with Equation 10.11. The shaft power of the gas turbine, which is an input of this equation, can be calculated using Equation 10.12. As this power is variable over time it needs to be integrated over that time. By multiplying the shaft power with the brake specific fuel consumption of the current phase, as found in Subsection 7.3.1, the weight of the fuel in N can be found. Dividing this by the gravitational acceleration will give the total amount of fuel used in kg.

$$m_{fuel} = \int \frac{P_{s_{gas}} BSFC}{g} dt \tag{10.11}$$

10.3. VERIFICATION AND VALIDATION

To check the reliability of the model of the Bombardier Q300 it needs to be compared to reality. This is done by first verifying the model to check if the model solves what it is expected to solve and second validating to ensure outcomes can be used in the real world.

10.3.1. VERIFICATION

In order to verify the model of the Bombardier Q300 first unit tests were performed on each mission phase. Following this the entire model was verified by altering input values and seeing if the outcomes changed as expected.

Unit test
Each mission phase has a separate unit in the model. Once a mission phase was modelled unit test are performed. First it is checked for syntax errors, following this the outcomes are compared to calculations done by hand to verify that the unit is working as expected. Small coding errors were fixed and in some cases mathematical errors were corrected. The resulting units are all verified. The results can be seen in Table 10.2. Deviations of the fuel burn in the unit tests can be explained by the simplified approach that was taken for the hand calculations. While the model is numerically integrated over time, for the hand calculations assumptions were made in order for it to be solvable.

Model verification
With all units verified the entire model was created by integrating all units into one program. This model is verified by altering inputs and seeing if the outcome changes as expected. The outcomes can be seen in Table 10.3. This completes the verification of the model.

Table 10.2: Verification of the units

Mission Phase	Output fuel burn [kg]	Calculated value [kg]
Engine Start	97.5	97.5
Taxi	97.0	97.0
Take-off	6.5	7.2
Climb	210.1	201.2
Change speed	32.4	32.1
Cruise	1735.3	1744.2
Descent	21.4	22.1
Loiter	40.9	41.3
Landing	5.7	5.9

Table 10.3: Verification of the complete model

Complete model test	Expected behaviour	Model Behaviour
Decreasing Cruise Height	Increase in total Fuel Consumption	Increase in total Fuel Consumption
Lowering Surface Area	Decrease in total Fuel Consumption	Decrease in total Fuel Consumption
Decreasing Cruise Velocity	Decrease in total Fuel Consumption	Decrease in total Fuel Consumption
Decreasing Range	Decrease in total Fuel Consumption	Decrease in total Fuel Consumption

10.3.2. VALIDATION

Now that the model is verified, it needs to be validated to ensure its reliability. This is done by taking the base model and comparing the outcomes to values from the Bombardier Q300 itself. The total fuel consumption for the Bombardier Q300 was found for a range of 924 NM with a payload of 5000 kg [65]. This also includes fuel reserves for loiter and diversion. In the model a diversion of 100 NM is taken into account. The results of the model and a comparison between the model and the Bombardier Q300 can be found in Table 10.4. Since the deviation between the model and reality is small the model is considered to be validated.

Table 10.4: Validation of the model

Model Fuel Consumption	Bombardier Q300 Fuel Consumption	Deviation [%]
2579.9	2528	2.05

10.4. HYBRID ELECTRIC MODEL: E-GLE

In order to estimate the performance of the E-gle a hybrid electric model was made. This was done by adjusting the model of Q300, after it was verified and validated. This is done not only by adjusting input values, but also the code of the model was changed to implement the simulation of DEP and electrical engines. Those changes are explained in this section. Subsection 10.4.4 describes the integration of all subsystems in the model.

10.4.1. SHAFT POWER GENERATION

In a hybrid electric aircraft the shaft power generation differs from a conventional aircraft. In this section, it is discussed where the shaft power, that is being delivered to the propellers and to the on-board systems, comes from. The power from the gas turbine uses the energy source fuel while the power delivered by the electric engines and distributed lift propellers is delivered by the batteries.

Gas turbine
As the power for propulsion can now be delivered by multiple sources as can be seen in Equation 10.12, the gas turbine can be scaled down. The gas turbine will operate at full power during take of and climb, and will stay on idle during descent just like in the baseline model. However, the power setting during loiter and cruise is determined by the amount of power the electric engines are able to deliver during these phases and the power required to keep a constant airspeed, in those phases the power required is equal to the power delivered from the engines. The distributed lift propellers will be folded and therefore will not use any power. Subsequently, if the power setting of the electric engines is known, the total power needed from the gas turbines can be calculated. During the descent, the engines will stay on flight-idle as turning off the engines will result in a safety issues, turning on engines in mid-air is harder due to the lower density. In the model this is implemented by having a variable power setting for the gas turbines in cruise and loiter depending on the shaft power required and the shaft power generated by the electric engines.

$$P_{a_{total}} = (P_{s_{gas}} + P_{s_e})\eta_{prop_{thrust}} + P_{s_{dep}}\eta_{prop_{dep}} \tag{10.12}$$

Electric Engine
The electric engine will be used as an auxiliary motor. It was determined that it is most beneficial to fly at maximum power during take off and climb, therefore the electric engines will use full power during those phases. An advantage is that the power of electrical engines does not degrade with increasing altitude as it is not dependent on the mass flow. Furthermore, the engines will be used during cruise and loiter. The power setting of the engine in these phases depends on the available battery energy that is left in the engines. The program iterates the available battery energy for cruise and loiter from which the power setting can be determined. The electric engines will shut down during the descent phase. This is implemented in the model by first, adding an electric shaft power source and secondly, changing the power setting of the electric engines per phase.

Distributed lift Propellers
During take-off, initial climb, and landing the aircraft will need to use the distributed lift propellers in order to stay airborne. The propellers create extra thrust and increase the lift generation. Since every propeller has an electric engine, extra power is required from the batteries during this phase. In the model the use of extra power for the take-off, initial climb and landing is taken into account, but since the distributed propeller only provides effective thrust at low speed this is not taken into account in the model.

10.4.2. ENERGY SOURCE

In the hybrid electric model, the energy comes from two sources, namely fuel and the batteries. In this section, it is discussed how the fuel mass and battery mass are calculated.

Batteries
Batteries provide power to the electrical engines, distributed lift propellers and the auxiliary power (i.e cabin, cockpit). With Equation 10.13 the total battery mass can be calculated. The described model determines the power at each time instance of the whole mission. If this power is integrated over time, the total energy needed from the battery can be calculated. It is important to also take into account the efficiency's of the system. The electric motors are divided by the efficiency of the motor and controller. Both the auxiliary energy and the shaft energy still need to be divided by the efficiency of the battery. This results in the total energy the battery should contain. Since the life-cycle of the battery depends on the depth of discharge [66], a 20% margin is added to the battery weight. Finally by applying the energy weight density, in this design a specific energy of 500 Wh/kg is used, the mass of the battery can be found.

$$m_{batt} = \int \left(\frac{P_{s_{motor}} + P_{s_{DEP}}}{\eta_{controller}\eta_{motor}} + P_{aux} \right) \frac{1}{E_s \eta_{batt}} dt \tag{10.13}$$

Fuel
The amount of fuel used is calculated the same way as with the bombardier. Different values for the BSFC were used since the E-gle uses different engines.

10.4.3. DRAG REDUCTION

Drag reduction is mostly realised in 2 ways. First a lower surface area can be realised, since the wing is designed for cruise conditions as discussed in Chapter 5. This can easily be implemented in the model of the Q300; only the surface area needs to be changed. Furthermore, drag reduction is realised by having the turboprop engines at the tip of wing. The vortices that are generated at the wing tip due to pressure difference of the upper and lower part of the wing are countered by the propellers and therefore the induced drag decreases. In Chapter 5 it is estimated that wing tip propeller would decrease the induced drag by 35%. Therefore the induced drag in the model is simply multiplied with 0.65.

10.4.4. COMPLETE MODEL

To finalise the design of the E-gle the model as described above is combined with the models for aerodynamics, structures and propulsion. This results in a iterative model that converges to a value for all design parameters of the E-gle and takes into account design choices from all subsystems. The flow of the model is shown in Figure 10.1, it continues to iterate untill all values are no longer deviating more than 1%.

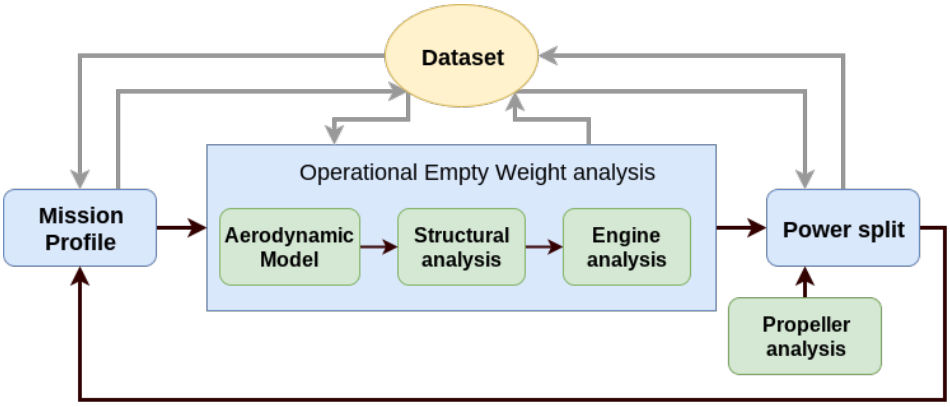

Figure 10.1: Flow diagram of the complete model. Black arrows indicate the flow of calculations, whilst grey arrows indicate the flow of data.

10.5. RESULTS

This section describes the results and conclusions that result from the program. First the cruise height is chosen, secondly the optimal number of electrical engines is discussed. Following this the mission profile is explained accompanied by a presentation of the power split. Finally a comparison is made to the Bombardier Q300.

10.5.1. CRUISE HEIGHT

In order to choose the most optimal cruise height the program evaluate the aircraft for several height. Normally flying higher is more efficient, because the density at high altitude is low and therefore the drag and thus the required power are low as well. However it costs time and energy to reach such an altitude. Especially for short flight it might be interesting to fly at lower altitudes.

Figure 10.2 shows that the optimal height fuel wise is around 6 km. However, a high altitude means, with a constant airspeed, an increase in surface area. This is less favourable as this will increase the weight of the total aircraft, but more importantly, increases the moment arm of the tip mounted engines. In Chapter 9 it was found it was very hard to estimate the effect of the wing tip engines on the wing and aircraft structure and therefore great uncertainty still exist at this topic. Increasing the moment arm was therefore found not to be ideal.

In addition an analysis was done on the height of different mission ranges. As the maximum range of the aircraft is 500 NM it is most likely that airliners will use it on flights in the range 300 to 500 NM. In Figure 10.2 the required fuel mass versus the range is plotted for several cruising altitudes. It can be seen that at an 500 NM range the least fuel is required for the 6 km height. However, for ranges shorter than 470 NM, the aircraft consumes less fuel for a cruise height of 5 km. The minimum cruising height is 5 km in order to be able to fly over high mountain ranges as the Alps and Pyrenees.

The busiest flying routes cover a distance of less than 500 NM[1] Therefore it was found ideal to optimise the aircraft for fuel use for this range, while it is still able to meet the 500 NM range requirement. The uncertainty of the effect of the weight of the wing tip propeller on the aircraft structure and a lower fuel consumption for ranges shorter than 470 NM are the motivation to choose for a cruising altitude of 5km.

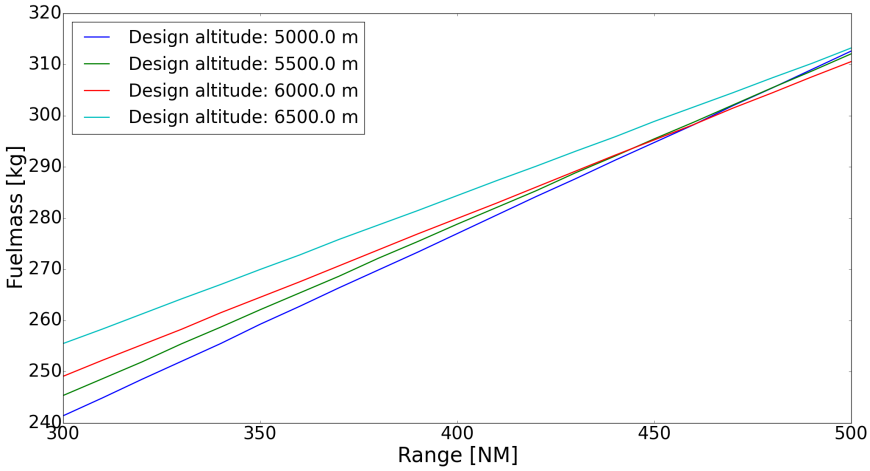

Figure 10.2: Fuel used at several height relative to the the range the aircraft will fly

10.5.2. NUMBER OF ELECTRICAL ENGINES

The optimal number of electric engines was determined using Figure 10.3. In Figure 10.3 can be seen that the efficiency of the system goes up for increasing number of engines. This is logical as the efficiency of the electrical system is higher than that of the gas turbine system. However, it is interesting to note the the behaviour of the curve. First the efficiency increases exponentially, but from 5 engines and more it transform to a more linear behaviour. This can be explained by the fact that 5 electrical engines can provide just enough power to fly the aircraft on battery power only. Therefore the number of engines in the range of 0 to 5 increases the efficiency greatly, because they affect the cruise phase, which is the major part of the flight. Adding more engines will increase the efficiency of the system but not as drastically as before. These engine will only affect the take-off, climb and acceleration phases, which are a smaller part of the entire mission.

[1] http://www.iata.org/pressroom/pr/Pages/2016-07-05-01.aspx. [Online; accessed 19 June 2017]

It should be noted that in these graphs it is assumed that the electrical engine will provide maximum power during cruise and loiter unless this is more than required. Therefore, increasing the number of engines will increase the total battery mass as more electrical energy is required to feed the electrical engines. This increases the total drag and energy required, but since electrical engines have a significantly higher efficiency over gas turbines the total efficiency of the aircraft increases. Furthermore, an even amount of engines is preferred, because the electrical engines will be installed in 2 gas turbines. An odd number of engines will result in an uneven power distribution over the aircraft making it asymmetrical and complex. The optimal amount of engines would be 5 according to Figure 10.3. However as discussed before an odd number of engines is not preferred and the amount of engines should be limited in order to limit aircraft weight. Hence, a total amount of 4 electrical engines was chosen.

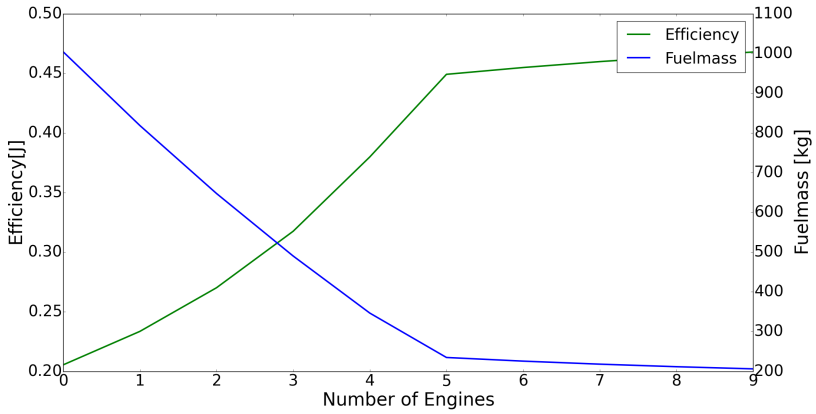

Figure 10.3: Efficiency and fuel mass relative to the number of electrical engines

10.5.3. GAS TURBINE SIZING

With the amount of electrical engines known also the amount of shaft power generated by the electric engines is given. From the model the total shaft power needed to perform manoeuvres during critical situations is given. First of all a climb gradient of 1.2% needs to be maintained during climb with one engine inoperative[20], secondly the E-gle needs to be able to climb at a rate of 500 ft/min at service ceiling in order to change altitude quickly enough to avoid collisions[67]. Thirdly it is checked if the aircraft produces enough power to accelerate to cruise velocity. From the power required the shaft power required can be calculated by taking into account efficiency of the propellers, next the shaft power from the electrical engines is subtracted to find the shaft power the gas turbines need to deliver. The results are displayed in Table 10.5. It can be seen that the climb rate at service ceiling is critical for the power required from the gasturbine.

Table 10.5: Shaft Power required from the gas turbines.

	One Engine Inoperative	Climb at service ceiling	Acceleration to Cruise
Total Power Required [MW]	1.88	2.39	1.37

10.5.4. MISSION PROFILE

The mission profile as discussed in Section 3.1 was used as an input. By combining the results, a graph could be made with corresponding velocities and height as can be seen in . This gives an overview of the final mission profile. In Figure 10.5 the power split throughout the mission can be seen. The blue line is the total shaft power, which is a sum of the green and red lines. The red line represent the gas turbine power and the green line the shaft power generated by the electrical motors. Note that during take-off, climb, acceleration the electrical engine and gas turbine are both providing full power as described in Section 10.4. It is interesting to note that the maximum power of the electrical engine stays constant over altitude while the power of the gas turbine drops with increasing altitude. This is because the power of the gas turbine engine is dependent on the mass flow. A higher mass flow means more energy that can be put into the air during a certain time and thus a higher total power can be achieved. Electrical engines however are independent of mass flow and therefore are not subject to this phenomenon.

During the cruise phase it was found it was most efficient to let the electrical engines provide maximum power. This is logic as the efficiency of the electrical system is higher than the efficiency of the gas turbine system. The 4 electrical engines together cannot provide enough power to let the aircraft fly fully electric during cruise and therefore the gas turbine is needed to provide the remaining required power.

During the loiter phase the aircraft requires less power and therefore the electrical engines are able to provide all the required power. However due to safety reasons the gas turbine engine will not be turned off. The gas turbine will provide power at the flight idle setting and the all the remaining power will be delivered by the electrical engines. In the descent and landing phases the gas turbine engine will also provide flight idle power. As no extra power is required the electrical engines are shut down during these phases

In Figure 10.5, the extended mission profile, in case of emergency, is taken into account. As this is normally not the case the aircraft was not optimised for this profile in terms of efficiency and fuel consumption. Therefore the electrical engine is not used and all required power comes from the gas turbine. Only the electrical engines of the high-lift propellers are used during take-off and descent.

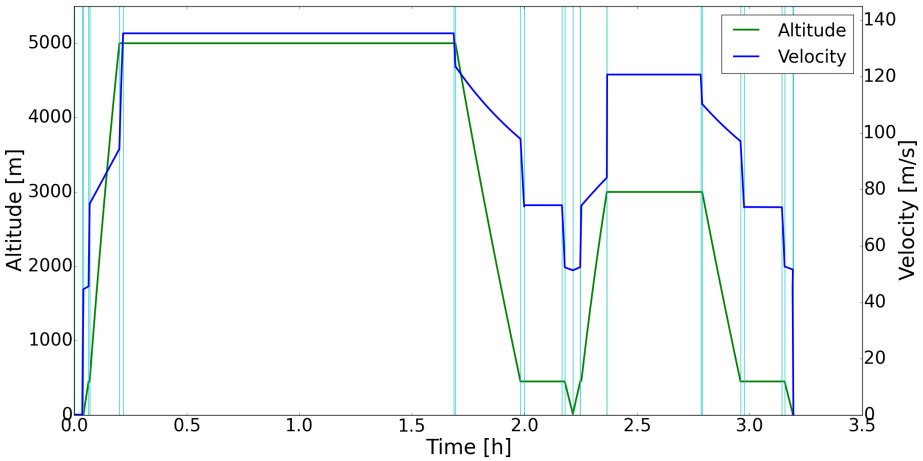

Figure 10.4: Height and velocity of the E-gle mission

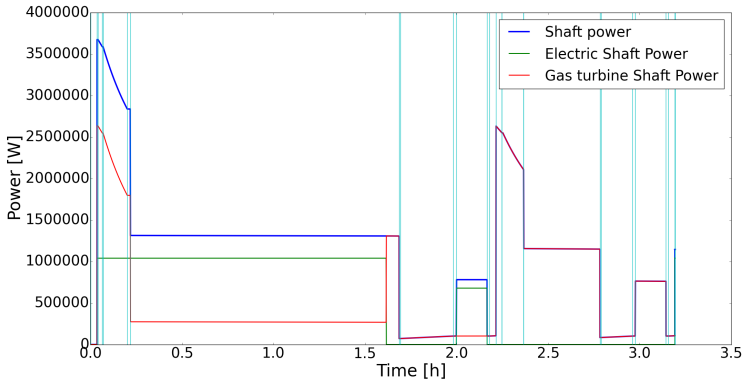

Figure 10.5: The power split of the electrical engine and gas turbine during the E-gle mission, light blue lines indicate the start of a new mission phase.

10.5.5. BATTERY AND FUEL MASS

The battery and fuel mass can now be calculated, because the required power at each time instance can be retrieved from Figure 10.5. Therefore the total required energy for the electrical engines and gas turbine can be determined. Using Equation 10.13 and Equation 10.11 the battery mass and fuel mass can be calculated respectively. Afterwards an

overview was created about how the battery energy and fuel used, which can be seen in Figure 10.6. Note that during take-off the battery energy drops relatively fast, because the DEP propellers and the electrical engines are used at full power. The first 2.25 hours represent the normal flight. At this stage the electrical energy is used as much as possible and therefore a rather steep decrease of the battery energy can be seen in this period, while the fuel mass decreases slowly. The extended mission starts after the first 2.25 hours. In this period it is the other way around, because the extended mission is primarily performed with fuel energy. The battery energy still decreases because the energy is used for on board power supply and DEP propellers during take-off and landing.

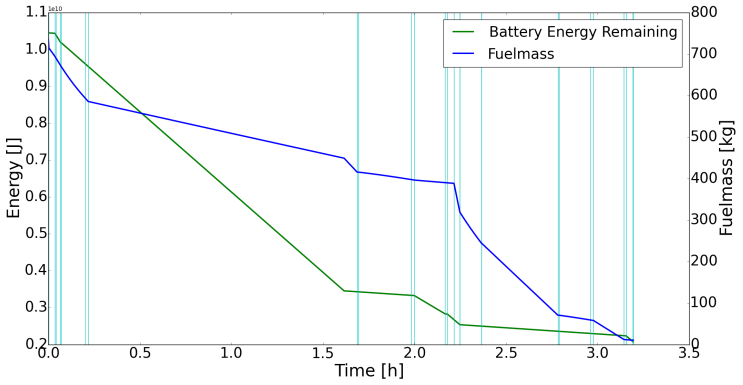

Figure 10.6: The battery energy and fuel mass over time, light blue lines indicate the start of a new mission phase.

10.5.6. COMPARISON TO BOMBARDIER Q300

In order to investigate the advantages and drawbacks of the E-gle a comparison is made to a competitor, namely the Bombardier Q300. A comparison is made for the amount of fuel burned and the total efficiency of each aircraft. Here efficiency is defined as the energy required for the mission over the total energy on board in batteries or fuel. As can be seen in Figure 10.7 the E-gle outperforms the Bombardier Q300, it burns only a quarter of the fuel. From calculations it has also been derived that the Bombardier Q300 has a total efficiency of 22% whilst the E-gle has an aefficiency of 38%, its total efficiency is 16 percent points higher. This can mainly be attributed to 3 aspects: The wingtip-propellers, the reduce in wing surface area due to DEP, and the use of electrical motors which are significantly more efficient than gas turbines. However a side note should be made, although the bombardier often performs short range missions it is capable of reaching destination 924 NM away. The E-gle can not do this with the current technology.

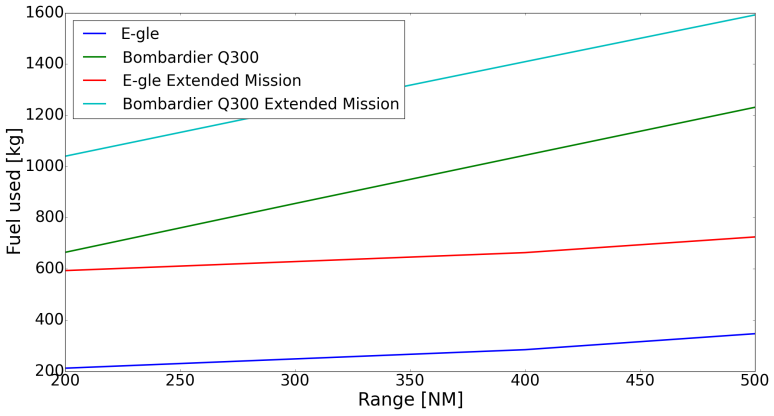

Figure 10.7: Fuel used during different ranges for the E-gle and Bombardier Q300 for both a normal flight and the extended profile with diversion.

10.6. PERFORMANCE OF THE FINAL DESIGN

In this section the overall performance of the E-gle is evaluated. As an input the design from the previous chapter are taken. First the payload range diagram is discussed, then take-off and landing and finally the climb.

10.6.1. PAYLOAD-RANGE DIAGRAM

To visualise the range performance of the E-gle a payload-range diagram is created. During a standard mission the aircraft would use 320 kg of fuel to fly a payload of 5000 kg over a distance of 500 NM. The rest of the flight is on batteries which take up 5805 kg of the MTOW. It needs 450 kg of reserve fuel for diversion. The OEM is 8910 kg. When this range does not suffice extra fuel can be used during cruise decrease the power drawn from the batteries. When taking on more fuel however less payload can be taken since the MTOW cannot be exceeded. When the maximum fuel capacity of 1288 kg is reached (the volume of the inner wingbox), the range can be extended even further by reducing the payload even more. When the payload is zero the maximum range is reached, also called the ferry range. All this can be seen in Figure 10.8.

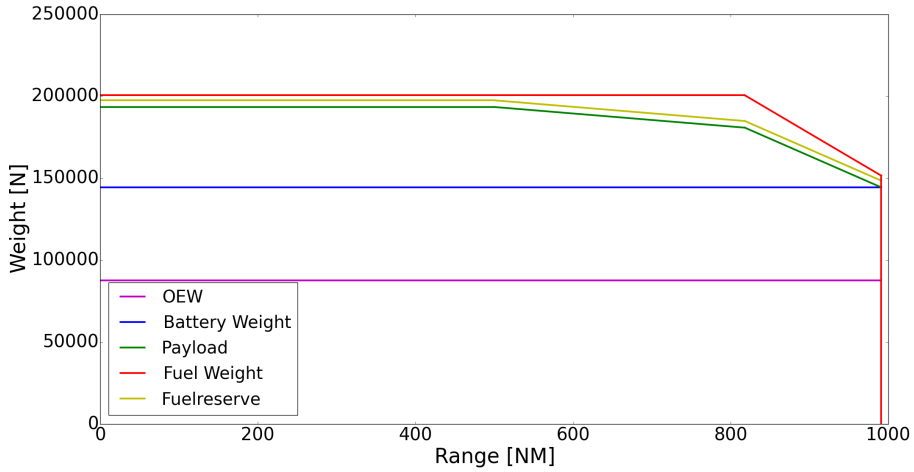

Figure 10.8: Payload-range diagram for the E-gle.

10.6.2. TAKE-OFF AND LANDING

In the requirements it is mentioned that the E-gle should be able to take-off in 1200 m and be able to land in 1100 m. In order to check whether the aircraft is able to meet these requirements the take-off and landing lengths are computed. In [61] it is stated that the take-off length can be determined using Equation 10.14, while the landing distance can be computed with Equation 10.15. The screen height that was taken was 15.2 m[61]. Furthermore, the barred T and D are the average values of the thrust and drag during the take-off and landing phase. These two parameters are calculated using a velocity of $V_{TO}/\sqrt{2}$ and $V_T/\sqrt{2}$ for the take-off and landing respectively. All other parameters were gathered from the performance program as described in Section 10.4.

It was found that the take-off requirement is met when the main engines operate at full power together with the DEP. The landing requirement is met when the aircraft is able to deliver a total reverse thrust of 19000 N. The aircraft is able to give 20000 N of reverse thrust according to Chapter 7 and therefore the landing requirement is also met. The final take-off and landing field length are 1090 m and 1190 m respectively.

$$s_{TO} = \frac{WV^2}{2g\left(\bar{T} - \bar{D} - \bar{D_g}\right)} + \frac{\frac{1}{2g}V_{scr}^2 - \frac{1}{2g}V_{LOF}^2 + h_{scr}}{sin\gamma_{scr}} \tag{10.14}$$

$$s_{Land} = \frac{\frac{1}{2g}V_A^2 - \frac{1}{2g}V_T^2 + h_{scr}}{\frac{1}{2}sin\gamma_A + \frac{C_D}{C_L}} + \frac{W}{2g}\frac{W}{S}\frac{2}{\rho}\frac{1.15^2}{C_{L_{max}}}\frac{1}{\bar{D} + \bar{D_g}} \tag{10.15}$$

10.6.3. CLIMB

The maximum climb performance was calculated using Equation 10.2. Figure 10.9 gives an overview of the rate of climb for several heights expressed in metres relative to velocity. In this graph it can be easily seen that for each height there is an optimal velocity. This is the velocity at which the power required is the smallest resulting in a maximum excess power. The optimal velocity increases with increasing height as the drag curve shifts to the right due to lower densities. Furthermore, the maximum power of the gas turbine decreases with increasing height and therefore the maximum rate of climb will decrease as well. Note that at high velocities the rate of climb at high altitudes can be higher than the rate of climb at low altitudes. Electrical engine power does not decrease with increasing altitude and thus the benefit of reduction in power required excels the penalty of a lower power available for these cases.

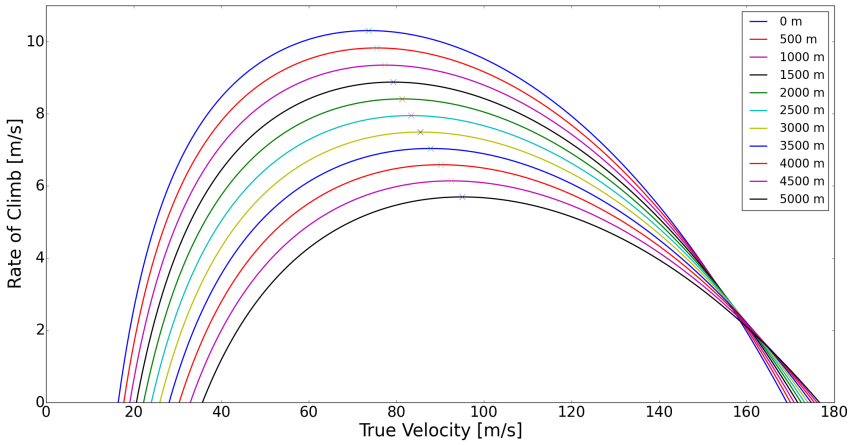

Figure 10.9: The rate of climb for several height relative to velocity

11

Operations, Maintenance & Production

To operate the E-gle in a sustainable manner an guideline for operations and maintenance need to discussed. This is done in Section 11.1 and Section 11.2. After this a production plan is presented in order to assemble the E-gle from start to finish in Section 11.3.

11.1. Operations & Logistics Concept Description

An important quantity for airlines is the time the aircraft is stood still at the gate between flights, which is defined as the turnaround time. During the turnaround time, a large amount of actions need to performed in a short amount of time, in order to make the aircraft flight ready as quickly as possible. An overview of the most important of these action for the E-gle can be seen in Figure 11.1. In this diagram, the beginning and end of the turnaround time are indicated by diamonds, instantaneous actions are indicated by trapezoids and continuous processes are indicated by rectangles. It is important to note that the size of a box does not necessarily give an indication of the time required to performed that task. The sized of the boxed used the diagram serve to give an indication of which action are performed in parallel and which are performed in sequence. All the different tasks described in the diagram are explained below.

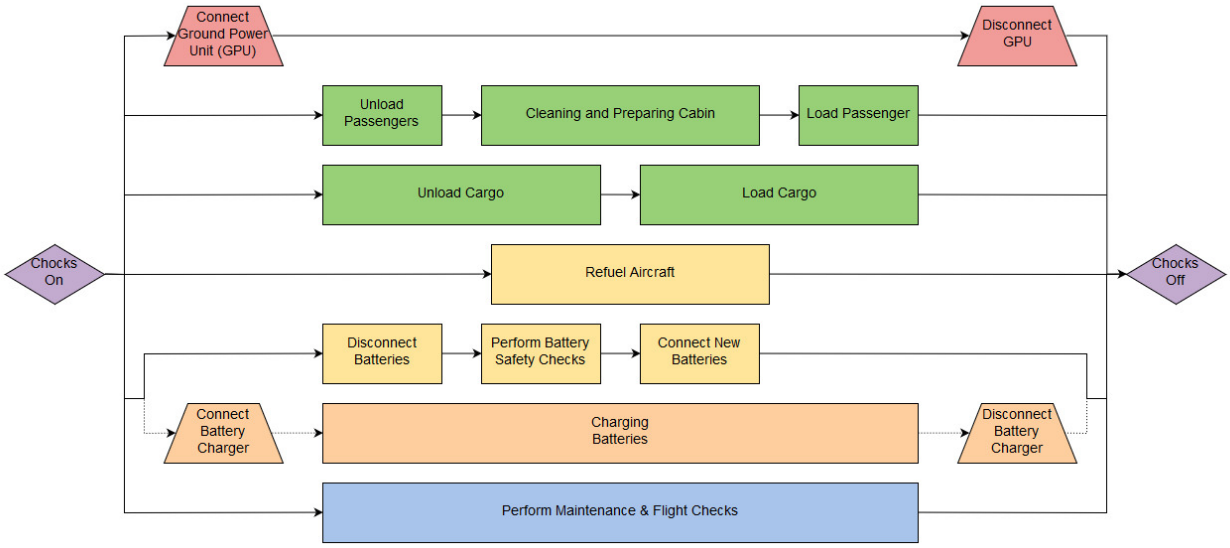

Figure 11.1: A block diagram of the actions required to be taken during turnaround time

11.1.1. ENERGY RESUPPLY

Once the aircraft reaches the specified gate, chocks are placed on the wheels, keeping the aircraft on its place and starting the turnaround time. Once the turnaround time starts, some instantaneous actions are performed. First, the aircraft is connected to the ground power unit (GPU), in order to provide power to the on-board systems, without using fuel. Next, the energy storage systems of the aircraft are resupplied. This can be split into battery swapping, battery charging and refuelling.

Battery Swapping
When the aircraft is landed and stands at the gate, the battery has decreased to 20% of its total energy capacity. Therefore the batteries either need to be charged or swapped. Charging the batteries, all or part of them, till they're full will take 6 hours. This is more than twice the flight time for a 500 NM mission. This was found unacceptable and therefore swapping batteries becomes far more interesting.

Swapping batteries is much faster than charging. The idea is to make a removable battery stack that can be easily removed and installed in the time the aircraft is on the ground. Tesla started testing battery swapping with model S users in California. The cars can switch in less than 90 seconds. Battery swapping demands facilities that can charge the battery packs. Also, vehicles needs to be designed that can change the battery in a fast way without damaging the batteries.

Battery Charging
As mentioned above, it is beneficial for the operation of the aircraft if the batteries are swapped instead of re-charged. However, it is possible that an airline is interested to fly to an airport without the facilities to swap the batteries and recharge them separate from the aircraft. Moreover, it is possible that, in case of emergency, the aircraft has to divert to an airport without the aforementioned facilities. This means that the batteries must be able to be recharged without swapping them, meaning that they are charged when in the aircraft.

This leads to an enormous increase in turnaround time, as fully recharging the batteries takes around six hours. It is therefore best for the design if charging the batteries without swapping them is limited to an absolute minimum. If charging the batteries is strictly necessary, the turnaround time can be limited in two ways. First, the batteries can be charged for a small percentage, after which the aircraft makes a short flight to an airport which has the proper facilities to swap the batteries. Second, the batteries can be charged up to a fraction where the aircraft is able to perform the take-off and landing, whereas the rest of the flight is performed on kerosene. It is important to note that this requires the fuel tanks to be large enough for this amount of fuel. However, as the original amount of fuel is very low, not enough space is available in order to accommodate this. Moreover, the space otherwise available in the wings could not be used for battery storage, as the batteries would not be accessible for swapping.

Refuelling
The turnaround time of regular aircraft is limited by the time it takes to refuel the aircraft. This is due to the fact that, for safety reasons, you are not allowed to refuel the aircraft while passengers are de-boarding or boarding [68]. The refuelling of the E-gle is very similar to that of a regular aircraft, as kerosene is used and the fuel tanks are still placed in the wings. However, the refuelling phase is impacted by the fact that the aircraft only takes fuel with it in order to assist the batteries during certain flight phases and in case of possible diversion. A quick estimation based on the current design indicates that it needs around 25 percent of what a comparable aircraft needs for a mission with a similar range. This implies that the turnaround time can be significantly decreased compared to these reference aircraft, as the time of the critical case is reduced. Research suggest that a reduction in turnaround time of 17% percent can be obtained using a battery swap[ping technique [69]. This is very beneficial for the design, as a shorter turnaround time leads to more flights, making the aircraft more profitable, especially for shorter range flights [70].

11.1.2. CARGO AND PASSENGERS

The loading and unloading of the E-gle is very similar to that of regular aircraft. As mentioned before, the refuelling of the aircraft takes significantly less time than for other aircraft, meaning that other phases become more critical for the turnaround time. This implies that a more effective loading and unloading of the cargo hold and a faster preparation of the cabin can lead to an even shorter turnaround time. Therefore, it is very beneficial for the operations and cost effectiveness of the aircraft if it has two cargo doors.

[1] https://player.vimeo.com/video/68832891?portrait=0&title=0&byline=0&color=&player_id=68832891.[Online; accessed 19 June 2017]

11.1.3. MAINTENANCE AND FLIGHT CHECKS

The maintenance and flight checks performed during the turnaround time mainly consist of checks and small repairs and is indicated in blue in Figure 11.1. Large maintenance session including both inspections and repairs and are not included in the diagram. They are performed on a scheduled basis when the aircraft is grounded for a larger amount of time. All the different types of maintenance performed and their frequencies at which they are performed are discussed in Section 11.2.

11.2. MAINTENANCE

The technical maintenance of the aircraft plays a crucial role in ensuring a safe, punctual and cost-effective flight operation of an airline. In addition, maintenance planning is necessary to ensure the airworthiness of the aircraft. A large part of the maintenance procedure are the same for conventional aircraft as for the E-gle Those procedures can be found in the Maintenance and Inspection Procedures Manual. However, there are certain design characteristics that change the maintenance procedures for the E-gle. The components that are affected the most are the batteries, electric motors, high-lift propellers, hybrid turboprop, wing, and the power management. The maintenance of these components will be discussed in the upcoming subsections.

11.2.1. BATTERIES

All battery technologies require scheduled checks to ensure safety. These check need to be based on the flight time, charge cycles and age of the battery. Battery maintenance is particularly crucial for the E-gle since the majority of the flight is battery powered. The following are some important maintenance procedures for the batteries.

- Perform periodic checks for the voltage levels. Inspect deviations from crucial battery parameters such as open circuit voltage, operating voltage, energy efficiency, specific energy, and cyclic stability on a regular basis.
- Perform visual inspection of the overall external and internal condition of the battery, electrolyte residue and bulging battery cells.
- For maintenance of the zinc electrode, perform checks to see the level of zinc utilisation. This has be to above a minimum of 60% to ensure efficient operation.
- In case the voltage checks display large disparity in cell voltages, but the battery looks good visually, then the battery needs to be removed from the aircraft and put on a constant current to charge until the cells display stable voltages.
- Perform general overhaul when defective cells are found, if the battery has failed the capacity check or if the visual condition of the battery indicates the need for major cleaning.
- Perform check for the system that supplies air to the batteries to ensure there are no blockages or forming of ice.

11.2.2. POWER DISTRIBUTION SYSTEM

The power distribution system (PDS) consists of a power converter, voltage regulator, current regulator, transformer and wiring. For DEP to be implemented successfully, it is imperative to ensure there are no flaws in the PDS. Further, it has to ensured that the control system performs necessary DEP initiations; during low speed flight, the low lift propeller system needs to be activated and during cruise, the blade folding mechanism of the lift propellers and battery recharging needs to be activated. Some important maintenance procedures are listed below.

- Perform check on the control system that activates/deactivates DEP on a daily basis.
- Visual inspection of wiring on a monthly basis to check for any sort of insulation failures, to avoid chances of short circuit.
- Voltage and current tests on a monthly basis to ensure they remain below maximum rating of the devices.
- Perform regular checks on safety devices like fuse links.

11.2.3. ELECTRIC MOTORS

All the lift propellers have an electric motor that provides power to the propeller. One of the main advantages of using an electric motor instead of combustion engines is the decrease in maintenance costs.

It is estimated that the maintenance can be reduced by 35% for electric vehicles compared to combustion vehicles [71]. This is because electric engines have far less moving parts than combustion engines, making it simpler and easier to maintain. [1]. However, electric engines still need maintenance. An overview of what kind of maintenance is required can be found below. [2]

- Perform visual inspection on monthly basis.
- Perform basic cleaning, wipe off dust, dirt, oil, etc. on a monthly basis.
- Clean out vent screens and fans on a quarterly basis.
- Semi-annually lubricate bearings, vacuum or blow out interior, check commutator and brushes leads, check brush spring tension, test field coils, test armature windings, check electrical connections.
- Perform noise and vibration inspections on a semi annual basis.

11.2.4. HYBRID: GASTURBINE-ELECTRIC ENGINE

The E-gle will use conventional turboprop engines for which it is sufficient to use current maintenance procedures described in the Maintenance and Inspection Procedures Manual. As for the electric motor, maintenance procedures are described in Subsection 11.2.3. The mechanical coupling and controllability of the the parallel hybrid configuration is quite complex since power needs to be regulated from two separate power sources. It is highly crucial to ensure proper functioning of the drive shaft which connects the gas turbine and motors to the propellers. Inspection should be performed on a regular basis to check for frictional wear. Cleaning and greasing need to be performed on a monthly basis.

11.2.5. HIGH-LIFT PROPELLERS

The aircraft has an increase in amount of propellers. Therefore, it is expected that the total maintenance cost and time of propeller will increase. However, the individual propeller maintenance will decrease. Namely, a fixed pitch was chosen. This simplifies the design making it more robust and easier to maintain. Furthermore, there will be multiple identical electric engine-propeller combinations. Therefore, parts do not have to be used specifically for one of the engines, but can be used for multiple engines. This decreases the cost of the parts [44]. Special thought also has to be given to the accessibility of the propellers since the E-gle has a high wing configuration. A special platform would be beneficial. The propellers are built so that they are easy to access for maintenance.

11.2.6. WING

The wing has a load case that differs from conventional aircraft. A tip mounted turboprop increases bending stress during taxiing and has an undesirable effect on flutter. As this is unconventional it is advised to increase inspection of the wing. In Chapter 9 it was found that the root is the most critical point of the structure. Multiple solutions to prevent failure were obtained. However, the uncertainty of these measures is still significant. Therefore, extra visual inspection should be done at the root chord of the aircraft. Furthermore, the wing carries 2 hybrid turboprops and 20 smaller electric engines for the DEP propellers. As the attachment of so many engines to the wing is unusual, extra visual inspection at those places is required. It is important to make sure enough hatches are placed in the wing in order to make the inspections easier and faster. These inspections can be scaled down when the use of distributed electric propulsion and wingtip mounted engines is increased as more knowledge on these topics will be available. Therefore, the uncertainty will go down and less inspection is required.

[1] https://avt.inl.gov/sites/default/files/pdf/fsev/compare.pdf[Online; accessed 19 June 2017]
[2] http://www.ohioelectricmotors.com/2015/07/a-general-guide-to-dc-motor-maintenance/.[Online; accessed 19 June 2017]

11.3. PRODUCTION PLAN

This section describes the manufacturing, assembly and integration of the aircraft after the design phase. This is illustrated in flow diagrams containing parallel and subsequent order in Figure 11.2 and shows the general overview of the production process. The production of this aircraft is not very different from other aircraft, which are build at this moment. Only the battery and DEP require different installation and are elaborated on in Subsection 11.3.1. First all the small components need to be produced in batches to quickly manufacture the larger components. Next, the larger components can be produced such as the fuselage, wing and engines. Afterwards the main fuselage and the engines can be assembled, also the smaller components such as doors and the interior can be produced. Finally all the components can be installed on the main fuselage and the final phase of the production can be started. This final phase is integrating all the components and making the aircraft complete with the final details.

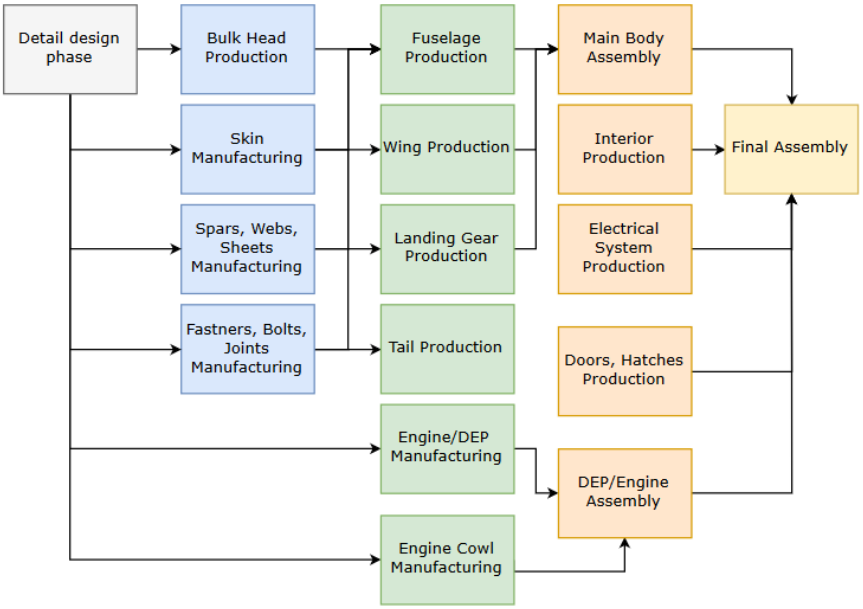

Figure 11.2: Production flow diagram

In Figure 11.3 the chain of design, suppliers, production and customers can be seen. After the design phase different suppliers need to be found to produce parts, where their specialisation is needed. Parts which can be self produced can be built in a production facility. First a "Parts Manufacturer Approval" certificate and other certificates need to be obtained before production can begin [72]. When all the suppliers are selected and parts are produced in batches, the production can start. When the aircraft is finalised, it will be delivered directly to the customer. Feedback can be delivered by the customer to adapt the design during the production phase to improve the following aircraft delivered.

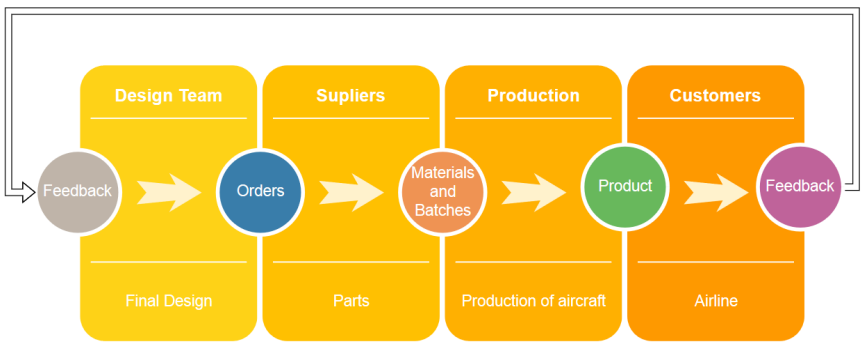

Figure 11.3: Design, supply, production and customer chain

11.3.1. DEP and Battery Production

In this section a more detailed production of the DEP and batteries are explained, which are the main differences between the E-gle and a normal regional airliner. The different parts are explained and discussed. Finally the assembly is discussed.

DEP Parts

- High lift blades: The material was chosen to be aluminium, further explained in Subsection 7.2.5. Due to high loads on the propeller a manufacturing way needs to be chosen to increase the strength and the life-time of the blades. A suitable production method is forging or casting with a heat treatment to increase the material strength. The production of the blades can be best performed by a company who is specialised in this field, since this part is critical for the safety of the passengers.
- Spinner: The material for the spinner is also selected to be aluminium to reduce the cost of the aircraft. The spinner can be produced using a press, since it possesses a conical shape, which can easily formed. The part can also be produced in a series, like a batch. This part can be self produced, since it is not critical part of the aircraft.
- Cowling: The Cowling is the skin around the motors and provides protection and increases the aerodynamic characteristics. This part can be made from aluminium or carbon fibre depending on the cost and final weight, during the detail design phase. The cowling needs to be easily removed to perform motor maintenance. To allow this a system needs to be installed to open. Therefore this cowl is best made in two parts and afterwards linked with a joining system, such as a hinge.
- Motor: The electrical motor is best bought directly from a external supplier. These components require a lot of knowledge to produce and there are several companies already supplying strong electrical motors.
- Fairing: The fairing is there to acquire a smooth connection between the engine and the wing. This fairing can be made out of aluminium and needs to be strong enough to carry the weight of the high-lift motors. They can be self produced using presses because of their round forms.
- Folding mechanism: The folding mechanism for the propeller is a difficult part and explained in Subsection 7.2.4. Due to the automatic opening system a spring should be applied to the propeller and a electro-magnet to keep the propellers closed during cruise. This is a new mechanism that has not yet been applied and is not a proven flight design. This part can best be produced self or in combination with a supplier who is specialised in propeller systems.

DEP Assembly and Integration

The DEP propellers can best be already assembled individually before placing it on the main wing. The wiring can then be connected to the engine Afterwards the cowling can be placed over the engine to achieve the final result. The folding mechanism can then be finalised and tested to work properly. An overview of a high-lift propeller assembly can be seen in Figure 11.4 with all the parts indicated.

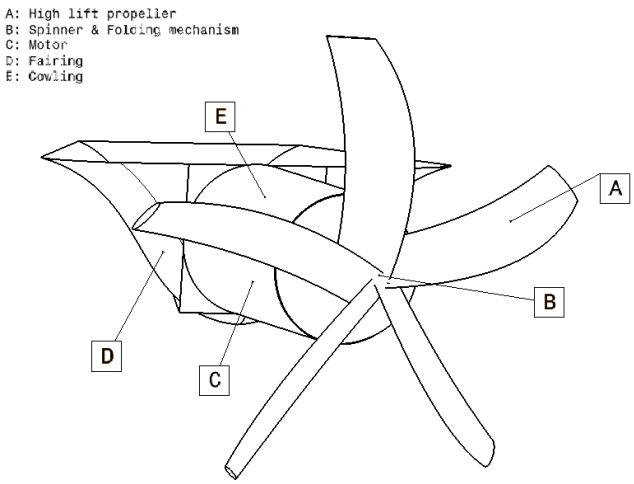

Figure 11.4: DEP production overview

Battery Parts

- Battery housing: The battery housing for the Zn-air batteries are important to maintain their specific energy and a high number of cycles until replacement. Therefore the housing needs to be airtight to prevent humidity. The casing is best made of a polyester-like material, since carbon fibre is too expensive and aluminium too heavy. These cases can be directly bought from suppliers and offer places for cable input. The corners can be tightly sealed using a gel or a kit.
- Battery cells: The cells can be ordered from companies and placed inside the battery housing. They can be stacked to acquire the right voltage and current.
- Loading system: The batteries need to be easily removable from the aircraft. A sliding system need to be present to unload and load the batteries from the aircraft as fast as possible. The sliding can be bought from regular companies and the battery case needs to be modified to fit these rails.

Battery Assembly:
The batteries can be directly assembled before loaded onto the aircraft. This is needed to also achieve the possibility to swap the batteries at the airport where possible. The battery housings then can be separately charged. The precise battery assembly is more suited for detailed design.

12

SUSTAINABILITY

The definition of sustainable development is defined as development that meets the needs of the present without compromising the ability of future generations to satisfy their own [73]. Sustainability can be divided into three different categories, namely ecological, social and economical sustainability. Social sustainability primarily focuses on the employees' mental and physical well-being and is therefore out of the scope of this project. Economical sustainability deals with the financial solvency of the project and will be treated in Section 13.3. Because of these reasons, ecological sustainability is focused on in this chapter.

Ecological sustainability is necessary to reduce the impact the design has on the environment. The design must meet the following goals along with the relevant requirements mentioned in Section 3.3 in order to be sufficiently ecologically sustainable [74].

Sustainability goals

1. Reduction of the material requirements (total mass consumed).
2. Reduction of the energy intensity (energy consumed during the lifecycle of the aircraft).
3. Reduction of toxic dispersion (release of toxic substances to all media).
4. Enhancing material recyclability (reuse of materials or energy).
5. Maximum sustainable use of renewable resources (avoid depletion of finite resources).
6. Extend product durability (optimise product life).
7. Increase of service intensity (create value-added while reducing environmental impacts).

This chapter will go through sustainability in the chronological order of the E-gle's life, by starting at the beginning of life with production in Section 12.1, after which the operational life is dicussed with the noise and emissions the aircraft produces in Section 12.2 and Section 12.4 and their reduction in Section 12.3 and Section 12.5 respectively and ending with the aircraft disposal in Section 12.6.

12.1. PRODUCTION

The production starts after the design phase and contains the manufacturing of all components and the continuous assembling until the final product is established. The production plan has already been described in Section 11.3 and describes the manufacturing, assembly and integration of the aircraft. This section focuses on how the whole production phase can be made sustainable to allow future generations to live in a world as humankind experiences it today.

Currently, in the production phase of an aircraft, several components are produced by different companies all around the world. All these components have to be delivered to a location where the final assembly happens. All these parts, which can be quite large, have to be transported resulting in a lot of external services which have to be used. Required services are ships, aircraft and ground transport systems to bring the components to the location of final assembly. These services have to be built and also produce emissions, therefore the use of external services have to be limited during the production phase. To limit the use of external services, the production of the different parts should be as close as possible to the location of the final assembly, preferably at the same location. However, this should not effect the quality of the products neither increase the cost significantly.

During the production phase, a significant amount of tools are required to manufacture the aircraft. Tools range from small to tighten bolts to large forklift trucks used to relocate large bulks of materials. Tools are often made from materials that are easily recyclable like steels and plastics. When it is decided that several tools will not be used anymore, they have to be sorted properly and delivered to an organisation specialised in recycling.

Bigger tools like the forklift truck make use of an energy source to operate. A lot of models use fuel as their power source. However, the development already led to electric alternatives which could be driven by green energy. The goal is to have only electric tools to reduce the emissions during the production phase.

Not only the location and equipment used during the production are important, also the factory itself. There are already companies working on energy neutral factories [75] to reduce emissions and costs during production. To make the factory more environmentally friendly, several actions can be undertaken. It is desirable that the isolation is sufficient, this will reduce the use of heaters in the winter and air conditioning in the summer. To make the factory even more friendly to the environment, solar panels can be placed on the roof to further reduce the emissions during production.

The E-gle is produced mostly out of composites, mandated by the need to reduce the weight. This is a distinguishing factor between the E-gle and current regional aircraft and makes it important to assess how the production of composite structures compares sustainability wise to more common materials such as steel and aluminium. The energy used to manufacture composite parts is less than that of steel and aluminium and due to their resistance to corrosion and fatigue they last longer and do not require corrosion inhibiting substances [76]. The CO_2 emissions during production are reduced significantly when made use of composites instead of aluminium [77]. This finding is supported by the comparison of the composite CFRP to aluminium in Figure 12.1 which shows that the overall CO_2 emission decrease by 32 %. Carbon fibre reinforced polymers (CFRP) are commonly used in aerospace industry due to their high strength-to-weight ratio [78].

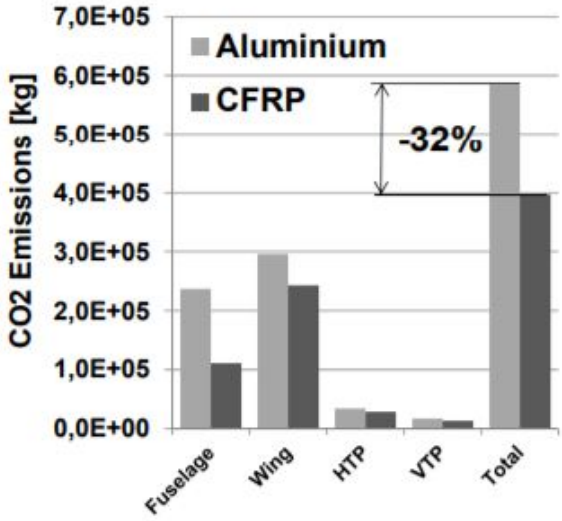

Figure 12.1: Distribution of CO_2 emissions for aluminium and CFRP [77]

The last part of the production that is discussed, is the batteries. The main benefit of the Zn-Air batteries are that they can be charged with green energy which reduces the aircraft's emissions significantly. The production of these batteries require the metal zinc, which is a very common material, making the risk of running out very small. A large amount of it is also located within the United States, making the transportation costs small [79]. The batteries' cathode is oxygen which can be obtained from the air around the aircraft.

12.2. NOISE

The noise produced by the aircraft consists of two main parts, namely the propulsion noise consisting of the jet engine and the propellers and the airframe noise which consists of the noise produced by the wing, tail, landing gear and high lift devices. Since the DEP propellers are very important to the project, the propeller noise is addressed in more detail. Finally verification and validation is performed and the noise is calculated for the certification procedures to determine whether the noise requirement is met. Figure 12.2 has a visual representation of the three test situations used and the axis and angle definitions used in the rest of this section. The three conditions are approach, where the aircraft is approaching the runway, lateral where the aircraft is taking off and fly-over just after the runway.

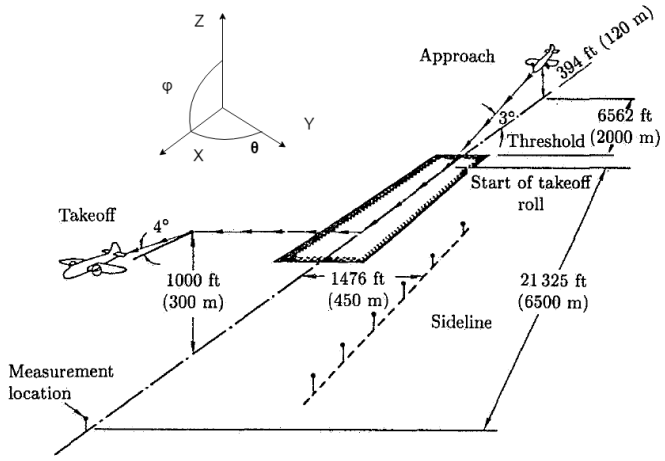

Figure 12.2: Noise certification conditions [80]

12.2.1. JET NOISE

To determine the jet noise, the book *Jet noise prediction using the Lighthill acoustic analogy* by R. H. Self is used [81]. Firstly the noise intensity produced by the jet exhaust is calculated with Equation 12.1. In this equation $A(y_1)$ is the area of the shear layer, $q(y_1,\omega)$ is the source distribution, ρ_0 and a_0 are the freestream density and speed of sound respectively. The geometry of the jet exhaust can be seen in Figure 12.3. The shear area multiplied with the source distribution is integrated from four times the nozzle diameter to 100 metres, which is thought of as a sufficiently accurate distance.

$$I_\omega(r) = \frac{\omega^4.}{32\pi^3 \cdot \rho_0 \cdot a_0^5 \cdot r^2} \int A(y_1) q(y_1,\omega) dy_1 \tag{12.1}$$

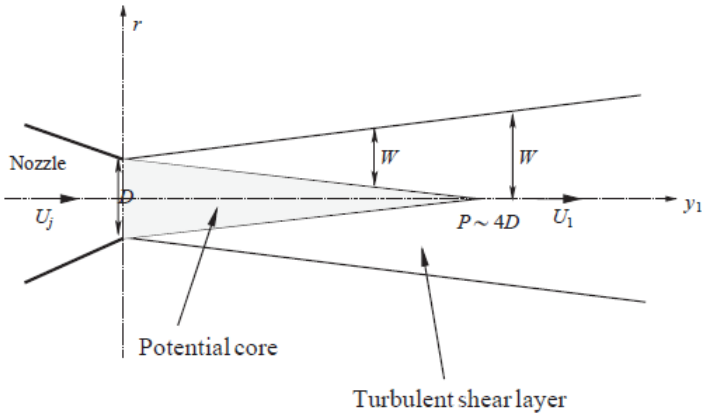

Figure 12.3: Simple schematic structure of a jet [81]

The area of the shear layer can be determined in a fairly simple manner by using Equation 12.2 in which D_{nozzle} is the diameter of the exit nozzle which is 18.6 cm for the jet engine used.

$$A = \begin{cases} \pi D_{nozzle} W, & y_1 < P \\ \pi W^2, & y_1 > P \end{cases} \tag{12.2}$$

$$P = 4D_{nozzle} \tag{12.3}$$

$$W = y_1 \cdot D_{nozzle} / P \tag{12.4}$$

The source distribution is calculated in a more complicated manner by using Equation 12.5. $l_\parallel$ and $l_\perp$ are the eddy lengthscales which are equal to $0.3W$ and $0.3l_\parallel$ respectively. U_c is the eddy convection velocity and is equal to $0.6U_1$. The mean centreline velocity u is calculated with Equation 12.6 and the turbulent eddy lifetime τ_s is calculated using Equation 12.7, where St is the Strouhal number.

$$q(y,\omega) = 2\pi l_\parallel l_\perp^2 \cdot \tau_s \cdot u^4 \cdot exp\left(-\frac{\omega^2(l_\parallel \cos^2(\phi) + l_\perp^2 \sin^2(\phi)}{4a_0^2}\right) exp\left(-\frac{\omega^2(1 - M_c \cdot \cos(\phi))^2}{4U_c^2}\right) \tag{12.5}$$

$$u = 0.15\frac{2P \cdot V_{jet}}{P + y_1} \tag{12.6}$$

$$\tau_s = \frac{D_{nozzle}/(1 + 0.5St)}{U_c} \tag{12.7}$$

$$St = \frac{f \cdot D_{nozzle}}{V_{jet}} \tag{12.8}$$

The results are presented in Figure 12.4 for the approach conditions, where one can note that the noise has a peak at low frequencies and drops off very quickly after that due to the rapidly diminishing exponents in $q(y,\omega)$.

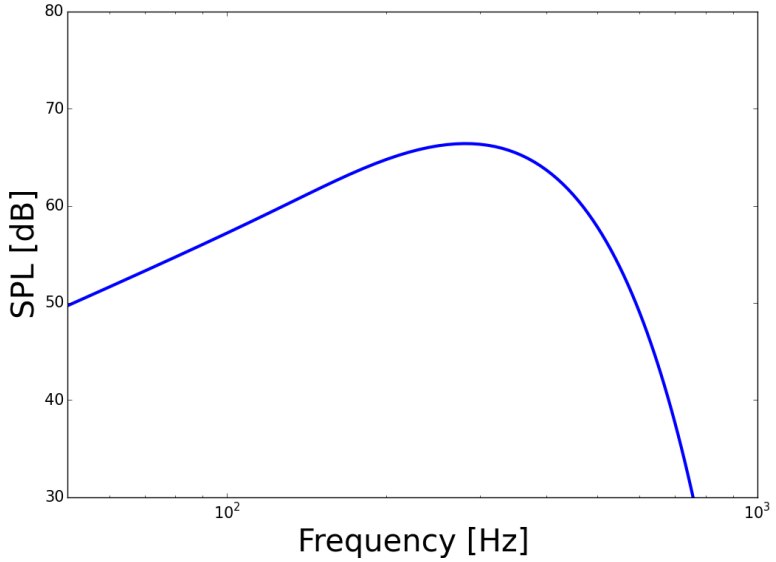

Figure 12.4: SPL of the jet exhaust

12.2.2. PROPELLER NOISE

The propeller noise consists of harmonic and broadband noise. For the calculation of the propeller noise the book *Aeroacoustics of Flight Vehicles* written by H. Hubbard is used [80].

The harmonic noise is generated by each blade's passing, at integer multiples m of the fundamental frequency f_0.

$$f_0 = \frac{N_B \cdot RPM}{60} \tag{12.9}$$

This noise is calculated with the noise pressure P_m, as shown in Equation 12.10. In this equation N_B is the number of propeller blades, r is the aircraft distance from the observer, R_{prop} is the propeller radius and a is the speed of sound. M_t and M_x are the rotational Mach number and the Mach number in the x-direction respectively.

$$P_m = \frac{m \cdot N_B \cdot M_t \cdot \sin(\theta)}{2\pi r \cdot R_{prop}(1 - M_x \cdot \cos(\theta))}\left(\frac{T \cdot \cos(\theta)}{1 - M_x \cdot \cos(\theta)} - \frac{P}{z_{eff}^2 \cdot M_t^2 \cdot a}\right)\psi_L \cdot J_{mN_B} \tag{12.10}$$

The angle θ is the retarded radiation angle, which is calculated with Equation 12.11 where θ_1 is the observational angle as shown in Figure 12.2.

$$\cos(\theta) = \cos(\theta_1)\sqrt{1 - M_x^2 \sin^2(\theta_1)} + M_x \sin^2(\theta_1) \tag{12.11}$$

The factor J_{mN_B} is the Bessel function, which can be calculated as shown by Equation 12.12, where z_{eff} is a constant equal to 0.8 [80].

$$J_{mN_B} = J_{mN_B}\left(\frac{mN_B \cdot z_{eff} \cdot M_t \cdot \sin(\theta)}{1 - M_x \cdot \cos(\theta)}\right) \tag{12.12}$$

$$x = \frac{m \cdot N_B \cdot z_{eff} \cdot M_t \cdot \sin(\theta)}{1 - M_x \cos(\theta)} \tag{12.13}$$

The final component that still needs to be known is the noncompactness factor ψ_L, which can be calculated using Equation 12.14. In this equation $\bar{c}_{prop}$ is the average chord of the blade and D_{prop} is the diameter of the propeller.

$$\psi_L = \frac{\sin(X)}{X} \tag{12.14}$$

$$X = \frac{m \cdot N_B \cdot M_t \cdot \frac{\bar{c}_{prop}}{D_{prop}}}{M_r(1 - M_x \cos(\theta))} \tag{12.15}$$

Now that this factor is also known, the sound pressure level SPL is calculated using Equation 12.16 in which P_{ref} is the reference sound pressure and equal to 20.

$$SPL_h = 20 \cdot \log\left(\frac{P_m}{\sqrt{2}P_{ref}}\right) \tag{12.16}$$

Now that the harmonic noise is known, the broadband noise can be calculated with Equation 12.17. This is the noise that is produced randomly. This equation depends on the over-all sound pressure level and the frequencies $\tilde{\omega}$ and the frequency at which the SPL is maximum, $\tilde{\omega}_{max}$.

$$SPL_{1/3} = OASPL + 10 \cdot \log\left(0.613\left(\frac{\tilde{\omega}}{\tilde{\omega}_{max}}\right)^4 \left[\left(\frac{\tilde{\omega}}{\tilde{\omega}_{max}}\right)^{3/2} + 0.5\right]^{-4}\right) \tag{12.17}$$

The frequency at which the SPL is maximum is the first harmonic of the propeller, thus equal to f_0 and thus $\tilde{\omega}_{max}$ can be obtained by substituting this into Equation 12.18. In this equation V is the velocity and δ^* is the thickness of the boundary layer which can be calculated with the Reynold's number and the mean aerodynamic chord of the propeller.

$$\tilde{\omega} = \frac{2\pi f \cdot \delta^*}{V} \tag{12.18}$$

$$\delta^* = 0.047 \cdot \bar{c}_{prop} \cdot Re_{\bar{c}_{prop}}^{-1/5} \tag{12.19}$$

The next unknown in Equation 12.17 is OASPL, presented in Equation 12.20. To be able to calculate this sound level, the retarded radius r_e and the directivity factor D must be known. These can be calculated using Equation 12.21 through Equation 12.25

$$OASPL = 10\log\left(M^5 \frac{\delta^* R_{prop}}{r_e^2} D\right) \tag{12.20}$$

$$D \equiv \frac{2\cos^2(\theta_e/2)}{[1 - (M - M_c)\cos(\theta_e)]^2(1 - M\cos(\theta_e))} \tag{12.21}$$

$$r_e = \frac{1 - M^2}{\sigma + M_x} \tag{12.22}$$

$$\theta_e = \cos^{-1}\left(-\frac{x}{r_e + M}\right) \tag{12.23}$$

$$\sigma^2 \equiv x^2 + \beta^2 z^2 \tag{12.24}$$

$$\beta^2 \equiv 1 - M^2 \tag{12.25}$$

Now that the SPL can be calculated, results can be obtained which are presented in Figure 12.5 for the approach conditions. The peaks represent the propeller harmonics, whilst the base represents the broadband noise.

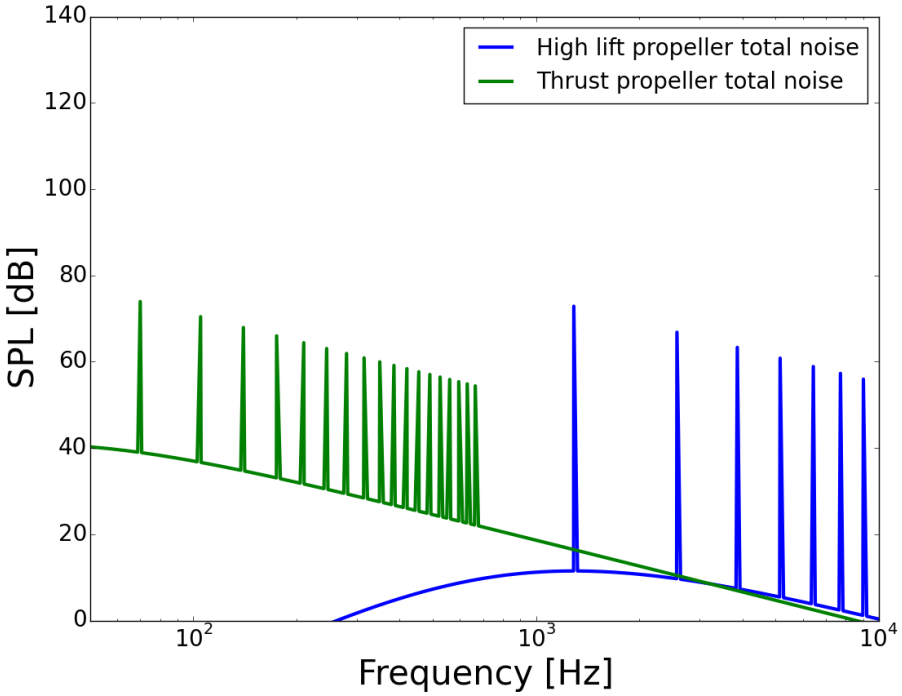

Figure 12.5: SPL of the high lift and thrust propellers

12.2.3. AIRFRAME NOISE

The airframe noise consists of wing, horizontal tail, front and rear landing gear and flap noise. For this the method by M. R. Fink is used, expressed in *Airframe Noise Prediction Method* [82]. First, the wing and horizontal tail noise is calculated, which is done with the same equations. The sound pressure level is calculated similarly to that of the broad-band propeller noise, by using Equation 12.26. This equation depends on the over-all sound pressure level (OASPL), the frequency f and the frequency at which SPL is maximum f_{max}, which is calculated with $f_{max} = N_{Str} \cdot V / t_w$, where N_{Str} is the Strouhal number and is taken to be 1.3 [83].

$$SPL = OASPL + 10 \cdot \log\left(0.613 \left(\frac{f}{f_{max}}\right)^4 \left[\left(\frac{f}{f_{max}}\right)^{3/2} + 0.5\right]^{-4}\right) - 0.03 \left|\frac{f}{f_{max}} - 1\right|^{3/2} \tag{12.26}$$

The OASPL with directivity is calculated using Equation 12.27 in which 104.3 dB is an empirical term for low-speed aircraft, ND is a noise factor for the trailing edge high lift device interference which is 0 due to the simplicity of the E-gle's high lift devices. Since the wingspan b_w is known, only the thickness of the turbulent boundary layer must be computed which is done using Equation 12.28, which is dependent on the wing geometry and the kinematic viscosity.

$$OASPL = 50 \cdot \log\left(\frac{V_{kt}}{100kt}\right) + 10 \cdot \log\left(\frac{\delta_w b_w}{z^2}\right) + 8 \cdot ND + 10 \cdot \log\left(cos(\phi) \cdot \sin(\theta) \cdot \cos(\theta/2)\right)^2 + 104.3dB \tag{12.27}$$

$$\delta_w = 0.37 \left(\frac{S_w}{b_w}\right) \left(\frac{V \cdot S_w}{b_w \cdot \nu}\right)^{-1/5} \tag{12.28}$$

The landing gear noise is estimated separately for the front and rear landing gear, since the front landing gear consists of two and the rear of four wheels per strut. The sound pressure level is calculated identically for both, namely with Equation 12.29 in which D_{wheel} is the diameter of the wheel.

$$SPL = 60 \cdot \log\left(\frac{V_{kt}}{194kt}\right) + 20 \cdot \log\left(\frac{D_{wheel}}{r}\right) + 10 \cdot \log\left(10^A + 10^B\right) \tag{12.29}$$

The values for A and B are different for two wheel and four wheel landing gears and are calculated using Equation 12.30 and Equation 12.31.

$$A = \begin{cases} 13 + \log\left(4.5\left(\frac{fD_{wheel}}{V}\right)^2\left[12.5 + \left(\frac{fD_{wheel}}{V}\right)^2\right]^{-2.25}\right) & \text{2 wheels} \\ 12 + \log\left(\left(\frac{fD_{wheel}}{V}\right)^2\left[0.4 + \left(\frac{fD_{wheel}}{V}\right)^2\right]^{-1.6}\right) & \text{4 wheels} \end{cases} \tag{12.30}$$

$$B = \begin{cases} 13 + \log\left(2\left(\frac{fD_{wheel}}{V}\right)^2\left[30 + \left(\frac{fD_{wheel}}{V}\right)^8\right]^{-1}\left(\frac{0.34H_{LG}}{D_{wheel}}\right)\sin^2(\phi)\right) & \text{2 wheels} \\ \left[12 + \log\left(7\left(\frac{fD_{wheel}}{V}\right)^3\left[1.06 + \left(\frac{fD_{wheel}}{V}\right)^2\right]^{-3}\right)\right]\sin^2(\phi) & \text{4 wheels} \end{cases} \tag{12.31}$$

The last component of the airframe noise is the flap noise, which is calculated with Equation 12.32. The subscript F denotes flap geometry, where δ_F is the flap deflection. G6 is an empirical factor that is used for single and double slotted flaps, such as the ones used on the E-gle, whose equation varies with the ratio fc_F/V.

$$SPL = G_6 + 10 \cdot \log\left(\frac{S_F \cdot \sin^2(\delta_F)}{z^2}\right) + 60 \cdot \log\left(\frac{V_{kt}}{100kt}\right) + 20 \cdot \log\left(\sin(\theta) \cdot \cos^2(\phi) \cdot \sin(\theta + \delta_F)\right) \tag{12.32}$$

$$G_6 = \begin{cases} 99.0 + 10 \cdot \log\left(\frac{fc_F}{V}\right), & fc_F/V < 2 \\ 103.82 - 6 \cdot \log\left(\frac{fc_F}{V}\right), & 2 \leq fc_F/V < 20 \\ 135.04 - 30 \cdot \log\left(\frac{fc_F}{V}\right), & 20 \leq fc_F/V \end{cases} \tag{12.33}$$

Now that all the airframe noise has been determined, the results are shown in Figure 12.6 for the approach situation. The wing produces the most noise, followed by the rear landing gear at low frequencies and the tail at higher frequencies.

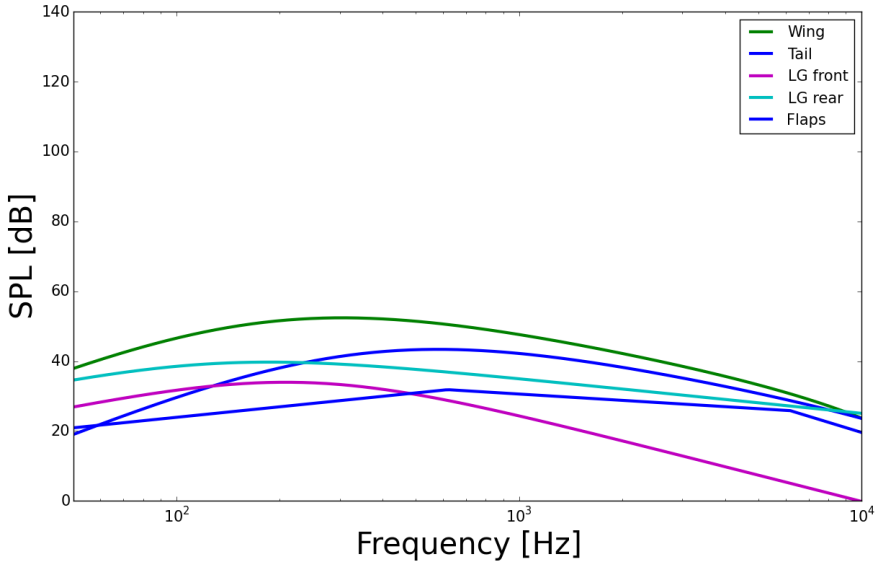

Figure 12.6: SPL of the various airframe components

12.2.4. NOISE CORRECTION

When SPL_{total} at each frequency is known as shown in Figure 12.7, the noise can be corrected for by atmospheric attenuation, annoyance, tone and duration. Duration and tone correction will be performed at a later phase of the design. In this section the noise for the lateral case is used.

The atmosphere absorbs sound energy, especially at higher frequencies, and for an accurate result this effect has to be taken into account. The sound reduction per 100 metres α is calculated with Equation 12.34, according to the book *Elements of Aviation Acoustics* by J. J. Ruijgrok [84]. In this equation the temperature T is expressed in degree Celsius.

$$\alpha = 10^{[2.05\log(f/1000)+1.14\cdot10^{-3}T-1.917]} + \eta(\delta)\cdot 10^{[\log(f)+8.43\cdot10^{-3}T-2.76]} \tag{12.34}$$

The result of this correction for the lateral case can be seen in Figure 12.8, where one can note that at high frequencies the sound is reduced significantly.

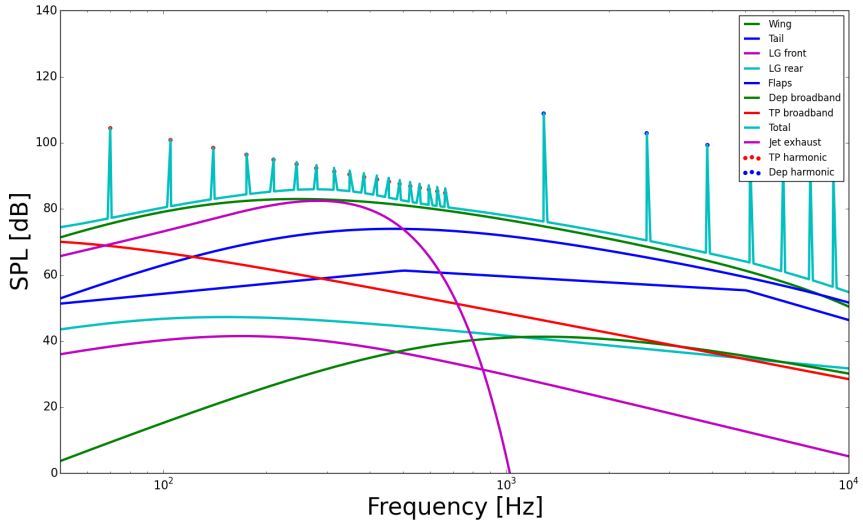

Figure 12.7: SPL of all the noise producing components

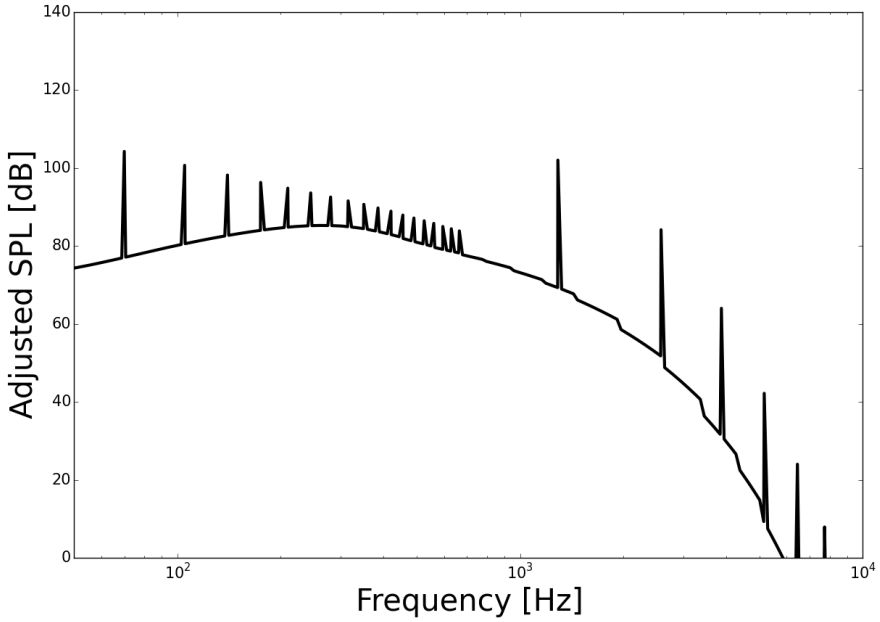

Figure 12.8: SPL adjusted for atmospheric attenuation.

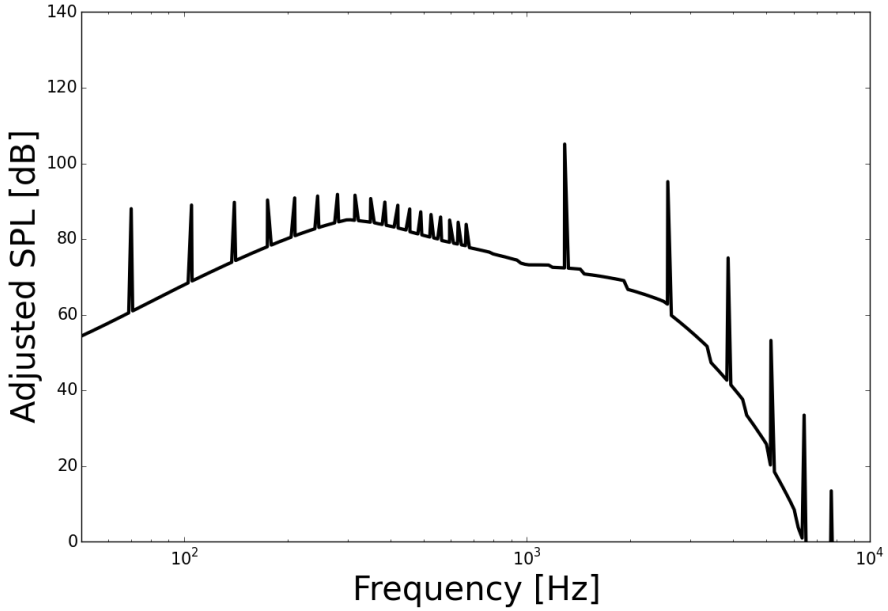

Figure 12.9: SPL adjusted for annoyance and atmospheric attenuation

By using 24 frequency bands, the annoyance correction can be calculated using Equation 12.35 and Equation 12.36, where $n(k)$ is the largest of the 24 values [85]. The value of 40.0 in Equation 12.36 is the reference sound pressure. Since a reference sound value of 0.0 dB has been used throughout the calculations, this value was used instead. Tone and duration correction would likely lower the effective perceived noise level, however, since it is not taken into account PNL is equal to the perceived noise level $EPNL$.

$$N(k) = 0.85n(k) + 0.15\sum_{i=1}^{24} n(i,k) \qquad (12.35)$$

$$EPNL = PNL(k) = 40.0 + \frac{10}{\log(2)}\log(N(k)) \qquad (12.36)$$

12.2.5. NOISE VERIFICATION AND VALIDATION

To check whether the results are sensible, verification must be performed. This is done first for the jet noise, then for the propeller noise and lastly for the airframe noise.

The jet noise was verified by using the comparison results of a small jet engine, with $M_j = 0.67$ and a D_{nozzle} of 0.0254 metres, shown in Figure 12.10. The calculated result shown in Figure 12.11 differs substantially from the comparison data unfortunately. From the exponents in Equation 12.5 it is expected that noise drops off sharply with frequency, as happens in the calculated results, however, this does not occur for the comparison data. Because of these substantial differences, the jet noise result is not very noteworthy.

Due to the high amount of very detailed inputs required for the propeller noise calculation, direct comparison is difficult. Therefore, the decision was made to compare the general result with an unspecified propeller as shown in Figure 12.12. One can observe in the calculated noise in Figure 12.13 that the harmonic peaks both show a decline in strength, although it is more pronounced for the comparison data. The broadband noise with respect to the harmonics is also higher for the comparison data than it is for the calculated result, however, both decline with frequency after the first harmonic.

The airframe noise is compared to that of an Airbus A320 presented in Figure 12.14 and Figure 12.6, which despite being a lot larger can still offer useful information with regards to frequency and the relative sizes of the components. Both are on their approach. For the A320, the wing noise is the highest with the landing gear just below that, whereas the opposite is the case for the E-gle. This is likely due to the much smaller wing.

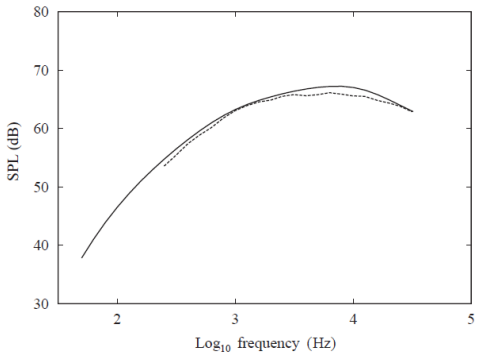

Figure 12.10: Comparison jet noise data [81]

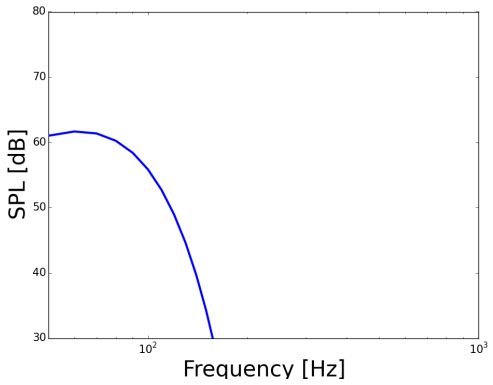

Figure 12.11: Jet noise results

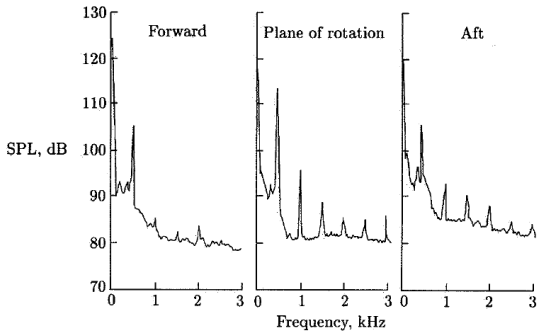

Figure 12.12: Comparison data of an unspecified propeller [80]

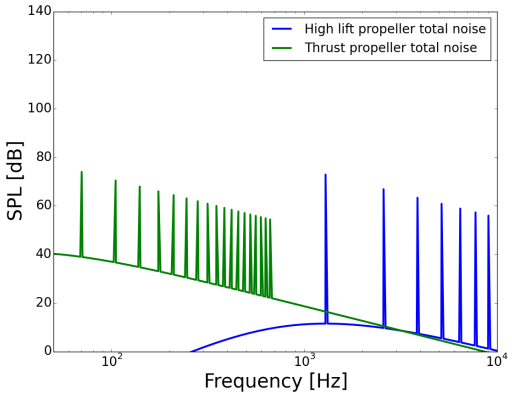

Figure 12.13: Propeller results for the high lift and thrust propellers

What can also be seen is that the flap noise is shifted down and to higher frequencies, which is sensible due to the smaller and simpler flap set-up and both of them show two kinks, one around a frequency between 10^2 and 10^3 and another between 10^3 and 10^4 Hz. All airframe components also show a maximum at a frequency in the order of hundred, similar to the verification data. Because of these reasons, the airframe noise calculations appear to be correct.

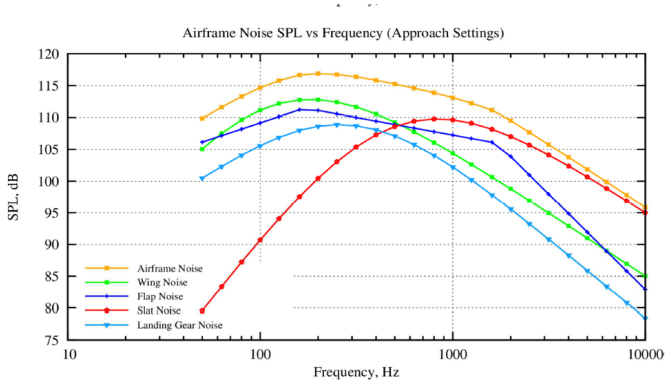

Figure 12.14: Comparison data of an Airbus A320 [86]

12.2.6. NOISE RESULTS

The effective perceived noise levels for the three test situations, along with the certification requirements are shown in Table 12.1. A power was used of 100 kW for the high lift propellers through all three test conditions. For the thrust propellers, a power of 3.5 MW was used for the lateral and fly-over, whilst 2.5 MW was used for the approach. The velocities used are 46.0 m/s for lateral, 53.9 m/s for fly-over and 56.6 for the approach. A Bombardier Q300 was used as the reference aircraft [19]. The aircraft meets all the JAR 36 requirements and is quieter than its competitor in all categories, however the requirement that the aircraft is 15 dB lower than a comparable regional aircraft is not met. The aircraft has a cumulative certification noise of 86.1 dB. In the next section noise reduction will be looked at as a way to lower this noise in the future.

Table 12.1: Results compared with certification requirements

	JAR 36 requirement [dB]	**Bombardier Q300 [dB]**	**Result [dB]**	**Difference E-gle and JAR 36 [dB]**	**Difference E-gle and Q300[dB]**
Lateral	94	86.9	85.3	- 8.7	- 1.6
Fly-over	89	80.0	75.1	- 13.9	- 4.9
Approach	98	93.3	76.1	- 21.9	- 17.2

12.3. NOISE REDUCTION

The most important noise sources to reduce are the thrust propeller noise, which is dominant at low frequencies, the jet engine noise which is dominant at slightly higher frequencies and finally the high lift propeller noise which is the highest and at the frequency range which is perceived the worst.

The primary means of lowering the jet exhaust noise is by lowering the exhaust velocity. This can be achieved by using more powerful electric motors for the thrust propeller, which would reduce the power the gas generator needs to generate. Additionally, noise suppressing measures can be fitted to the engine, such as liners which can achieve a reduction of up to 5 dB. Furthermore, chevrons can be fitted which would be directed inward with respect to the jet [87] and flow mixers can be used to reduce the flow mixing sound between the jet exhaust and the ambient air, which can reduce noise by 4 dB [88]. All of these efforts increase the weight and drag, which increases fuel consumption and can thus have a negative over-all impact on the sustainability.

The propeller noise can be reduced by changing the operating conditions or the design parameters. The most significant way to achieve a reduction in noise is by changing the way the propeller operates is by lowering the propeller tip speed [80]. The decision was made to have a tip speed equal to 0.8 times the speed of sound for performance reasons. Lowering the tip speed would lower the frequency, which is beneficial for both propellers but primarily the high lift propeller would benefit due to its harmonics being located in the region having the highest relative SPL. The effect of the tip speed on the blade's noise can also be reduced by increasing the sweep angle, which is currently zero degrees. The effect of sweep on propeller performance has thus far not been analysed, which makes it an interesting point to research in the future, however, this has a higher effect for transonic cruise speeds [80].

By changing the design of the propeller, noise can also be reduced. Having a larger diameter or more blades reduces the blade loading and thus reduces the noise produced [80], however, having a higher blade-count also increases the frequency and thus has to be done carefully. A larger diameter is also beneficial for performance reasons so seems to be an ideal way to reduce noise, however for the high lift propellers the maximum allowable diameter is limited by the required induced velocity and the power the motors can deliver and thus cannot be increased significantly unless the aerodynamic requirements are lowered. Furthermore, to allow for their folding the diameter is generally limited. Additionally, the blade shape or airfoil can be changed, which has a complicated effect on the performance and noise produced. For reasonable designs a noise reduction of around 3 dB can be achieved. The final point of interest is to use syncrophasing, which uses phase differences between the propellers as a way to cancel the noise [80].

12.4. EMISSIONS

Aircraft engines produce emissions in the form of carbon dioxide (CO_2), which comprises about 70% of the exhaust, and water vapour (H_2O), which comprises about 30%. Less than 1% of the exhaust is composed of pollutants like nitrogen oxides (NO_x), oxides of sulphur (SO_x), carbon monoxide (CO), partially combusted or unburnt hydrocarbons (HC),

particulate matter (PM) and other trace compounds. The level of these emissions is quantified by emission indices (EIs) that specify how many grams of the substance are released per one kilogram of fuel burned.

The emissions of NO_x, CO and HC depend on the internal conditions of the engine. NO_x is produced primarily through reactions between oxygen and nitrogen in the high temperature regions of the engine combustor. Therefore NO_x emissions are sensitive to the combustor pressure and temperature, the fuel flow rate and the geometry of the combustor. Conditions favourable to CO and HC production are attained at low engine power settings where the temperature is low and the combustion is less efficient that is, incomplete combustion occurs. Therefore, EIs of NO_x, CO and hydro-carbons are engine specific and they vary from engine to engine.

To compare the emissions produced by E-gle to conventional regional turboprop aircraft, the Bombardier Q300 is chosen as the reference aircraft. The emission indices of the various byproducts are found based on statistical data from several engines in [89]. Further for a range of 500NM, the E-gle requires 320kg of fuel, while the Q300 requires 1159kg of fuel. Table 12.2 shows the details of the emissions produced and the percentage difference. It is seen that the E-gle has 72% lower emissions.

Table 12.2: Comparison of emissions between E-gle and Bombardier Q300

		E-glekg>kg	**Bombardier Q300kg>kg**
Fuel required over 500 NM range		320	1159
Emissions	Emission index (EI)g/kg>g/kg		
CO_2	3149	1007.68	3649.69
H_2O	1230	393.6	1425.57
SO_x	0.84	0.268	0.973
CO	4.875	1.56	5.65
NO_x	23.1077	7.394	26.781
HC	1.5637	0.500	1.812
Total emissions		**1411.002**	**5110.477**
% Difference		**-72.39 %**	

It must be noted that this is only the direct emissions produced by the aircraft during flight. There also exist indirect emissions due to the production of electricity that is required to recharge the batteries on ground. This is expected to be only a small proportion considering the fact that more than 40% of the energy needs in 2030 will be met by renewable energy sources [90]. Assuming, that the power generation method in power plants burns fuel in the same fashion as the gas turbines in the aircraft, it is calculated that equivalent fuel weight of 92 kg needs to be accounted for along with fuel weight of 320kg for E-gle. This results in a total equivalent fuel weight of 412 kg. Now performing the same emission analysis with the emission indices as in Table 12.2, a total of 1815.784 kg of emissions is obtained. Finally, the resultant emissions comes out to be 64.5% lower than that of comparable regional turboprop aircraft.

12.5. EMISSIONS REDUCTION

The E-gle already meets the emission requirement due to using a high amount of batteries, but to further reduce the environmental impact of the aircraft the existing emissions can be reduced even further.

Nitrogen oxides contribute to global warming and an increase in ozone at lower altitudes where the aircraft operates and in contrast, deplete the ozone layer at higher altitudes. Additionally, they cause acid rains, produce smog and are toxic. The production of NO_x is significantly higher when the flame temperatures inside the engine are very high, thus keeping the combustion temperature lower is beneficial for sustainability, however, also lowers the performance. Additionally, making the flame zone more lean also reduces the NO_x produced by 15% to 40% and can be achieved with a lean head end liner. Furthermore, water injection lowers it dramatically, however the water quality has to be high and the addition of water injection adds substantial weight [91]. The NO_x in fuels is also a major contributor to emissions, but aviation kerosene has only a very small concentration of N_2 [92].

Carbon monoxide is extremely toxic and thus, its emittance has to be reduced as much as possible. To prevent the production of carbon monoxide, a sufficiently lean fuel-to-air ratio has to be used to avoid incomplete combustion, which is normally only a problem during minimum load conditions or start-ups. It can also be reduced by lowering the amount of water injected and closing the inlet guide vanes [91].

Removing particulates from the emissions is largely done by changing the fuel composition. By washing, filtering or centrifuging the fuel, contaminants such as heavy metals are removed. The amount of sulphur oxides can be reduced by using fuel with a lower sulphur content [91].

12.6. STRUCTURE DISPOSAL

The structure consists of two primary materials, aluminium and composites. Recycling of composites is as of yet unpopular. Limited demand for recycled composites, high recycling cost and lower quality of the recyclates are preventing composite recycling from being commercially attractive. Furthermore, the heterogeneous nature of composites makes it difficult to separate the reinforcement from the polymer frequently resulting in high energy requirements or use of hazardous chemicals. However, efforts exist within the aerospace industry with associations such as AFRA and PAMELA to develop technologies to recycle composites and the energy use has already been decreased to roughly 10% of that required to produce the material. Because of this, it is likely that when the end of life of the E-gle occurs, the composites within the structure can be recycled [93]. Due to the advantages composites pose for sustainability with regards to production and operational life and the high likelihood that end of life recycling will be realistic in the future, they are seen as having excellent sustainability.

Aluminium is also highly recyclable, due to the following characteristics. Aluminium is resistant to corrosion and thus, retains a high value after use, the energy required and carbon dioxide produced to recycle is only 5% of that to produce it and the versatility of the alloys leads to many potential uses [94]. Recycling of aluminium is also already commonplace, with around 75% of aluminium in the aerospace industry being recycled in the year 2000 and rising [95].

12.7. BATTERY DISPOSAL

A key aspect of the sustainability is the batteries, which have to be disposed of. Due to the hazardous effect zinc has on soil and waterways, it is paramount that the batteries are disposed of in a proper manner [96]. This is done by extracting the zinc and other metals in the battery which can then be re-used by the industry, after which the remaining materials are harmless and can be further recycled. The spent zinc can be electrochemically regenerated, which requires energy, but can be done with sustainable energy sources such as solar power. Since zinc-air batteries have already seen use, in for instance the form of hearing aids, the recyclability has been investigated thoroughly and is already applied in industry [97]. This can be done by using the Modified Zincex process, which has higher zinc recovery efficiency, higher selectivity, better electroextraction performance and is environmentally safer than the current zinc recovery methods [98].

13

Design Evaluation

In order to check if the goals set at the beginning of the project have been met, the design of the E-gle will be evaluated. This will be done by first performing a sensitivity analysis and a risk analysis. This is followed by a detailed financial analysis and the return on investment is calculated. Next the RAMS criteria for the E-gle are presented and finally a compliance matrix is shown.

13.1. Sensitivity Analysis

In this section the sensitivity of the design to critical design inputs is tested. This is done in order to investigate the influence of change of important design parameters or subsystem characteristics.

During the design phase technological advancement may progress faster or slower than initially expected. It is also possible that the design choices change after deeper analysis. With the help of a sensitivity analysis the viability of the design can be guaranteed. First a sensitivity analysis for the battery specific energy is given, followed by an analysis of the MTOW.

13.1.1. Battery Specific Energy

During the preliminary design phase it was already discovered that there is uncertainty about the development in the battery industry. New battery concepts are discovered and developed with high specific energies that are capable of powering aircraft, but the outcome in 15 years is hard to predict. If the specific energy of batteries develops at a different rate than expected this has an influence on the entire concept of the E-gle.

The specific energy of the battery is directly related to the power setting of the gas turbine and the MTOW. A lower specific energy increases the MTOW, since the batteries become heavier. It also reduces the electric energy on board which leads to a higher power setting for the gas turbine. This in turn results in a lower efficiency and an increase in the emissions of greenhouse gasses. To investigate the impact of the battery specific energy the E-gle has been designed multiple times. Each time the battery specific energy was altered to investigate the influence on the entire design and the environmental effect.

In Figure 13.1 the effect of the battery specific energy on the MTOW and battery mass can be seen. It is expected that the specific energy of a zinc-air battery is 470 Wh/kg in 2025. Should it be lower due to a lack of progress in the battery industry the MTOW and battery mass increases. If the specific energy increases due to new technologies or different battery concepts, the weight then decreases. The limiting factor is the MTOW since it is capped at 22000 kg. This leads to a required specific energy of at least 420 Wh/kg. This needs to be monitored throughout the entire design process.

To investigate the effect of the battery specific energy on the environment, a closer look was taken at the fuel used during flight. The results are visible in Figure 13.2. With the current design the fuel mass is 735 kg of which 415 kg is reserve fuel for diversions. It can be seen that a 100% increase in specific energy reduces the fuel onboard by 25% (again including reserve fuel). The amount of fuel burned has a direct relationship to the emissions and greenhouse gasses expelled, therefore the emissions are also lowered by 25%. Thus an increase in battery specific energy has a positive effect on environmental sustainability of the aircraft.

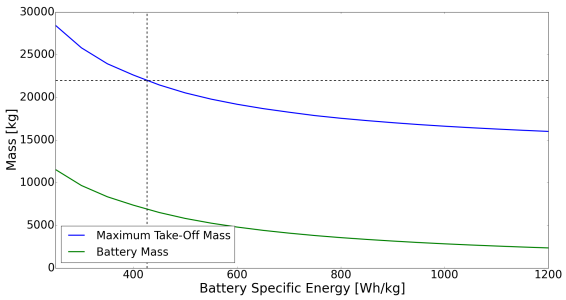

Figure 13.1: Maximum take-off mass and battery mass as a function of the battery specific energy.

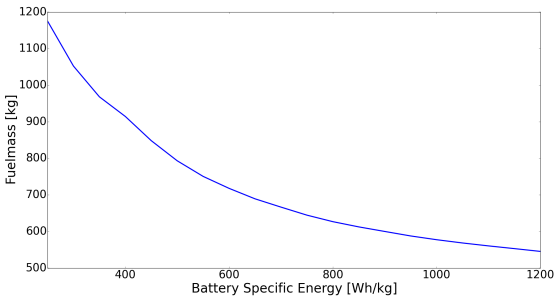

Figure 13.2: Maximum take-off mass and battery mass as a function of the battery specific energy.

13.1.2. MAXIMUM TAKE-OFF WEIGHT

Due to the "snowball effect" (when an aircraft becomes heavier it becomes even heavier due to the increase in drag leading to an increase in fuel mass), the E-gle is also analysed for its sensitivity with regards to an increase in MTOW. At this stage of the design process the MTOW is likely to change due to uncertainties in the design and subsystems. No detailed design has been performed, implying that the OEW and thus the MTOW will change.

In this case the original E-gle design is used, but the MTOW is changed to investigate the effect on energy used during the flight and the efficiency of the aircraft. The results are seen in Figure 13.3. From the graph it can be concluded that, as was expected, a lighter aircraft requires less energy. It can also be seen that a lighter aircraft will operate more efficiently, due to the fact that more of its energy used can come from batteries which operate more efficiently than the gas turbines. No limiting factors and major risks are seen from this analysis, but if the aircraft becomes heavier the operational cost will also increase due to higher fuel burn and more maintenance. The efficiency decreases negatively affects the sustainability and the attractiveness of the E-gle for airliners reduces.

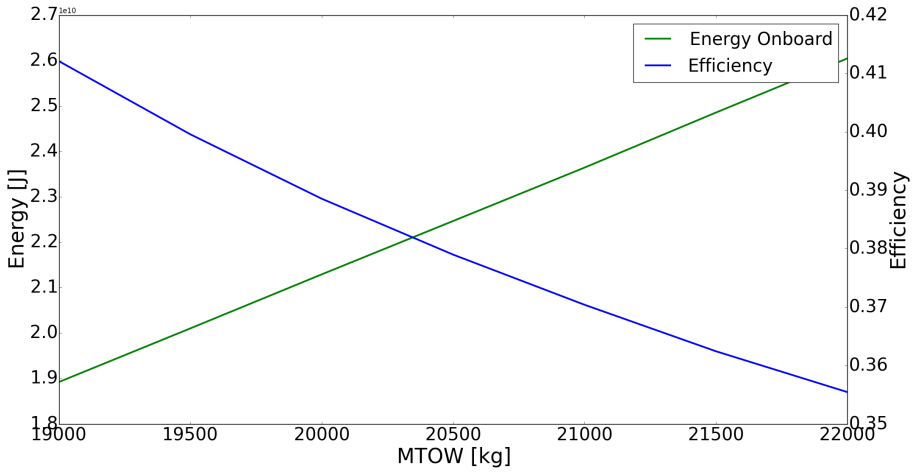

Figure 13.3: Energy needed on-board for the flight and efficiency as a function of maximum take-off weight.

13.2. TECHNICAL RISK ASSESSMENT

The objective of technical risk assessment is to identify, assess and mitigate the risks that may occur in the development of the system or the product, with the consequence that technical performance, schedule or cost requirements are not met. The structure of this section is fashioned in a systematic manner that reflects the sequential flow of risk evaluation. This can be viewed in Figure 13.4.

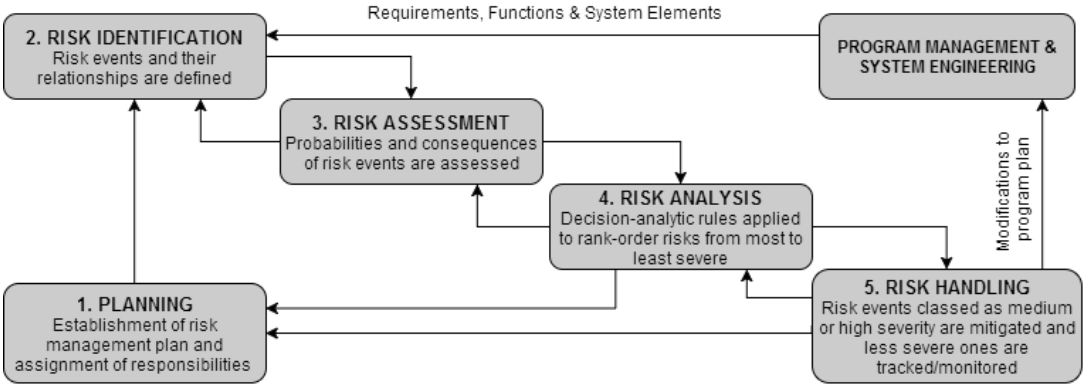

Figure 13.4: Fundamental steps in risk management process[1]

13.2.1. RISK PLANNING

The E-gle is a hybrid electric aircraft designed for regional transport. It is a new concept involving futuristic aspects, innovative design techniques and thus, a rigorous risk management must be performed to ensure safe operations. A strategic approach has been followed in order to achieve this.

The team has appointed two risk managers who constantly keep track and record the identified risks for the project. Every group member is approached by the risk managers to notify them about the risks involved in their respective subsystems. These risks are appended, quantified in the record and the possible mitigation procedures are thought of in order to reduce their magnitude. A risk map prior to and after mitigation is generated to visualise the effect of the appropriate actions undertaken.

13.2.2. RISK IDENTIFICATION AND ASSESSMENT

In this section the risks of the various subsystems and those related to the cost and scheduling of the project are identified, after which an initial risk map is created.

PERFORMANCE

1. **Low wingtip propeller efficiency:** The engines placed on the tip of the wing are rotating in the opposite direction of the vertices created by the wing at that point. This is done in order to reduce the induced drag produced by these vertices. The total reduction in induced drag is estimated to be around 35% [23–25]. If this reduction in drag can not be obtained, this will result in an increase in drag. This will decrease the performance of the aircraft and will result in the snowball effect.
2. **Low battery specific energy:** Currently, the batteries available on the market reach specific energies up to 250 wh/kg. Around 2025 zinc air batteries are expected to have an specific energy of 470 wh/kg. If this prediction can not be reached by 2025, the aircraft's weight could increase significantly. This would result in a decrease in performance.
3. **Overdesign:** In the process of evaluating the performance of the aircraft during the take-off and landing phases, the thrust generated by the high-lift propellers was not considered. This in turn leads to an overdesign that has a snowball effect on the rest of the subsystems, thereby increasing the weight of the aircraft.

[1] https://www.mitre.org/publications/systems-engineering-guide/acquisition-systems-engineering/risk-management [Online; accessed 21 June 2017]

AERODYNAMICS

4. **Folding of propellers:** High-lift propellers are used as high lift devices in order to aid in take-off and landing. During cruise they are retracted, as the wings are already designed to provide the required lift. In case the propellers fail to fold in, a significant amount of drag is created.
5. **Flaps not deployable:** The E-gle has a split flap which is deployed at the time of landing. The effect of this device is an increase in lift in addition to the amount produced by the high-lift propellers. Consequently, there is an increase in the drag required for landing. The failure of this flap will make it difficult for the pilot to land. Firstly, because the aircraft will need to fly at a higher speed and secondly, the landing field length may not be sufficient.
6. **Stall at low altitude:** When an aircraft goes below its stall speed the lift decreases resulting in an imbalance in the equilibrium. In order to counteract this effect, the angle of attack is increased but if increased beyond the critical value, the lift is reduced further and the airplane falls. This phenomenon is more critical at low altitude as it is harder to recover from.

STABILITY AND CONTROL

7. **Control surfaces failure:** Loss of control in flight has been one of the most significant causes of fatal aircraft accidents for many years. This may occur due to the failure of elevator, ailerons, or rudder. The former is the most critical as it ensures longitudinal stability of the aircraft. The failure of one control surface induces high stresses on the remaining ones or on the structure it is connected to, leading to hazardous events[1].
8. **Unexpected shift in c.g.:** During the design phase the centre of gravity of the aircraft plays a mayor role on the stability. If the c.g. is more in front this might overload the nose landing gear and make it more difficult to pitch-up during take-off. If the c.g. is more aft, the aircraft might tip over or be unstable in flight.

PROPULSION

9. **Electric motor control failure:** Two most critical problems with electric motors are electric overload and overheating. The former occurs when the system tends to draw more current than allowable which is unpredictable and has quite a big impact. The latter occurs if the system is over design temperature, causing the heat conducting capacity to reduce at an alarming rate.
10. **Governor failure:** The governor is a complex mechanism which enables the propeller blades to achieve a variable pitch. If there would be a malfunction with this mechanism, the thrust propellers would not be able to achieve their optimal pitch angle. This decreases the efficiency of the propeller during operation. There will be a reduction in performance and increase in fuel consumption, however, the aircraft will be able to operate safely.
11. **Gearbox/engine failure:** In case an engine would fail, the other engine should be designed in order to maintain altitude. However, unlike conventional aircraft, the E-gle has its thrust engines located on its wing tip. This imposes a higher moment which has to be managed by the aircraft. The impact is already reduced by designing an horizontal tail for one engine inoperative conditions. However, landing during bad weather and cross winds remains critical.

POWER

12. **Air entry obstruction:** During operations, air out of the atmosphere is used to keep the batteries functioning. When the passage is obstructed during flight, parts of the power system cannot operate properly, reducing the amount of available energy.
13. **Batteries degradation:** Degradation is a phenomena in which batteries decline to a lower quality. The batteries obtain a reduced amount of capacity and are therefore not sufficient enough to be used in the E-gle. Degraded batteries have to be replaced or repaired in time as they reduce the performance and safety of the aircraft.
14. **Power distribution failure:** With the parallel hybrid electric configuration and high-lift propellers, the power distribution plays a mayor role. If this system does not operate correctly, the high-lift propellers might deactivate or stay activated. Furthermore, insulation failure could cause short circuit or voltage and current failure. This can result in high power dissipation, which produces heat and could even lead to fire.

[1] http://www.skybrary.aero/index.php/Loss_of_Control [Online; accessed 21 June 2017]

15. **Poor battery management system:** The battery management system manages the charging and discharging of the batteries. If the temperature, voltage or current diverge from their optimal state, a loss of propulsion can occur. In case of a short circuit, the battery system can overheat and eventually catch fire or explode.
16. **Fuel leakage:** In case of a leakage in the fuel tank, the amount of fuel will decrease. This has an impact on the performance of the aircraft, as the aircraft has to land earlier and won't be able to finish its mission. In the unlikely event that the aircraft's fuel tank will be empty before the climb is finished, it won't be able to continue its climb on batteries.

STRUCTURES

17. **Unreliable structural analysis:** The structural analysis was done in two different manners. One being an estimation method for conventional aircraft, which doesn't take into account flutter or engine placement. The other being a program which has the exact loading diagram of the E-gle, but does not take into account buckling or flutter. Neither methods take flutter into account. An estimation for the addition in structural weight was based on a paper covering aeroelastic flutter for a wing with DEP. It is likely that the combination of these methods result in an underestimation of the actual wing weight. This has a great impact on both take-off weight and performance [56].
18. **Landing gear problems:** Nowadays, landing gears are designed in order to absorb heavy impacts. If the landing gear has any problems such as a failing retraction mechanism, the aircraft might have to do a gear up landing. Although the likelihood is low, the impact can be high due to the fact that the bottom of the fuselage stores the batteries. These batteries might catch fire during this rough landing.
19. **Fatigue failure:** A common risk of any aircraft is fatigue. It cannot be avoided, but regular inspections and replacements have to be performed to minimise structural damage.

COST AND SCHEDULE

20. **High development costs:** No similar aircraft has been designed yet using the combination of batteries and DEP, making it more difficult to predict the development costs. The occurrence of higher costs are probable and have marginal impacts like less profit or higher selling price.
21. **Overpriced permanent magnets:** The electric motors installed in the engines use strong permanent magnets to function. The most widely used type is a permanent magnet made from an alloy of neodymium, iron and boron to form the $Nd_2Fe_{14}B$ tetragonal crystalline structure. Chinese manufacturers, being a dominant force in neodymium magnet production, are reluctant to export this rare material and thus their costs have skyrocketed.
22. **Competitors enter the market:** In the next decade, the availability of fossil fuels will certainly decrease and more people are therefore considering renewable energy. It is just a matter of time until other companies develop similar aircraft. This results in a more competitive market and therefore selling this aircraft can become difficult.
23. **Not meeting NASA N+3 requirements:** The development of the hybrid aircraft using DEP is mainly set up to meet the environmental goals of NASA N+3. The requirements set in these goals are challenging and when these requirements are not satisfied, the aircraft is less appealing to the customers.
24. **Technology maturity:** The development of the aircraft is also dependent on the maturity of the required technology. Currently the batteries are not developed well enough to deliver sufficient power, however it is predicted that in 2025 the development has reached a point where it does. Predictions are not fully reliable and there is always a chance that these predictions do not come true.
25. **Decrease in benefits from government:** Projects focusing on electrical, fuel efficient vehicles receive many advantages from the governments such as subsides and tax reduction. The evolution of these advantages is not well known, however. In case they would decrease, funding will have to be found elsewhere.
26. **New certification regulations:** Before a newly developed aircraft model may enter into operation, it must obtain a type certificate from the responsible aviation regulatory authority. Since E-gle is an electric aircraft, the regulations are different than conventional. Certain certification changes may not influence the fulfilment of the design, however, others may, resulting in cost and schedule constraints.

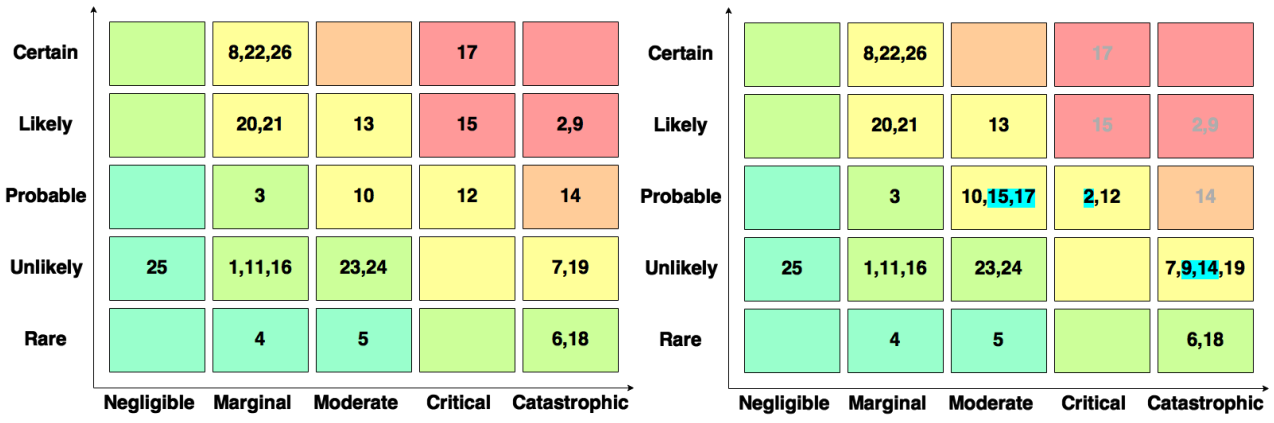

(a) Risk map before mitigation

(b) Risk map after mitigation

Figure 13.5: Level of risk mitigation in the form of risk maps

13.2.3. RISK ANALYSIS AND HANDLING

In this section the three most important risks are analysed in more detail and how they are mitigated is discussed.

2. **Low battery specific energy:** The characteristics of the batteries are not known in great detail since the batteries have not been used for these kind of applications before. The aircraft's weight is one of the main parameter influencing the performance of the aircraft. With the batteries being an important subsystem of the aircraft and the weight being highly dependent on the future improvements of the batteries, this imposes a high risk.

Since the batteries are a crucial part of the aircraft the impact can't be reduced completely. As can be seen in Section 13.1, the batteries should obtain a minimum specific energy of 420 Wh/kg by 2030. If this in not reached by 2030 the maximum take-off weight will exceed its limit. In order to reduce the risk, the mitigation of the risk has to be done from the beginning of the design process. This is done by creating a detailed mass budget. By continuously updating and managing the mass budget throughout the design process the probability and impact of this risk are reduced. Furthermore, this risk can be reduced by working closely together with external suppliers.

9. **Electric motor control failure:** As previously mentioned, the common causes for electric motor failure are over-current and overheating. To avoid an over-current, there are some devices that need to be installed that can prevent it from happening. These devices are usually wired in the circuits and will automatically shut down the extra amount of current flowing in the circuit.

Excessive heat in motors can cause a number of performance problems. Overheating causes the motor winding insulation to deteriorate quickly. For every ten centigrade rise in temperature, the insulation life is cut in half. It has been concluded that more than 55% of the insulating failures are caused by over heating.

Overheating occurs due to a number of factors. Every electric motor has a design temperature. If a motor is started at a bad current value, it starts operating in a much warmer condition than the design temperature. It is very important that the motors should be matched with their ideal current values.

Overheating also occurs when an electric motor is forced to operate in a high temperature environment. This causes the rate at which heat can be conducted to reduce at an alarming rate. The area where electric motors are operating must have a proper cooling system and a ventilation system should be there in case the cooling system stops working[1].

14. **Power distribution failure:** Another big risk identified at this stage of the project is the malfunction of the power distribution system (PDS). The probability of occurrence and the consequence of failure are both extremely high on the risk map. With DEP, it is important that the power is well distributed among the multiple propellers. However, this risk differs with the different concepts considered in this report. The final propulsion architecture suggests one motor per lift propeller and two per cruise propeller. The risk would therefore be lower than if several propellers would depend on a single electric motor. However, the failure of the PDS is still possible.

[1] http://www.brighthubengineering.com/commercial-electrical-applications/78579-determining-causes-for-electric-motor-failure/ [Online; accessed 21 June 2017]

It can be a problem with the control system to activate and deactivate DEP, insulation failure causing electrocution and short circuit or even voltage and current failure. Short circuits must be avoided because they lead to high power and current dissipation, producing very high temperatures. In case the batteries are shorted, they are also discharged very quickly.

Power distribution failure can also be caused by electromagnetic interference, generated by the controller or other external source. It is therefore important to perform regular inspections, as described in Section 11.2 in order to avoid power distribution problem, but also fire and explosion. On top of the regular maintenance, the system will be originally designed in such a way that enough insulators are placed and fixed, and wiring is properly tested and indicated and redundancies are built in the wiring system, such as fuses and parallel circuits. All the subsystems must be extensively tested before putting them together. Further, testing should be performed on the overall system.

15. **Poor battery management system:** The battery management system (BMS) is of paramount importance to ensure safe flight. It is an electronic system managing the state of the batteries during charge and discharge. Several parameters are controlled, such as voltage, temperature and the current. In case one of the parameters diverges from its optimal state, a loss of propulsion can occur during flight, requiring the aircraft to land sooner. Furthermore, problems can also occur on the ground such as short circuiting and overheating of the battery system. Fire or explosion might also occur in case the overheating becomes too important. In case a fire occurs during flight, other systems necessary to propel the aircraft can be harmed, jeopardising the flight. Because the consequences of this risk are very dangerous, it is important to develop a complete mitigation plan.

As described in the paragraph about PDS failure, when batteries are short circuited, the high power dissipation causes overheating and can lead to fire or explosion. In order to limit the damages on other systems, the fire must be contained with a battery casing which should be airtight if possible.

The chosen batteries are Zinc Air batteries. They have never been used on an aircraft because the technology is not ready yet. Technology maturity is therefore an important risk for this project. This type of batteries is sensitive to extreme temperatures and humidity so enough precaution must be taken to ensure safe batteries operation. Other downsides of Zinc Air batteries are the high self discharge rate and the air supply system that needs to provide enough oxygen to the batteries. In order to maximise the probability of having the technology ready on time, investment must be sufficient for the development of this new technology. Responsibilities must be shared with the supplier, as well as the development cost in case it is higher than expected. Finally, extensive verification and validation must be performed with internal and external experts.

16. **Unreliable structural analysis:** This risk is quite different from the other risks as it is internal to the team. Only limited time was allocated to perform its analysis. At present, only strength analysis was performed in depth, however, since E-gle is more susceptible to flutter due to its high aspect ratio a proper flutter study needs to be done to ensure that the wing sustains all the loads occurring during the mission. Additionally, weight increase due to buckling was also obtained from literature that does not exactly emulate the wing being designed for this mission. The probability of occurrence and impact of this risk can be vastly reduced by following a detailed aeroelastic analysis using the tools developed specifically for this purpose.

13.3. FINANCIAL ANALYSIS

This section describes the financial analysis of E-gle. Cost is a major parameter that an airline considers when looking for a new aircraft. In order to sell it for a low price, the aircraft manufacturers must reduce the life cycle cost as much as possible, in order to keep a profit margin for themselves. Aircraft cost estimation is mostly statistical, based on actual cost of prior aircraft. However, cost is dependent on production rate and the amount of aircraft produced. The production learning curve describes this phenomenon: the more aircraft produced, the more the manufacturer learns and the faster and cheaper it becomes to produce he next aircraft. But the cost also varies with the location where the aircraft is being developed, the timescale and other parameters. Two requirements must be considered in this section.

CON-CST-01 The Direct Operating Cost (DOC) shall be 25% lower than current regional transport turboprop.
CON-CST-02 The increase in purchase cost shall not be higher than 10 % of the purchase cost of the current regional transport turboprop.

These requirements are based on a comparison between the E-gle and current regional transport aircraft. Because actual cost varies a lot between different operational practices, methods to estimate the cost usually show the relative cost estimation variation between different designs. This report will focus on the differences and particularities that the E-gle presents, compared with other regional transport aircraft.

The life cycle cost (LCC) can be decomposed in research, development, test and evaluation (RDT&E), production, ground support equipment and initial spares, special construction, operations and maintenance and disposal. The sizes of each element are proportional to the magnitude of their costs for a typical aircraft. Each section will be analysed in order to determine the similarities and differences between the E-gle and typical regional transport turboprop. The cost estimations are based on the methods presented in *Aircraft Design: A Conceptual Approach* by D. P. Raymer [16]. Cost estimation relationships (CER) are developed for the aircraft companies and potential customers. They are expressed in either cost or labour hours. Labour hours can be converted into cost by multiplying by the appropriate hourly rate.

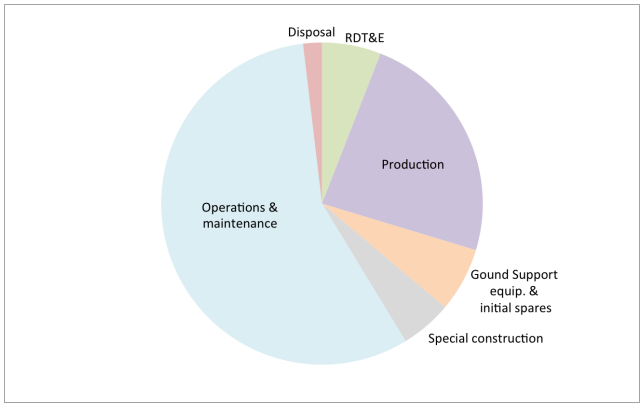

Figure 13.6: Elements of Life Cycle Cost [16]

13.3.1. RDT&E AND PRODUCTION COSTS

RDT&E includes technology research, design engineering, prototype fabrication, flight and ground testing and evaluations for operational sustainability. It also includes certification cost for civil aircraft. The magnitude of this section does not vary on the number of aircraft produced. The production cost includes the material cost to build the airframe, engines, and avionics. It also includes the production tooling cost, the manufacturer's overhead, administrative expenses and the labour cost. The production cost varies with the number of aircraft manufactured. Due to the learning curve and the investment in tools to produce the first aircraft, the production cost decreases with increasing the number of aircraft produced. The purchase price must cover the RDT&E and production costs, as well as a profit for the manufacturer. CERs are usually developed with RDT&E and production costs combined. The model used in this section is the Development and Procurement Costs of Aircraft model (DAPCA) [16]. The final equation to calculate the cost of RDT&E and production is given in Equation 13.1. This method estimates the amount of hours required by the engineering, tooling, manufacturing and quality control groups. These values are multiplied with the corresponding hourly rates in order to determine the cost. Based on statistics data the costs of development support, flight-test and manufacturing material are calculated [16].

$$\text{RDT\&E} + \text{flyaway} = H_E R_E + H_T R_T + H_M R_M + H_Q R_Q + C_D + C_F + C_M + C_{eng} + C_{av} + C_{sp} + C_{int} \tag{13.1}$$

The variables are the number of aircraft built, influencing the production cost, the empty weight, maximum velocity, number of flight tests, engine maximum thrust, Mach number and the turbine inlet temperature. These variables are different for the Bombardier Q300 and the E-gle. 263 [1] Bombardier Q300's aircraft were produced between 1989 and 2009, giving a rate of one aircraft every month on average. To ease the comparison between the two aircraft, it is first assumed that the total number of aircraft produced is the same for the E-gle. However, this number will be higher when the aircraft comes out because of a high demand and will decrease more rapidly because of technology development, with batteries and motors becoming even more efficient, bringing other aircraft on the market.

[1] https://www.aircraftcompare.com/helicopter-airplane/Bombardier-Q300/98[Online; accessed 26 June 2017]

The engine on the Bombardier Q300 is the PW123 and costs 800,000 USD [99]. The engine on the E-gle is the GE CT7-2A, unfortunately no cost estimation could be found, so it was estimated to be 700,000 USD because it is less powerful than the PW123. An extra category was added to the cost estimation of the E-gle: the propulsion system without the gas turbines. Details can be found in Table 13.1. These values were found from the cost estimation from the student team Nova Electric Racing from Delft University of Technology. They have a cost estimation for the electric motor Emrax 268 and other subsystems. From there, values for the turbo electric hybrid system were estimated. DAPCA estimates the interiors (seats, closets, lavatories, etc) to be 1250 USD per passenger for regional transport and the avionic costs 7-13 USD per gram [16]. The highest value was selected and from an example, it is assumed that the avionics have a mass of 200 kg in the E-gle [16].

Finally, the cost of RDT&E and flyaway for the Bombardier Q300 was found to be 14.7 M USD, when benefits are added, the value becomes comparable with the purchase price of 17.0 M$. The cost of RDT&E and flyaway for the E-gle was found to be 15.6% higher, with a value of 17.0 M USD.

However, the requirement CON-CST-02 stipulates that the purchase cost shall not be higher than 10% of the purchase cost of the regional transport aircraft. Increasing the number of aircraft produced decreases the production cost. Therefore, in order to meet the requirement of purchase cost, a minimum of 281 aircraft must be produced and sold, assuming the same profit margin (as a percentage of RDTE and flyaway cost) as the Bombardier Q300. With a total production of 281 aircraft, the RDT&E and production cost of the E-gle is estimated to be 16.2 M USD.

Table 13.1: Propulsion system cost estimation without gas turbines and thrust propellers

DEP system	Cost	**Turbo electric system**	Cost	**Other**	Cost
EM: Emrax 268	100000	EM: Siemens SPD60	24000	Batteries	261180
Motor controller	60000	Motor Controller	12000	Wiring	500
Sensors	7000	Sensors	1400	Circuit breaker	200
Cooling	1400	Cooling	280	BMS	1000
Propellers	4000			Margin	818
	172400		**37680**		**59102**
Total Cost					**470400**

13.3.2. OPERATIONS AND SUPPORT

Operations and support cost is the largest part of the LCC as can be seen in Figure 13.6. It represents the total cost to own and operate an aircraft, composed of the direct operating cost (DOC) and indirect operating cost (IOC). DOC groups fuel, oil, batteries, crew personnel, ground personnel, and maintenance as shown in Figure 13.7 [100]. IOC groups the insurance, indirect costs, and depreciation. Several methods exist to estimate the cost, but the majority only estimates the DOC and are all based on the *Standard Method of Estimating Comparative Direct Operating Costs of turbine Powered Transport Airplanes*. For commercial aircraft the operations and support cost is roughly composed of 38% fuel, 25% maintenance, 24% crew personnel, 12% depreciation and 1% insurance with the rest being negligible [16]. However, these values vary considerably and in particular with the E-gle, for which fuel is not the main energy source anymore. First, the DOC of the Bombardier Q300 is presented, followed by the E-gle, focusing on the differences between the two aircraft.

DIRECT OPERATING COST

DOC is the sum of all the cost elements related to flight operations. Again, following the steps described by Raymer [16], the parameters can be estimated. Converting the percentages of fuel/oil, crew personnel and maintenance to DOC only, the fuel/oil category represents 44%, maintenance 29% and crew personnel 27% of the DOC. These numbers are validated with the analysis of the Q-Series provided by Bombardier [101].

In the design mission, most of the fuel is burned, except the fuel for the loiter and to reach another airport. However, the aircraft almost always lands with an important volume of fuel that can be used for the next flight. The amount of fuel used every year can be estimated by multiplying the average yearly flight hours per aircraft, by the average fuel burnt per hour, which is determined by the total duration and fuel burnt from a typical mission profile. A civil aircraft flights on average 2500 to 4500 hours per year (FH/YR/AC), here, the average is taken: 3500 hours [16]. The average cost of jet fuel from May 2016 to May 2017 is 0.37 USD/litre.

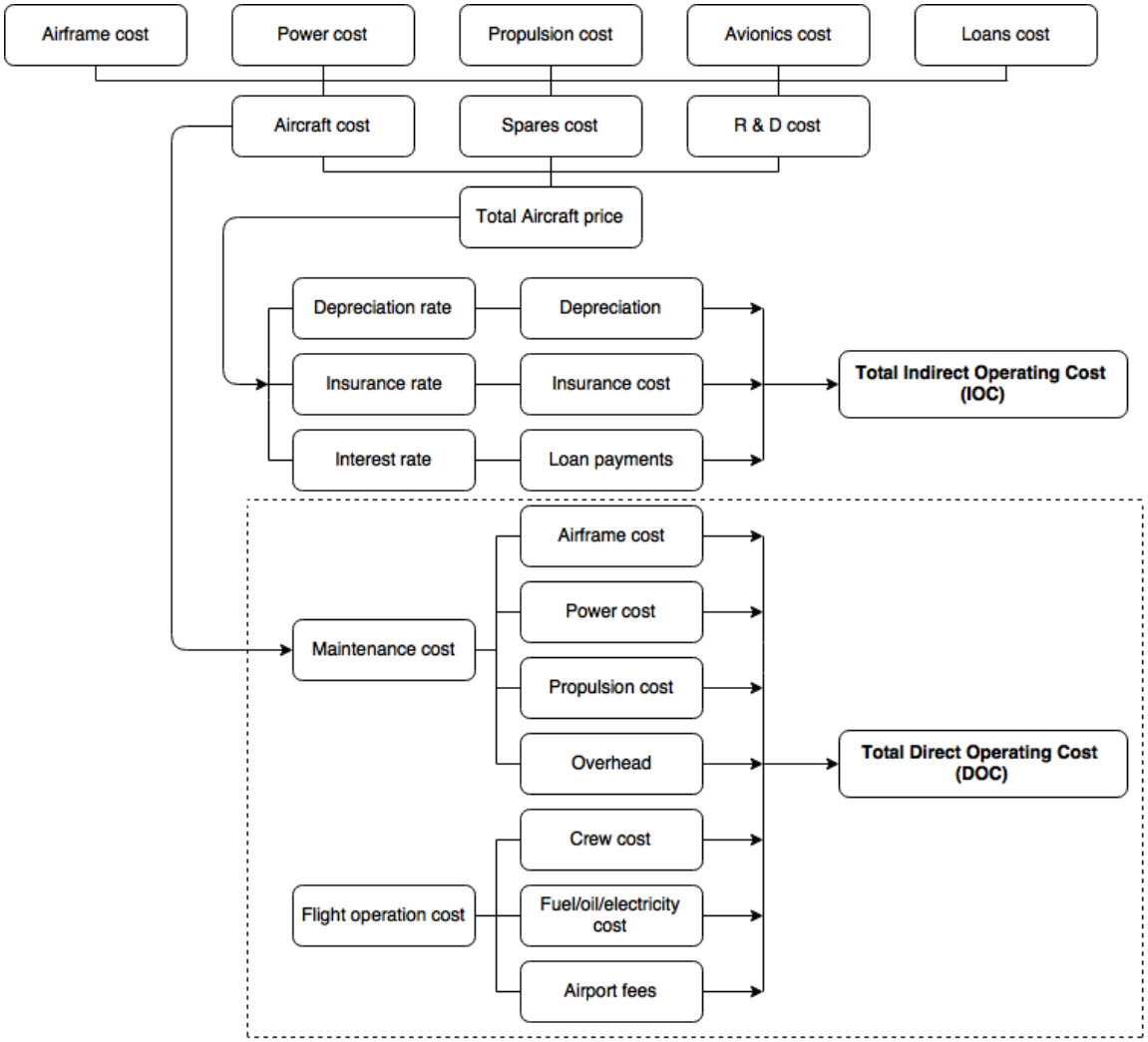

Figure 13.7: Direct operating cost components

From the document *Q series analysis* from Bombardier [101], the fuel usage is 855.5 litres/hour. In total, 1.1 M USD is spent every year per aircraft for fuel. The oil cost is neglected because it is on average only 0.5% of the fuel cost.

The cost for the crew personnel can also be estimated using Raymer's method. Although the results can differ a lot from one aircraft to another, it gives a rough estimate. Because it is just the difference between the Bombardier and the E-gle being investigated and the method is similar for both aircraft, this estimation is sufficient at this stage of the project. In general, a 50 passengers aircraft has a crew of 3 people. The cost can be estimated with equation Equation 13.2. With a cruise velocity of 528 km/h and a take-off gross weight of 19,505 kg, the three-man crew cost is estimated to be 461.2 USD/block hour. A block hour is the duration during which the aircraft is in use, from when the blocks are removed from the wheels to when they are placed again behind the wheels. The block speed of the Q300 is 487.63 km/h and the range is 1558 km. Therefore, the standard value for block hours of the Q300 is 3.2 hours. In order to have this cost in USD/YR/AC as well, the unit of block hours (BH) need to be converted into years. The flight hours per year, FH/YR, were estimated to be 3500. On average, an aircraft takes about 15 minutes for the ground manoeuvre and 6 minutes for air manoeuvre. Therefore, the FH for a standard flight of the Q300 is 21 minutes less than the BH, 2.85 hours. A final value of 1.8 M% USD/YR/AC was found for the crew salaries.

$$\text{Three-man crew cost} = 72\left(V_c \frac{W_0}{10^5}\right)^{0.3} + 172 \tag{13.2}$$

The last section to analyse is the maintenance cost. Maintenance is required after a certain number of flights (cycles) or flight hours. Maintenance is mainly calculated with Maintenance Man hours per Flight Hour (MMH/FH) and material cost. Standard values are presented in Raymer [16].

Multiplying the MMH/FH of 5 by the labor wrap rate of 73 USD and the FH/YEAR (3500 FH/YR/AC), the value of 1.3 M USD is found. The total materials cost is determined by the material cost per FH by using Equation 13.3, multiplied by the FH per year (3500) plus the material cost per cycle in Equation 13.4 times the cycles per year (1346). Following Equation 13.5, a final value of 0.48 M USD per year per aircraft was found. In total, 1.8 M USD is required per year per aircraft for the maintenance of the Q300.

$$\frac{\text{material cost}}{\text{FH}} = 3.3\left(\frac{C_a}{10^6}\right) + 10.2 + \left[58\left(\frac{C_e}{10^6}\right) - 19\right] N_e \tag{13.3}$$

$$\frac{\text{material cost}}{\text{cycle}} = 4.0\left(\frac{C_a}{10^6}\right) + 6.7 + \left[7.5\left(\frac{C_e}{10^6}\right) + 4.1\right] N_e \tag{13.4}$$

$$\text{material cost} = \left(\frac{\text{material cost}}{\text{FH}} \cdot \frac{\text{FH}}{\text{YR}}\right) + \left(\frac{\text{material cost}}{\text{cycle}} \cdot \frac{\text{cycles}}{\text{YR}}\right) \tag{13.5}$$

In comparison to the initial division of the DOC into fuel, crew salaries and maintenance, the ratio between salaries and maintenance is reasonable but the fuel cost seems rather low. The reason for this might be that the equations are taken from the book *Supersonic and Subsonic, CTOL and VTOL, Airplane Design* by G. Corning [102]. It is very likely that the division of the DOC among the three main sections was different, mainly due to the lower price of fuel. Based on the initial ratio presented in this section, the fuel would cost around 2.7 M USD/YR/AC. Finally, the total DOC is estimated to be 6.5 M USD/YR/AC for the Bombardier Q300.

In order to calculate the DOC of the E-gle, the main differences must be analysed. The crew salaries stay the same, but the two other categories differ. Although the new propulsion system will require extra maintenance for the motors, the power distribution and the structure due to the increase in load on the wings,the MMH/FH is assumed to stay constant since the aircraft has a similar size as well as two gas turbines, these two factors being the main source of MMH/FH. However, the material cost for maintenance will differ. The main factor will be the batteries since they have a life cycle much lower than other structural or propulsion components.

With a life cycle of 10000 hours, the batteries must be replaced every 2.86 years. The life span of the electric motors is estimated to be 20 years. If the total cost of the electric motors, 124,000 USD, is divided into a cost per year a value of 6200 USD is found. These two new cost categories are added to the new value of 0.46 M USD of material cost, based on the mass of the E-gle. The new maintenance cost is estimated to be 1.9 M USD including MMH/FH. The other components that are added in the E-gle can be neglected. In total, it can be noticed that there will be a small increase in the maintenance cost. The fuel consumption of the E-gle is estimated to be 75% lower than the Q300. Therefore, the fuel cost is 0.7 M USD. The cost of electricity must be added to the fuel cost category. From the data published by the *U.S. Energy Information Administration*, the average price of electricity in the United States was estimated to cost 9.44 cents/kWh [1] in April 2017. The energy cost is estimated to be 328.7 USD/flight. More details on the characteristics of the batteries can be found in Section 8.1. This costs a total of 0.44 M USD/YR/AC. Now the total DOC of the E-gle is estimated to be 4.8 M USD/YR/AC.

Table 13.2: DOC comparison between the Q300 and the E-gle

	Q300 [M USD]	**Cost E-gle [M USD]**
Fuel	2.9	1.1
Crew salaries	1.8	1.8
Maintenance	1.8	1.9
Total	**6.5**	**4.8**

The DOC of the E-gle is 26.2% lower than the DOC of the Bombardier Q300, the requirement CON-CST-01 is therefore met.

[1] https://www.eia.gov/electricity/monthly/epm_table_grapher.php?t=epmt_5_6_a[Online; accessed 27 June 2017]

The cost of ground support equipment, initial spares, special construction and disposal is calculated next. Initial spares add 10 to 15% of the aircraft price, so 2.2 M$ for the Q300 and 2.4 M USD for the E-gle. The E-gle requires special infrastructure on the ground in order to swap the batteries easily, safely and rapidly. Disposal cost is 2% of the LCC or 6.7% of the RDT&E and production cost, so 1 M USD for the Q300 and 1.3 M USD for the E-gle [16].

13.3.3. COST BREAK-DOWN STRUCTURE

The Cost Break-down Structure (CBS) is a breakdown that identifies all the cost elements of the project development in order to satisfy the needs and requirements of the project. That is the development and production cost of the product that was preliminarily designed during the DSE. The CBS presented in Figure 13.8 focuses on the post-DSE cost elements.

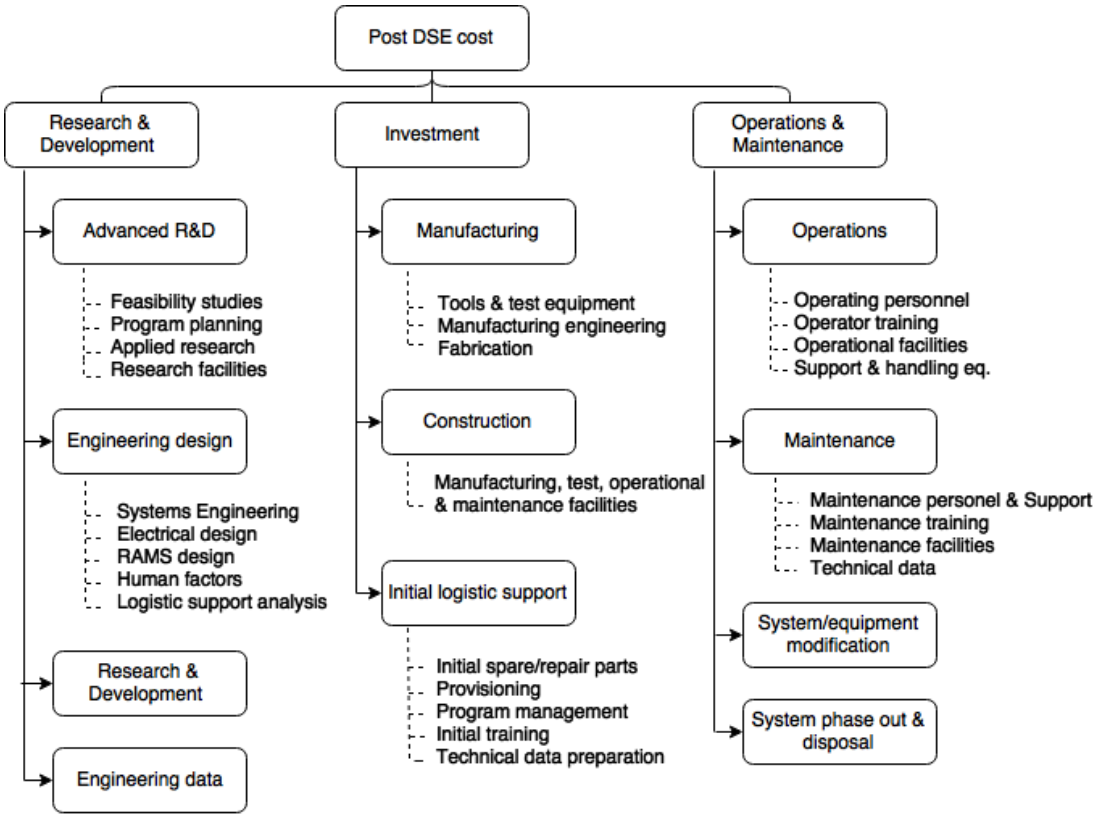

Figure 13.8: Cost breakdown structure for the post DSE phases

13.3.4. RETURN ON INVESTMENT

Return on Investment (RoI) measures the return on investment, relative to investment costs. It is used to compare several investments, by comparing their efficiency. The result of the RoI is expressed as a percentage or a ratio. It is desired to have a high RoI.

The RDT&E and production cost decrease exponentially when increasing the number of aircraft produced. In order to reduce the cost, it is necessary to sell as many E-gles as possible. The purchase cost of the Bombardier Q300 is 17 M USD. One of the main parameters that an airline looks at when looking after a new aircraft is the purchase and operational cost. Selling the E-gle for the same price, 17 M USD, for an aircraft that has a lower direct operating cost (DOC) and a green image, but for which employees (pilots, engineers, workers) must be formed and uncertainties about the aircraft are present, would place the aircraft in a good position on the market.
Based on the equations presented in Raymer [16], producing 281 aircraft is necessary to start reimbursing the investment of the manufacturer. However, 404 must be sold to cover all the investment costs. This number is very large so it would be preferable to increase the purchase price, in order to make sure that any investment is reimbursed as soon as possible, with a limited amount of aircraft built.

The purchase cost of 20 M USD is therefore selected. With this price, a number of 212 aircraft must be sold in order to generate profit. In order to calculate the RoI, it is assumed that 2 E-gles are built every month, during 10 years. With a total of 240 aircraft built, the RoI can be calculated as can be seen in Equation 13.6 [1] where the costs are expressed in million USD.

$$\text{RoI} = \frac{\text{Gain from investment} - \text{Cost of Investment}}{\text{Cost of Investment}} = \frac{3647.7 - 3643.6}{3643.6} = 0.00125 \tag{13.6}$$

It can be seen that the result is very low. In order to increase this ratio, one should consider to increase the purchase price or to build more aircraft in the same amount time.

13.4. RELIABILITY, AVAILABILITY, MAINTAINABILITY AND SAFETY CHARACTERISTICS

In order to quantify the operational effectiveness the Reliability, Availability, Maintainability and Safety Characteristics (RAMS) are calculated. RAMS characteristics indicate the effectiveness and profitability of the aircraft's operational cycle where higher values are better. In this section all above mentioned characteristics are quantified or taken from reference aircraft. Since the RAMS characteristics can not yet be determined during this stage of the design the results of this section should be seen as a goal for further design phases.

In an ideal world an aircraft would be constructed once and continue to fly until its end of life. In this case the reliability and availability would be equal to 1 and maintainability and safety would not be necessary, however, this is impossible. if an aircraft is not maintained the reliability reduces affecting the availability and safety. Performing scheduled maintenance increases the reliability of each subsystem and the system as a whole. If a subsystem fails this negatively affects the availability and maintainability of the aircraft, defects lead to unscheduled maintenance reducing the availability of the aircraft. To ensure a subsystem failure does not result in a system failure safety philosophies can be applied to increase the reliability of the system as a whole. When the maintainability of the aircraft is high, the repair time is low and this increases the availability of the aircraft.

13.4.1. RELIABILITY

Reliability gives the probability that the aircraft can operate failure free during a given interval [103]. Since the E-gle is a complex system with multiple subsystems each subsystems influences the reliability of the aircraft as a whole. Since not all subsystems are critical a failure at subsystem level does not necessarily mean a complete system failure. Therefore only the critical subsystems are included when calculating the reliability of the system. First a list of subsystems is given with their respective reliability, secondly the reliability of the system is discussed. At this stage of the design the reliability of each subsystem and the system as a whole can not yet be calculated and thus, as mentioned above, the reliability as discussed in this chapter should be seen as a goal.

Reliability of Subsystems and the complete System
When calculating the reliability of the system, each subsystems needs to be taken into account. The reliability of a subsystem can be calculated using Equation 13.7, where MTBF is the mean time between failure and t is the interval or mission time [103].

$$R(t) = e^{\frac{-t}{\text{MTBF}}} \tag{13.7}$$

Since the design is not yet at a stage where the reliability of each subsystem can be calculated, values will be taken from reference aircraft and adjusted for the mission of the E-gle and its unique design. Table 13.3 shows the reliability for each subsystem [104]. The power subsystem is still uncertain due to the lack of information and testing of the batteries, since this is also a unique characteristic of the E-gle no reference data can be used. Other subsystems include the flight control computer, flight instrumentation, communication systems and the navigation system. To analyse the reliability of the entire aircraft all subsystems have to be taken into account. This done using Equation 13.8.

$$R_{\text{system}} = \prod R_{\text{subsystems}} \tag{13.8}$$

[1] http://www.investopedia.com/terms/r/returnoninvestment.asp[Online; accessed 27 June 2017]

If defects occur, whether critical or non-critical, the aircraft will have to undergo maintenance reducing the availability. This has a negative affect on the sustainability of the aircraft.

Table 13.3: Reliability of all subsystems

Subsystems	**Reliability**
Airframe (Structures and Aerodynamics)	0.99825
Propulsion System	0.99969
Power System	0.99994
Other Subsystems	0.98115
Total Reliability	0.98307

13.4.2. AVAILABILITY

Availability is defined as the total operational time over the total time. It can be defined in percentage or as days per year. For aircraft with short ranges, the availability is lower due to the fact that maintenance is required more often [105] and aircraft movement is often limited during nighttime when the airport is located in an urban area [106]. In general the availability for a regional turboprop aircraft is around 50%. Since the E-gle is electric and more silent than its competitors it can take off and land during nighttime at more airports resulting in a higher availability.

In order to reach these values the E-gle will need regular servicing and maintenance sessions to keep the reliability high. In order to keep these sessions from interfering with operating times and reducing the availability, they can be planned during nighttime when flight movements are restricted. Unscheduled maintenance however cannot be planned, but in order to keep availability high, unscheduled maintenance should not last longer than 24 hours [103].

13.4.3. MAINTAINABILITY

In order to have sufficient reliability and availability the E-gle needs maintenance. Scheduled maintenance sessions can ensure the aircraft does not need unscheduled repairs. In general this does not differ greatly from regular aircraft, but the E-gle has some additional subsystems to inspect as explained in Section 11.1. To reach the target availability repairs should be completed within 24 hours. Since the E-gle is a state of the art aircraft, self diagnostic software can assist mechanics which reduces the repair time. Also the standardisation of equipment and interchangeable hardware modules such as electric engines can lower the complexity of repairs, this needs to be taken into account during the design phase.

13.4.4. SAFETY

During the aircraft's lifetime, it is continuously in contact with human interaction. During the production and maintenance, people are working close to the aircraft. During flight, a large amount of passengers are present in the E-gle and have to be transported safely from one location to another. Current aircraft are very safe and compared to cars, buses and bicycles it is responsible for the least amount of deaths per km travelled [60]. Overall safety has to be established by the joint contribution of the manufacturer, operator and authorities.

Seventy percent of the fatal accidents involve human factors. To prevent structural failure, safety requirements have to be established. These requirements are related to strength, load cases and life time. Each requirement has its own unit of time, for example 'flights' or 'flying hours'.

Different design philosophies can be applied; safe life, fail safe or damage tolerance. Safe life is the flight hours, landings or number of flights of a structure during which there is a low probability that the aircraft's strength is going to degrade below its design strength. During the design life, fatigue failure is not likely to occur because a reasonable safety factor is applied. However, fatigue can be an issue when the design life is increased due to economical reasons, when loads are higher than expected, improvement of methods (resulting is smaller safety factors) or the use of different materials that are more sensitive to crack growth and residual strength. A drawback of the safe life approach is that the design is over-built, which means it is not economical friendly. To counteract these drawbacks, other design philosophies were developed like the fail safe design. Fail safe applies on structures or systems that do not cause dangerous situations for human beings after failure. The chance that a structure or system fails is small due to reliability, quality and maintainability requirements, however there is always a possibility that a part of the aircraft fails.

The aviation authorities are very strict concerning safety; when a section fails, this should not harm the passengers or the environment. The fail safe concept is economically more viable than a safe life design. The third design philosophy is damage tolerance. Damage tolerance reflects the ability of a design to sustain anticipated loads in the presence of accidental damage, fatigue or corrosion until it is detected through malfunctions or inspections and is repaired. Damage tolerance is not a replacement for safe life or fail safe, it has to be used in combination with one of them. Damage tolerance includes durability, the ability of the design to sustain degradation to a certain extent so they can be controlled by inspection and economically acceptable maintenance programs.

The question that arises is the following: should either a safe life or fail safe design be applied on a certain structure? The benefit of safe life is that it reduces the likelihood of any failure and unplanned maintenance. The benefit of fail safe is that it is possible to manage easily damage after failure. There is no established method to determine which method has to be applied.

When a safe life design is considered, extensive testing and analysis are required to estimate the functional time of a component. Since it is not possible to determine exactly how long the component will last, a reasonable safety factor has to be applied to prevent catastrophic failure. Techniques to consider a proper fail safe design involve redundancies: when a critical subsystem fails and causes serious losses, back-up systems are required. Also several load paths have to be possible to transfer the loads via different paths after a certain part has failed.

As mentioned earlier, the interaction between different disciplines; the operator, manufacturer and the authorities accomplish the safety of the aircraft. Because there is no established method for determining which philosophy has to be applied, the involved parties have to use their judgement on a case-by-case basis. When inspection is not possible, safe life has to be chosen to guarantee a functioning structure. Also when it is very expensive to repair or replace certain components, safe life is the most appropriate approach. When parts are easy to repair and easily inspected, the fail safe philosophy has to be chosen. When a certain part of the aircraft is very critical and it is hard or impossible to make it redundant, safe life has to be chosen. These approaches are visualised in Figure 13.9.

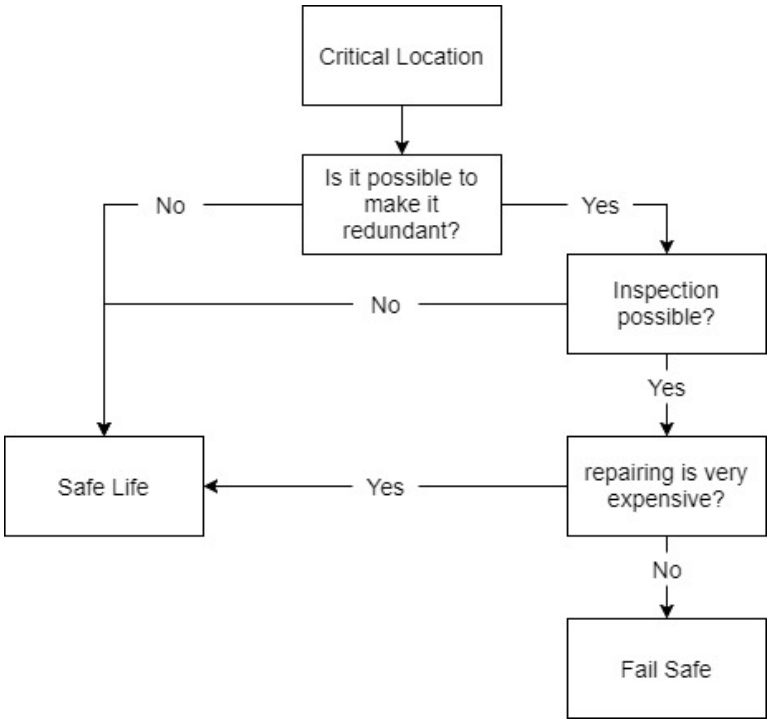

Figure 13.9: Design approach concerning safety

For each design part of the E-gle this design approach has to be followed. It is applied to different safety critical functions of the E-gle and is presented in Table 13.4. It is not possible to make the fuselage, wings and control surfaces redundant and therefore safe life will be applied to these components. The aircraft engines and propellers are designed in such a way that when an engine fails, the aircraft can still operate. Next to that, the engines and propellers are repairable and inspectable. Therefore fail safe is chosen for the wingtip and high-lift propellers.

For the fuel tank and landing gear it is not possible to make it redundant because there is not enough space for that in the aircraft, therefore the safe life approach is considered for these parts. It is most convenient to place the batteries in one compartment, but a complete battery system failure when a small failure occurs has to be avoided. Therefore, the batteries are placed in different compartments to avoid overall battery failure. The last critical function described is the flight data system. A lot of on-board systems are powered electrically and very few mechanically. The flight data system provides inputs and data from the pilot or autopilot to functional components of the aircraft. Failure of this system is very critical, therefore a redundant system has to be installed.

Table 13.4: Design Approach concerning safety for different structures

Critical Function	Safe Life	Fail Safe
Fuselage	✓	
Main Wing	✓	
Tail configuration	✓	
Control Surfaces	✓	
High-lift Propellers		✓
Wingtip Propellers		✓
Fuel Tank	✓	
Batteries		✓
Landing Gear	✓	
Turboprop		✓
Flight Data System		✓

Not only during the flight phase risks occur to people close to the aircraft. When the E-gle is on the ground passengers and their luggage have to enter and leave the aircraft. Meanwhile, the aircraft is provided with enough fuel and the batteries are swapped to ensure the next flight can be fulfilled. These proceedings can cause dangerous situations and therefore will be discussed in more detail to ensure safety.

To be sure that no accidents regarding fuelling happen such as ignition and leakage, safety measures have to be taken [107]. Only trained personnel and vehicles from approved organisations can carry out the fuelling procedure. Each aircraft should have a sufficient amount of fire extinguishers available to counteract starting fires. To ensure nobody smokes near the fuelling devices and areas, prominent "no smoking" signs have to be posted in each fuel servicing vehicle. Next, each fuel system should be able to quickly and completely shut off the fuel flow in case of emergencies. Lastly, a fire brigade should be nearby to be able to extinguish a large fire.

The last part discussed for safety are the measures taken to ensure safe battery swapping. The risks that occur during swapping and which could cause dangerous situations for involved people are stated here. When the batteries are taken outside the aircraft, they are exposed to the local environment which could include rain, snow, hail, heat or cold. This could cause safety issues because the batteries' protection could be damaged. If leaks are present, water could enter the battery system resulting in fire. To ensure no water or hail will be in touch with the batteries, which could pose a serious danger to the people involved, a shelter roof has to be placed above the swapping configuration.

13.5. REQUIREMENTS COMPLIANCE MATRIX

In Table 13.5 and Table 13.6, the requirement compliance matrix can be seen. It gives an overview of which of the requirements originally imposed on the design have been met and which have not at this stage and in which part of the report a justification for this can be found. Moreover, it allows for comment on interesting information concerning certain requirements, for example for the requirements that have not been met.

Table 13.5: First part of the compliance matrix

Requirement ID	Requirement	Check	Section	Comment
CON-CST-01	The direct operating cost (DOC) shall be 25% lower than current regional aircraft.	✓	13.3.2	-
CON-CST-02	The increase in purchase cost shall not be higher than 10% of the purchase cost of current regional aircraft.	✓	13.3.1	-
CON-SDL-01	The preliminary design shall be completed in ten weeks.	✓	15.1	-
CON-SDL-02	The preliminary design shall be completed by ten designers.	✓	15.1	-
CON-MRK-01	The aircraft shall be market-ready by 2030.	✓	14.3	-
TEC-PRE-A01	Propellers shall be accessible for inspection.	✓	11.2.5	-
TEC-PRE-B01	The cargo holds shall be accessible via a cargo ramp.	✓	6.1.1	-
TEC-PRE-B02	The aircraft shall have capacity for 50 passengers.	✓	6.1.1	-
TEC-PRE-C01	The aircraft shall be charged, from empty to full, within the turn around time of the Q300.	X	11.1.1	The charging time for Zn-air batteries is 6 hours. Battery swapping is the alternative that has been chosen in this research.
TEC-PRE-C02	The aircraft shall be fuelled, from empty to full as fast as the refuelling of the Q300.	✓	11.1.1	-
TEC-PRE-C03	The charging and fueling process shall pose no danger to anyone within or near the aircraft or charging equipment.	✓	13.4.4	-
TEC-PRE-D01	The aircraft shall be sufficiently manoeuvrable to use general airport taxiways.	X		Unfortunately this is not checked yet. Could be done with a landing gear analysis.
TEC-INF-A01	The aircraft shall have a maximum take-off field length of 1200 m.	✓	10.6.2	-
TEC-INF-A02	MTOW shall not exceed that of the Bombardier Q300 multiplied with a factor 1.1.	✓	4.1.3	-
TEC-INF-B01	The aircraft shall have a climb rate as described in CS25.119,121	✓	10.5.3	-
TEC-INF-C01	Range shall exceed 500 nautical miles with normal reserves.	✓	10.5.4	-
TEC-INF-C02	Cruise speed shall be 500 km/hr.	✓	10.5.4	-
TEC-INF-D01	The aircraft shall have a maximum landing field length of 1100m.	✓	10.6.2	-
TEC-INF-D02	The landing gear shall be able to withstand a landing gear load of 2g.	✓	9.7	-
TEC-INF-E01	The aircraft shall have stable eigenmodes.	✓	6.4	The spiral motion is marginally unstable.
TEC-INF-E02	The aircraft shall be stick-fixed stable.	✓	6.3.2	-
TEC-INF-E03	The aircraft shall be stick-free stable.	✓	6.3.2	-

Table 13.6: Second part of the compliance matrix

Requirement ID	Requirement	Check	Section	Comment
TEC-INF-F01	The aircraft shall have a turning performance as described in CS-25.	X		Unfortunately this is not checked yet. This could be done by doing turning calculations.
TEC-INF-F02	The aircraft shall be able to perform a cross wind landing procedure as described in CS25.	✓	6.3.3	-
TEC-INF-F03	The aircraft shall be able to have a take-off pitch rate as described in CS25.	✓	6.3.2	-
TEC-PST-A01	Routine maintenance items shall facilitate easy removal.	✓	11.2	-
TEC-PST-A02	Hatches shall be placed in the wing and fuselage to allow for access and inspection.	✓	11.2.6	-
TEC-SUB-A01	The design shall be made with a battery specific energy of 500 Wh/kg	✓	10.4.2	-
TEC-SUB-A02	The battery system shall have a casing that prevents fire from reaching other parts of the aircraft.	✓	13.2.3	-
TEC-SUB-A03	The energy mass shall stay within its mass budget of 6264 kg.	X	4.1.3	The energy mass exceeded its budget. However, there is enough contingency to mitigate the problem.
TEC-SUB-A04	Environmentally friendly disposal of the batteries shall be possible at end of life.	✓	8.1	-
TEC-SUB-A05	The power subsystem shall be at least as safe as the power subsystem of Q300.	✓	13.4.4	-
TEC-SUB-B01	No structure shall have plastic deformation below ultimate load.	✓	9.6	Flutter has not yet been taken into account in a detailed model.
TEC-SUB-B02	No (parts of a) structure shall fail below failure loads.	✓	9.6	-
TEC-SUB-B03	Structures shall have sufficient stiffness to not limit operation of the aircraft due to operational forces.	✓	9.6	-
TEC-SUB-B04	The structure shall be corrosion resistant.	✓	9.5	-
TEC-SUB-B05	The structure shall be able to endure for 30 years.	X		No fatigue analysis was done. This should be done in the next research phase.
TEC-SUB-B06	The structure shall stay within its mass budget of 4962 kg.	✓	4.1.3	-
TEC-SUB-C01	DEP shall be used to increase dynamic pressure for the wing.	✓	5.3.2	-
TEC-SUB-C02	The propulsion subsystem shall adhere to CS-25E.	X	7.4	There is no certification yet for this kind of aircraft in CS-25.
TEC-SUB-C03	The propulsion subsystem shall stay within its mass budget of 2196 kg.	✓	4.1.3	-
TEC-SUB-C04	The aircraft emissions shall be 50% lower compared to current conventional regional aircraft.	✓	12.5	-
TEC-SUB-C05	The cumulative certification noise impact shall be 15 dB lower compared to current regional transport turboprop aircraft.	X	12.2.6	The noise requirement was not met. The aircraft noise characteristics are similar to that of the Q300. The aircraft complies with the JAR 36 noise requirement.

14

Project Design & Development Logic

This chapter displays a logical order of the work done so far and the work that needs to be done from here on. Firstly, the design development of the E-gle at a conceptual level is explained in Section 14.1. Secondly, an insight into the post-DSE activities is given in Section 14.2. Lastly, the different phases of aircraft development after the conceptual design phase are included in the form of a Gantt chart in Section 14.3

14.1. Conceptual Design Development

The design synthesis exercise includes only the conceptual design of the aircraft. It consists of multiple phases where extensive brainstorming sessions were conducted to come up with new concepts, disregard unfeasible concepts and improve the selected ones.

The first phase was project planning. In this phase, the project was logically organised. All the tasks to be done were listed and put in the form of a work flow diagram, work breakdown structure and a Gantt chart, highlighting important milestones and deadlines. Additionally, a team organisation diagram was made to allocate roles and responsibilities to the team members.

The second phase was the baseline review. In this report, all the functions of the system were determined and from them, the system requirements were derived with some requirements being classed as key or driving requirements. These were presented in the form of a functional flow diagram and a requirement discovery tree. Furthermore, design option trees containing all possible concepts, were generated for different subsystems. Feasible combinations were briefly analysed and selected for trade-off. Additionally, resources were allocated, budgets were framed, risks were assessed and a sustainable development strategy was formulated.

The third phase was the mid-term review. This phase mostly involved performing extensive trade-offs in order to come up with the best aircraft design. Every subsystem was individually studied and results were gathered. Following from the trade-off outcomes, a sensitivity analysis and verification and validation procedures were performed to ensure quality assurance of the chosen concept. As an electric aircraft is a new concept, changes in operations and logistics exist; these were briefly discussed and possible modifications were suggested. Updates were made to the technical risk assessment and sustainable development strategy.

The last phase is the final review. The chosen design configuration is designed in the final phase for its aerodynamic characteristics, electric and hybrid electric propulsion, battery sizing, performance, acoustics, emissions, cost, etc. A requirement compliance matrix was generated to give on overview which requirements have been met. Additionally, a future outlook is presented in which the post-DSE activities are discussed and a detailed cost breakdown structure is presented. Further research and recommendations are mentioned for the detailed design phase.

14.2. Post-DSE Activities

The design synthesis exercise terminates with the final preliminary design of the E-gle. There are several procedures to be followed after that point. Figure 14.1 shows the progression in a workflow diagram. Three broad divisions can be realised from this figure, the first being the detailed design phase, the second being the production phase and the third being the operations phase.

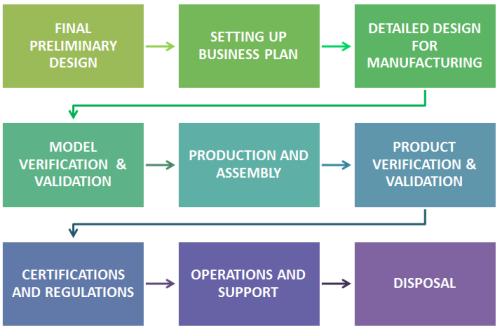

Figure 14.1: Post-DSE activity flow

Once the final preliminary design is well documented and presented to pertinent stakeholders, the next step is to search for business officials who are willing to invest in the product development. This involves framing of detailed budgets, setting up bank accounts and making negotiations with the clients.

After the contracts have been signed and made formal, the detailed designing is initiated. Some of the components to which high priority is given are as follows:

- Wing Design
- Tail Design
- Fuselage Design
- Landing Gear
- Propulsion System
- Battery Functioning & Performance
- Equipment/Subsystems
- Integration
- Wind Tunnel Testing
- Weight Distribution
- Performance & Stability Analysis
- Control Surfaces Design

In this phase, a computer model is perfected and every minute detail is implemented into the simulation so that it can be used for CFD and FEM analyses. Moreover, wind tunnel tests and different structural failure tests are performed at this stage. Finally, the design can be optimised for the design parameters that satisfy the project requirements. Engineering drawings for all the components are produced with very specific dimensions for manufacturing reasons. Once the individual subsystem tests have been conducted a full scale model test is conducted and the findings are documented. The design can be reiterated if are any deviations from the expected results.

After receiving a green signal from the detailed design phase, production and assembly plans are worked out. This involves acquisition of parts and components from different manufacturers, arranging transport facilities and setting up the assembly line. Furthermore, the product verification and validation procedures must be executed. These include passing the flight readiness and critical design reviews.

The aircraft is then taken for certification and regulations. This process involves acquiring approval for the items shown below. Once the aircraft is certified, it is ready for operation. After completing its operational life, the aircraft retires and is disposed.

- Aircraft Software
- Engines, Propellers, Batteries
- Human safety factors
- Technical Standard Orders
- Parts Manufacturer Approval
- Original Design Approval Process
- National Automated Conformity Inspection Process

14.3. PROJECT GANTT CHART

In order to make sure the aircraft is ready by the year 2030, a Gantt chart was made for the tasks to be performed until that period. The activities can be broadly divided into three major phases, first being the detailed designed phases, second being the production phase and third being the operations phase. Breakdown of each phase can be viewed in Figure 14.2.

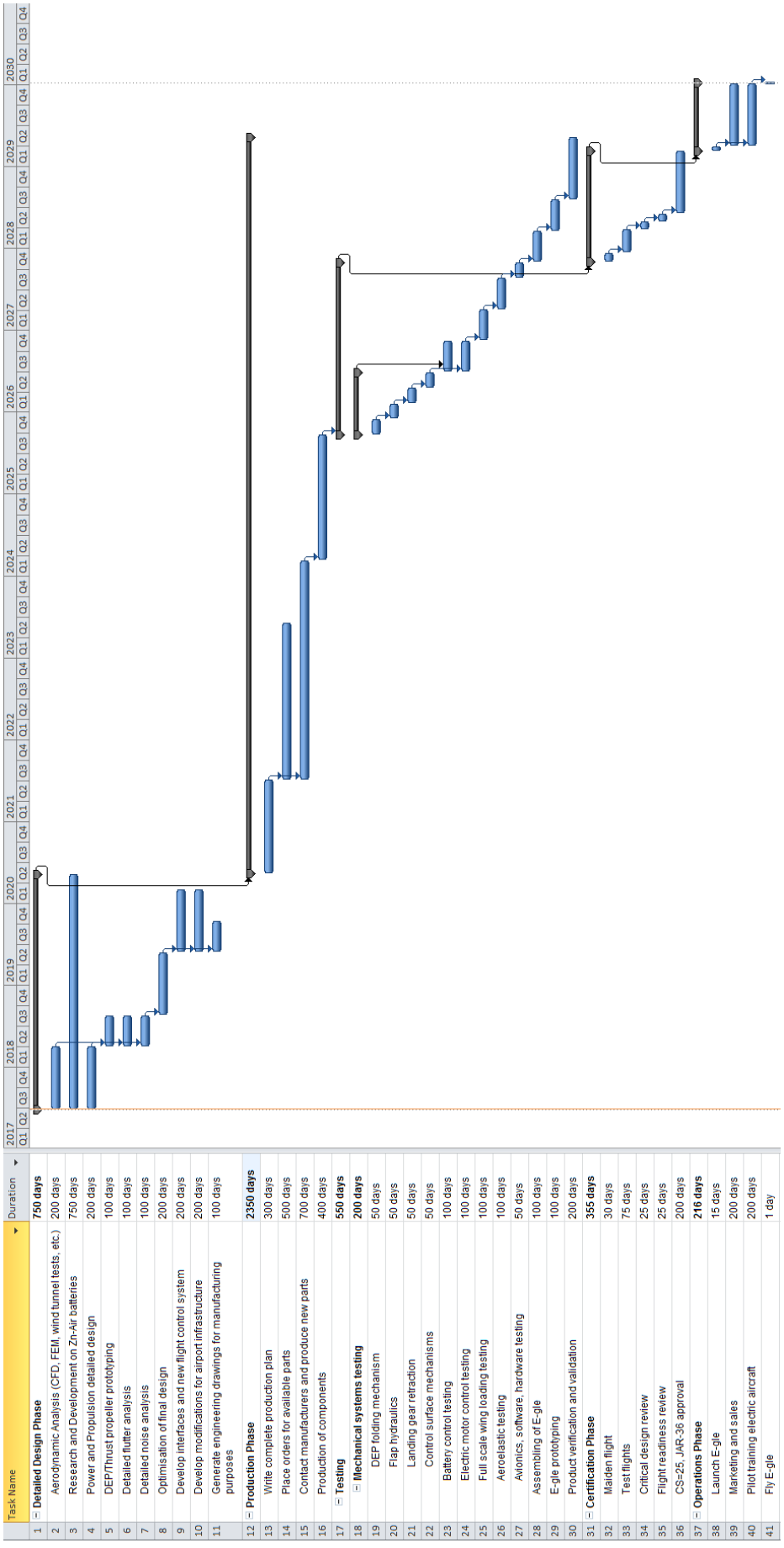

	Task Name	Duration
1	**Detailed Design Phase**	**750 days**
2	Aerodynamic Analysis (CFD, FEM, wind tunnel tests, etc.)	200 days
3	Research and Development on Zn-Air batteries	750 days
4	Power and Propulsion detailed design	200 days
5	DEP/Thrust propeller prototyping	100 days
6	Detailed flutter analysis	100 days
7	Detailed noise analysis	100 days
8	Optimisation of final design	200 days
9	Develop interfaces and new flight control system	200 days
10	Develop modifications for airport infrastructure	200 days
11	Generate engineering drawings for manufacturing purposes	100 days
12	**Production Phase**	**2350 days**
13	Write complete production plan	300 days
14	Place orders for available parts	500 days
15	Contact manufacturers and produce new parts	700 days
16	Production of components	400 days
17	**Testing**	**550 days**
18	**Mechanical systems testing**	**200 days**
19	DEP folding mechanism	50 days
20	Flap hydraulics	50 days
21	Landing gear retraction	50 days
22	Control surface mechanisms	50 days
23	Battery control testing	100 days
24	Electric motor control testing	100 days
25	Full scale wing loading testing	100 days
26	Aeroelastic testing	100 days
27	Avionics, software, hardware testing	50 days
28	Assembling of E-gle	100 days
29	E-gle prototyping	100 days
30	Product verification and validation	200 days
31	**Certification Phase**	**355 days**
32	Maiden flight	30 days
33	Test flights	75 days
34	Critical design review	25 days
35	Flight readiness review	25 days
36	CS=25, JAR-36 approval	200 days
37	**Operations Phase**	**216 days**
38	Launch E-gle	15 days
39	Marketing and sales	200 days
40	Pilot training electric aircraft	200 days
41	Fly E-gle	1 day

Figure 14.2: Planning of post-DSE activities in the form of a project Gantt chart

15

Conclusion

In order to meet the environmental goals of NASA N+3 and Flightpath 2050, there is a need to design aircraft that efficiently uses alternate, cleaner energy sources over conventional propulsion techniques. This project aims to design a hybrid regional passenger aircraft that can cover a range of at least 500 NM. The aircraft makes use of a hybrid power supply in which the power is delivered by both batteries and fuel. Distributed electric propulsion is used to increase the dynamic pressure during take-off and landing which allows the wing to be optimised for cruise and limiting the use of high lift devices.

First, the project results will be discussed in Section 15.1 and the main characteristics of the E-gle aircraft can be found in Table 15.1. This is followed by the recommendations of this project, stating on which topics the focus should lie future design phases in order to realise this project.

15.1. Project Results

In Chapter 5 it was found that the two main ways to reduce the drag of the aircraft are the wingtip propellers and the smaller surface are. The wingtip propellers lead to a decrease in induced drag of 35%, as they counteract the wingtip vortices. Moreover, the reduction in wing size due to the wing being sized for cruise condition, leads to a decrease of the total drag of around 30%.

The propulsion components and architecture were discussed in Chapter 7. A parallel turbo-electric hybrid system was chosen because of the redundancy of the system and its lower required power output from the gas turbine, making the design lighter and cheaper. The configuration will have two hybrid turbo-electric propellers, which both have one gas turbine, the GE-CT7-2A, and 2 electric motors, the Siemens SPD60. Furthermore, there will be 20 high-lift propellers, driven by 20 Emrax-268 electric motors. The thrust propellers have 2 blades and use variable pitch to increase their efficiency. The DEP propellers will have 8 propeller blades due to a limited allowable propeller diameter.

In Chapter 8 it is discussed how the aircraft gets its power. The energy comes partly from Jet A-1 fuel and partially from Zn-Air batteries. The advantage of Zn-Air is the relatively high specific energy and volume density. Disadvantages are the charging time and life cycle of the battery. If demand rises and research is intensified, these challenges can be mitigated. In Chapter 11 it was chosen to swap the batteries instead of recharging them directly. This reduces the turn around time making it possible to make more trips, which is cost efficient.

The wing weight and body weight were computed in Chapter 9. The wing weight is 2040 kg, which is slightly higher than the wing weight of similar aircraft. The fuselage weight was estimated to be 1530 kg, which is similar to reference values. Al-7050 and Al-2024 were the chosen materials for the wing structure. Al-7050 was chosen for its high strength and Al-2024 for its fatigue resistance.

The performance of the aircraft was treated in Chapter 10. The optimal cruising height for the E-gle was found to be 5000 m, because for short distances the benefit of lower drag at a high altitude does not outweigh the penalty of the extra energy and time needed to reach that altitude. The E-gle was found to be much more fuel efficient than the Q300. For the same range of 500 NM, the Q300 burned 1159 kg of fuel, while the E-gle only burned 320 kg of fuel. The battery mass for this mission was 5804 kg. Furthermore, an optimal efficiency was reached at a number of engines for which the cruise flight could be flown purely on electrical power.

In Chapter 12 the noise and emissions of the aircraft were evaluated. The noise did not meet the requirement stated of the project, but the noise level was considerably lower than the JAR-36 noise requirement and lower in all categories compared to the Bombardier Q300. The emission requirement was easily met with a total direct emissions reduction of 72.4%. If the emissions of the production of the electrical energy is taken to account the emission reduction reduces by 64.5%.

The risks of the design were evaluated in Section 13.2. One of the most important risks is a potentially low battery specific energy in the year 2025, as this will increase the weight quite drastically. Another important risk is power distribution and electric motor control failure. This increases the chance of fire during flight and a total failure of the system will make it very hard to land as the aircraft is dependent on the extra dynamic pressure on the wing created by the high-lift propellers. Finally, there is still an uncertainty in the required strength and stiffness of the wing, which can increase the weight.

According to Section 13.3, the direct operating cost of the E-gle can be reduced by 25% compared to the Q300, making it financially more attractive than its competitors. Furthermore, Chapter 2 states that the busiest flight routes can be covered with a 500 NM range. However, the acquisition cost of the aircraft is 10% higher than that of the Q300. This is mainly due to a major increase in the amount of electrical engines, increasing the complexity of the system and thus increasing the costs.

Altogether, the E-gle reduces emissions by having higher aerodynamic and propulsive efficiency, while reducing operating costs as well. In this way, the E-gle contributes to a greener future in aviation in a financially attractive way.

Table 15.1: Aircraft Characteristics of the E-gle

Parameter	Value	Unit	Parameter	Value	Unit
Passengers	50	-	Aspect Ratio	15	-
Cruise Height	5000	m	DEP Engines	20 x 100	kW
Cruise Velocity	500	km/h	Electrical Engines	4 x 260	kW
Range	500	NM	Gas Turbine	2 x 1200	kW
MTOW	20446	kg	Take-Off Field Length	1090	m
OEW	8909	kg	Landing Field Length	1190	m
BW	5804	kg	Stall Velocity Sea Level	46.0	m/s
MFW	1288	kg	RD&T and Production Cost	16.1 million	USD
MPW	5000	kg	Direct Operating Costs	4.8 million	USD/year
Surface Area	39	m^2	Cumulative Certification Noise	86.1	dB
Wing Span	24.2	m	Direct Emission Reduction	72.4	%

15.2. RECOMMENDATIONS

One of the main recommendations is further research into the wingtip propeller benefits. There are currently only a few articles available which explain the reduced induced drag caused by the wingtip propellers and methods to determine this benefit have not yet been developed. Furthermore, no research has been done into the effect of wingtip propellers on the structure of the aircraft. Flutter is going to play a crucial role in the design the wing. However, as it is hard to make a model to describe this phenomena, very basic computations were done during the current research. Developing a more detailed model, for example using a FEM analysis, is crucial for the implementation of the effects of wingtip propellers, as the uncertainty at this is stage is still very large.

A more detailed approximation of the lift distribution and the effect of distributed electric propulsion with accurate software is advised. In addition, wind tunnel tests should be done to validate the results of this report. The Oswald efficiency factor in this report was based upon statistical data, but as the E-gle uses a significantly different concept than existing aircraft, the accuracy of the Oswald factor can be improved.

More research on the specific energy and recharge capabilities is advised for the power part of the project. Currently the charging time is 6 hours, which is more than twice the mission time. Moreover, technology readiness level of the batteries is low. However it is expected that these problems will resolve when further research is conducted due the increase in demand. Furthermore, battery swapping needs extra attention, as this technology is not used as standard routine. The infrastructure of such an operation can also be explained in more detail in further research.

Parallel hybrid engines are used in cars, but further research can be done in up-scaling this technology for a power range applicable to aircraft. Especially the integration of the two system is a point of interest. At the moment it is still unclear how the systems interact at certain power settings. For example, if the gas turbine works at flight idle while the electrical engine works on full power.

For the market analysis it is important that in the next stage of the design process a business plan is developed. It should contain the financial plan, a market strategy and investment plan.

During the preliminary design process it was found that it might be interesting to investigate a fully electric aircraft. In order to make this feasible, the range requirement needs to be more flexible and the development time needs to be longer. This gives the industry the chance to increase battery specific energy and reduces the required energy needed to perform the mission. Moreover, full hydrogen flight is an interesting option, but the technical readiness level is still low and therefore the time constraints should be relaxed. Especially in combination with electric fight, hydrogen has great advantages with the possibility to use superconducting engines together with the relatively high specific energy and reasonable energy density characteristics of hydrogen in comparison with batteries.

A research field that might be more realistic in the given time constraint is a hybrid aircraft that does not make use of distributed electric propulsion. Especially for longer ranges this concept might be more efficient and less complex than a hybrid design with DEP. Longer ranges means flying at higher altitudes, which when the cruise speed is fixed results in a relatively high required surface area that diminishes the main benefit of DEP. Leading to the possible conclusion that benefits of the DEP are outweighed by the extra mass added to the aircraft.

BIBLIOGRAPHY

[1] A. M. Stoll, J. Bevirt, M. D. Moore, W. J. Fredericks, and N. K. Borer, "Drag Reduction Through Distributed Electric Propulsion," 2014.

[2] A. Gohardani and G. Doulgeris, "Challenges of Future Aircraft Propulsion: A Review of Distributed Propulsion Technology and its Potential Application for the All Electric Commercial Aircraft," 2010.

[3] Airbus, "Airbus Global Market Forecast," 2016.

[4] Boeing, "Boeing Current Market Lookout," 2016.

[5] Bombardier, "Bombardier Business Aircraft Market Forecast," 2016.

[6] Bombardier Aerospace, "Bombardier Q300 Datasheet."

[7] Fokker, "Fokker 50 datasheet."

[8] Embraer, "Embraer ERJ 140 Datasheert."

[9] ATR, "ATR 42-500 Datasheet."

[10] Tupolev, "Tupolev-124 Datasheet."

[11] Aviator Media, "Aircraft compare database," 2017.

[12] International Civil Aviation Organization, *Operation of Aircraft, Annex 6, Part 1*. 2009.

[13] B. S. Blanchard and W. J. Fabrycky, *Systems engineering and Analysis*. Prentice-Hall.

[14] J. Scanlan, "Sample Aircraft Weight Estimates," 1995-2004.

[15] C.Downing, "An Introduction to Airline Communication Types," 2016.

[16] D. P. Raymer, *Aircraft Design: A Conceptual Approach*. American Institute of Aeronautics and Astronautics, Inc., 2004.

[17] E. Torenbeek, *Synthesis of Subsonic Airplane Design*. Cluwer Acedemic Publishers, 1982.

[18] D. G. S1, "Midterm report," 2017.

[19] Jane's Information Group, "Jane's all the world's aircraft," 2017.

[20] European Aviation Safety Agency, *Certification Specifications for Large Aeroplanes CS-25*. 2007.

[21] D. Steenhuizen and A. Elham, "AE2111-II, Wing Design Part 1-4," 2015.

[22] N. K. Borer, J. M. Derlaga, K. A. Deere, M. B. Carter, S. A. Vikken, M. D. Patterson, B. L. Litherland, and A. M. Stoll, "Comparison of Aero-Propulsive Performance Predictions for Distributed Propulsion Configurations," 2017.

[23] L. R. Miranda and J. E. Brennan, "Aerodynamic Effect of Wingtip-Mounted Propellers," 1986.

[24] J. C. Patterson and G. R. Bartlett, "Effect of Wing-Tip Mounted Pusher Turboprop on the Aerodynamic Characteristics of a Semi-Span Wing," 1985.

[25] M. H. Snyder, "Effects of a Wingtip-Mounted Propeller on Wing Lift, Induced Drag, and Shed Vortex Pattern," 1968.

[26] A. M. Stoll and G. V. Mikic, "Design Studies of Thin-Haul Commuter Aircraft with Distributed Electric Propulsion," 2016.

[27] D. S. M. Nita, "Estimating the Oswald Factor from Basic Aircraft Geometrical Parameters," 2012.

[28] I. H. Abbott and A. E. V. Doenhoff, *Theory of Wing Sections*. Dover Publications, 1958.

[29] J. Roskam, *Airplane Design, Part VI: Preliminary Calculation of Aerodynamic, Thrust and Power Characteristics*. DARcorporation, 1985.

[30] M. D. Patterson, "Conceptual Design of High-Lift Propeller Systems for Small Electric Aircraft," 2016.

[31] M. D. Patterson and B. J. German, "Simplified Aerodynamics Model to Predict the Effect of Upstream Propellers on Wing Lift," 2015.

[32] M. D. Patterson, B. J. German, and N. K. Borer, "A Simple Method for High-Lift Propeller Conceptual Design," 2016.

[33] M. D. Patterson, J. M. Derlaga, and N. K. Borer, "High-Lift Propeller System Configuration Selection for NASA's SCEPTOR Distributed Electric Propulsion Flight Demonstration," 2016.

[34] G. L. Gentry, M. A. Takallu, and Z. T. Applin, "Aerodynamic Characteristics of a Propeller-Powered High-Lift Semispan Wing," 2016.

[35] Mcdonnell Douglas Astronautics Company, "The USAF Stability and Control Digital DATCOM," 1979.

[36] G. L. Rocca, "AE3211-I, Design for AC longitudinal stability," 2017.

[37] M. Sadraey, *Aircraft Design: A Systems Engineering Approach*. 2012.

[38] J. Roskam, *Airplane Design, Part II: Preliminary Configuration Design and Integration of the Propulsion System*. DARcorporation, 1985.

[39] Holy Cows Inc., "DATCOM Method," 2010.

[40] Holy Cows Inc., "Aircraft Coefficient Comparisons Between Datcom and Published Data," 2011.

[41] J. A. Mulder, W. H. J. J. van Staveren, J. C. van der Vaart, E. de Weerdt, C. C. de Visser, A. C. in 't Veld, and E. Mooij, "AE3202 Flight Dynamics Lecture Notes," 2013.

[42] J. V. Bogaert, "Assessment of Potential Fuel Saving Benefits of Hybrid-Electric Regional Aircraft," 2015.

[43] R.H.Lenssen, "Series Hybrid Electric Aircraft Comparing the Well-to-Propeller Efficiency With a Conventional Propeller Aircraft," 2016.

[44] S. Gudmundsson, *General Aviation Aircraft Design : Applied Methods and Procedures*. Butterworth-Heinemann, 2014.

[45] R. Vos, J. A. Melkert, and B. T. C. Zandbergen, "Aerospace Design and Systems Engineering Elements I," 2017.

[46] R. Eppler, *Airfoil Design and Data*. 1990.

[47] L. W. Traub, *Inverse Propeller Design for a Prescribed Chord or Blade Angle*. Embry Riddle Aeronautical University, 2017.

[48] MT-Propeller, "MTV-8 Variable Pitch Propeller," 2005.

[49] G. V. Brown, A. F. Kascak, and B. Ebihara, "NASA Glenn Research Center Program in High Power Density Motors for Aerospacepropulsion," 2005.

[50] M. J.Fu, Z.P.Cano, "Electrically Rechargeable Zinc–Air Batteries: Progress, Challenges, and Perspectives," 2017.

[51] Y.Li, M.Gong, Y.Liang, and J.Feng, "Advanced Zinc-Air Batteries Based on High-Performance Hybrid Electrocatalysts," 2013.
[52] D.Linden and T.B.Reddy, *Handbook of batteries*. 2002.
[53] C.Pornet, S.Kaiser, A.T.Isikveren, and M.Horung, "Integrated Fuel-Battery Hybrid for a Narrow Body Sized Transport Aircraft," 2014.
[54] E. Torenbeek, "Development and Application of a Comprehensive, Design-sensitive Weight Prediction Method for Wing Structures of Transport Category Aircraft," 1992.
[55] T. H. G. Megson, *Aircraft Structures for Engineering Students*. 2012,.
[56] S. An, "Aeroelastic Design of a Lightweight Distributed Electric Propulsion Aircraft with Flutter and Strength Requirements," 2015.
[57] J. C. O. Lopes, "Material Selection for Aeronautical Structural Application," 2008.
[58] R. Vos and J. A. Melkert, "Aerospace Design and Systems Engineering Elements I," 2017.
[59] S. T. Chai and W. H. Mason, *Landing Gear Integration in Aircraft Conceptual Design*. 1996,.
[60] R. Alderliesten, "AE1102-I Introduction to Aerospace Engineering I," 2014.
[61] G. Ruijgrok, *Elements of Airplane Performance*. Delft Academic Press, 2009.
[62] M. Voskuijl, "AE2230-I Flight and Orbital Mechanics," 2016.
[63] A. Filippone, *Advanced Aircraft Flight Performance*. Cambridge University Press, 2013.
[64] AE3205 - Simulation, Verification and Validation, "Flight Performance of the Fokker 50,"
[65] Bombardier Aerospace, "Bombardier Q300," 2006.
[66] J. Park, G. Nam, and J. Cho, "Perspective of Zn-Air Batteries," 2015.
[67] U.S. Department of Transportation, "Pilot's Handbook of Aeronautical Knowledge," 2016.
[68] H. Fricke and M. Schultz, "Delay Impacts onto Turnaround Performance," 2009.
[69] M. Mirza, "Economic Impact of Airplane Turn-Times," 2008.
[70] M. Schmidt, "A Review of Aircraft Turnaround Operations and Simulations," 2017.
[71] J. Arshad, *A Cost Benefit Analysis of Electric and Hybrid Electric Vehicles*. University of Chicago, 2014.
[72] United States Department of Transportation, "Federal Aviation Administration," 2017.
[73] World Comission on Environment and Development, *Our Common Future*. Oxford University Press, 1987.
[74] A. Azapagic, S. Perdan, and R. Clift, *Sustainable Development in Practice*. John Wiley Sons, 2004.
[75] I. Takeshita, "Gigafactory Tesla," 2013.
[76] F. O'Brien-Bernini and O. Corning, "Composites and Sustainability – When Green Becomes Golden," 2011.
[77] M. Weiss and V. Gollnickx, "Aircraft Production - Ecological assessment in the pre-design stage," 2013.
[78] T. Tanimoto, J. Fujimoto, T. Tamura, K. Todome, M. Adachi, Y. Suzuki, and K. Kauchi, "Static and Fatigue Properties of CFRP/Damping-Material Laminatese," 2001.
[79] K. R. Long, J. H. D. Jr., and S. Ludington, "Significant Deposits of Gold, Silver, Copper, Lead, and Zinc in the United States ," 2000.
[80] H. H. Hubbard, *Aeroacoustics of Flight Vehicles: Theory and Practice*. NASA Langley Research Center.
[81] R. H. Self, *Jet Noise Prediction Using the Lighthill Acoustic Analogy*. University of Southampton.
[82] M. R. Fink, *Airframe Noise Prediction Method.* U.S. Department of Transportation Federal Aviation Administration.
[83] J. C. Hardin, D. J. Fratello, and R. E. Hayden, *Prediction of airframe noise*. National Aeronautics and Space Administration.
[84] J. J. Ruijgrok, *Elements of Aviation Acoustics*. 2004,.
[85] G. S. Hreinsson, *Aircraft Noise*. Virginia Polytechnic Institute and State University, 1993.
[86] A. K. Sahai, *Consideration of Aircraft Noise Annoyance during Conceptual Aircraft Design*. RWTH Aachen, 2016.
[87] L. Leylekian, M. Lebrun, and P. Lempereur, "An Overview of Aircraft Noise Reduction Technologies," 2014.
[88] O. Bschorr, "Noise Reduction for Propellers," 1972.
[89] D. K. Wasiuk, M. H. Lowenberg, and D. E. Shallcross, "An Aircraft Performance Model Implementation for the Estimation of Global and Regional Commercial Aviation Fuel Burn and Emissions," 2014.
[90] U.S. Energy Information Administration, *International Energy Outlook 2016*. 2016.
[91] G. D. M. R. Pavri, *Gas Trubine Emissions and Control*. GE Energy Services, 2001.
[92] J. P. van Buijtenen, W. P. J. Visser, S. Shakariyants, and F. Montella, *Gas Turbines, Propulsion and Power, AE2–203*. Materials Park Ohio, 2011.
[93] Y. Yang, R. Booma, B. Irion, D. van Heerden, P. Kuiper, and H. de Wit, "Recycling of Composite Materials," 2012.
[94] J. A. S. Green, *Aluminum Recycling and Processing for Energy Conservation and Sustainability*. Materials Park Ohio, 2007.
[95] K. J. Martchek, "Modelling More Sustainable Aluminium," 2006.
[96] A. Haque, V. Subramanian, and R. J. Gibbs, "Copper, Lead, and Zinc Pollution of Soil environment," 2009.
[97] Y. Li and H. Dai, "Recent Advances in Zinc–Air Batteries," 2014.
[98] G. Díaz and D. Martín, "Modified Zincex Process: the Clean, Safe and Profitable Solution to the Zinc Secondaries treatment," 1994.
[99] F. International, "The Market for Aviation Turboprop Engines," 2010.
[100] R. Hamann and M. van Tooren, "Systems engineering & Technocal management techniques," 2017.
[101] Bombardier, "Bombardier Q series analysis."
[102] G. Corning, *Supersonic and Subsonic, CTOL and VTOL, Airplane Design*. 1976,.
[103] H. P. Barringer, "Availability, Reliability, Maintainability, and Capability," 1997.
[104] D. Pettit and A. Turnbull, *General Aviation Aircraft Reliability Study*. NASA.
[105] M. Mirza, "Economic Impact of Airplane Turn-Times," 2008.
[106] F. Wubben and J. Busing, "Night time restrictions at Amsterdam-Schiphol An international comparison ," 2004.
[107] H.L. Smith III, "Standards for Aircraft Fuel Servicing Fuel Safety Training," 2013.

A

APPENDIX

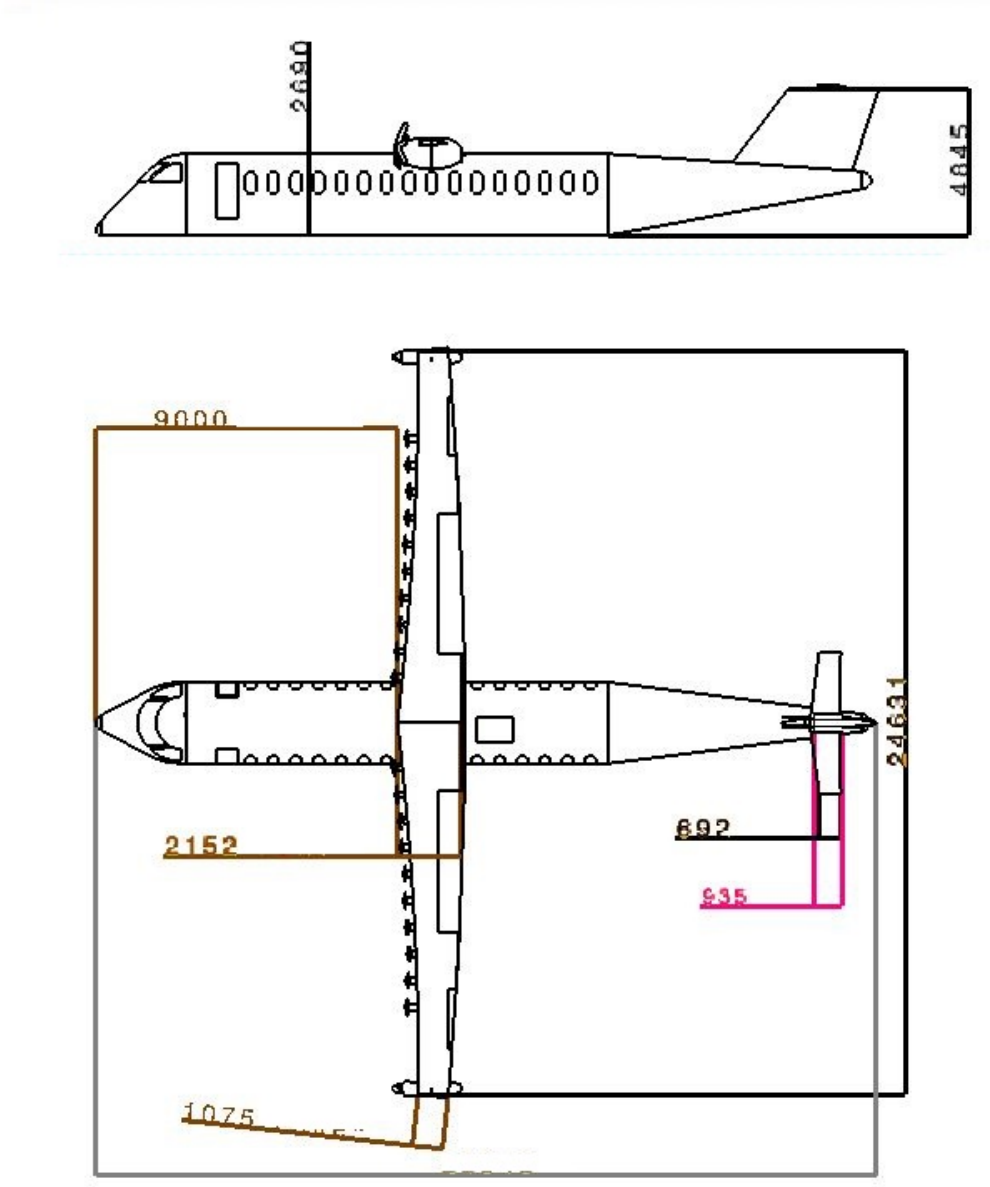

Figure A.1: Drawings of the E-gle